MECHANISMS OF TURBULENT FLAME PROPAGATION

BY

RAMZY G. ABDEL-GAYED
B.Sc., G.I.Mech.Eng., M.I.Combustion

Submitted in fulfilment of the requirements
for the degree of Doctor of Philosophy

DEPARTMENT OF MECHANICAL ENGINEERING,
THE UNIVERSITY OF LEEDS

JULY 1978

"IN THE NAME OF ALLAH,

THE BENEFICENT, THE MERCIFUL"

Dedicated to my Parents

"Now the puzzle is complete; the sum is right;
and I hardly know whether to be glad or sorry
that the work is done"

Oliver C. de C. Ellis
A history of fire and flame

ABSTRACT

Measurements are reported of premixed hydrogen-air turbulent burning velocities, made by the double kernel method during explosions. Turbulence was created by four high speed fans driven by electric motors within the explosion vessel. This arrangement created a central region of uniform, isotropic turbulence in which all measurements were made.

The ratio of turbulent to laminar burning velocity correlates well with both the turbulent Reynolds number of the reactants and the ratio of laminar burning velocity to r.m.s. turbulent velocity. The use of hydrogen-air mixtures has extended the data on premixed turbulent combustion to régimes with higher values of the last dimensionless ratio. At high values of the ratio there is evidence of a wrinkled laminar flame structure, but at lower values a small scale eddy structure seems to be dominant.

A two eddy theory of turbulent combustion is presented. This rests upon the assumption, supported by a good deal of experimental evidence, that two scales of eddy are particularly important. One is associated with the integral scale of turbulence, the other with the Kolmogorov microscale. It is assumed that all the material in the large eddies is used in the formation of the smaller dissipative eddies. It is assumed that laminar flame propagation occurs through the large eddies, whilst two approaches are

considered in the case of dissipative eddies. In the first approach, laminar flame propagation across a vortex tube is employed, whilst in the second the concept of a reaction time in the vortex tube is used.

It is shown that the rate of burning in small eddies can be many times greater than that in large eddies. Theoretical values are obtained for the ratio of turbulent to laminar burning velocity, in terms of turbulent Reynolds number and the ratio of laminar burning velocity to r.m.s. turbulent velocity. These are in fair agreement with experimental values, but more data are required on the intermittency and chemical lifetimes of small eddies.

Experiments are reported on the effect of turbulence upon flammability limits. These are narrowed as turbulence increases, but counter-action may be taken by increasing the spark iginition energy and by establishing the initial flame in a shielded region where the turbulence is reduced. The relevance of the theory to these results is discussed.

Finally, the application of these findings in practical combustion chambers is discussed.

ACKNOWLEDGEMENTS

The author would like to thank Dr. Derek Bradley for his guidance, advice, many valuable discussions and continuous encouragement throughout the supervision of this work.

In addition, the author is grateful for the assistance given by the technical staff of the Thermodynamics Laboratory, and is also grateful to Leeds University and the Science Research Council for providing part financial support.

CONTENTS

PAGE

PAGE

CHAPTER 1

INTRODUCTION

1.1 GENERAL INTRODUCTION

Practical combustion usually involves turbulent flames as, for example, in petrol and diesel engines, gas turbine and ramjet combustion chambers, and furnaces. Turbulent flame propagation is also an important feature of explosions in both mines and buildings. There is now a widely recognised need for fundamental research into this mode of combustion, in support of current efforts to improve the fuel economy, combustion intensity and exhaust emissions of all types of combustion system. Unfortunately, the structure of turbulent flames and the processes governing their rate of propagation are not readily amenable to theoretical analysis. Although the basic features of laminar flame structure and propagation are clearly understood, no comparable understanding of turbulent flames has yet been achieved. Improvement, through experiment and theory, of the understanding of premixed turbulent flames is the prime aim of the present work.

Qualitatively, the effects of turbulence upon combustion have been known for many years. Mallard and Le Chatelier (1) noted that turbulence increased both energy transfer and flame surface area and also formed new centres of inflammation. Effectively, they were anticipating three different models of turbulence combustion and also implying that no single one of them would be comprehensive. Historically, models for turbulent flames

have lagged behind contemporary understanding of isothermal turbulence in non-reacting systems. The latter, in turn, has been conditioned by the degree of sophistication of the available experimental techniques for turbulence studies.

Most early studies of turbulent flames were directed towards an understanding of flame propagation in a spark ignition engine and these have been reviewed by Wheeler (2). Pressure records were obtained, sometimes flame speeds were measured, but no attempts were made to deduce labouratory values of turbulent burning velocity. Since then many measurements have been taken on burners and in explosion vessels.

The advent of the laser Döppler anemometer in the last few years is helping to give a better understanding of the structure of turbulence and its role in combustion (3).

Although much research has been done on the nature of turbulent combustion, no simple theory has yet been established which adequately describes the burning processes. This may be explained by the extreme complexity of these processes, in which the chemical reactions are complicated and are associated with spatially and temporary varying temperatures, concentrations and velocities.

A completely analytical theory of turbulent combustion might be developed by extensions of the statistical theory of turbulence to include fluctuations

of temperature, species concentration, velocities and chemical reaction rates. Several years ago both Von Kármán (4) and Hawthorne (5) recommended this type of approach, but as the statistical theory has not yet reached the stage where it predicts isothermal time averaged quantities, it cannot be extended to include chemical reactions. Flame propagation is governed by the conservation equations for global mass, species and energy. These equations along with appropriate chemical rate data have been used to predict the burning velocity, temperature and composition profiles for laminar flames with reasonable accuracy (6,7). However, for turbulent conditions if the conservation equations include terms for all the fluctuating quantities and then are expanded, various double and triple correlations arise. It is not surprising that attempts to solve the equations have resorted to the various priori assumptions needed to close the conservation equations (8-10).

Apart from the works of Prudnikov (11,12), Raushenbakh et al (13) and Predvoditelev (14,15) which retain some aspects of statistical nature of turbulence, the remaining analytical predictions of the turbulent burning velocity, u_t, result in grossly oversimplified relationships. The various approaches have been reviewed by Andrews, Bradley and Lwakabamba (16). More recently Bray and Moss (17) have developed a model for premixed turbulent flames. They assumed that combustion occurs through a global, one-step, irreversible chemical reaction.

They also used a probability density function and obtained time-averaged values of thermodynamic variables within the flame. These variables were then used, along with conservation equations derived from the exact equations of turbulent reacting flow to establish a set of equations for the flame. If a probability density function based on concentration is assumed, these model equations form a closed set, which provide a complete description of time-averaged mean and fluctuating properties. This model has been developed further by Bray and Libby (18) to predict flame speed and structure.

1.2 MEASUREMENTS INVOLVING FAN-GENERATED TURBULENCE

The observation of free flame propagation in a closed vessel obviates the complications of flame stabilisation. The use of such vessels fitted with a fan was pioneered by Schloesing and de Mondesir in 1864 and their work formed the basis for Mallard and Le Chatelier's (1) observation of enhancement of the rate of flame propagation due to turbulence. The creation of turbulence by fans in closed vessels has several advantages over its creation in continuous flow systems. Semenov (19) has shown that if four identical fans are symmetrically disposed within a closed vessel and rotated at the same speed a central region exists of uniform isotropic turbulence. Pre-pressure period flame propagation occurs within this region, in which a fairly

spherical turbulent flame will propagate (19,20). It also offers good possibilities for detailed investigation of the structure of isotropic turbulence, in which there is no mean flow velocity. Thus the eddies will not have a convective velocity superimposed on them, which might preclude detailed study of individual eddy lifetimes.

In an explosion a single flame propagating through the unburnt gases facilitates a study of the flame structure without the complication of a fluctuating flame brush which occurs in stabilised turbulent flames. On the other hand, when hot wire anemometers are used to characterise the turbulence of the cold gas some problems arise due to the rectification of the velocity fluctuations by the hot wire (19-22), and these are demonstrated and discussed in Chapters 3 and 4 of the present thesis.

Karpov et al (20) and Sokolik et al (23) used a nearly spherical vessel equipped with four stirrers driven by electric motors for the determination of turbulent burning velocities from pressure-time records and flame radius-time photographs.

Another method of creating turbulence in a closed vessel has been used by Ohigashi et al (24). In this a screen rapidly moved magnetically across the closed vessel just prior to ignition, but this involves problems due to the different rates of turbulence decay across the vessel. A similar arrangement has been used recently by Iinuma (25), who concluded that the characteristics of the turbulence so generated was very complicated and could not be measured in detail.

Ono et al (2) have used a configuration of four fans mounted behind four changeable perforated plates, which form four sides of the combustion chamber, with two windows to form the other sides.

In the Mechanical Engineering Department, at Leeds University, Andrews (26) experimented with an apparatus similar to that of the Russian group but with the fan driven by air turbines. He measured turbulent burning velocities by both the double kernel method and also the flame speed-gas velocity method. He suggested that for isotropic turbulence, the ratio of turbulent to laminar burning velocity, u_t/u_ℓ, could be correlated with the Taylor turbulent Reynolds number of the unburnt gas, R_λ, equal to $u'\lambda/\nu$, where u' is the r.m.s. turbulent velocity, λ is the Taylor microscale of turbulence and ν the kinematic viscosity.

Subsequently, Lwakabamba (27) used the same apparatus, and presented values of u_t, for methane and ethylene-air mixtures. Arising from his results a secondary influence was suggested, in that values of u_t/u_ℓ tended to be less at a given Reynolds number for those mixtures with a higher value of u_ℓ.

1.3 THE PRESENT WORK

To elucidate this last possibility, it was decided to measure turbulent burning velocities by the double kernel method for mixtures with significantly higher values of

laminar burning velocity than previously investigated. For this reason, hydrogen-air mixtures, some of which give high values of u_ℓ, were used in the same apparatus, but the original air turbines were replaced by electric motors and the shaft sealing improved.

The present study suggests that for isotropic turbulence, the ratio u_t/u_ℓ can be correlated with both u_ℓ/u' and the turbulent Reynolds number, R_L, equal to $u'L/\nu$, where L is the integral scale of turbulence. Other workers' data, drawn from a variety of rigs, over a wide range of burning conditions, mixtures and turbulent parameters, correlate well with the proposed parameters and this is demonstrated in Chapter 5.

The effect of turbulence on flame propagation limits was studied and ciné schlieren flame photographs were used to examine the structure of turbulent flames. These revealed the importance of the small eddy structure as the turbulence increases.

In Chapter 6, a two eddy theory of burning is presented, based on the experimental studies. The theory predicts the volumetric rates of burning in both large and small eddies, the burning velocity ratio u_t/u_ℓ, and the flame thickness ratio δ_t/L. The theory gives theoretical support to the proposed correlations of the experimental data given in Chapter 5.

Finally the current findings are applied to problems of lean burning in gasoline engines in Chapter 7.

1.4 NOMENCLATURE

L	integral scale of turbulence
R_L	$\frac{u'L}{\nu}$
R_λ	$\frac{u'\lambda}{\nu}$
u_ℓ	laminar burning velocity
u_t	turbulent burning velocity
u'	r.m.s. turbulent velocity
δ_t	turbulent flame thickness
λ	Taylor microscale of turbulence
ν	kinematic viscosity

1.5 REFERENCES

1. E.MALLARD and H.L. LE CHATELIER, Ann. Mines Paris 4, 343 (1883).

2. R.V.WHEELER, The inflammation of mixtures of ethane and air in a closed vessel: the effects of turbulence, J.Chem.Soc. 115, 81 (1919).

3. P.MOREAU and A.BOUTIER, Laser velocimeter measurements in a turbulent flame, Sixteenth Symposium (International) on Combustion, The Combustion Institute: Pittsburgh, 1747 (1977).

4. T.VON KÁRMÁN, Comments in round table discussion on turbulent flames, Fourth Symposium (International) on Combustion, p.924, Williams and Wilkins: Baltimore (1953).

5. W.R.HAWTHORNE, Selected combustion problems, fundamental and aeronautical applications, Butterworths, London, p.267 (1954).

6. G.DIXON-LEWIS, Flame structureand flame reaction kinetics I, Proc.Roy.Soc. (London), Ser.A, 298, 495 (1967).

7. G.DIXON-LEWIS, Flame structure and flame reaction kinetics II, Proc.Roy.Soc.(London), Ser.A, 307, 111 (1968).

8. W.T.SYNDER, Preliminary observations of one-dimensional turbulent propane air flames, Eighth Symposium (International) on Combustion, p.573 Williams and Wilkins: Baltimore (1962).

9. H.S.SANEMATSU, Turbulent flame propagation in a homogeneous gas mixture, Combustion and Flame 13, 1 (1969).

10. F.A.WILLIAMS, An approach to turbulent flame theory, J.Fluid Mech. 40, 401(1970).

11. A.G.PRUDNIKOV, Equation of turbulent flame, The Third All-Union Congress on Combustion Theory, Vol.1, Flame Propagation and Detonation in Gas Mixtures, Moscow 1960, p.100.

12. A.G.PRUDNIKOV, The determination of the average parameters of a turbulent flame, Izv.Akad.Nauk SSSR, Otd.Tech.Nauk, Energetika i Automatika No.1, p.43 (1960).

13. B.V.RAUSHENBAKH, S.A.BELLY, I.V.BESPALOV, V.Ya.BORODACHEV, M.S.VOLYNSKY and A.G.PRUDNIKOV, Physical basis of the working process in combustion chambers of jet engines, Mashinostroyeniye: USSR (1964). (English Translation: FTD-MT-65-78 (1967).)

14. A.S.PREDVODITELEV, On rates of chemical reactions in turbulent flows, The Third All-Union Conference on Combustion Theory, Vol.1, Flame Propagation and Detonation in Gas Mixtures, Moscow 1960, p.138.

15. A.S.PREDVODITELEV, The rates of chemical reactions in turbulent streams (Basic formulation of the theory), Inzhenemo-Fizicheskii Zh. 11, p.3 (1960). (English Translation: NLL RTS-1817 (1961).)

16. G.E.ANDREWS, D. BRADLEY and S.B.LWAKABAMBA, Turbulence and turbulent flame propagation - a critical appraisal, Combustion and Flame 24, 285 (1975).

17. K.N.C.BRAY and J.B.MOSS, A unified statistical model of the turbulent premixed flame, University of Southampton Report A.A.S.U. No.335 (1974).

18. K.N.C.BRAY and P.A.LIBBY, Interaction effects in turbulent premixed flames, The Physics of Fluids 19, 1687 (1976).

19. E.S.SEMENOV, Measurement of turbulence characteristics in a closed volume with artificial turbulence, Combustion, Explosion and Shock Waves 1, 57 (1965).

20. V.P.KARPOV, E.S.SEMENOV and A.S.SOKOLIK, Turbulent combustion in an enclosed space, Dokl. Akad. Nauk SSSR128, 1220 (1959).

21. Y.OHTA, K.SHIMOYAMA and S.OHIGASHI, Vaporization and combustion of single liquid fuel droplets in a turbulent environment, Bulletin of the JSME 18, 47 (1975).

22. S.ONO, M.TSUGE, M.KURUSU and I.FUKUE, A study on the influence of the scale of turbulence on the burning rate in a vessel, Bulletin of the JSME 19, 547 (1976).

23. A.S.SOKOLIK, V.P.KARPOV and E.S.SEMENOV, Turbulent combustion of gases, Combustion, Explosion and Shock Waves 3, 36 (1967).

24. S.OHIGASHI, Y.HAMAMOTO and A.KIZIMA, Effects of turbulence on flame propagation in closed vessels, Bulletin of the JSME 14, 849 (1971).

25. K.IINUMA, A study of turbulent flame propagation in closed vessels, Automobile Exhaust Clarification Study Group, Japan, March 1977.

26. G.E.ANDREWS, Laminar and turbulent flame propagation, Ph.D. thesis, Dept. of Mechanical Engineering, Univ.Leeds (1972).

27. S.B.LWAKABAMBA, Turbulent flame propagation in closed vessels, Ph.D. thesis, Dept. Mechanical Engineering, Univ.Leeds (1975).

CHAPTER 2

DERIVATION OF TURBULENT TRANSPORT COEFFICIENTS FROM TURBULENT PARAMETERS IN ISOTROPIC TURBULENCE

CHAPTER 2

DERIVATION OF TURBULENT TRANSPORT COEFFICIENTS FROM TURBULENT PARAMETERS IN ISOTROPIC TURBULENCE

2.1 INTRODUCTION

Fundamental statements of the conservation equations for turbulent flow involve neither a length scale nor the concept of turbulent diffusivity, ε. Nevertheless, because of the incompleteness of fundamental data, these concepts continue to be used both in experimental anemometry and in solutions of complex flow problems.

In the computational solutions of those flow systems which involve the turbulent transport of energy, mass, and momentum, the associated transport coefficients are sometimes conveniently expressed in terms of the turbulent Reynolds number, R_L(1,2). This parameter also has been used in the correlation of data on turbulent burning velocities (3-5) and in the present studies. In this approach to turbulent flow it is important, therefore, to ascertain the interrelationship between turbulent transport coefficients and turbulent Reynolds number. In the present work this will be expressed through the employment

of the ratio of turbulent diffusivity to kinematic viscosity, ε/ν, which is termed the turbulent transport number. The task is to find the relationship between the two dimensionless numbers.

Initially, the relationship is sought for isotropic turbulence. The present state of theories of turbulence does not enable a theoretical relationship to be obtained, but many experimenters have derived values of ε/ν from measurements of flow in circular tubes which involve all three transportable quantities at different flow Reynolds numbers, Re. Also some measurements have been derived for flow between two parallel plates. This Chapter first reviews this work and then the measurements of turbulent parameters: macroscale, L, microscale, λ, and r.m.s. turbulent velocity u'. These measurements enable R_L, equal to $u'L/\nu$, at a given position, to be related to Re. From the interrelationships thus derived it is possible to express ε/ν as a function of R_L. Hopefully, for isotropic turbulence, this is a unique relationship which is independent of the flow system.

2.2 THE RELATIONSHIP BETWEEN ε/ν AND Re

2.2.1 Pipe Flow

Many experimenters have shown, through the technique of hot wire anemometry, that the turbulence in the vicinity of the centre line of a circular pipe is close to isotropic (6-9). Figure 2.1 shows experimentally

determined values of ε_y/ν in the radial direction for this region in developed flow, plotted against Re. Of these data points 58% are referred to by the original workers as being on the pipe axis and 89% are for a value of dimensionless radius of less than 0.1. Values are based upon mass, energy, and momentum transfer and the general scatter of the points obscures any tendency there might be for ε_y/ν to depend upon which of the three quantities is being transferred. This is in line with recent studies carried out by Quarmby and Quirk (45). Table 2.1 summarises the techniques used for the measurements reported in Refs. (10-25).

Semi-theoretical values of ε_y/ν also have been derived from velocity profiles. For a long time there was uncertainty concerning the distribution of turbulent diffusivity for momentum in the core region of the pipe (22). The velocity distribution of Nikuradse implied that it fell to zero at the axis, but Reichardt (26) measured the velocity profile and proposed an empirical expression for the distribution of eddy diffusivity of momentum.

$$\varepsilon_y^+ = (K_v/6)(1 - a^2)(1 + 2a^2) \qquad (2.1)$$

where $\varepsilon_y^+ = \varepsilon_y/u^* R$,

a is the radius ratio $= r/R$,

K_v = von Kármán constant

and u^* is the friction velocity, given by (9, p.31)

$$u^* = 0.1\ (Re)^{7/8}\ \frac{\nu}{R} \qquad (2.2)$$

With a value of K_v equal to 0.4 (26) Eqs. (2.1) and (2.2) yield

$$\varepsilon_y/\nu = 0.00667\ (Re)^{7/8}\ (1 - a^2)(1 + 2a^2) \qquad (2.3)$$

and on the axis of the pipe (a = 0) this yeilds

$$\varepsilon_y/\nu = 0.00667\ (Re)^{7/8} \qquad (2.4)$$

The equation appears as the straight line in Fig. 2.1.

Brinkworth and Smith (23) modified Reichardt's expression by proposing alternative values for the constants. From their measured velocity profiles they obtained a value of K_v equal to 0.378. Their expression, for 50,000<Re<350,000, yields

$$\varepsilon_y/\nu = 0.0063\ Re^{7/8}\ (1 - a^2)(1 + 2a^2) \qquad (2.5)$$

and at the axis

$$\varepsilon_y/\nu = 0.0063\ (Re)^{7/8} \qquad (2.6)$$

This equation appears as the broken line in Fig. 2.1. Further modifications to Reichardt's model have been made by Travis et al (27) and expressions given for ε_y/ν across the pipe diameter.

Powe et al (28) have used a somewhat different approach, which is based upon the equation of Laufer (7) for the Reynolds stress, $\overline{uv}$, where u and v represent the axial and radial fluctuating velocity components,

respectively. For this purpose they employed the velocity profile expression given by Kays (29) for the central region, and that given by Longwell (30) for the wall region. Experimental data for these expressions were taken from Refs. 31 and 32. The turbulent diffusivity for momentum was obtained from the expression (33),

$$\varepsilon_y = - \overline{uv} \left(\frac{\partial U}{\partial y}\right)^{-1} \qquad (2.7)$$

in which U is the mean velocity component in the axial direction and y is the distance measured in the radial direction. The three values of ε_y/ν obtained in this way for the pipe axis from Ref. (28) are shown in Fig. 2.1. The figure shows that Eq. (2.4) agrees well with the experimental results.

2.2.2 Parallel Plate Chanel Flow

For fully developed turbulent flow in a parallel plate channel Laufer (44) was the first to show, through the technique of hot wire anemometry, that the turbulence in the vicinity of the centre line is isotropic. Figure 2.2 shows experimentally determined values of ε_y/ν in the radial direction, for this region in developed flow, plotted against Re_p, based upon the distance apart of the plates. Values are based upon mass, energy, and momentum transfer and the general scatter of the points again obscures any tendency for ε_y/ν to depend upon the quantity transferred. Table 2.2 summarises the techniques used for the measurements reported in Refs. (20,46-48). The

equation of the line through the points is

$$\varepsilon_y/\nu = 2.67 \times 10^{-3} (Re_p)^{1.028} \qquad (2.8)$$

$$\text{for} \quad 2.5 \times 10^3 < Re_p < 6 \times 10^4$$

2.3 THE RELATIONSHIPS BETWEEN MEASURED TURBULENCE PARAMETERS AND Re

2.3.1 Pipe Flow

These are shown in Figs. 2.3-2.5. Baldwin and Walsh (24) made hot wire anemometer measurements in developed turbulent air flow at the core of a 203 mm diameter pipe. The measured length scale was that of the Eulerian macroscale in the axial direction, L_x. The value of the transverse Eulerian scale in the radial direction, L_y, is one half of this value (34-36). Because the transport processes at present under consideration are in the radial direction, it is the value L_y that is used in the evaluation of the turbulent Reynolds number R_L, in conjunction with the r.m.s. turbulent velocity for this direction, v'.

Powe et al (8,37) have more recently used hot wire anemometry in turbulence measurements of air flow in a pipe of 305 mm. diameter, for all three directions. Length scale measurements were made only for one value of Re. In Mickelsen's (18) mass transfer studies hot wire anemometry was employed to measure r.m.s. turbulent velocity and Taylor microscale in the axial direction.

In the work of Lawn (38) air was blown along a honed tube of 144.3 mm diameter and microscales were determined by hot wire anemometry for all three directions. In the earlier work of Robertson et al (39), air was blown, at three different values of Re, along a 76 mm diameter smooth pipe. The microscale of turbulence in the axial direction, λ_x, was measured in two ways: first, by the use of a differentiating circuit to give the time derivative of the fluctuating signal and second, from the turbulent energy spectrum. The microscale in the radial direction, λ_y, shown in Fig. 2.5, was obtained from $\lambda_y = \lambda_x 2^{-\frac{1}{2}}$ (35).

Pike et al (40) used the laser Doppler shift technique to measure r.m.s. turbulent velocities in water flow in a pipe. The values obtained compared well with those from hot wire measurements in carbon dioxide, at the same Reynolds number.

Figure 2.3 shows the variation with Re of the ratio of the r.m.s. turbulent velocity for the radial direction to the mean centre line axial velocity, v'/U, at the pipe axis. This relationship is expressed by

$$\frac{v'}{U} = 0.087\ (Re)^{-0.079} \qquad (2.9)$$

$$\text{for } 10^4 < Re < 7 \times 10^5$$

Figure 2.4 shows the variation of the ratio of the radial macroscale to the pipe diameter, L_y/d, at the pipe axis, whilst Fig. 2.5 shows the corresponding

variation for the radial microscale ratio, λ_y/d. The latter relationship is expressed by

$$\frac{\lambda_y}{d} = 0.097\ (Re)^{-0.136} \qquad (2.10)$$

for $4\times10^4 < Re < 7 \times 10^5$

2.3.2 Parallel Plate Channel Flow

Few measurements have been made in parallel plate channel flow when compared with pipe flow. Laufer (44) was the first to make a thorough study of turbulent channel flow. He employed hot wire acemometry to measure r.m.s. turbulent velocity, macroscale, and Taylor microscale for developed air flow in a 12:1 aspect ratio channel. The Reynolds number range was 24,600 to 123,200 and measurements were made for all three directions.

Clark (49) used hot wire anemometry to measure r.m.s. turbulent velocity in air flow in a 12:1 aspect ratio channel, with a suction system, for the Reynolds number range of 30,000 to 91,200.

Hussain and Reynolds (50,51) and Acharya and Reynolds (52) have more recently employed hot wire anemometers to measure r.m.s. turbulent velocity for air blown along a turbulent channel with a relatively higher aspect ratio (18:1) than before. The range of Reynolds number used was 27,600 to 64,600.

Figure 2.6 shows the variation with Re_p of the ratio of the r.m.s. turbulent velocity for the radial

direction to the mean centre line axial velocity, v'/U, at the channel axis. The relationship may be expressed by

$$\frac{v'}{U} = 0.109\ (Re_p)^{-0.137} \qquad (2.11)$$

for $2\times10^4 < Re_p < 1.5\times10^5$

Figure 2.7 shows the variation of the radial microscale to the channel width, λ_y/y_o, at the channel axis. The relationship between this and the Reynolds number may be expressed by

$$\frac{\lambda_y}{y_o} = 9.726\ (Re_p)^{-0.499} \qquad (2.12)$$

for $2\times10^4 < Re_p < 1.5\times10^5$

It is easily shown from this equation and Eq. (2.11) that $R_{\lambda y}$ and Re_p are related by

$$R_{\lambda y} = 1.06\ (Re_p)^{0.364} \qquad (2.13)$$

for $2\times10^4 < Re_p < 1.5\times10^5$

Figure 2.8 shows these results in the form of the variation of radial turbulent Reynolds number based on macroscale, R_{Ly}, at the channel axis, with the channel flow Reynolds number, Re_p.

2.4 THE RELATIONSHIP BETWEEN R_L AND R_λ FOR ISOTROPIC TURBULENCE

The macro and micro scales are not independent

variables, but are interrelated. From a consideration of the steady state turbulent energy balance, in which the energy dissipation rate in isotropic turbulence is equated to the rate at which the large eddies supply energy it can be shown (3,35), that

$$\frac{L_y}{\lambda_y} = \frac{A}{40} R_{\lambda y} \qquad (2.14)$$

where $R_{\lambda y} = v'\lambda_y/\nu$ and A is a numerical constant of order unity.

Values of L_y/λ_y were obtained from the full line curves in Figs. 2.4 and 2.5 for values of Re in the range 4×10^4 to 7×10^5. Values of $R_{\lambda y}$ were calculated from the data of Figs. 2.3 and 2.5 for different values of Re and the relationship between the two Reynolds numbers was found to be

$$R_{\lambda y} = 8.42 \times 10^{-3} (Re)^{0.785} \qquad (2.15)$$

$$\text{for} \quad 4 \times 10^4 < Re < 7 \times 10^5$$

This is also the equation of the line shown in Fig. 2.9.

These data enabled an experimental relationship to be obtained between L_y/λ_y and $R_{\lambda y}$. This was found to be

$$\frac{L_y}{\lambda_y} = \frac{R_{\lambda y}}{42.4} \text{ for } 10 < R_{\lambda y} < 350 \qquad (2.16)$$

and is shown by the full straight line in Fig. 2.10. If this relationship is of general validity, irrespective of the mode of turbulence generation, it should apply also

for other isotropic flow systems.

From measurements of grid generated turbulence Dryden (41) previously has proposed a value of 48.64 for the denominator on the right hand side of equation (2.16). However, the present author is grateful to Mr. N. Gat (53) for pointing out that this value is erroneous, and that the origin of the error lies in the omission of a factor of two in Eq. (17.2) of Ref. (41). When this is corrected the relationship becomes

$$\frac{L_y}{\lambda_y} = \frac{R_{\lambda y}}{24.32} \quad \text{for } R_{\lambda y} > 10 \qquad (2.17)$$

and this is shown by the broken line in Fig. 2.10. The "y" direction is again that transverse to the flow. Also shown in this figure are experimental points in the régime $29 < R_{\lambda y} < 74$ obtained by Uberoi and Corrsin (42) in studies of grid generated turbulence in a wind tunnel.

Two experimental points are shown for higher values of Reynolds number, from the data of McQuivey and Richardson (43) on water flow in an open channel. These are for a position at half the depth; hot film anemometry was employed, but turbulence fell short of complete isotropy. Three experimental points are shown from the measurements of Laufer (44) on the flow of air at the centre line of a rectangular duct. These measurements give rather higher values of L_y/λ_y than do those of Ref. (42). Also shown in this figure are experimental points obtained by Comte-Bellot and Corrsin (54) in studies of grid generated

turbulence in a wind tunnel. In general, the experimental results of Refs. (37,42-44,54) give support for Eq. (2.16).

The results of Ballal and Lefebvre (55) on grid generated turbulence in a combustion chamber, are also shown in Fig. 2.10. They indicate both a large scatter and also higher values of L_y/λ_y than have been obtained previously. In the calculations of the length scale, L_y, these authors have used an erroneous expression, top equation on p. 221 in Ref. (55), in which u'^2 is missing from the denominator. In discussions with the present author and Dr. D. Bradley, Dr. Ballal (56) suggested that the printed values in Ref. (55) are $L_y/2$ and not L_y, due to a mistake in a computer programme. Accordingly, in the calculation of data for Fig. 2.10 from that of Ref. (55) values of L_y were taken to be twice those given in the reference.

The present author has no explanation for the discrepancy between these results and those of other workers but would opine that Eq. (2.16) is reasonably valid in view of its closeness to the measurements of the other workers on a variety of rigs.

It is easily shown from this equation that the two turbulent Reynolds numbers are related by

$$R_{\lambda y} = 6.5\, R_{Ly}^{0.5} \qquad \text{for } 10 < R_{\lambda y} < 350 \qquad (2.18)$$

Also it is easily shown from this equation and

Eq. (2.7) that R_{Ly} and Re, at the axis of pipes, are related by

$$R_{Ly} = 1.67 \times 10^{-6} (Re)^{1.57} \qquad (2.19)$$

for $4\times10^4 < Re < 7\times10^5$

2.5 THE RELATIONSHIP BETWEEN ε/ν AND R_L FOR ISOTROPIC TURBULENCE

In the light of the good agreement, revealed in Fig. 2.1, between Eq. (2.4) and the experimental points for all three transfer processes, this equation was combined with Eq. (2.19) to yield the following relationship between turbulent transport number and turbulent Reynolds number:

$$\frac{\varepsilon_y}{\nu} = 11 \; R_{Ly}^{0.56} \qquad \text{for } R_{Ly} > 100 \qquad (2.20)$$

Insufficient data are available to establish comparable relationships for the other orthogonal directions.

Equation (2.20) was applied to the parallel plate channel flow, using the only available measured point from the data of Ref. (46), in the range of $R_{Ly} > 100$. The value of R_{Ly} obtained in this way is plotted in Fig. 2.8. This also shows a good agreement with the directly measured values of R_{Ly} made by Laufer (44) and is an indication that Eq. (2.20) is independent of the flow system.

In the computational methods developed by Spalding and coworkers for turbulent flow an effective viscosity, μ_{eff} is employed (1). The value of this is related to turbulent parameters through the use of a function, C_μ. With ρ as the density of the fluid, the value of μ_{eff}, which is equal to $\rho\varepsilon$, is given by

$$\rho\varepsilon = \mu_{eff} = \rho\, k^{\frac{1}{2}}\, L\, C_\mu \tag{2.21}$$

in which, k, the turbulent kinetic energy is given by the sum of the three components of energy:

$$k = \frac{1}{2}\,(u'^2 + v'^2 + w'^2) \tag{2.22}$$

A consideration of these relationships for isotropic turbulence and the "y" direction gives

$$C_{\mu y} = 1.5^{-0.5}\,\frac{\varepsilon_y}{\nu}\,R_{Ly}^{-1} \tag{2.23}$$

and from Eqs. (2.20) and (2.23)

$$C_{\mu y} = 9.06\,R_{Ly}^{-0.44} > 100 \tag{2.24}$$

2.6 CONCLUSIONS

(1) A survey of experimental results shows a similar correlation between ε_y/ν and Re at the axis of pipes and parallel plate channel, for mass, energy and momentum transfer. This is given by Eq. (2.4) for pipe flow and Eq. (2.8) for parallel plate channel flow.

(2) A survey of turbulence measurements at the axis shows the r.m.s. turbulent velocity to be related to centre line velocity by Eq. (2.9) for pipe flow and Eq. (2.11) for parallel plate channel flow. The Taylor microscale is related to the diameter by Eq. (2.10) for pipe flow and related to the channel width by Eq. (2.12) for parallel plate channel flow.

(3) For isotropic turbulence a new relationship is proposed between L_y and λ_y. This is given by Eq. (2.16).

(4) It is proposed that for isotropic turbulence, the turbulent transport number and turbulent Reynolds number are related by

$$\frac{\varepsilon_y}{\nu} = 11 \quad R_{Ly}^{0.56} \quad \text{for} \quad R_{Ly} > 100$$

TABLE 2.1 Pipe Flow Techniques for Experimental Determination of ε_y/ν.

(MA) indicates mass, (MO) momentum, and (E) energy transport.

Reference No.	Technique
10 (MA)	CO_2 and H_2 diffused into air flow.
11 (MA)	Water soluble dye injected into water.
12 (MA)	Water soluble dye injected into water.
13 (MA)	Natural gas injected from pipe along pipe axis.
14-16 (MA)	Central pipe supply of CO_2 and H_2, diffusing into air. KCl solution diffusing through water.
17 (MA)	Small central point source injected N_2O into air.
17 (MO)	Velocity profiles by pitot tube.
18 (MA)	Helium diffused into air flow in large pipe.
19 (MA)	NaCl solution diffused from point source into water flow.
20, 21 (MO)	Measurement of pressure gradient and velocity distribution in air.
22, 23 (E)	Temperature distribution in preheated water measured with thermistors.
24 (E)	Central line source of heat, of varying size, in air. Radial temperatures measured with thermocouples.
25 (E)	Temperature distribution of air.

TABLE 2.2 Parallel Plate Channel Flow Techniques for Experimental Determination of ε_y/ν.

Same notations as Table 2.1.

Reference No.	Technique
20 (MO)	Measurement of pressure gradient and velocity distribution in air.
46 (MA)	Water vaporisation from wall. Air, CO_2, and helium also used.
47 (E)	Temperatures of the upper and lower surfaces of channel maintained at constant, but different, values. Temperature distribution of air stream ascertained from resistance of a short length of platinum wire.
48 (E)	Upper plate maintained at a higher temperature than lower one. Measurement of temperature distribution in air.

2.7 NOMENCLATURE

A	numerical constant, (see Eq. (2.14)
C_μ	a function for determining μ_{eff}, (see Eq. (2.21))
d	pipe diameter
k	turbulent kinetic energy
K_v	von Kármán constant
L	Eulerian macroscale of turbulence
Re	pipe flow Reynolds number
R_L	turbulent Reynolds number based on macroscale, L
t	time
R_λ	turbulent Reynolds number based on microscale, λ
u	fluctuating axial velocity
u'	r.m.s. turbulent axial velocity
U	mean velocity component in axial direction
v	fluctuating radial velocity
v'	r.m.s. turbulent radial velocity
w'	r.m.s. turbulent velocity in third orthogonal direction
y	radial coordinate
y_o	channel width
ε	turbulent diffusivity
λ	Eulerian Taylor microscale of turbulence
μ_{eff}	effective viscosity
ν	kinematic viscosity
ρ	density
ε/ν	turbulent transport number

Subscripts

p	parallel plates channel flow
x	axial direction
y	radial direction

2.8 REFERENCES

1. A.D. GOSMAN, W.M. PUN, A.K. RUNCHALL, D.B. SPALDING and M. WOLFSHTEIN, Heat and Mass transfer in recirculating flows, Academic Press, London and New York (1969).

2. B.E. LAUNDER and D.B. SPALDING, Lectures in mathematical models of turbulence, Academic Press, London and New York (1972).

3. G.E. ANDREWS, D. BRADLEY and S.B. LWAKABAMBA, Turbulence and turbulent flame propagation - a critical appraisal, Combustion and Flame 24, 285 (1975).

4. G.E. ANDREWS, D. BRADLEY and S.B. LWAKABAMBA, Measurement of turbulent burning velocity for large turbulent Reynolds numbers, Fifteenth Symposium (International) on Combustion, p. 655, Pittsburgh: The Combustion Institute (1975).

5. F.C. GOULDIN, Statistical model for premixed turbulent flames, paper presented at the Central States Section and Western States Section , The Combustion Institute, Joint Meeting, San Antonio, Texas (1975).

6. H.L. DRYDEN, Turbulence and diffusion, Ind. Engng Chem. 31, 416 (1939).

7. J. LAUFER, The structure of turbulence in fully developed pipe flow, NACA, Report 1174 (1954).

8. H.W. TOWNES, J.L. GOW, R.E. POWE and N. WEBER, Turbulent flow in smooth and rough pipes, Trans. Am. Soc. Mech. Engrs 94, 353 (1972). (Series D, Journal of Basic Engineering.)

9. J.T. DAVIES, Turbulence phenomena - An introduction to the eddy transfer of momentum, mass, and heat, particularly at interfaces, p. 10, Academic Press, New York and London (1972).

10. W.L. TOWLE and T.K. SHERWOOD, Eddy diffusion - Mass transfer in the central portion of a turbulent air stream, Ind. Engng Chem. 31, 457 (1939).

11. G.V. EVANS, A study of diffusion in turbulent pipe flow, Trans. Am. Soc. Mech. Engrs 89, 624 (1967). (Series D, Journal of Basic Engineering.)

12. J.P. MALENGE and J. GOSSE, Étude expérimentale de la diffusion de matière par turbulence dans les conduits, Génie chem. 94 (1965).

13. W.G. SCHLINGER and B.H. SAGE, Material transfer in turbulent gas streams - concentric flow, Ind. Engng Chem. 45, 657 (1953).

14. D.L. FLINT, H. KADA and T.J. HANRATTY, Point source turbulent diffusion in a pipe, A.I.Ch. E. Jl. 6, 325 (1960).

15. H. KADA, Diffusion from a source of mass for turbulent flow of water and of slurries in a pipe, Ph.D. thesis, Uni. Ill., Urbana (1959).

16. H. KADA, M.Sc. thesis, Univ. Ill., Urbana, Oct. 1957.

17. A. QUARMBY and R.K. ANAND, Axisymmetric turbulent mass transfer in a circular tube, J. Fluid Mech. 38, 433 (1969).

18. W.R. MICKELSEN, An experimental comparison of Lagrangian and Eulerian correlation coefficients in homogeneous isotropic turbulence, NACA TN 3570 (1955).

19. H.C. GROENHOF, Eddy diffusion in the central region of turbulent flows in pipes and between parallel plates, Chem. Engng Sci. 25, 1005 (1970).

20. F. PAGE, W.G. SCHLINGER, D.K. BREAUX and B.H. SAGE, Point values of eddy conductivity and viscosity in uniform flow between parallel plates, Ind. Engng Chem. 44, 424 (1952).

21. W.H. CORCORAN, F. PAGE, W.G. SCHLINGER and B.H. SAGE, Temperature gradients in turbulent gas streams - Methods and apparatus for flow between parallel plates, ibid. 44, 410 (1952).

22. B.J. BRINKWORTH and P.C. SMITH, Radial distribution of diffusivity in the core of turbulent pipe flow, Chem. Engng Sci. 28, 1847 (1973).

23. B.J. BRINKWORTH and P.C. SMITH, Velocity distribution in the core of turbulent pipe flow, ibid. 24, 787 (1969).

24. L.V. BALDWIN and T.J. WALSH, Turbulent diffusion in the core of fully developed pipe flow, A.I.Ch.E.Jl. 7, 53 (1961).

25. C.A. SLEICHER, Experimental velocity and temperature profiles for air in turbulent pipe flow, Trans. Am. Soc. Mech. Engrs 80, 693 (1958).

26. H. REICHARDT, Vollständige darstellung der turbulenten geschwindigkeitsverteilung in glatten leitungen, Z. angew. Math. Mech. 31, 208 (1951).

27. J.R. TRAVIS, H.O. BUHR and A. SESONSKE, Model for velocity and eddy diffusivity distributions in fully turbulent pipe flow, Canadian Jl. of Chem. Engng 49, 14 (1971).

28. R.E. POWE, H.W. TOWNES and J.L. GOW, Mean velocity profiles for turbulent shear flow, Journal of Hydronautics 6, 60 (1972).

29. W.M. KAYS, Convective heat and mass transfer, p. 71, McGraw-Hill, New York (1966).

30. P.A. LONGWELL, Mechanics of Fluid Flow, p. 325, ibid.

31. J.L. GOW, Fully-developed turbulent flow in smooth and rough-walled pipe, M.Sc. thesis, Mech. Engng Dept., Montana State Univ., Bozeman, Mont. (1969).

32. R.E. POWE, Turbulence structure in smooth and rough pipes, Ph.D. thesis, Aerospace and Mech. Engng Dept., Montana State Univ., Bozeman, Mont. (1970).

33. H. SCHLICHTING, Boundary layer theory, chaps. 19-20, McGraw-Hill; New York (1968).

34. T. VON KÁRMÁN and L. HOWARTH, On the statistical theory of isotropic turbulence, Proc. R. Soc. 164A, 192 (1938).

35. J.O. HINZE, Turbulence, McGraw-Hill, New York (1959). In order of appearance in text, p. 172, p. 153, p. 185.

36. R.S. BRODKEY, The phenomena of fluid motions, p. 272, Addison-Wesley Publishing Company (1967).

37. R.E. POWE and H.W. TOWNES, Turbulence structure for fully developed flow in rough pipes, Trans. Am. Soc. Mech. Engrs 95, 255 (1973). (Series I, Journal of Fluid Engineering.)

38. C.J. LAWN, The determination of the rate of dissipation in turbulent pipe flow, J. Fluid Mech. 48, 477 (1971).

39. J.M. ROBERTSON, J.H. BURKHART and J.D. MARTIN, Study of turbulent flow in rough pipes, University of Ill., Theoretical and Applied Mechanics Rep. No. 279, Urbana (1965).

40. E.R. PIKE, D.A. JACKSON, P.J. BOURKE and D.I. PAGE, Measurement of turbulent velocities from the doppler shift in scattered laser light, Journal of Physics E1, 727 (1968).

41. H.C. DRYDEN, A review of the statistical theory of turbulence, Q. App. Maths. 1, 7 (1943).

42. M.S. UBEROI and S. CORRSIN, Diffusion of heat from a line source in isotropic turbulence, NACA Rep. 1142 (1953).

43. R.S. McQUIVEY and E.V. RICHARDSON, Some turbulence measurements in open-channel flow, Journal of the Hydraulics Div. 95, 209 (1969).

44. J. LAUFER, Investigation of turbulent flow in a two-dimensional channel, NACA Rep. 1053 (1951). (Supersedes NACA TN 2123, 1950.)

45. A. QUARMBY and R. QUIRK, Measurements of the radial and tangential eddy diffusivities of heat and mass in turbulent flow in a plain tube, Int. J. Heat Mass Transfer 15, 2309 (1972).

46. T.K. SHERWOOD and B.B. WOERTZ, Mass transfer between phases - role of eddy diffusion, Ind. Engng Chem. 31, 1034 (1939).

47. F. PAGE, W.H. CORCORAN, W.G. SCHLINGER and B.H. SAGE, Temperature and velocity distributions in uniform flow between parallel plates, Ind. Engng Chem. 44, 419 (1952).

48. E. VENEZIAN and B.H. SAGE, Temperature gradients in turbulent gas streams: Effect of viscous dissipation on evaluation of total conductivity, A.I.Ch.E. Journal 7, 688 (1961).

49. J.A. CLARK, A study of incompressible turbulent boundary layers in channel flow, Trans. Am. Soc. Mech. Engrs 90, 455 (1968). (Series D, Journal of Basic Engineering.)

50. A.K.M.F. HUSSAIN and W.C. REYNOLDS, The mechanics of a perturbation wave in turbulent shear flow, FM-6, Mechanical Engineering Dept., Stanford University, May 1970.

51. A.K.M.F. HUSSAIN and W.C. REYNOLDS, Measurements in fully developed turbulent channel flow, Trans. Am. Soc. Mech. Engrs 97, 568 (1975). (Series I, Journal of Fluids Engineering.)

52. M. ACHARYA and W.C. REYNOLDS, Measurements and prediction of a fully developed turbulent channel flow with imposed controlled oscillations, TF-8, Mechanical Engineering Dept., Stanford University, May 1975.

53. N. GAT, Private Communication, 2nd May 1977.

54. G. COMTE-BELLOT and S. CORRSIN, Simple Eulerian time correlation of full- and narrow-band velocity signals in grid-generated 'isotropic' turbulence, J. Fluid Mech. 48, 273 (1971).

55. D.R. BALLAL and A.H. LEFEBVRE, The structure and propagation of turbulent flames, Proc. Roy. Soc. 344A, 217 (1975).

56. D.R. BALLAL, Private Communication, 13th February 1976.

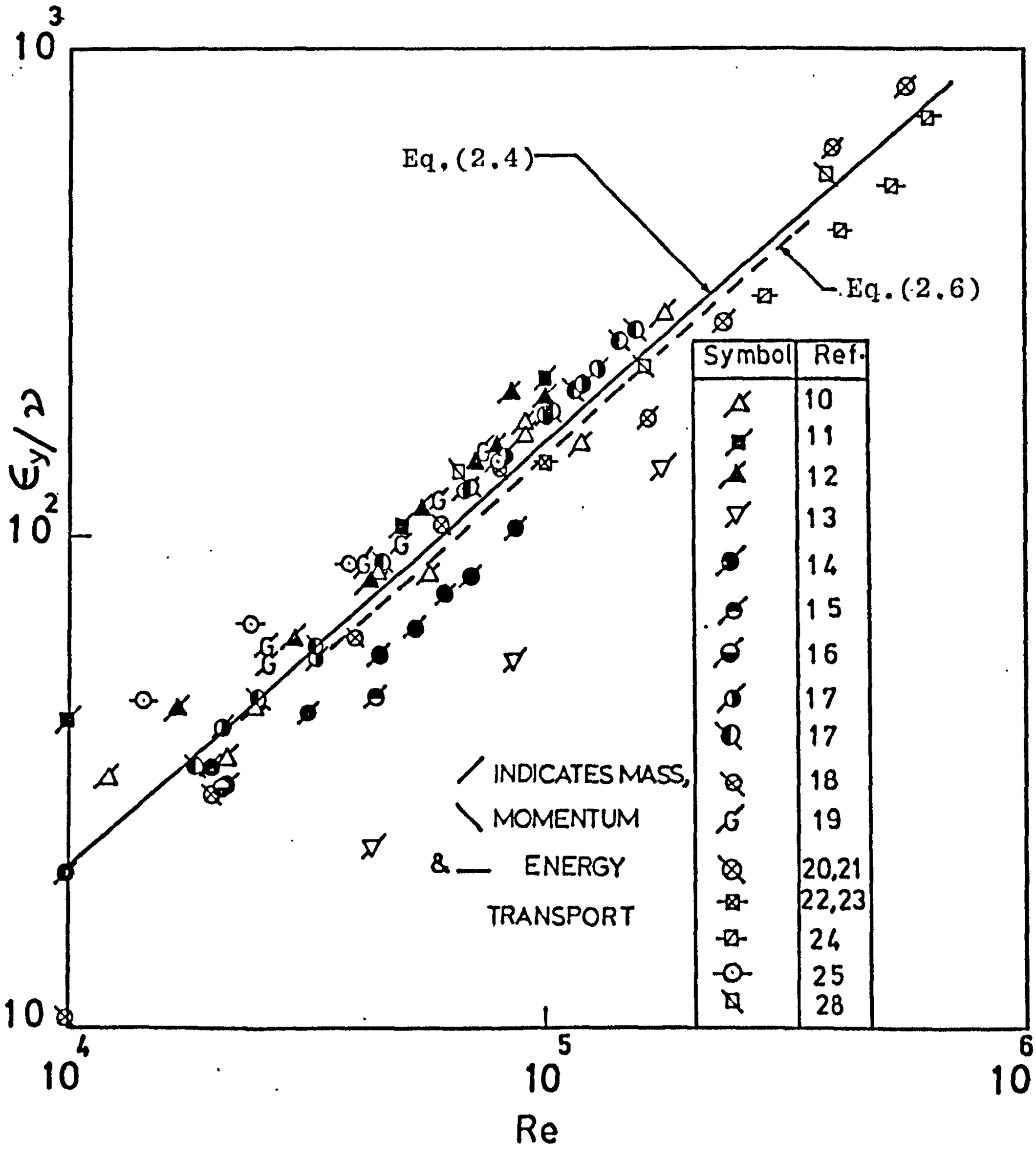

FIG.2.1 VARIATION OF RADIAL TURBULENT TRANSPORT NUMBER AT AXIS WITH PIPE FLOW REYNOLDS NUMBER

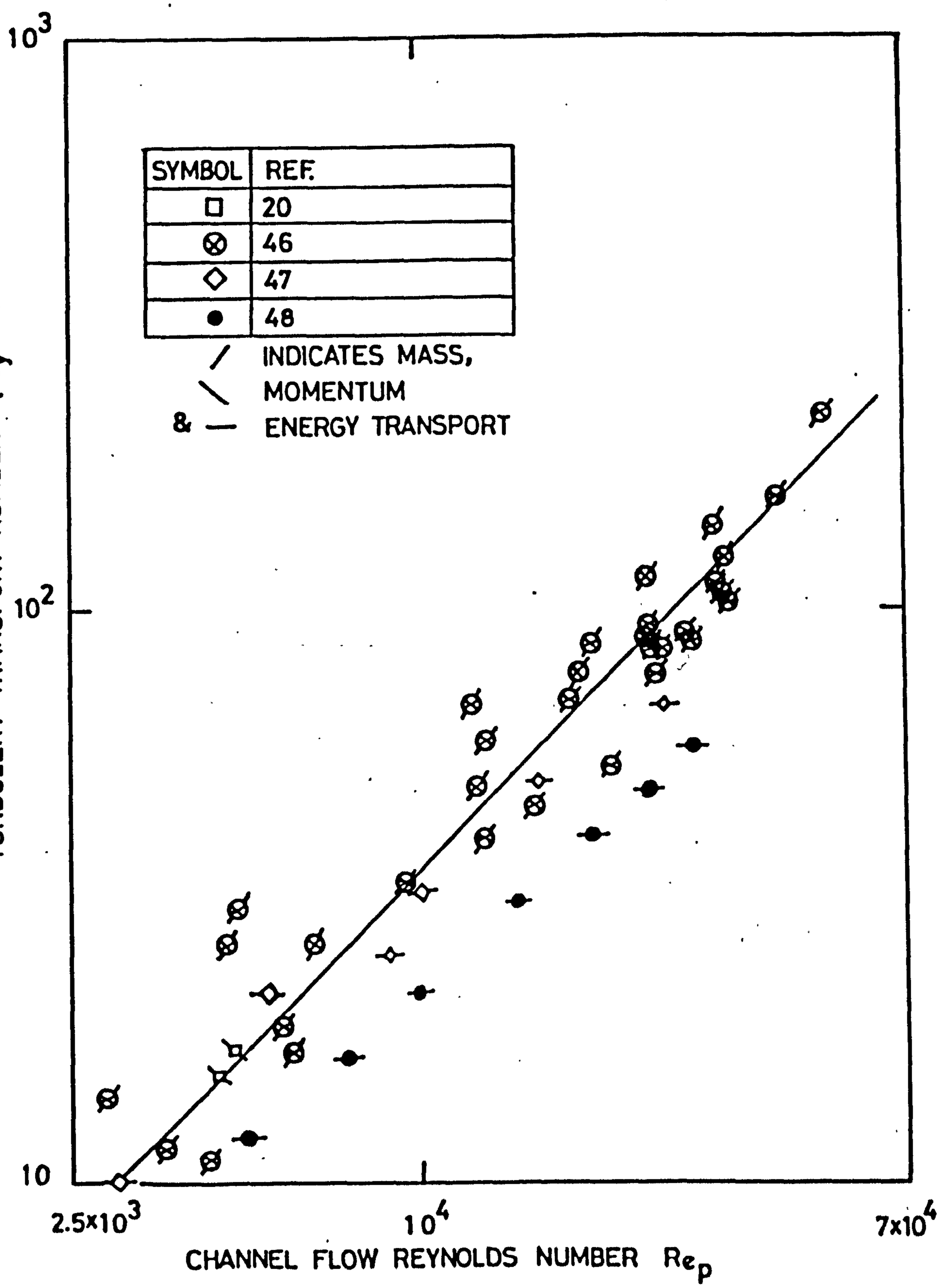

FIG.2.2 VARIATION OF RADIAL TURBULENT TRANSPORT NUMBER AT AXIS WITH CHANNEL FLOW REYNOLDS NUMBER

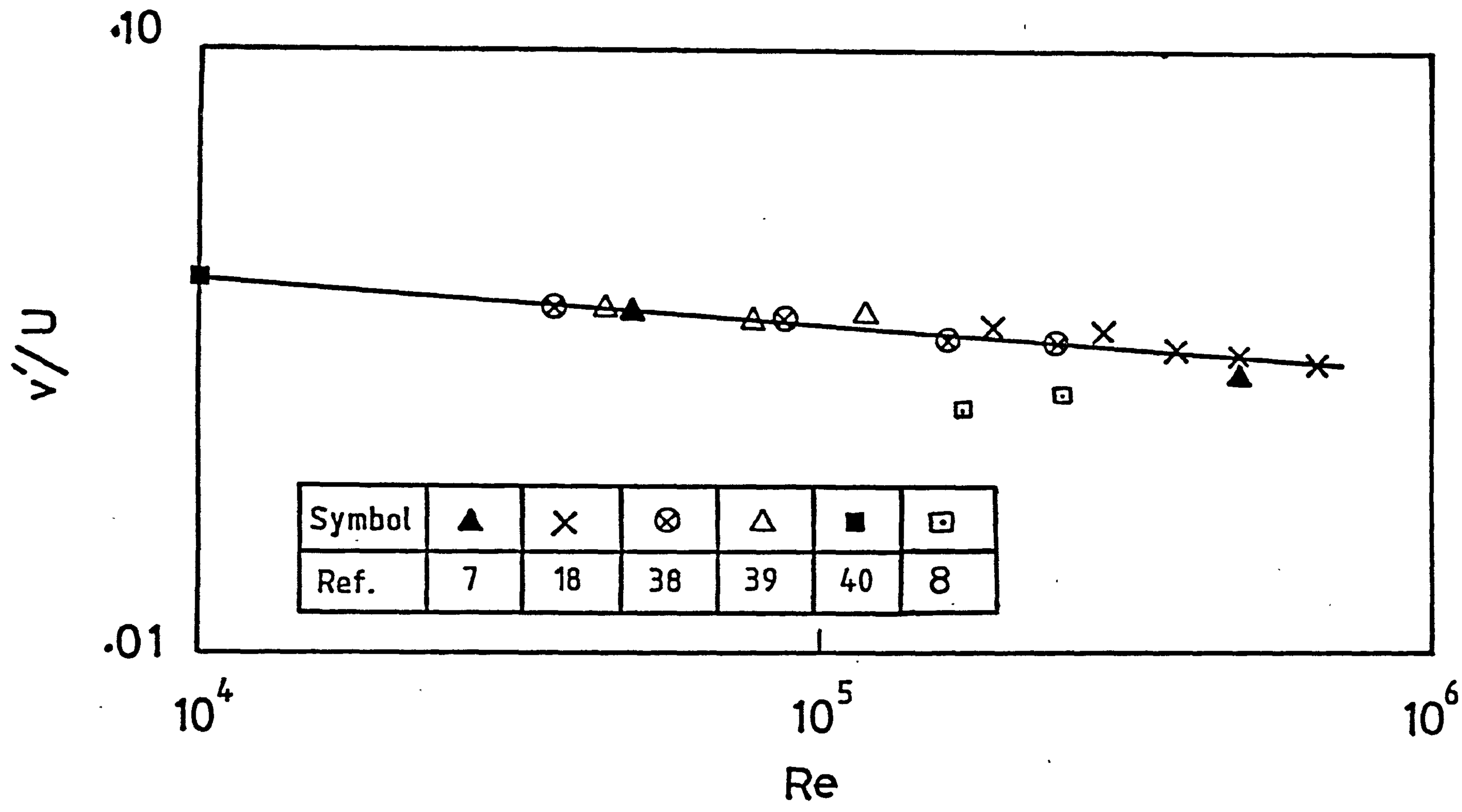

FIG.2.3 VARIATION OF RADIAL R.M.S. TURBULENT VELOCITY AT AXIS WITH PIPE FLOW REYNOLDS NUMBER

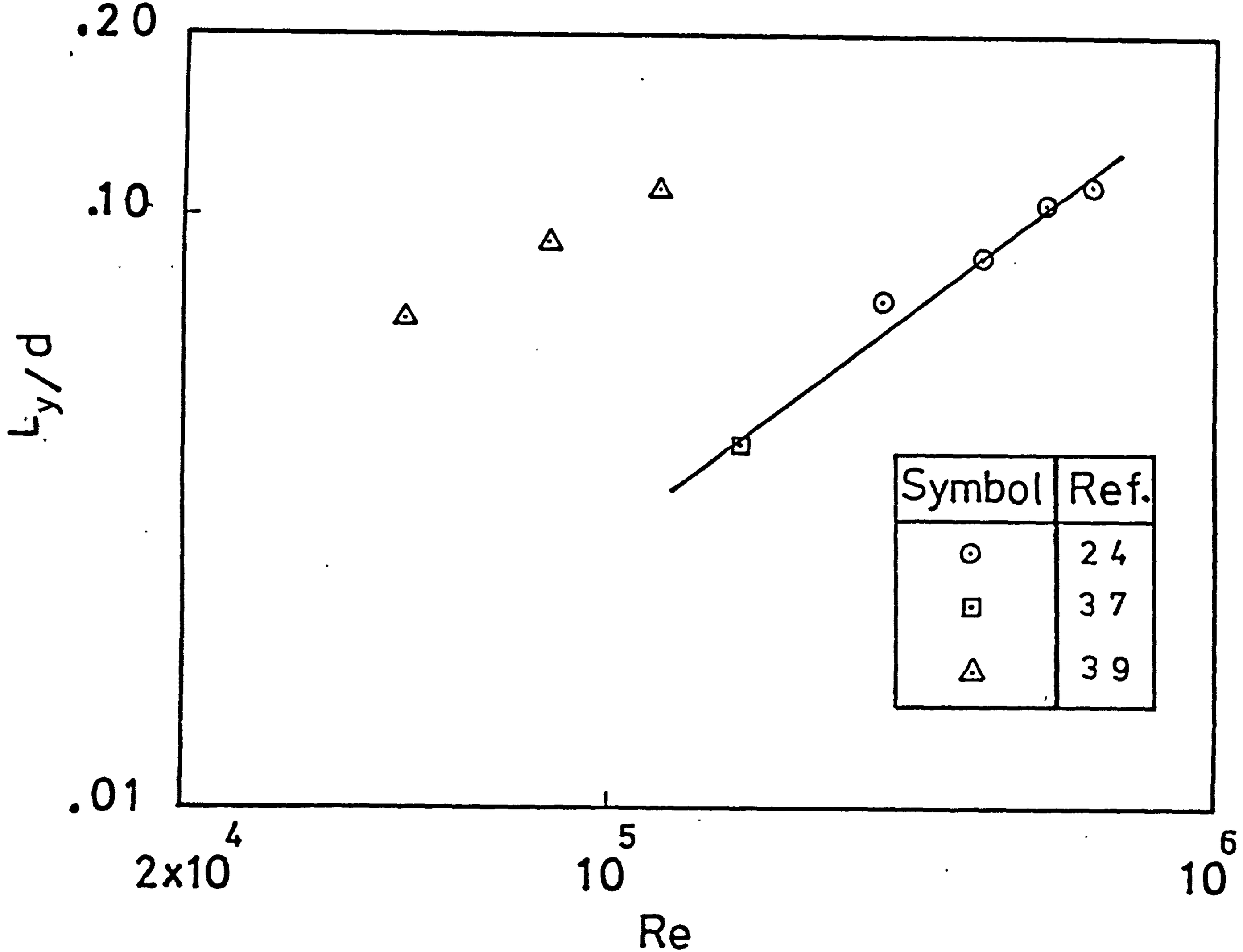

FIG.2.4 VARIATION OF RADIAL MICROSCALE AT AXIS WITH PIPE FLOW REYNOLDS NUMBER

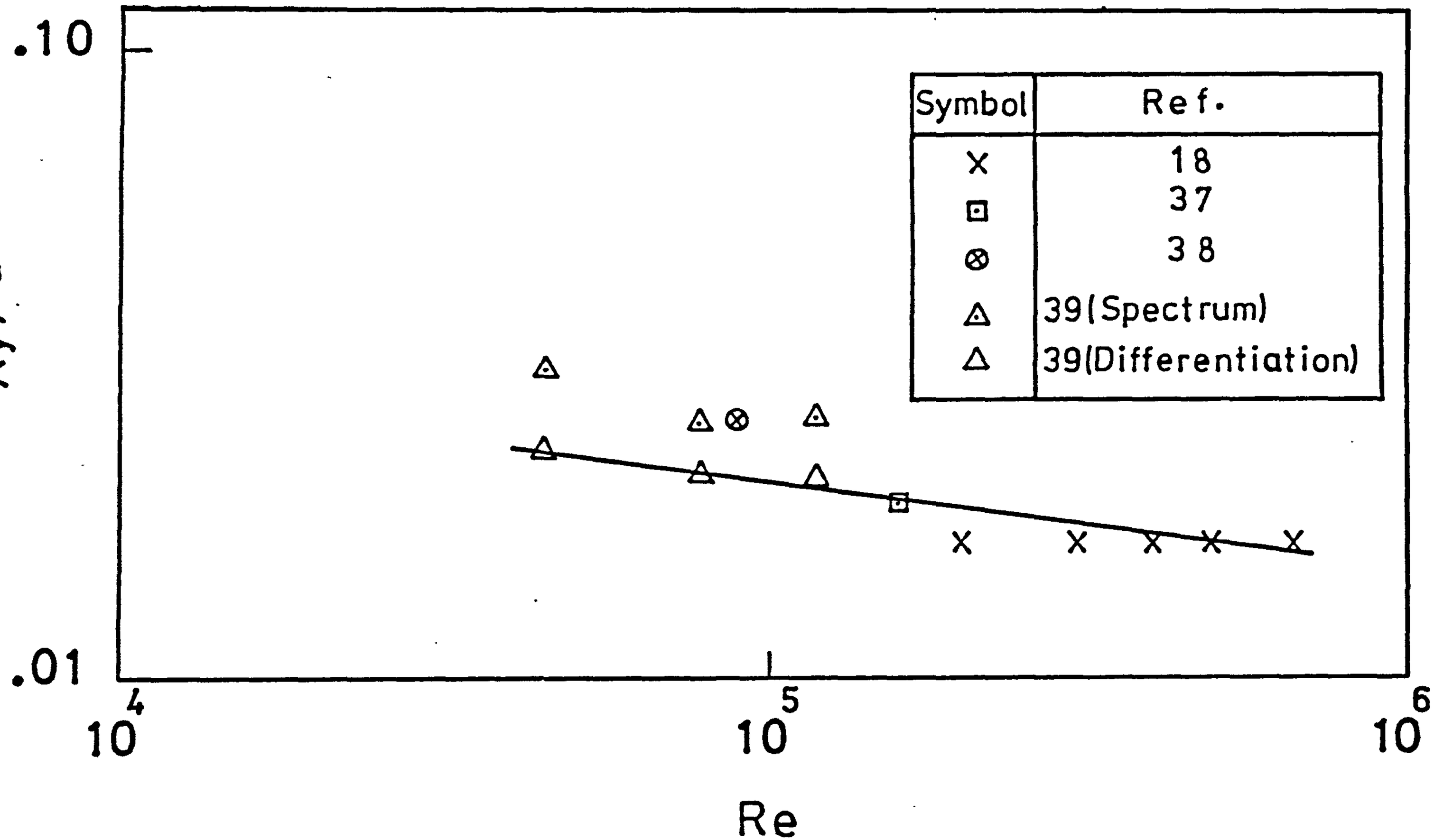

FIG.2.5 VARIATION OF RADIAL MICROSCALE AT AXIS WITH PIPE FLOW REYNOLDS NUMBER

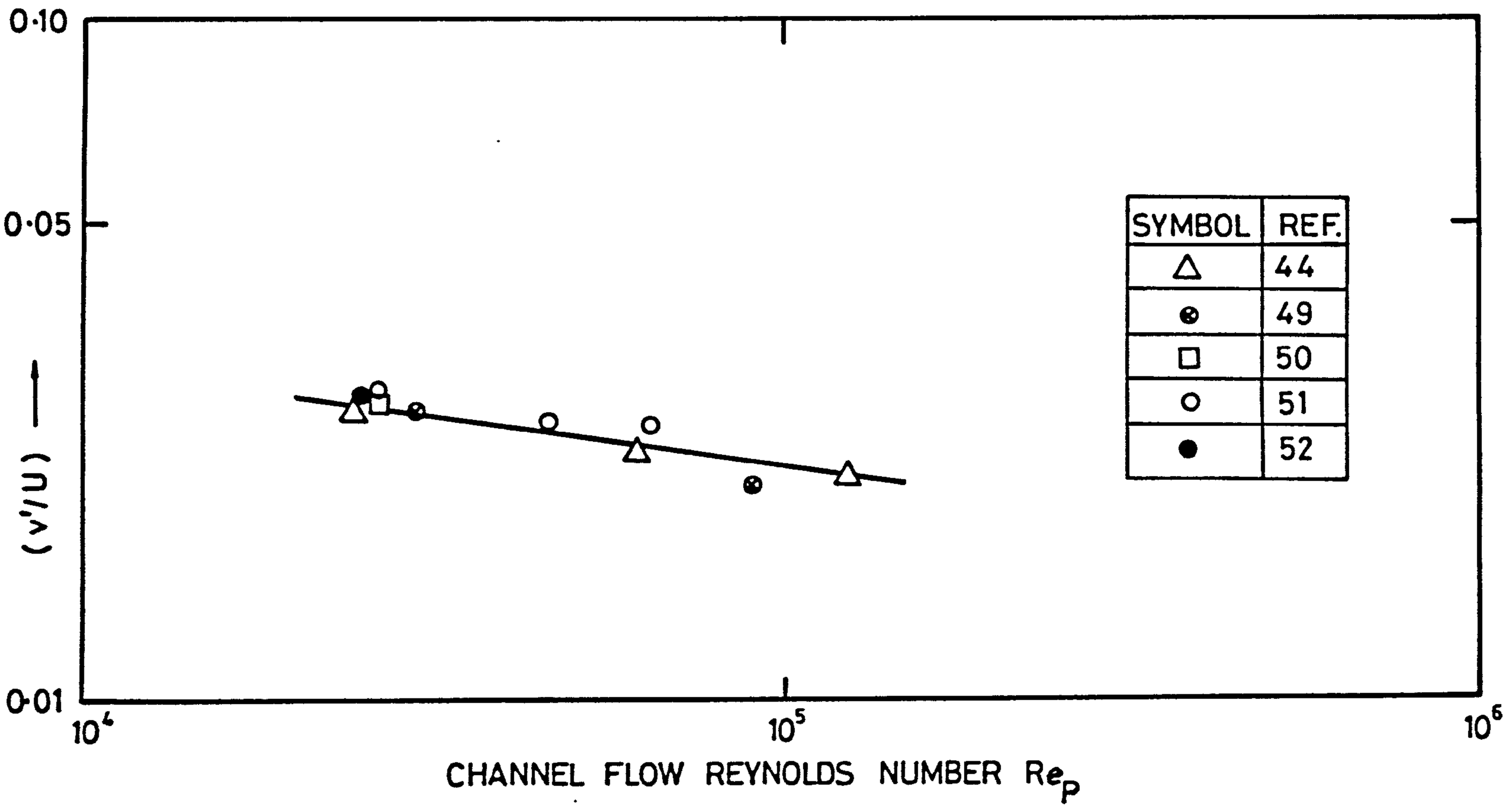

FIG.2.6 VARIATION OF RADIAL R.M.S. TURBULENT VELOCITY AT AXIS WITH CHANNEL FLOW REYNOLDS NUMBER

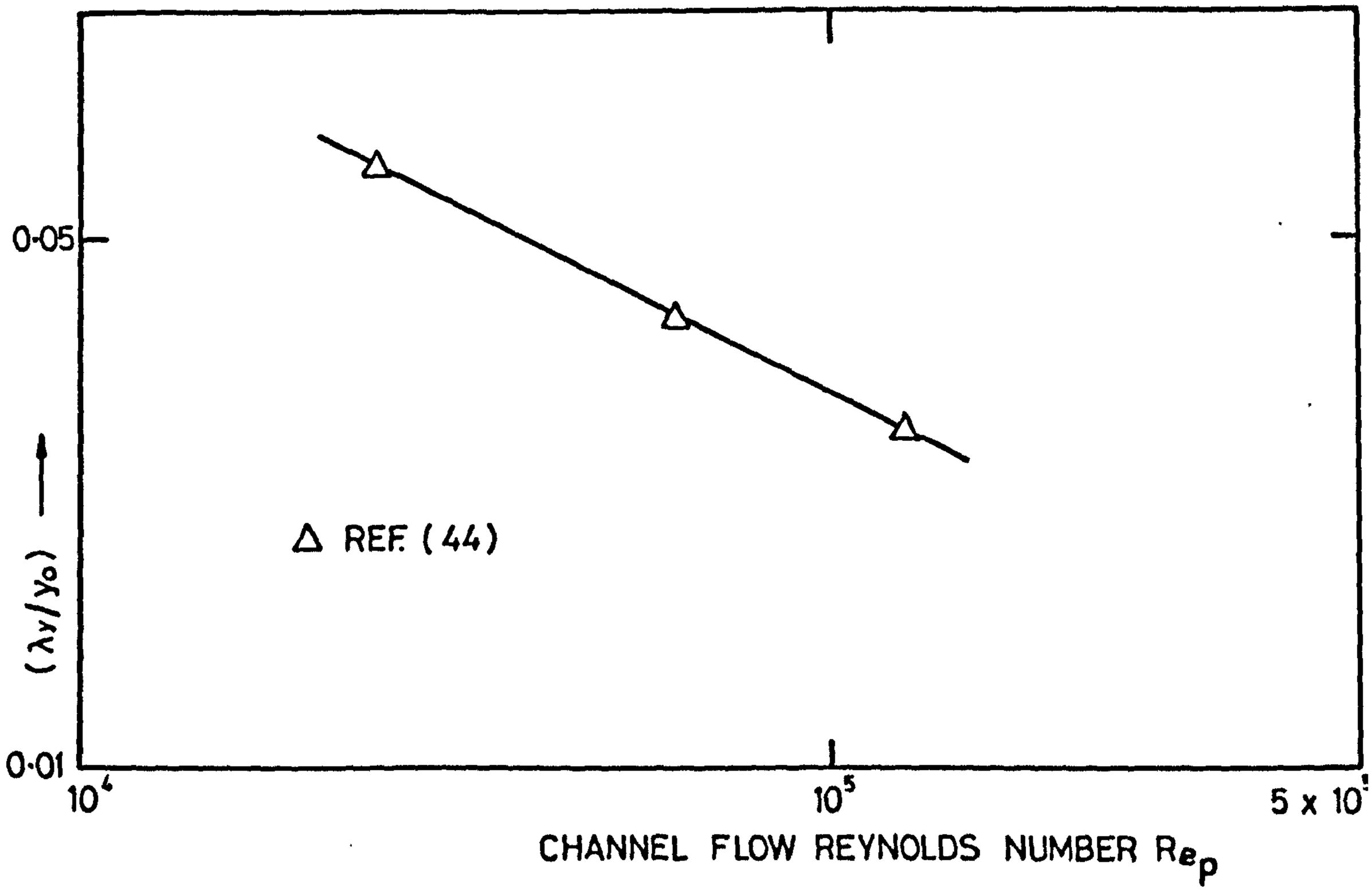

FIG. 2.7 VARIATION OF RADIAL MICROSCALE AT AXIS WITH CHANNEL FLOW REYNOLDS NUMBER

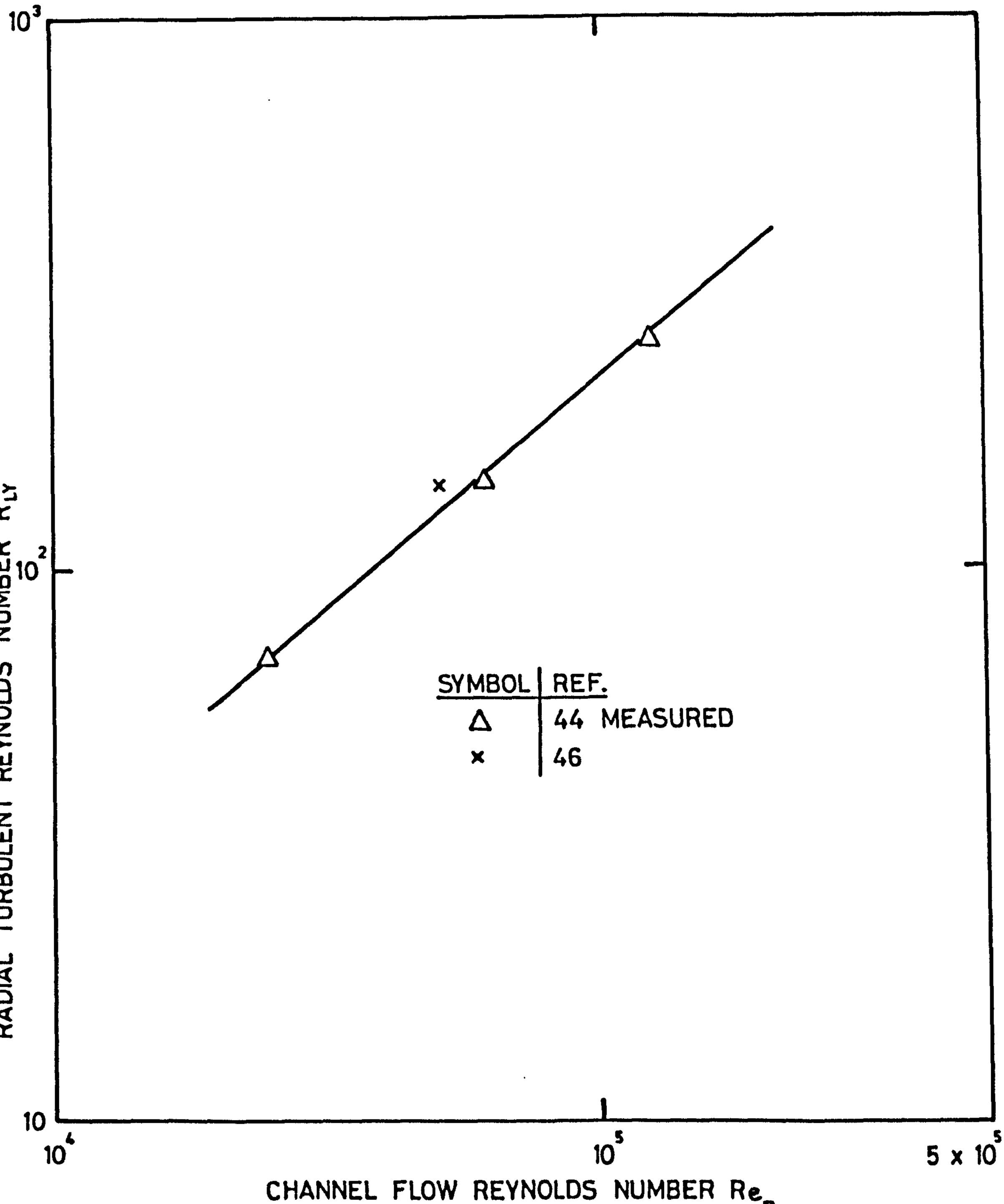

FIG. 2.8 VARIATION OF RADIAL TURBULENT REYNOLDS NUMBER R_{LY} AT AXIS WITH CHANNEL FLOW REYNOLDS NUMBER

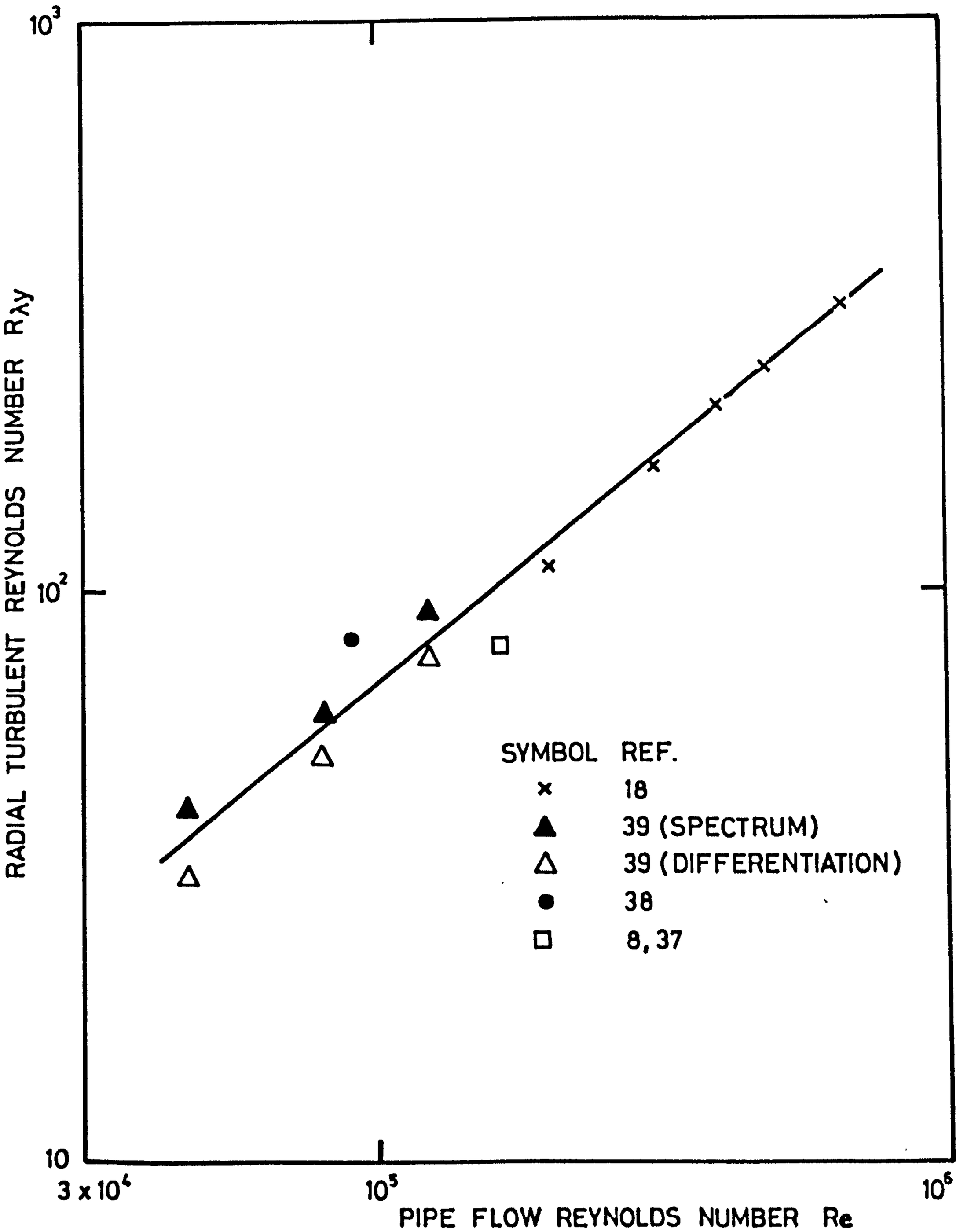

FIG. 2.9 VARIATION OF RADIAL TURBULENT REYNOLDS NUMBER $R_{\lambda y}$ AT AXIS WITH PIPE FLOW REYNOLDS NUMBER

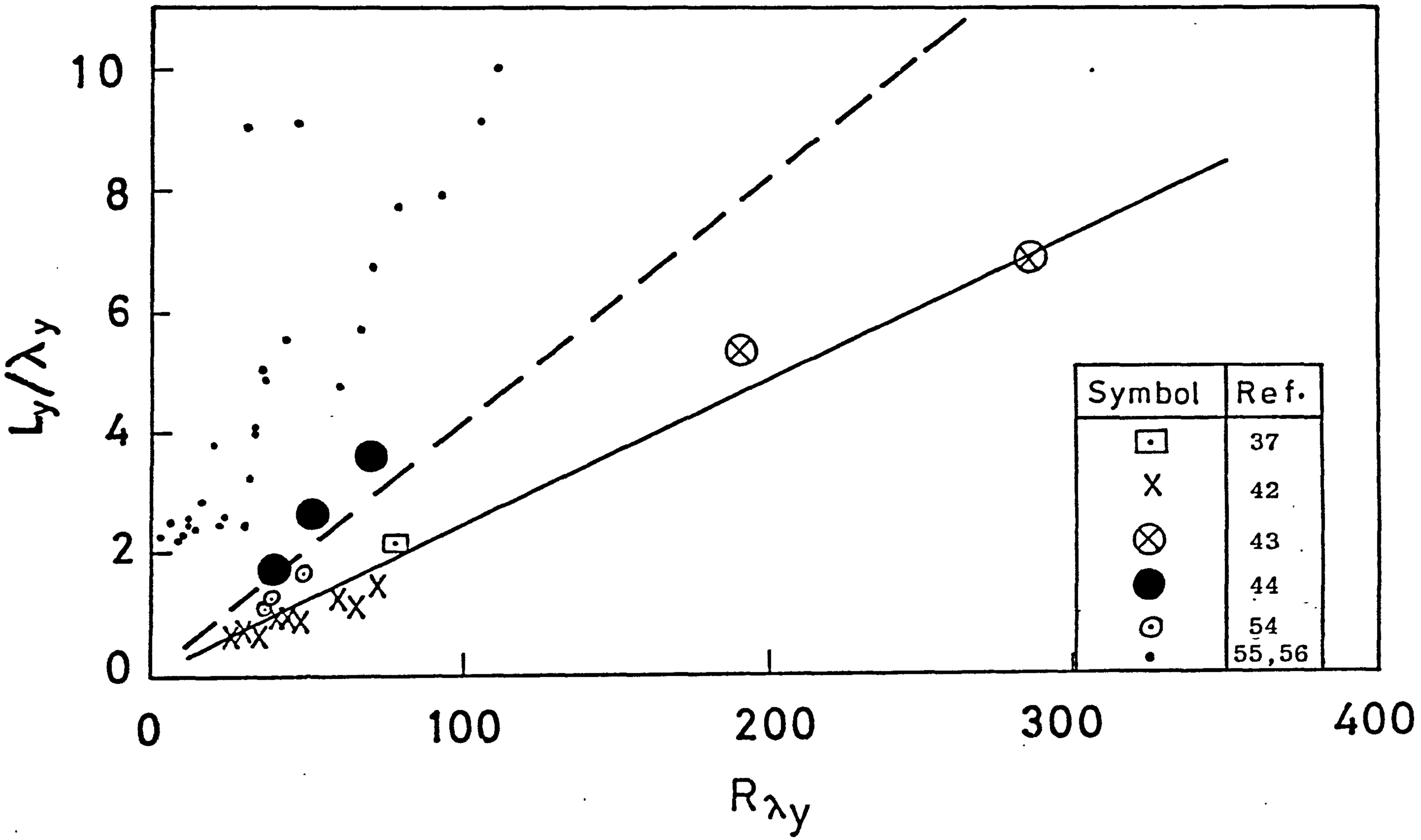

FIG.2.10 INTERRELATIONSHIP OF L_y/λ_y AND $R_{\lambda y}$ FOR DIFFERENT FLOW SYSTEMS

CHAPTER 3

APPARATUS AND EXPERIMENTAL TECHNIQUES

CHAPTER 3

APPARATUS AND EXPERIMENTAL TECHNIQUES

3.1 INTRODUCTION

In this Chapter, the basic apparatus and techniques used throughout the investigations are described. Only brief descriptions are given in those instances where comprehensive details are available elsewhere (1,2).

3.2 EXPLOSION VESSEL AND FANS

The vessel has been described in detail by Hundy (1) and Andrews (2). It consisted of a cast-steel 305 mm diameter cylindrical explosion vessel, 305 mm long and with 150 mm diameter windows in each end. These windows were fitted with schlieren quality glasses, 25.4 mm thick. They were concentric with the end plates, in order to study the whole flame during its pre-pressure period. A view of the vessel is shown in Fig. 3.1.

Four identical eight bladed fans were symmetrically positioned at 90^{o} intervals around the central circumference and at 45^{o} to the horizontal. Andrews (2) designed

the eight blade fans which were machined from a solid block of aluminium. Each blade was inclined at an angle of 30^{o} to the axis and was 50 mm wide, with inner and outer edges radiused to 90 mm and 140 mm respectively. The mean diameter of each fan was 147 mm and when they were all mounted in position they gave a central experimental region of 178 mm diameter.

Each fan originally was designed to be driven separately by a GAT IAM 1/8 horsepower air turbine with valves for independent speed control of each turbine, by means of a pressure regulator and flow controller. The air supply was from the departmental mains and, for higher fan speeds, air at higher pressures was drawn on a blow down system from large tanks in the laboratory. The fan speed was measured with a magnetic transducer and six symmetrical slots in the fan shaft. With this system the minimum stable speed of the fan was 500 r.p.m., whilst the maximum speed was 5,000 r.p.m. for very short periods or 4,000 for more sustained running.

Hydrogen and methane at low pressure were chosen for some of the experimental work for the reasons given in Chapters 1 and 4 respectively. The use of hydrogen and low pressure methane mixtures necessitated improved shaft sealing, in the form of Leybold Rotary Transmission units, type F65K. These comprise a combined vacuum sealing disc and ball bearing housing. The improved sealing necessitated a higher power to drive the fans, because of the increased

resisting torque of the seal. The original air turbines therefore were replaced by one horsepower d.c. motors (3), the speed of each of which could be independently and accurately adjusted via a four channel speed control unit supplied by Acel Systems Limited. The electric motors and fans were mounted to the vessel as illustrated in Fig. 3.2.

The control system comprised four independent motor speed control units, utilising thyristor control of the armature current and mounted within a wall mounted control cabinet. On the front panel of the cabinet were independent stop/start controls for each fan, together with a "mains on" and "motor running" lamps and four speed control potentiometers. The feedback control voltage was drawn from the armature back e.m.f.

In an explosion, increased pressure at the outside, remote circumferential face of the seal resulted in the seal being pressed tightly on to the shaft and this created excessive resisting torque. This was ameliorated by venting the remote side of the seal to atmosphere via a plastic tube.

The speed control range for these motors was between 200 and 10,000 r.p.m., but because of the resisting torque of the seals the maximum possible speed of an installed fan was 4,000 r.p.m. This could only be maintained for short periods and a speed of 3,500 r.p.m. was the maximum possible for sufficiently long periods. It would

be possible to achieve higher fan speeds by removing the seals.

The arrangement of the four fans within the vessel is shown in Fig. 3.3. The fans do not encroach into the central volume of the vessel, which spatially is equivalent to the constant pressure period of the explosion, within which the experimental measurements were made. The space between adjacent fans allows the insertion of spark plugs, tulip, hot wire anemometers and ionisation probes.

3.2.1 Ancillary Equipment

3.2.1.1 Storage Tank

A large pressure tank, of approximately 10 cu ft capacity, was used for the storage of gaseous mixtures. It was fitted with a multiway filling cork. This was connected to the calibration rig as described in Section 3.2.1.5 , and the mixtures made in the tank were easily withdrawn into it.

3.2.1.2 Spark Plug and Ignition Circuits

The spark plug body consisted of a mild steel externally threaded tube as the outer earthed conductor. A central steel rod served as the high voltage conductor; this was supported and insulated from the outer tube by a nylon sleeve, and bonded with an epoxy resin to form a gas tight seal. The high voltage electrode was screwed

into the end of the steel rod. The earth electrode consisted of a piece of stiff copper wire fixed to the outer steel tube between two threaded collars. The co-axial geometry was used to minimise electrical interference from the discharge circuit. A gap width of approximately 1.0 mm was used in the measurement of turbulent burning velocities. For the double kernel technique two such spark plugs were used and these were placed 40 mm apart in the central region of the vessel.

Two ignition circuits were used in the course of the experiments. The first circuit, unit (A), was designed to produce two sparks in precise synchronisation. The use of hydrogen mixtures with high burning velocities necessitated improved synchronisation of the two sparks. The two spark gaps were connected in series and were included in the same capacitive discharge circuit. This ensured that the two sparks formed simultaneously, for which a minimum voltage of 8 KV was necessary. The whole of the discharge circuit was enclosed in a shielded metal case, and the leads to the co-axial spark plugs were of co-axial cable to minimise the effects of electrical interference. The discharge system was electrically earthed directly to the mains supply and insulated completely from the explosion vessel, which was earthed separately.

The 0.05 μF capacitor bank was charged to 8KV from a D.C. high voltage generator to give a stored energy of 1.6 Joules. A few turns of copper wire on a 25.4 mm

diameter ebonite former were inserted in the discharge line to increase the inductance of the circuit and hence the duration of the discharge, which has been shown in certain circumstances to facilitate ignition (4,5). When a 300 V pulse was applied to the primary coil of the pulse transformer, the high voltage induced at the secondary terminal caused electrical breakdown at the trigger gap, followed by the simultaneous breakdown of the two spark gaps. This ignition circuit is shown in Fig. 3.4.

The second ignition circuit, unit (B), was a variable energy, variable frequency, ignition unit which produced a spark capable of igniting near-limit mixtures at high levels of turbulence. It was used throughout the investigations of the effects of turbulence upon ignition and propagation limits. The circuit is illustrated in Fig. 3.5. The three capacitors could be connected in several ways to give total capacitances of 1.5, 3, 4.5, and 6 μF, which, when charged to 2,000 volts, stored energies of 3, 6, 9, and 12 J, respectively. One of the four inductors could be connected in series with the capacitors to alter the discharge frequency. However, inductors of 2 and 16 μH were used for stored energies of 12 and 3 J, respectively, in order to keep the spark duration the same. The ignition spark was produced as a result of a discharge at an internal air gap, A, from a third electrode.

3.2.1.3 Pressure Transducer and Charge Amplifier

A Kistler piezo-electric pressure transducer and a Kistler type 568 charge amplifier measured pressures. The transducer, previously used by Lwakabamba (3), was of type 701 H with a working range of 0-600 atmospheres and rise time of 6 μ sec.

3.2.1.4 Hot Wire Probes

The hot wire probes were of the standard DISA type, 55F31 and 55A35. These supported the wires which had been welded to the probes by a spot welding DISA micromanipulator with a binocular microscope. The tungsten wires used in the course of the work were supplied by Johnson Matthey Co Ltd. Their diameter was 5 μm and their aspect ratio, L_w/d, was 234.

All of the hot wires were connected to the DISA 55D01 constant-temperature bridge anemometer by a 5 metre cable and were operated with an overheat ratio of 0.8. For air flow calibrations a DISA type 55D90 calibration unit was employed. This produced a free air jet from an air pressure of 1.2 MNm^{-2} absolute. This was capable of producing the full calibration velocity range of between 0.5 m sec^{-1} and 300 m sec^{-1}. It was possible to obtain a 5:1 velocity range at the touch of a button and a calibration curve could either be recorded automatically on an X-Y recorder, or manually from voltage readings on a DISA 55D30 digital voltmeter. The probes were mounted

so that their axis was parallel to the jet.

The turbulence in the explosion vessel is characterised by the absence of a mean flow velocity. The relationship between voltage and velocity for a constant-temperature anemometer is non linear. If the r.m.s. turbulent velocity, u', is large and if, the mean velocity, U, is small, fluctuations of voltage do not correspond linearly to those of velocity (15). In mean flow systems it is assumed that if u'/U is greater than a few percent reliable quantitative measurements cannot be obtained unless the wire signal is linearised. Obviously, in the present application linearisation of the signal was vital. A DISA 55D10 lineariser was used, with facilities for different velocity exponents. Figure 3.6 shows a typical calibration curve for a wire calibrated with velocity exponents, of 0.435, 0.450, 0.500 and 0.556. No value of exponent gave a perfectly straight calibration line, but with an exponent of 0.5, the recorded signal became almost linear with velocity for values greater than 0.8 m sec^{-1}. Linearity was not possible in the velocity range of less than 0.8 m sec^{-1} due to the influence of natural convection. The effect of non-linearity of the calibration curve is discussed in detail by Beér and Chigier (6). However, the error involved in assuming a linear relationship in the present vessel was small. The concurrent detailed investigations of McMahon (7) have shown it can be neglected, and velocity exponent of 0.5 was used throughout the work reported in the thesis.

The DISA 55D10 lineariser has an output of 0-10 volts for a given calibration velocity range. Alteration of this range easily could be achieved by adjusting the lineariser gain control. Thus the lineariser could also be used as an amplifier. Typical linearised velocity fluctuations in the vessel with the fans running are shown in Fig. 3.7 (a and b). Clearly the fans produce intermittent turbulence. If the lineariser gain was set too high then velocity fluctuations could overshoot the range, cut off, and result in an underestimation of the measured components. This is shown in Fig. 3.7(c). In quantitative determinations of u', the lineariser gain setting and exponent were maintained at the same value for the calibration and the measurements in the vessel.

3.2.1.5 The Tubular Calibration Rig

A 12.7 mm bore copper tube of 800 mm length was adopted for use as a second calibration rig to operate at different pressures with various gas mixtures and for lower velocities than could be measured with the DISA calibration rig. Gas velocities ranged from zero to approximately 5 m sec^{-1} at atmospheric pressure.

This rig was similar to that used by Andrews, Bradley and Hundy (8). The required gas mixture from the storage tank, or air from the atmosphere, was drawn along the tube via a buffer tank of 0.5 m^3 capacity to a vacuum pump. The volumetric flow rate was measured by a positive displacement gas meter of the Baird and Tatlock wet type.

Gas temperatures were always equal to the ambient values.

The gas velocity transverse to the wire was deduced from the known laminar velocity profile in the tube and the volumetric flow rate. For the fully developed profile, the velocity at the centre line is equal to twice the mean flow velocity (9). The variation of gas velocity along a wire of length 1.17 mm, centred on the tube axis, was less than 0.9%. Care always was taken to ensure that the flow was fully developed and that the wire was centred on the tube axis.

In both rigs, the wire was mounted, and adjusted by eye, to be normal to the flow. The wire was positioned at the centre of the tube, by traversing the wire radially until the maximum reading on the DISA 55D30 D.C. digital voltmeter was obtained. A diagram of the calibration flow system is shown in Fig. 3.8. When air was used it was drawn directly through the gas meter from the atmosphere, and regulations of the pressure and flow, rate were made by valves C and D. When gas mixtures were drawn from the storage tank, valve B maintained the pressure in the meter constant at one atmosphere. Readings were taken only when conditions were steady. Appropriate gaseous mixtures were prepared in the storage tank as described in Section 3.2.1.1.

Air was replaced by nitrogen where necessary in order to avoid flammable mixtures and any possibility of explosion due to ignition at the hot wire. The system

also was purged initially with nitrogen.

To check the accuracy of the rig a wire was calibrated in both this and the Disa rig with air and good agreement was obtained over the range 0.8 to 5 m sec^{-1}, as shown in Fig. 3.9. The calibration of a hot wire at low velocities (less than 1.5 m sec^{-1}) is shown in Fig. 3.10.

3.3 ANEMOMETRY MEASUREMENTS

The determination of turbulent parameters requires the measurements of u' and either the macroscale, L or the Taylor microscale, λ. Karpov et al (10), Semenov (11), Andrews (2), Ohta et al (12) and Ono et al (13), have investigated fan turbulence in closed vessels. The present cold turbulence investigations in the vessel were in collaboration with McMahon (7) and only a part of the results are reported in this thesis.

3.3.1 Measurements of The Degree of Isotropy

Karpov et al (10), Semenov (11) and Ohta et al (12) first showed the turbulence created by a symmetrical arrangement of fans in a closed vessel was isotropic. Isotropy simplifies the investigation of the structure of turbulence and the degree of isotropy created by the present arrangement of the fans has been investigated by Andrews (2). Essentially this involved determination of the correlation between two mutually perpendicular

turbulence velocities, u and v at a point. The correlation coefficient $R_{u\ v}$ is related to the Reynolds stress $\overline{uv}$. R_{uv} is defined by (14)

$$R_{uv} = \frac{\overline{uv}}{\sqrt{\overline{u^2}}\sqrt{\overline{v^2}}} \qquad (3.1)$$

For isotropic turbulence it will be zero, because of the random nature of the velocity fluctuations in all directions.

The experimental arrangement used by Andrews (2) is shown in Fig. 3.11. A DISA 55A32 45^{o}X hot wire probe was used for this, with linearised voltage conversion of the two signals by a DISA 55D10 lineariser, with a velocity exponent of 0.45, for each wire. For turbulence measurements in the plane of the two wires one wire responds to (u+v) and the other to (u-v), (15). The signal applied to a first DISA 55A06 random signal indicator and correlator sums and subtracts the two signals to yield the products 2u and 2v and these were correlated by another 55A06 correlator to give R_{uv}. Most of the results were within the R_{uv} band ± 0.05 for a distance of 80 mm either side of the vessel centre and for fan speeds up to the maximum value of 4,000 r.p.m. This low value showed the turbulence to be isotropic.

3.3.2 Measurements of R.M.S. Turbulent Velocity, u'

With the configuration of fans used there was no mean velocity of flow and the conventional concept of the relative intensity of the turbulence was meaningless.

The r.m.s. isotropic turbulence velocity, u', was measured with a DISA 55F31 miniature hot wire probe. The signals were processed by a 55D01 anemometer and 55D10 linear-iser.

Under more conventional conditions where the main stream velocity is larger than the amplitude of velocity fluctuation, the output signal of a hot wire anemometer includes both a time mean d.c. voltage component and an a.c. voltage component with positive and negative values about a time mean zero base at the d.c. voltage value (Fig. 3.12(a)). The r.m.s. turbulent velocity in such a case is easily determined from the a.c. component of the anemometer output by, for instance, a DISA r.m.s. volt-meter, type 55D35.

On the other hand, for the turbulent flow field of the present studies with no time mean approach flow, the hot wire was incapable of indicating the direction of flow, and the velocity fluctuations were effectively rectified. The output wave form is that of the rectified signal for a mean flow system (Fig. 3.12(b)). This signal includes a time mean d.c. voltage component, D, which was measured with a DISA type 55D30 d.c. digital voltmeter, whilst the r.m.s. value of the a.c. voltage component, a_1, about the pseudo d.c. voltage, D, (Fig. 3.12(c)) was measured with a DISA type 55D35 r.m.s. voltmeter.

The true r.m.s. voltage, $E = \sqrt{\overline{u^2}}$ (3.2)

,where the equality sign signifies "measures". The a.c. voltage component, a is defined by

$$a = \sqrt{\overline{(u - D)^2}}$$

$$= \sqrt{\overline{u^2} - 2\,\overline{D}\,\overline{u} + \overline{D^2}} \qquad (3.3)$$

Also, by definition, $\overline{u} = D$

Then
$$a = \sqrt{\overline{u^2} - D^2} \qquad (3.4)$$

Then, from Eq. (3.2), the voltage, E, corresponding to the effective r.m.s. velocity to which the wire responds is given by (10,16)

$$E = (D^2 + a^2)^{\frac{1}{2}} \qquad (3.5)$$

In systems with mean flow, the effect of the fluctuating turbulent velocity at right angles to the mean flow can be negligible (15). This is shown as follows:

The instantaneous component along the axis of the wire W + w, has no effect, and the wire responds to (15)

$$U_{eff} = \{(U + u)^2 + v^2\}^{\frac{1}{2}} \qquad (3.6)$$

In the present vessel, where there is no mean flow, U = 0. The turbulence is isotropic, namely, u' = v' = w'; and it is clear that in this case the wire responds to

$$U_{eff} = \{u^2 + v^2\}^{\frac{1}{2}} \qquad (3.7)$$

This result was also obtained by Semenov (11) in his

analysis of fan turbulence in closed vessels. Thus the calibration linked to "E" gives the "apparent" r.m.s. value of fluctuating velocity, u'_a, which parameter was used by Lwakabamba (3) directly measured in the vessel.

$$u'_a = \{\overline{u^2 + v^2}\}^{\frac{1}{2}}$$

$$= \{\overline{u^2} + \overline{v^2}\}^{\frac{1}{2}}$$

$$= (2)^{\frac{1}{2}}\, u' \qquad (3.8)$$

Thus the true r.m.s. value, u', is $(2)^{-\frac{1}{2}}$ times the apparent measured r.m.s. value.

There was some heating of the gas by the rotation of the fans and according to Bearman (17), the relative error in the velocity measured by a hot wire anemometer due to this is about 1% for a temperature change of $1^{o}C$. When the temperature variation was more than this value, the cold resistance of the wire was measured at the new temperature in order to select a value of operating wire resistance to maintain a constant overheat ratio (18,19). This rested upon the assumption of constant gas transport properties.

Horizontal and radial traverses of the wire (2) showed u' to be invariant with radius up to a value of 70 mm at fan speeds of 500 r.p.m., and up to a value of 50 mm for all fan speeds up to 4,500 r.p.m. The experimental arrangement is shown in Fig. 3.13.

3.3.3 Measurements of Scales of Turbulence, L and λ

Measurements of the integral scale, L and the Taylor microscale, λ, are connected with the study of the relationships between velocity fluctuations in space and with time at a given point. These two scales were obtained by the following three different methods.

3.3.3.1 Two Point Velocity Correlation Method

The integral scale of turbulence, L was obtained by the rather tedious process of two point velocity correlation. A 55A06 correlator was used with linearisation of both wire signals for different separation distances. Figure 3.14 shows the experimental arrangement. A correlation coefficient of unity was never obtained, possibly because of interference effects between the two wires at small separation (20). Neither was a coefficient of zero obtained at the largest possible separation within the homogeneous region of turbulence. The lowest value was 0.03, which was also obtained when one wire was removed from the vessel and immersed in an independent gas jet. The value of L was obtained by dividing the area under the correlation coefficient-separation curve between the maximum and minimum values of the coefficient by the differences between these values. A probe holder was designed and constructed of steel to enable the two probes to be moved independently of each other.

The Taylor microscale can be found by fitting a

parabola to the above two point velocity correlation curve, to pass through the points for small separation distances. Normally, this parabola would also pass through the point of correlation of unity. However, because such a coefficient was never obtained, the parabola was fitted to pass through the point of maximum observed correlation. The equation of the parabola becomes

$$y^2 = \lambda^2 \, (1-R_y/R_{ymax}) \qquad (3.9)$$

where R_{ymax} is the maximum observed correlation at a particular speed. The results are reported in Chapter 4.

3.3.3.2 Autocorrelation Method

The autocorrelation function is a measure of the similarity between a signal and a time-delayed form of itself. Thus the autocorrelation of the raw linearised hot wire signal should, on integration, yield an average time for the existence of a large eddy. Similarly the autocorrelation of $\frac{du}{dt}$ should yield an average time for the existence of the Taylor microscale eddies.

The autocorrelation measurements for the present vessel were obtained by Andrews (2) with a Hewlett Packard Model 3721A correlator, which produces a plot of the autocorrelation function against delay time. The auto-correlation curve for u was integrated to obtain the integral time scale, L_t. Taylor (21) first showed that L and L_t could be related by:

$$L = U \, L_t \qquad (3.10)$$

If no mean flow exists, as in the present vessel, the assumption used by Semenov (11) and given by Tabaczynski (22), as U = u', for obtaining the integral scale, L, is used

$$L = C_1 \, u' \, L_t \tag{3.11}$$

where C_1 is a constant of order one.

The Taylor micro time scale, λ_t, was obtained by Andrews (2) by using both a DISA 55A06 Random Signal Indicator and Correlator and the expression (23)

$$\lambda_t = \left[\overline{u^2} \;\Big/\; \overline{\left(\frac{du}{dt}\right)^2} \right]^{0.5} \tag{3.12}$$

and by assuming that λ_t, is the time taken for the auto-correlation function of $\frac{du}{dt}$ to be reduced to zero. The experimental arrangement is shown in Fig. 3.15. Taylor's hypothesis (21) defines the relationship between λ and λ_t as:

$$\lambda = U \, \lambda_t \tag{3.13}$$

In both cases, λ, was obtained from

$$\lambda = C_2 \, u' \, \lambda_t \tag{3.14}$$

where C_2 is constant of order one. The results are reported in Chapter 4. In the present work the values of C_1 and C_2 were taken as unity.

3.3.3.3 Power Spectral Density Method

The structure of a turbulent flow might be considered physically as a superposition of a large number of eddies with different sizes and angular velocities. A more detailed picture for the description of turbulence can be obtained from considerations of the distribution of energy. High frequency fluctuations of velocity might be regarded as associated with small eddies and low frequency fluctuations with large eddies. The frequency spectrum can be analysed with the aid of electric filters.

The linearised output signals from the hot wire were filtered by a DISA D25 auxiliary unit and then processed by a Brüel and Kjaer audio frequency spectrometer, type 2112, of frequency range 22-4,500 HZ, in conjunction with an extension filter set type 1620, for analysis of frequencies below 22 HZ down to 12.5 HZ. These enabled the bare linearised hot wire signal to be separated into its various frequency components and each frequency band to be studied separately. Basically, the audio frequency spectrometer consists of an input amplifier, a filter system of band-pass filters and weighing networks, and an output amplifier. The bandwidth of the filters was 1/3 octave throughout the present work. Fig. 3.16 shows the experimental arrangement.

The power spectral density function or energy spectrum, E(n), at the centre frequency, n, is defined as the square of the output divided by the bandwidth. The

length scales L and λ are related to E(n) and for conditions with mean flow the relationships are given by Hinze (14) as:

$$L = \frac{U}{4} \lim_{n \to 0} \frac{1}{u'^2} E(n) \qquad (3.15)$$

$$\frac{1}{\lambda^2} = \frac{2\pi^2}{U^2 u'^2} \int_0^\infty dn\ n^2 E(n) \qquad (3.16)$$

Taylor (21) defined a normalised power spectral density function F(n) by

$$F(n) = \frac{E(n)}{u'^2} \qquad (3.17)$$

In the present vessel, since there was no mean flow and the velocity fluctuations were effectively rectified by the hot wire, as discussed in Section 3.3.2; the term u'^2 in Eq. (3.17) was replaced by the square of the velocity corresponding to the a.c. voltage component a (see Eq. (3.4)). Then substitute Eq. (3.17) into Eqs. (3.15) and (3.16), and the assumption U = u', yield length scales given by

$$L = \frac{u'}{4} \lim_{n \to 0} F(n) \qquad (3.18)$$

$$\frac{1}{\lambda^2} = \frac{2\pi^2}{u'^2} \int_0^\infty dn\ n^2 F(n) \qquad (3.19)$$

The normalised power spectral density function F(n) satisfied the condition (14)

$$\int_0^\infty dn\ F(n) = 1 \qquad (3.20)$$

The values of L and λ were calculated from Eqs. (3.18) and (3.19) and the results are given in Chapter 4. At the highest frequencies the r.m.s. output of the audio frequency spectrometer was only slightly higher than the inherent broadband noise of the output amplifier. All readings were corrected by subtraction of the level of this noise.

3.4 OPTICAL SYSTEM AND PHOTOGRAPHY

The work reported in this thesis centres around optical recording of flame propagation in a spark ignited explosion. Of major importance was the measurement of burning velocity and the relationship between flame propagation and flame structure in the initial stages of the explosion. The technique employed was that of schlieren high speed photography.

Hundy (1) and Andrews (2) in their development of a suitable optical system studied the available optical techniques. Three techniques were selected: reflection plate schlieren interferometry, knife edge schlieren and wire diffraction schlieren interferometry. All three techniques used the optical arrangement shown in Fig. 3.17 for the reflection plate, and a change from one system to another merely involved the appropriate insertion at the schlieren focus. For the purpose of flame front definition and quantitative investigations of flame structure, it was noted that the last of these was superior to the others.

But the other two techniques were easier to adjust and gave adequate definition, so they were used throughout the work reported in this thesis.

3.4.1 Light Source

In recent years, the use of lasers as light sources has become common (24-26). Some holographic applications have been reviewed by Soroko (27) and various workers have investigated different optical arrangements (28-30) and their application to refractive index gradient measurements (31,32). Three dimensional holographic interferograms of a diffusion flame have been obtained by Alwang et al (33). However, for the present requirements, Andrews (2) has concluded that holographic systems were unjustifiably complicated, but that laser light sources, in one of the three suggested optical systems, was satisfactory and simple to use (34-37).

A Scientifica and Cook helium-neon portable laser (6328^{o}A) was used with a power output of 3.0 mw.

3.4.1.1 Laser Safety

The safety precautions required in the use of lasers are given in a Ministry of Aviation publication (38). In the present work danger would arise only if the beam should accidentally be focused on the retina. This was unlikely, but care was taken not to look directly into the beam, or its reflections. Nevertheless, frequent eye tests were essential during the course of this work.

3.4.2 Schlieren Arrangement

A diagram of the optical arrangement is shown in Fig. 3.17. The laser light was focused by a microscope lens placed directly in front of the laser. This focus was arranged to coincide with the focus of a large four inch diameter multicomponent lens and resulted in a four inch beam of parallel light. This passed through the two windows in the endplates of the cylindrical explosion vessel. An identical four inch diameter lens refocused the beam, either on to a knife-edge or a reflection plate, depending on requirements.

Accurate adjustment of the above system was imperative to obtain good results. All the optical devices were mounted on two one meter optical benches, positioned either side of the explosion vessel. The laser was mounted on a half meter optical bench of its own. After the beam had been aligned along both benches and through the centre line of the explosion vessel, the microscope lens was inserted and adjusted so that the enlarged beam passed through the first large lens. This was positioned to give a parallel beam of light by placing a plane mirror over the face of the lens and adjusting the lens position until the laser light was reflected back to focus at the microscope lens. Next, the windows of the vessel were aligned perpendicularly to the parallel beam of light. This was achieved by placing the plane mirror flat against the window and adjusting the angle of the first optical

bench until the light was again reflected back to a focus at the focus of the microscope lens. Finally, the second large lens was adjusted to be perpendicular to the parallel laser light using the same technique but altering the inclination of the second optical bench.

3.4.3 Schlieren Interferometry

The characteristic of schlieren interferometers is the very small shear between the interfering beams, instead of the large separation associated with Mach-Zehnder instruments. Also the shear always occurs after the single parallel light beam has traversed the optical inhomogeneity. With a laser source all parts of a plane and coherent wave front are identical, one beam can be inverted or rotated with respect to the other, as an alternative to being overlapped in any desired way, without detriment to fringe legibility and Tanner has reviewed some of these possibilities (39).

Since an unperturbed part of the wave front can be folded over that part which traversed the inhomogeneity, no separate reference beam is necessary; all that is required is a method of folding the wave at the schlieren focus in order to obtain interference fringes. This has been achieved by shearing the wave front with a reflection plate, by which means interference occurs between light waves reflected from the front and back surfaces of the reflection plate (24,40-43). The simplicity of this system and the possibility of obtaining quantitative interferograms

led to the adoption of this method of visualisation for explosion flames in the work of Hundy (1) and Andrews (2) and its continued use in the present work.

Experimental and theoretical details of this method have been fully discussed by Hundy (1). Consideration of the geometrical optics of the system yields an expression for the separation of those rays in the test section which interfere in the image plane. This separation distance depends on the angle of incidence of the reflection plate and its thickness. For quantitative results a large ray separation distance (large reflection plate thickness) is required, so that one ray can be considered to have passed through the flame while the other is unaffected. However, the number of fringes increases with the plate thickness and this places a practical limitation on the maximum ray separation. For qualitative flame visualisation studies the thickness and precise angle of the reflection plate are irrelevant.

3.4.3.1 Reflection Plates

Those designed by Hundy (1) were used in the present work. To safeguard against plate vibrations, they were mounted in plasticine on a lens holder which was positioned on the optical bench at the schlieren focus. The major advantage of this method was the ease with which interference fringes were obtained; the only necessary adjustment was the inclination of the reflection plate to an appropriate angle to the optical axis.

3.4.3.2 Optical Arrangement

The microscope objective was positioned to give a parallel beam at the test section and the reflection plate placed at the focus of the second lens. With a white card or similar object as a screen, the reflection plate was adjusted so that the beam fell on a place which was free of imperfections and gave a pattern of straight, even fringes. The incidence angle at the plate was set at approximately 50^{o}. For photography, the camera was focused on the spark gap. This was done by holding a small light inside the vessel, near the spark gap with the laser switched off.

3.4.4 Knife Edge Schlieren

In contrast to the reflection plate, the knife edge does need careful adjustment. When the knife edge is at the schlieren focus, diffraction effects are easily obtained.

The technique for the knife edge schlieren also has the same problem as that for the reflection plate, in that the variations in the inclination of the refractive index gradient to the knife edge can lead to different results. Displacement of the image of the source parallel to the knife edge produces no effect at the screen, and the edge must therefore be set perpendicular to the direction in which the density gradients are to be observed.

Andrews (2) recommended the use of an 'L' shaped

knife edge with the corner of the 'L' positioned at the schlieren focus, in an attempt to overcome directional effects caused by the use of simple vertical or horizontal knife edge. It was noticed during the double kernel investigations, which are discussed in Chapter 4, that an 'L' shaped knife edge gives good definition for one of the kernels but less so for the other. By employing 'V' shaped knife edges it was possible to obtain reasonable definitions for both kernels. Two simple razor blades stuck together in a 'V' shape were used.

3.4.5 High Speed Camera

A Fastax type W.F. 17 high speed ciné camera was used in conjunction with a Weinberg power control unit WG-15 and a programmer unit WG-25. The maximum framing speed of the camera was 8,000 frames per second and the film size was 16 mm. Built into the camera was a small neon lamp which calibrated the film at intervals of either one or ten milliseconds. The programmer unit was used for triggering and synchronisation, as described in Section 3.5.3.

For photography, the camera lens was positioned a few centimeters behind the schlieren focus so that the explosion vessel window filled the 16 mm frame. The lens was opened fully, to f 2.8 and focused on the filament of a small torch bulb placed at the centre of the vessel, just above the spark plug.

During the course of the work this camera developed a fault which impaired its smooth running and, as a consequence, it was replaced by a Hitachi model 16 HM high speed camera. This was used in conjunction with a 16 mm Gordon Advanced Camera Control System GC1026. The maximum framing speed of this camera was 10,000 frames per second.

The camera was equipped with LED timing lamps, the light from which was projected by lens on to the film. The timing light marked the film every m sec, with a burst of 10 marks every 10 m secs.

Ilford FP4 film was used in the high speed camera. This was chosen because it provided good contrast and responded to the laser wavelength. Often 25 ft lengths were used, but for hydrogen explosions, when the camera ran at near maximum speed, lengths of up to 100 ft were employed.

3.4.6 Tulip

In order to study the effect of high turbulence levels upon ignition and flame propagation it was decided to initiate flame propagation in a volume shielded from the full turbulence intensity. Initially a tulip-shaped glass shield was formed with the spark electrodes close to the base of what became known as the tulip. The definition of the flame front inside the tulip was very poor and this arrangement was replaced by a shield of two

schlieren quality glass plates orthogonal to the optical axis. Unfortunately, it was not possible even with this arrangement to obtain satisfactory flame visualisation with either schlieren or interference techniques because of the difficulty of aligning the two plates orthogonally to the optical axis. The two designs that eventually were employed are shown in Figs. 3.18 and 3.19.

For the design of Fig. 3.18, tulip A, the spark electrodes were shielded from the full turbulence intensity by two brass discs of 63.5 mm diameter mounted on the spark electrodes, as shown in the figure. The distance between the two discs could be easily varied.

The two spark plugs, described in Section 3.2.1.2, were mounted horizontally from either side of the vessel. The flat ended brass screw electrodes were screwed into the inner conductor of the spark plugs, to form a variable spark gap.

Each of the two discs was brazed to a threaded brass boss. These were screwed on to the electrodes and the thread enabled the distance apart of the two discs to be varied. In some experiments a further shielding was achieved by covering approximately the lower three-quarters of the circumferential gap between the two discs by a thin brass sheet.

In the course of the experiments reported in Chapter 4 it became clear that this volume was too large

and the flame movement away from the tulip was excessive.

To overcome this difficulty a cylindrical tulip of smaller volume, tulip B, was made which is shown in Fig. 3.19. A cylinder of 22 mm diameter and 39 mm internal height was mounted at the end of the horizontal electrode. This tulip is shown in position inside the bomb in Fig. 3.3.

The high voltage electrode consisted of a flat ended brass screw, screwed into the inner electrode. The earther electrode consisted of a brass disc attached to a thin steel vertical rod across the tulip diameter.

To estimate the turbulence intensity inside the tulip, a hot wire probe such as described in Section 3.2.1.4. was inserted inside the tulip. The value of u' was found to be less than 10% of the value outside the tulip. This low value enabled a flame kernel to become established in a region of low turbulence.

3.5 GENERAL EXPERIMENTAL TECHNIQUES

3.5.1 Preparation of Gaseous Mixtures

Due to the effective sealing of the fan shaft, the explosion vessel could be evacuated to a sufficiently low pressure for mixtures to be made up in the vessel. It was first washed out by evacuation to a pressure of less than one Torr and filled with atmospheric air; this process was repeated three times. The mixture components were

added, the smallest constituent first, to their respective partial pressure, and to a final pressure of one atmosphere. The mixture was allowed to stand for at least five minutes before explosion, with the fan running for good mixing.

For calibration experiments, all mixtures were prepared in the large tank described in Section 3.2.1.1.

3.5.1.1 Gas Purity

The methane was drawn from cylinders suppled by Air Products Ltd. The purity quoted by the suppliers was 95%. The hydrogen was supplied by the British Oxygen Company and was 99.99% pure. Air was taken from the atmosphere through a drying tube containing anhydrous calcium chloride.

3.5.2 Leak Testing

The equipment was tested periodically for leakage by evacuations to low pressure and observations for any pressure increase over a period of time. Leaks were located by the application of both air pressure and soap solution. The amount of leakage tolerated was such as to give 1 Torr increase in pressure per hour in the explosion vessel. For the storage tank any detectable increase in pressure over a period of 24 hours denoted too large a leak.

3.5.3 Synchronisation

A high speed camera control unit triggered the

spark and oscilloscope. A button on the unit started the camera, which after a preset length of film had run through (for the Fastax camera), or when the camera had attained its full speed (for the Hitachi camera), closed a relay which triggered the spark and the oscilloscope. The sequence is demonstrated diagrammatically in Fig. 3.20.

With the camera at full speed a relay in the camera control unit closed and discharged a capacitor through the gate of thyristor in the synchronisation unit, which caused a 0.1 μF capacitor to be discharged through the primary circuit of the pulse transformer in the ignition unit. The circuit is shown in Fig. 3.21.

3.5.4 Pressure Measurements

The equipment for pressure measurements is described in Section 3.2.1.3. The pressure transducer was mounted flush with the explosion vessel cylinder wall on the centreline. The transducer was calibrated by Lwakabamba (3) to obtain its sensitivity and the calibration was found to be linear. The pressure increases measured in these experiments took place over a period of approximately 5 m sec and this was large compared with the transducer rise time of 6 μ sec.

The charge amplifier was set to give an output of 1 m volt for every increase of 1 p.s.i. pressure. These settings were maintained for all the explosions.

3.5.5 Recording Techniques

Output voltages, such as those from the hot wire, pressure transducer and ionisation probe were displayed on the oscilloscopes and traces were photographed with oscilloscope cameras. The time base on the oscilloscopes was set so that a single sweep would cover the required period. The sweep was triggered at the beginning of the explosion and the camera shutter remained open whilst the event occurred. The illuminated graticule on the oscilloscope was also recorded on the photograph, and when quantitative data was required, measurements were made from the photograph with a travelling microscope.

Tektronix type 502 and type 551 dual beam, with type 11A5 plug-in units, oscilloscopes were used throughout.

3.5.6 Processing of Results

The high speed films were developed by a Gordon 16/35 negative film processing machine. They were later analysed with a P.C.D. Ltd., X-Y Digital Data Reader, type ZAE 1B. This had a 16 mm back projection facility which permitted analysis of still and ciné films from their blown up images (about 40 times) on a translucent screen with a reading area of 30 × 50 cm. The Reader also had a built-in scaling facility so that the actual distances between reference knife edges on the films could be set as a digital output such that all subsequent film measurements were in real distances along the vessel

centreline diameter. The films were measured frame by frame. To obtain a distance scale on the film a known calibration distance was required on it. Two razor blade edges, attached to the window, 60 mm apart, were used for this. Andrews (2) had shown that there was no distance error due to the camera being focused at the centre of the vessel.

3.6 NOMENCLATURE

a	a.c. voltage component, Eq. (3.4)
C_1	constant, Eq. (3.11)
C_2	constant, Eq. (3.14)
d	hot wire anemometer diameter
D	time mean d.c. voltage component
E	true r.m.s. voltage, Eqs. (3.2) and (3.5)
E(n)	power spectral density function or energy spectrum
F(n)	normalised power spectral density function
L	integral scale of turbulence
L_t	integral time scale
L_w	hot wire anemometer length
n	frequency
R_{uv}	the coefficient of correlation between fluctuating velocities u and v, Eq. (3.1)
R_y	the correlation coefficient between velocity at two points a distance y apart
t	time
u	instantaneous fluctuating velocity in the x direction
$\overline{uv}$	Reynolds stress
u'	r.m.s. turbulent velocity in the x direction, $\sqrt{\overline{u^2}}$
u'_a	"apparent" r.m.s. velocity directly measured in the present vessel
U	mean flow velocity in the x direction

U_{eff} effective cooling velocity

v instantaneous fluctuating velocity in the y direction

v' r.m.s. turbulent velocity in the y direction, $\sqrt{\overline{v^2}}$

w instantaneous fluctuating velocity in the z direction

w' r.m.s. turbulent velocity in the z direction, $\sqrt{\overline{w^2}}$

W mean flow velocity in the z direction

y separation distance

λ Taylor microscale of turbulence

λ_t Taylor micro time scale

3.7 REFERENCES

1. G.F. HUNDY, Flame propagation in closed vessels, Ph.D. thesis, Dept. Mechanical Engineering, Univ. Leeds (1969).

2. G.E. ANDREWS, Laminar and turbulent flame propagation, Ph.D. thesis, Dept. Mechanical Engineering, Univ. Leeds (1972).

3. S.B. LWAKABAMBA, Turbulent flame propagation in closed vessels, Ph.D. thesis, Dept. Mechanical Engineering, Univ. Leeds (1975).

4. D.R. BALLAL and A.H. LEFEBVRE, The influence of spark discharge characteristics on minimum ignition energy in flowing gases, Combustion and Flame 24, 99 (1975).

5. M. KONO, S. KUMAGAI and T. SAKAI, The optimum condition for ignition of gases by composite sparks, Sixteenth Symposium (International) on Combustion, p.757, The Combustion Institute: Pitsburgh (1977).

6. J.M. BEÉR and N.A. CHIGIER, Combustion Aerodynamics, p. 219, Applied Science Publishers Ltd, London (1972).

7. M. McMAHON, The influence of turbulence upon spark ignition, Ph.D. thesis, Dept. Mechanical Engineering, Univ. Leeds (1979).

8. G.E. ANDREWS, D. BRADLEY and G.F. HUNDY, Hot wire anemometer calibration for measurements of small gas velocities, Int. J. Heat and Mass Transfer 15, 1765 (1972).

9. J.G. KNUDSEN and D.L. KATZ, Fluid dynamics and heat transfer, McGraw-Hill, New York (1958).

10. V.P. KARPOV, E.S. SEMENOV and A.S. SOKOLIK, Turbulent combustion in an enclosed space, Dokl. Akad. Nauk SSSR 128, 1220 (1959).

11. E.S. SEMENOV, Measurement of turbulence characteristics in a closed volume with artificial turbulence, Combustion, Explosion and Shock Waves 1, 57 (1965).

12. Y. OHTA, K. SHIMOYAMA and S. OHIGASHI, Vaporization and combustion of single liquid fuel droplets in a turbulent environment, Bulletin of the JSME 18, 47 (1975).

13. S. ONO, M. TSUGE, M. KURUSU and I. FUKUE, A study on the influences of the scale of turbulence on the burning rate in a vessel, Bulletin of the JSME 19, 547 (1976).

14. J.O. HINZE, Turbulence - An introduction to its mechanism and theory, p. 59, McGraw-Hill, New York (1959).

15. P. BRADSHAW, An introduction to turbulence and its measurement, p. 119, Pergamon Press, Oxford (1971).

16. DISA Instruction and Service Manual for Type 55D35 RMS Voltmeter, Disa Elektronik A/S, Denmark.

17. P.W. BEARMAN, Corrections for the effect of ambient temperature drift in hot-wire measurements in incompressible flow, DISA Information No. 11, May 1971.

18. DISA Instruction and Service Manual for Type 55D01 Anemometer Unit, Disa Elektronik A/S, Denmark.

19. C. GAULIER, Measurement of air velocity by means of a triple hot-wire probe, Institut Français Du Pétrole, Division Applications, April 1976.

20. F.H. CHAMPAGNE, V.G. HARRIS and S. CORRSIN, Experiments on nearly homogeneous turbulent shear flow, J. Fluid Mech. 41, 81 (1970).

21. G.I. TAYLOR, The spectrum of turbulence, Proc. Roy. Soc A164, 476 (1938).

22. R.J. TABACZYNSKI, Turbulence and turbulent combustion in spark-ignition engines, Prog. Energy Combust. Sci. 2, 143 (1976).

23. DISA Instruction and Service Manual for Type 55A06 Random Signal Indicator and Correlator, Disa Elektronik A/S, Denmark.

24. L.H. TANNER, Some laser interferometers for use in fluid mechanics, J. Sci. Instrum. 42, 834 (1965).

25. M.J.R. SCHWAR and F.J. WEINBERG, Laser techniques in combustion research, Combustion and Flame 13, 335 (1969).

26. D.R. HERRIOTT, Some applications of lasers to interferometry, Progression Optics (ed. E. Wolf) 6, 171 (1967).

27. L.M. SOROKO, Holography and interference processing of information, Soviet Physics Uspekhi 90, 643 (1967).

28. L.H. TANNER, Some applications of holography in fluid mechanics, J. Sci. Instrum. 43, 81 (1966).

29. L.H. TANNER, The scope and limitations of three dimensional holography of phase objects, J. Sci. Instrum. 44, 1011 (1967).

30. J.G. BEESEY and G.E. MADDRIX, Simple holographic interferometer of the Rayleigh type, Rev. Sci. Instrum.41, 880 (1970).

31. A.G. HAVANER, Holographic applications in shadowgraph, schlieren, and interferometric analysis of heat transfer and fluid flow test subjects, ARL-70-0270 AD-717 702 (1970).

32. O.M. FREDRICK, Optical holography interferometry for space-time resolved refractive index measurement, Proc. 15th Annual Analytical Instrument Symposium, 5-7 May, 1969, New Orleans, La, p. 114-127.

33. W.G. ALWANG, L.A. CAVANAUGH and D. CAIN, The observation of three dimensional shadowgraph like images in holography of phase objects, Applied Optics 8, 1256 (1969).

34. R.J. GOLDSTEIN, Interferometer for aerodynamic and heat transfer measurements, Rev. Sci. Instrum. 36, 1408 (1965).

35. U. GRIGULL and H. ROTTENKOLBER, Two-beam interferometer using a laser, J. Opt. Soc. America 57, 149 (1967).

36. B.N. BASKAREV, V.M. EROSHENKO, A.A. MUSHINSKY and Y.N. TERENTIEV, Lasers as light sourses for Mach-Zehnder interferometers, Russian J. Engineering Physics 17, 261 (1969).

37. C.S. CHEN and J.D. BIRD, Alignment technique for the Mach-Zehnder interferometer using a laser, J. Phys. E: Sci. Instrum. 4, 157 (1971).

38. MINISTRY OF AVIATION, Laser Systems - Code of Practice, SJ 15219 (1965).

39. L.H. TANNER, The design of laser interferometers for use in fluid mechanics, J. Sci. Instrum. 43, 81 (1966).

40. A.K. OPPENHEIM, P.A. URTIEW and F.J. WEINBERG, On the use of laser light sources in schlieren interferometry Systems, Proc. Roy. Soc. A291, 279 (1966).

41. M.V.R.K. MURTY, The use of a single plane parallel plate as a lateral shearing interferometer with a visible gas laser source, Applied Optics 3, 531 (1964).

42. M.V.R.K. MURTY, Compact lateral shearing interferometer based on the Michelson interferometer, Applied Optics 9, 1146 (1970).

43. J.G. KEELEY and R.A. HARGREAVES, A rugged inexpensive shearing interferometer, Applied Optics 9, 948 (1970).

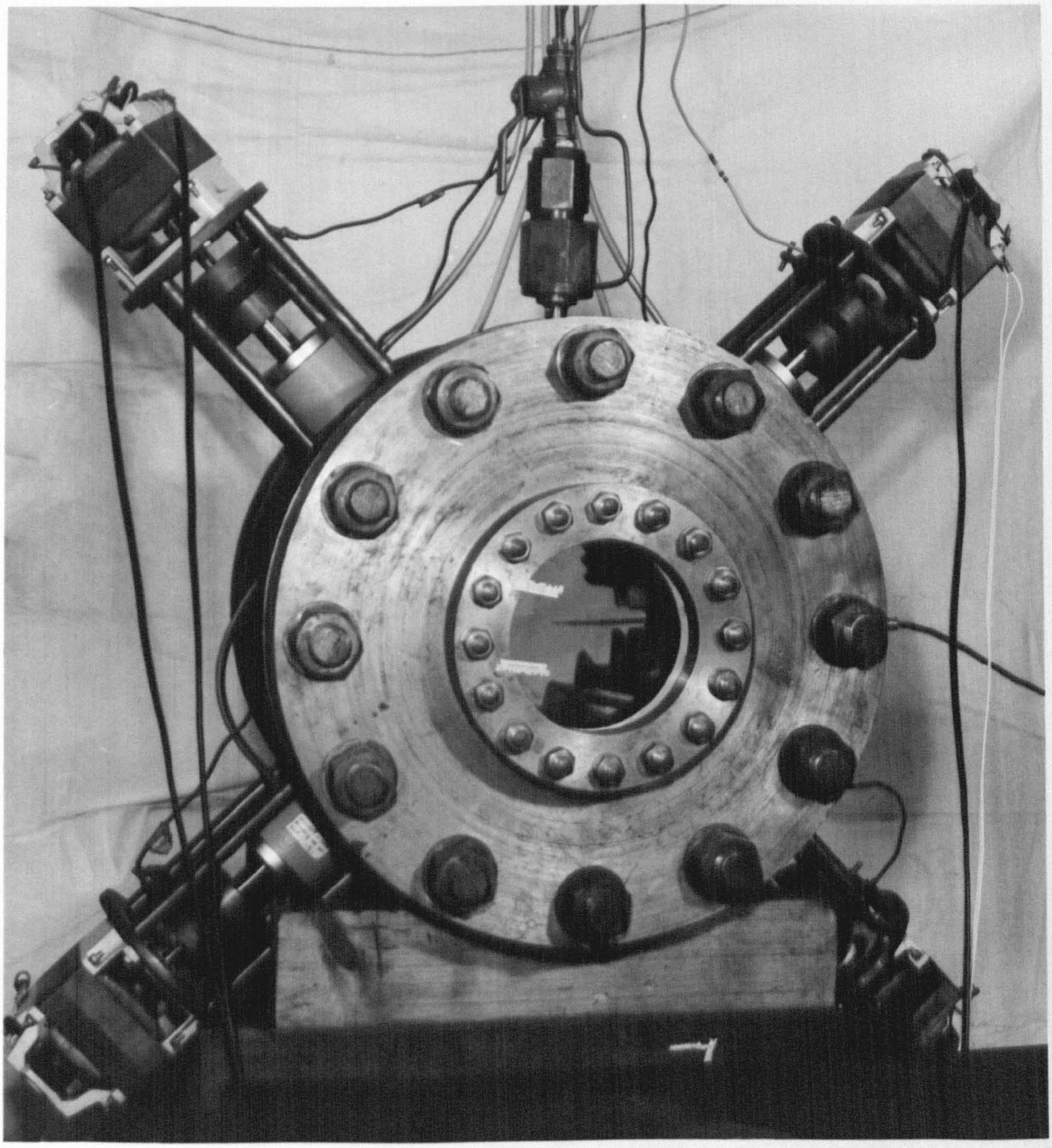

FIG. 3.1 TWELVE INCH DIAMETER EXPLOSION VESSEL

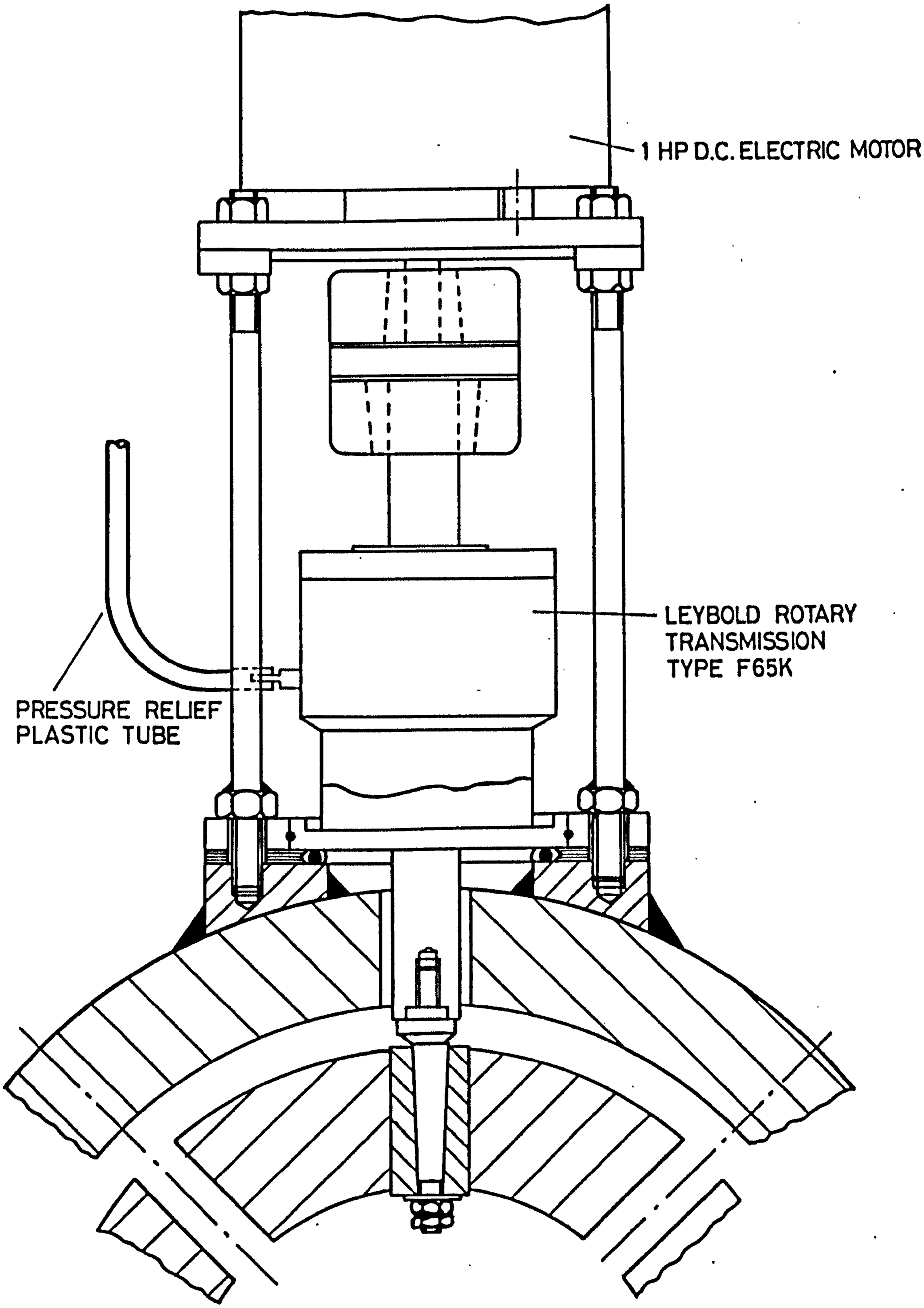

FIG. 3.2 PRESENT ASSEMBLY OF ELECTRIC MOTORS
AND FANS ON THE EXPLOSIVE VESSEL.

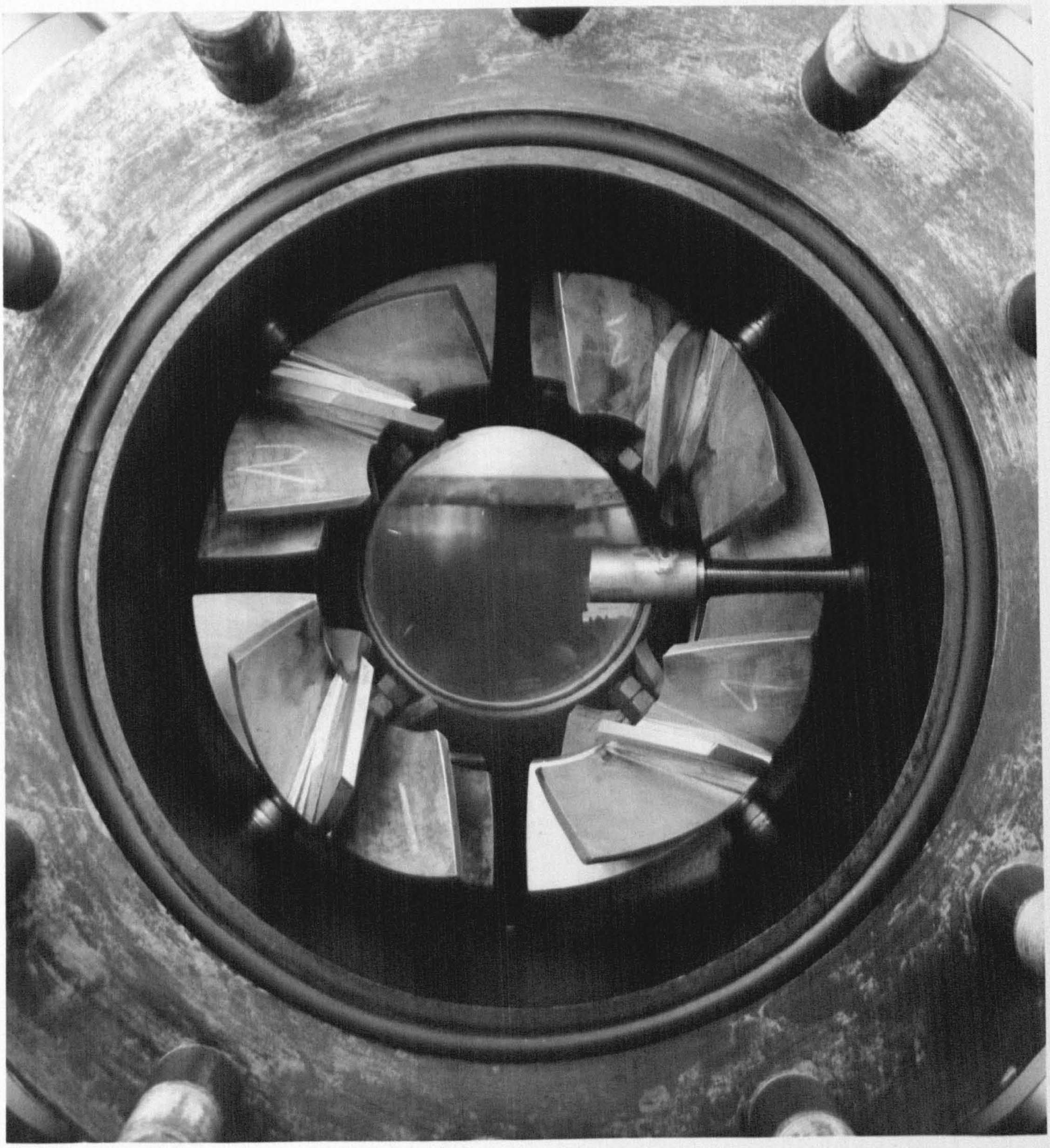

FIG. 3.3 FANS IN POSITION IN EXPLOSION VESSEL

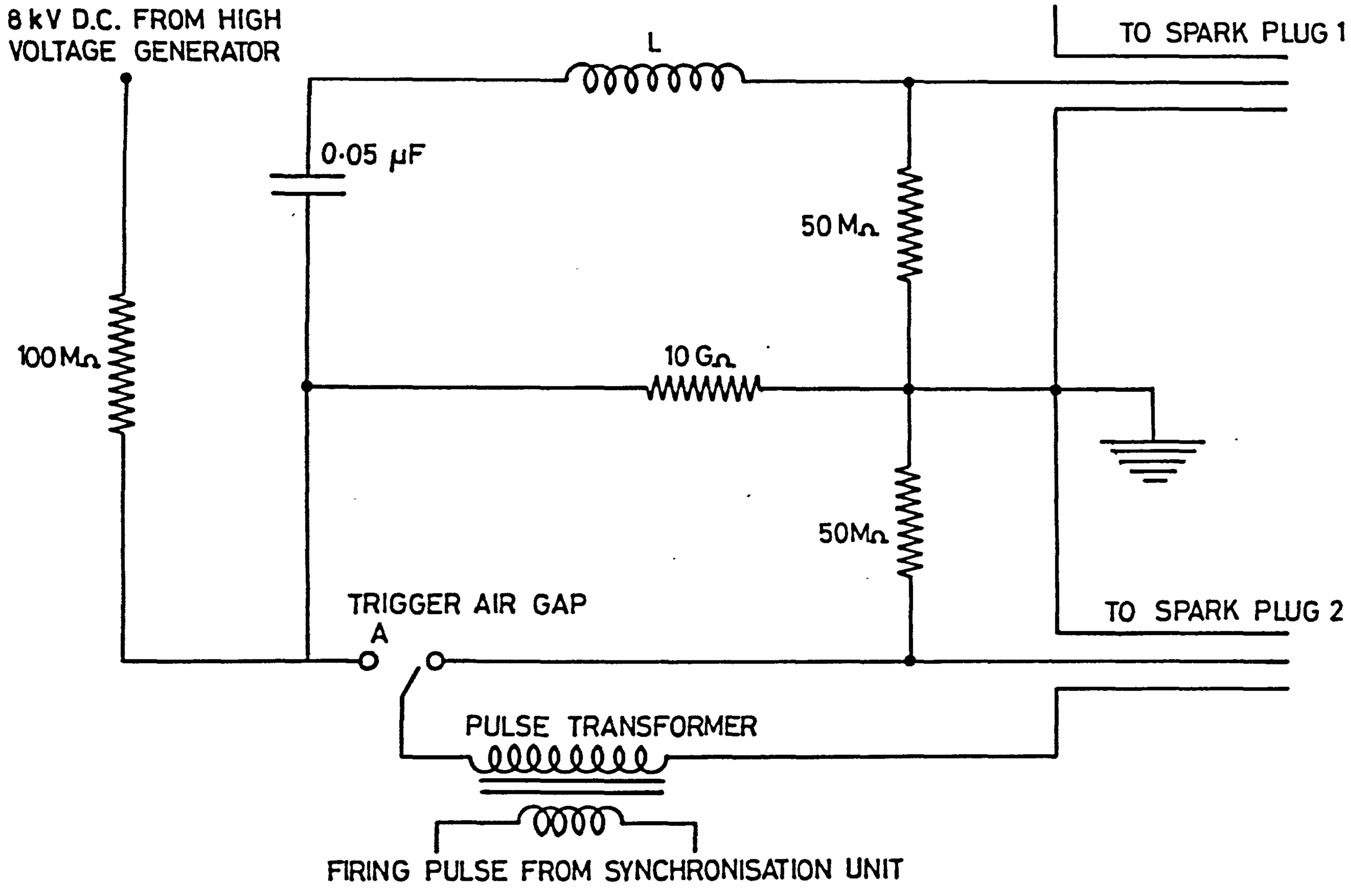

FIG. 3 . 4 CIRCUIT DIAGRAM OF IGNITION UNIT (A)

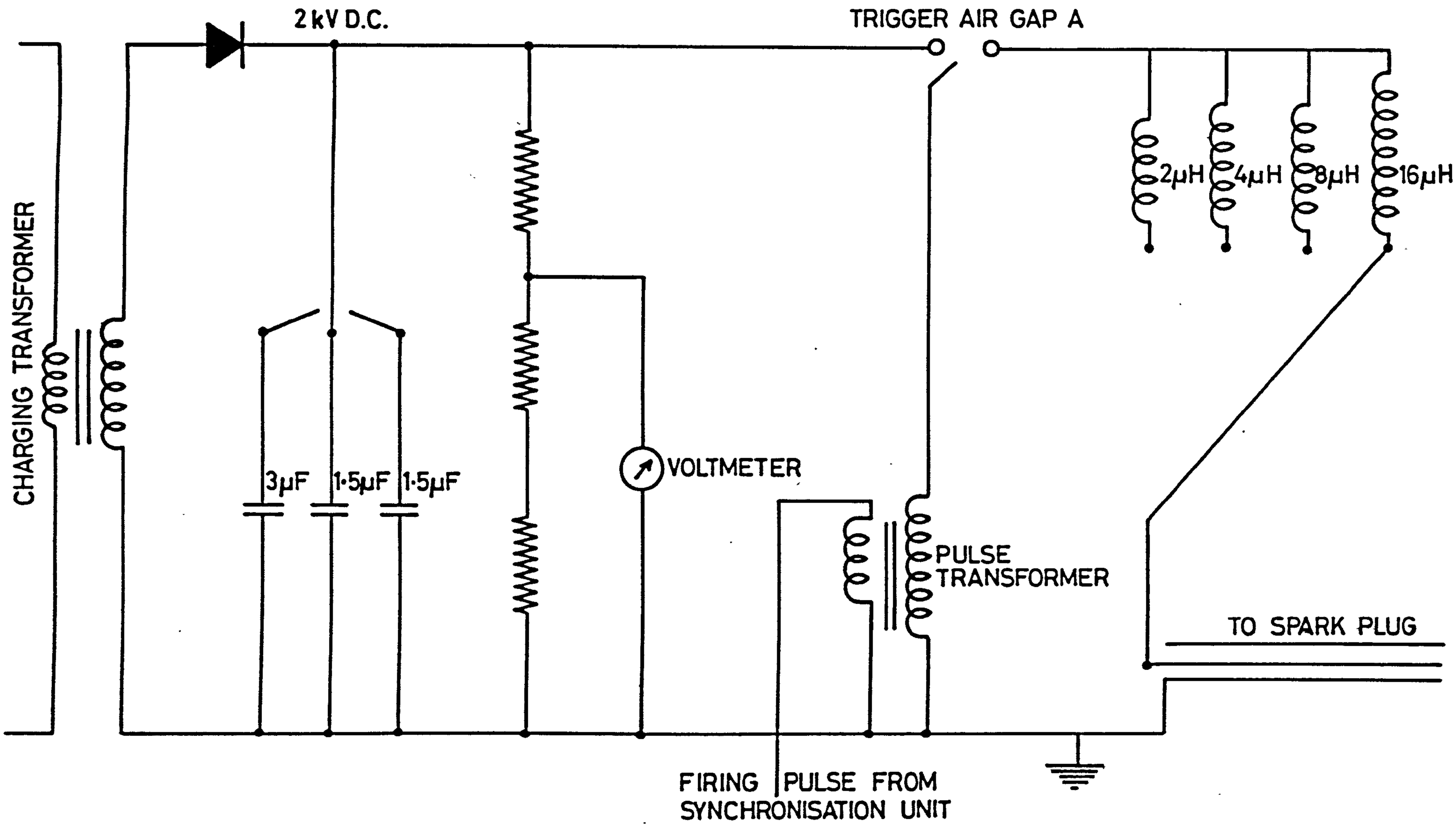

FIG.3.5 CIRCUIT DIAGRAM OF IGNITION UNIT (B)

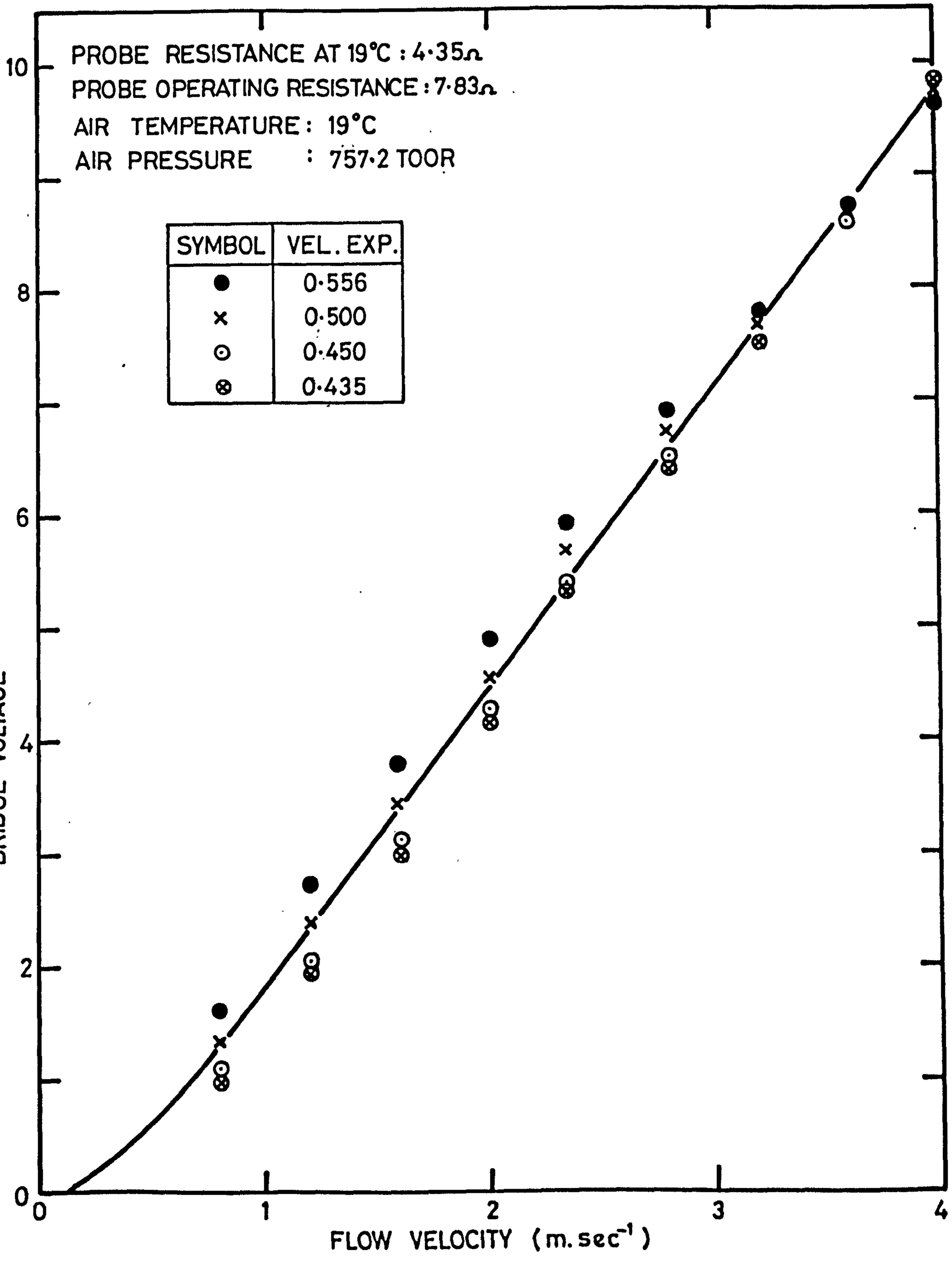

FIG. 3.6 EFFECT OF LINEARISED EXPONENT ON CALIBRATION CURVE

TYPICAL LINEARISED VELOCITY FLUCTUATIONS

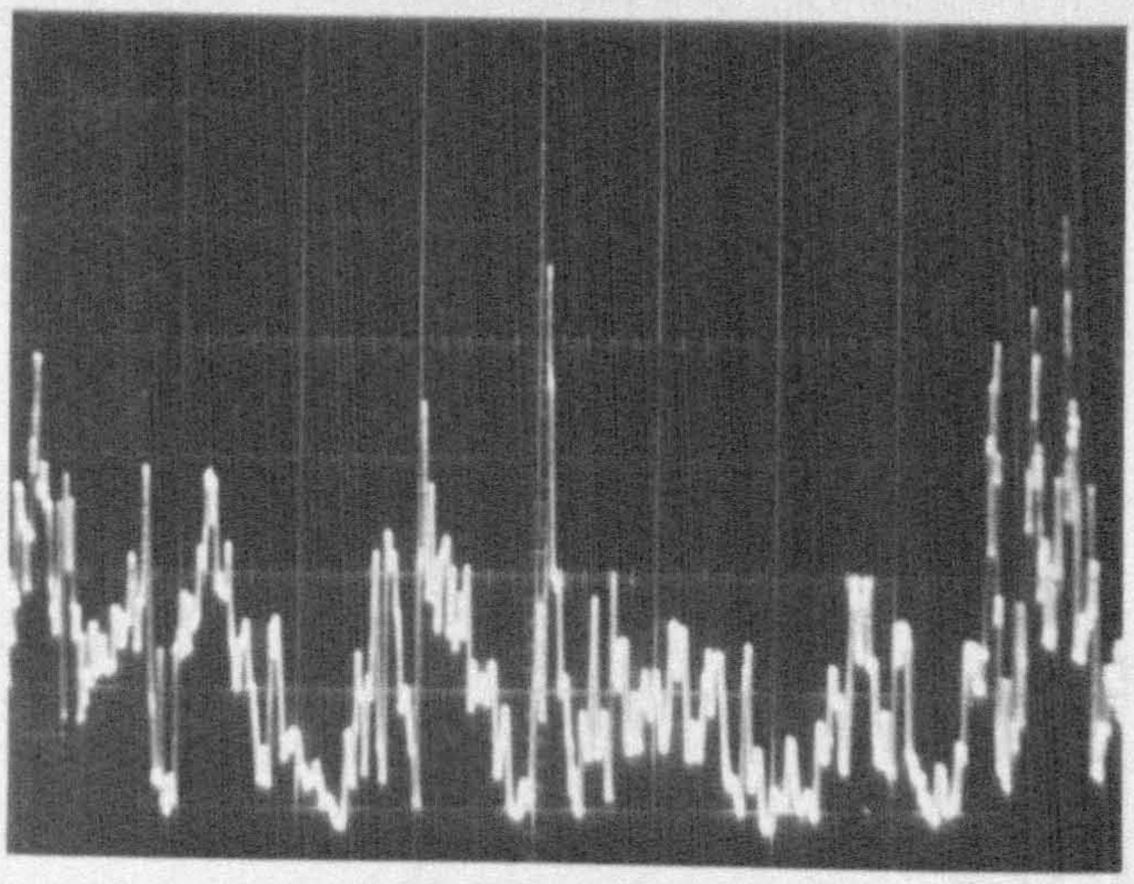

1,500 rpm

(a)

TYPICAL INTERMITTENT BURST OF TURBULENCE

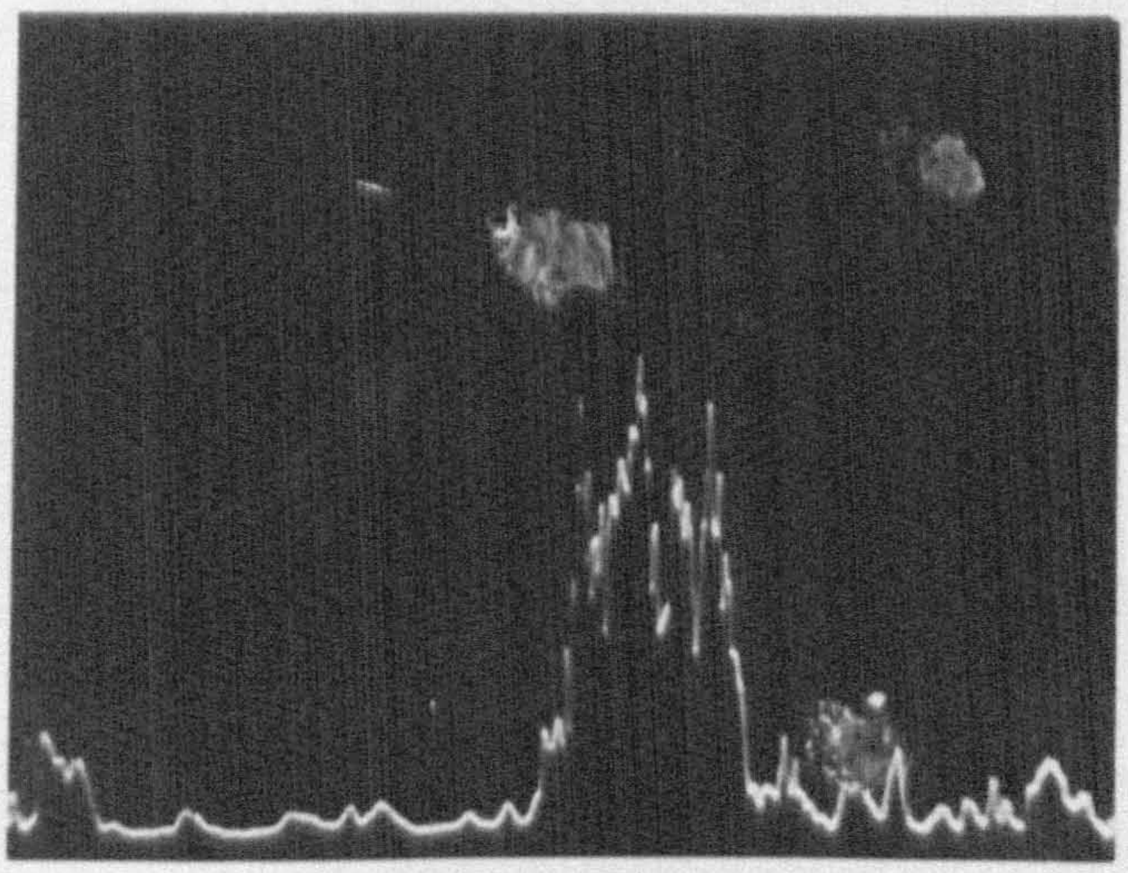

1,000 rpm

(b)

PEAK VELOCITY CUT-OFF DUE TO LINEARISER OVERSHOOT

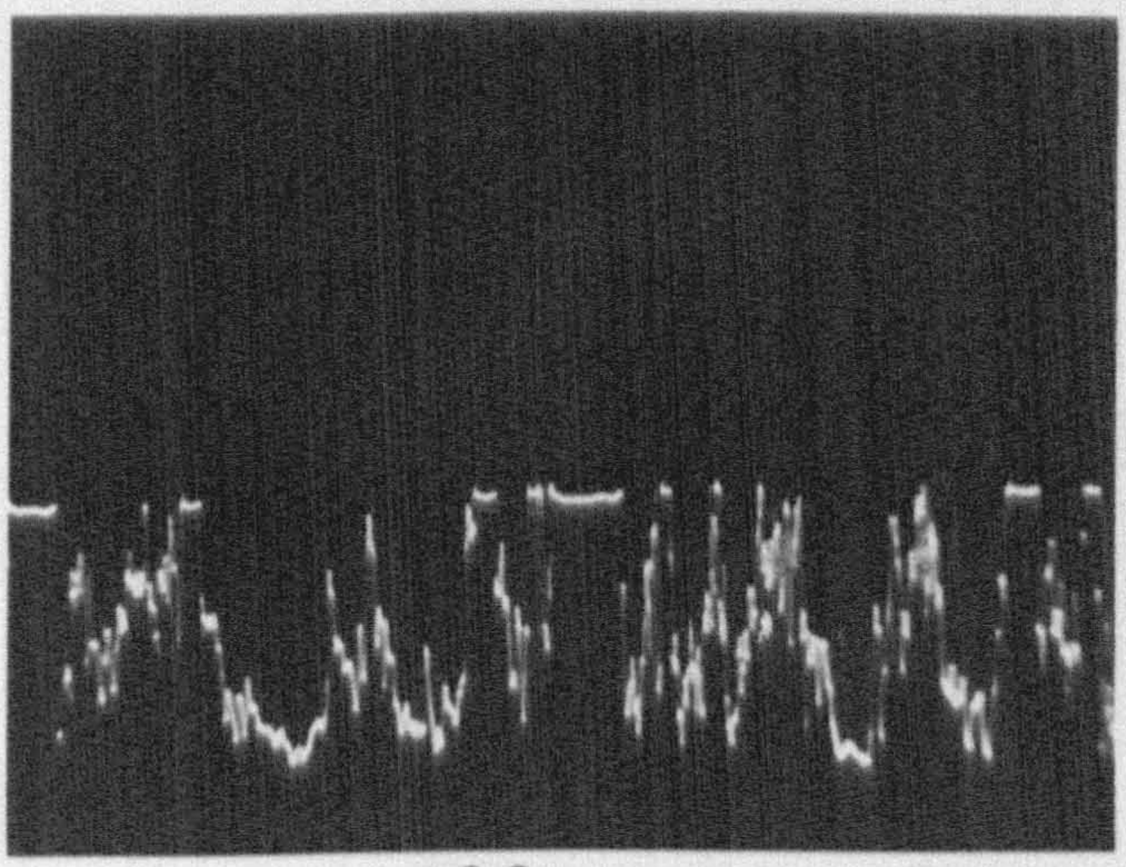

3,500 rpm

(c)

FIG. 3.7 VARIOUS ASPECTS OF THE LINEARISED VELOCITY SIGNAL

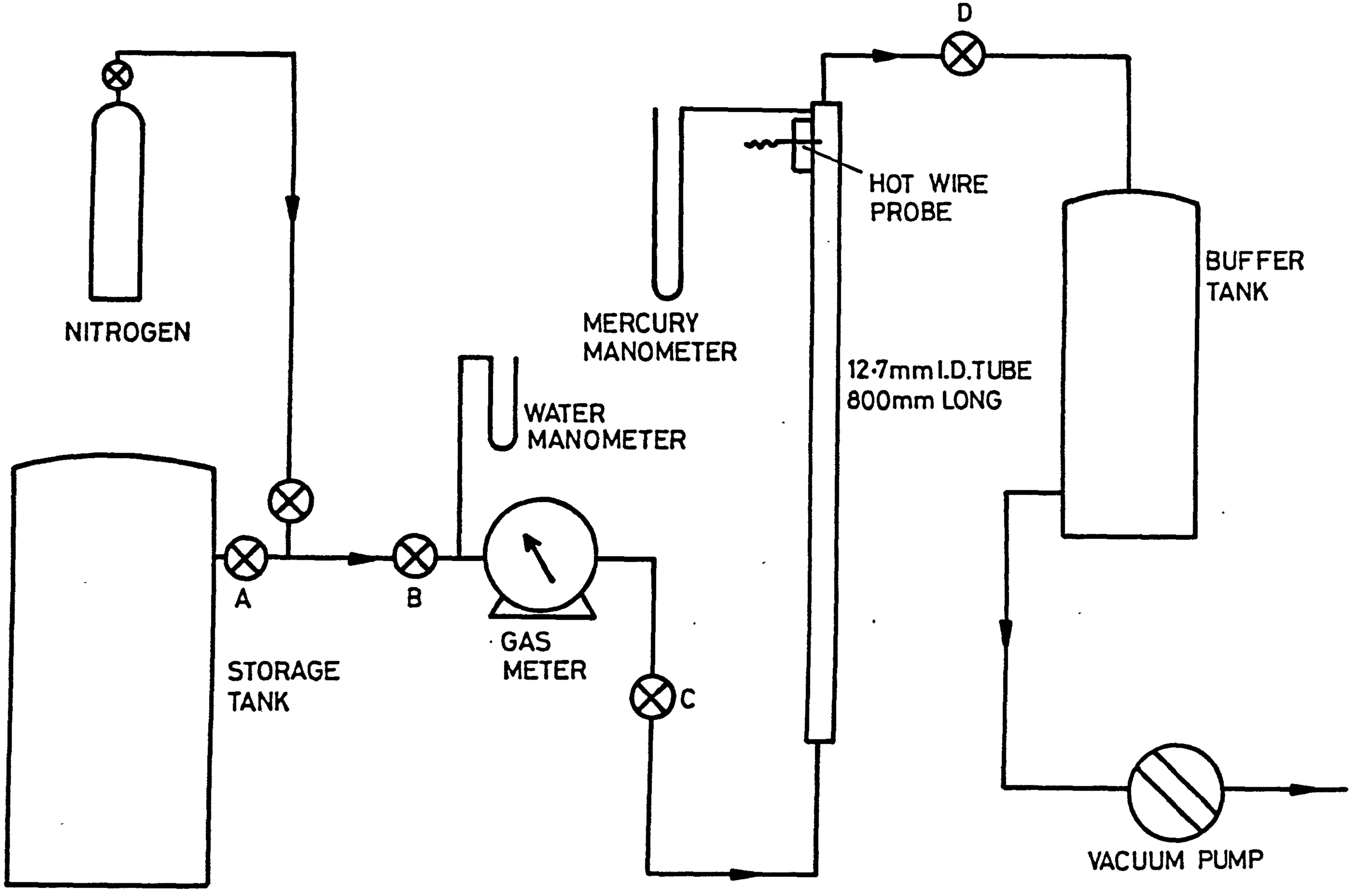

FIG. 3.8 FLOW DIAGRAM FOR THE TUBULAR CALIBRATION RIG

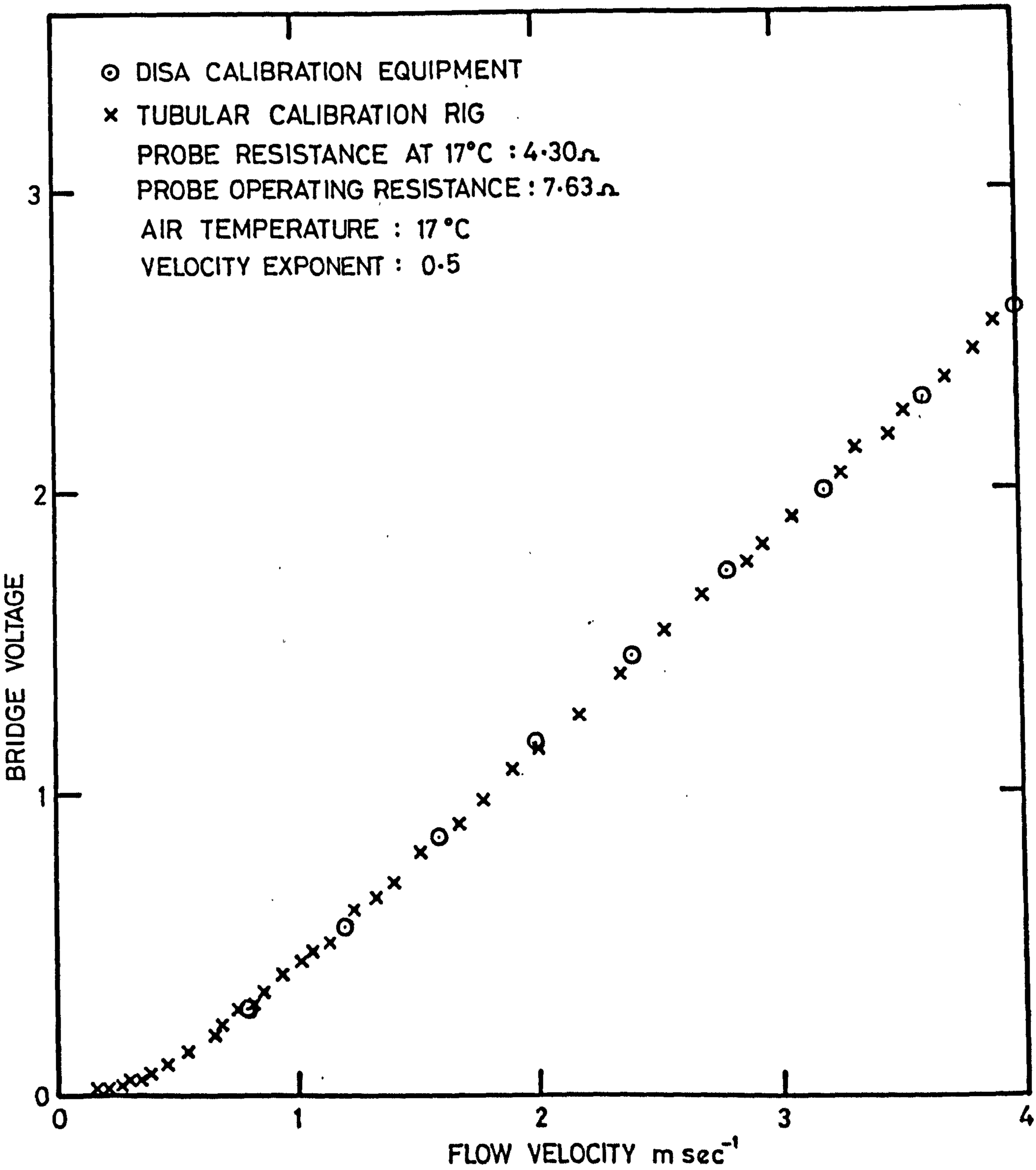

FIG. 3.9 CALIBRATION OF HOT WIRE IN BOTH DISA EQUIPMENT AND THE TUBULAR CALIBRATION RIG

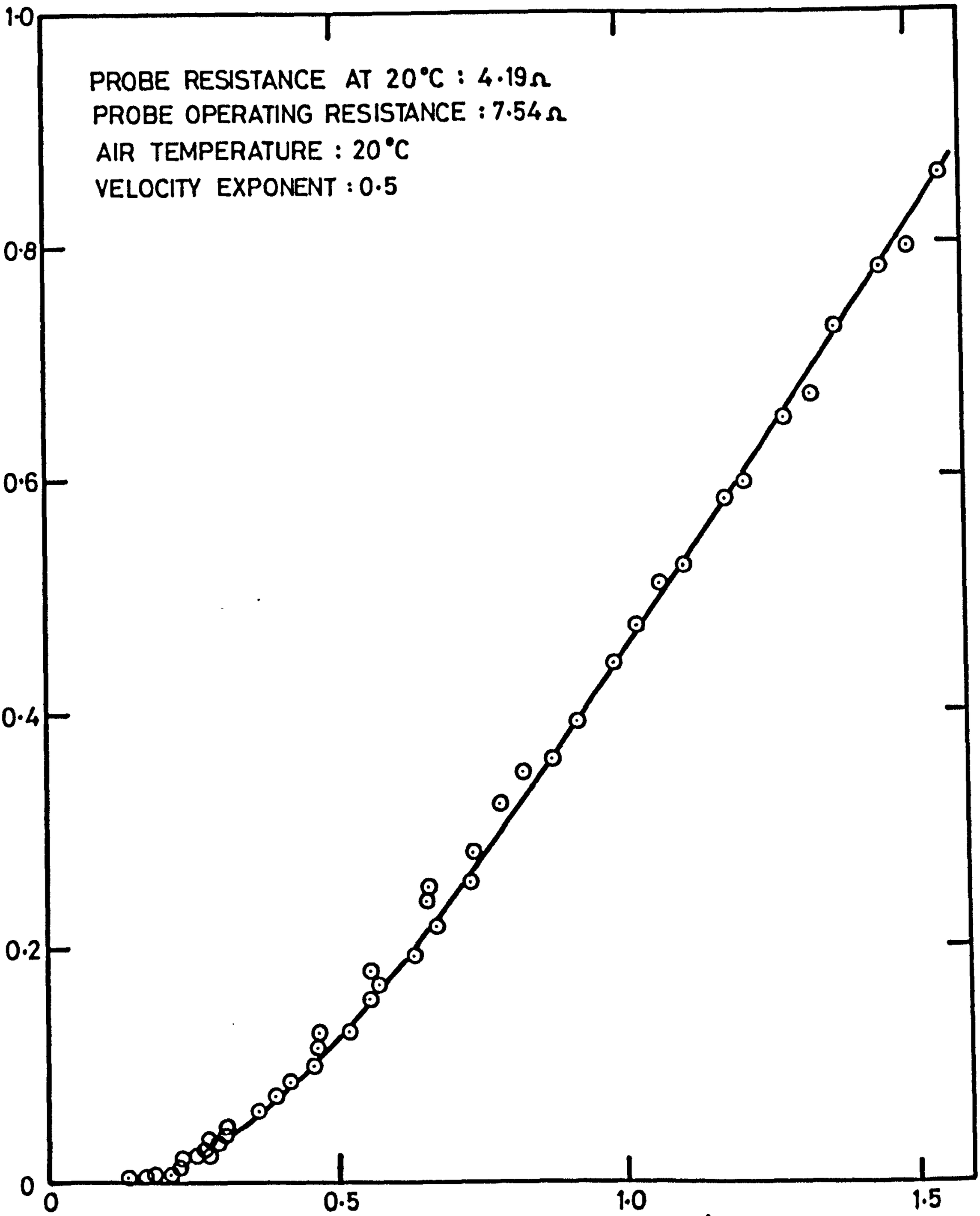

FIG. 3.10 CALIBRATION OF THE HOT WIRE AT LOW VELOCITIES

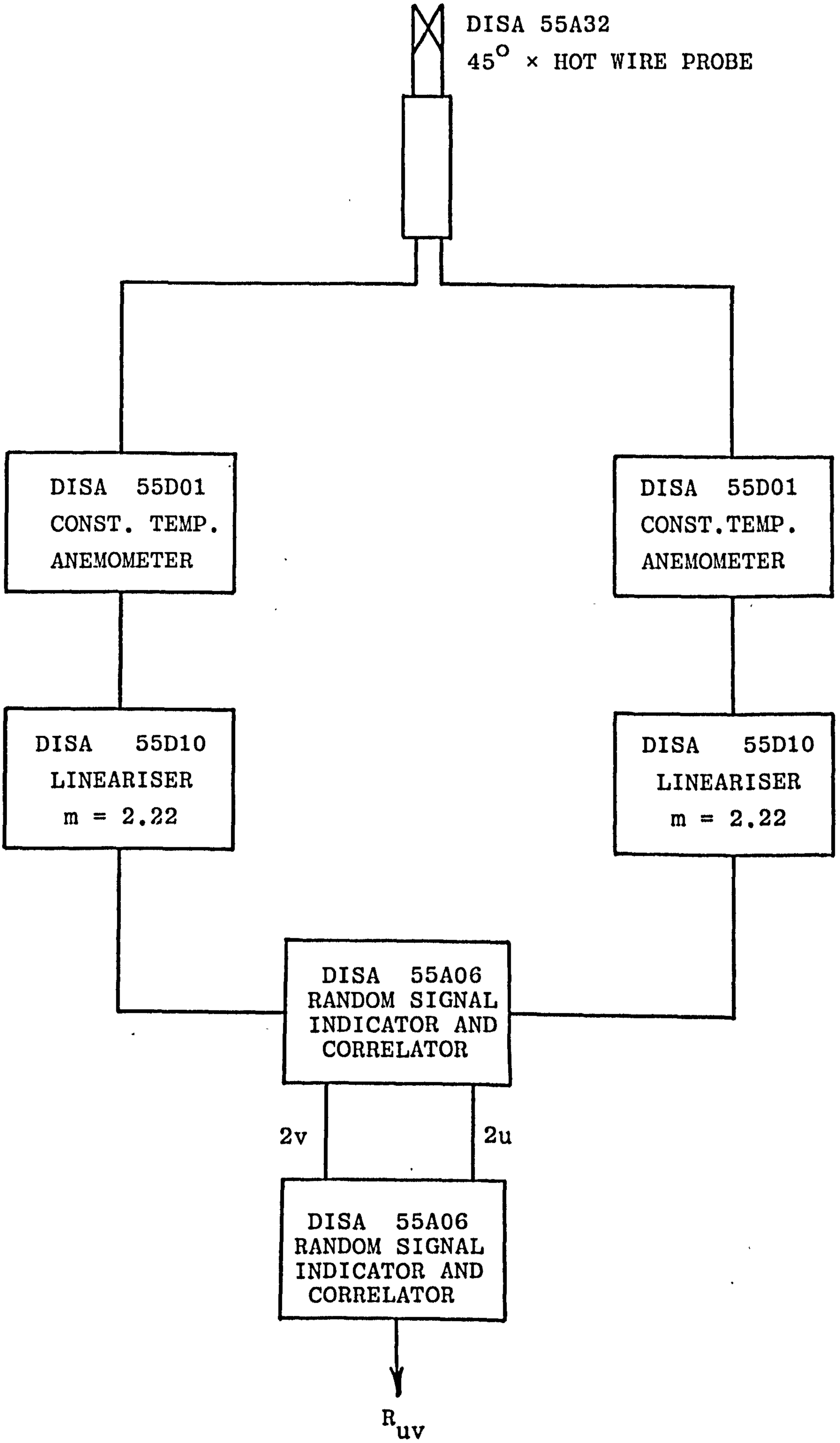

FIG.3.11 EXPERIMENTAL ARRANGEMENT FOR THE MEASUREMENT OF REYNOLDS STRESS

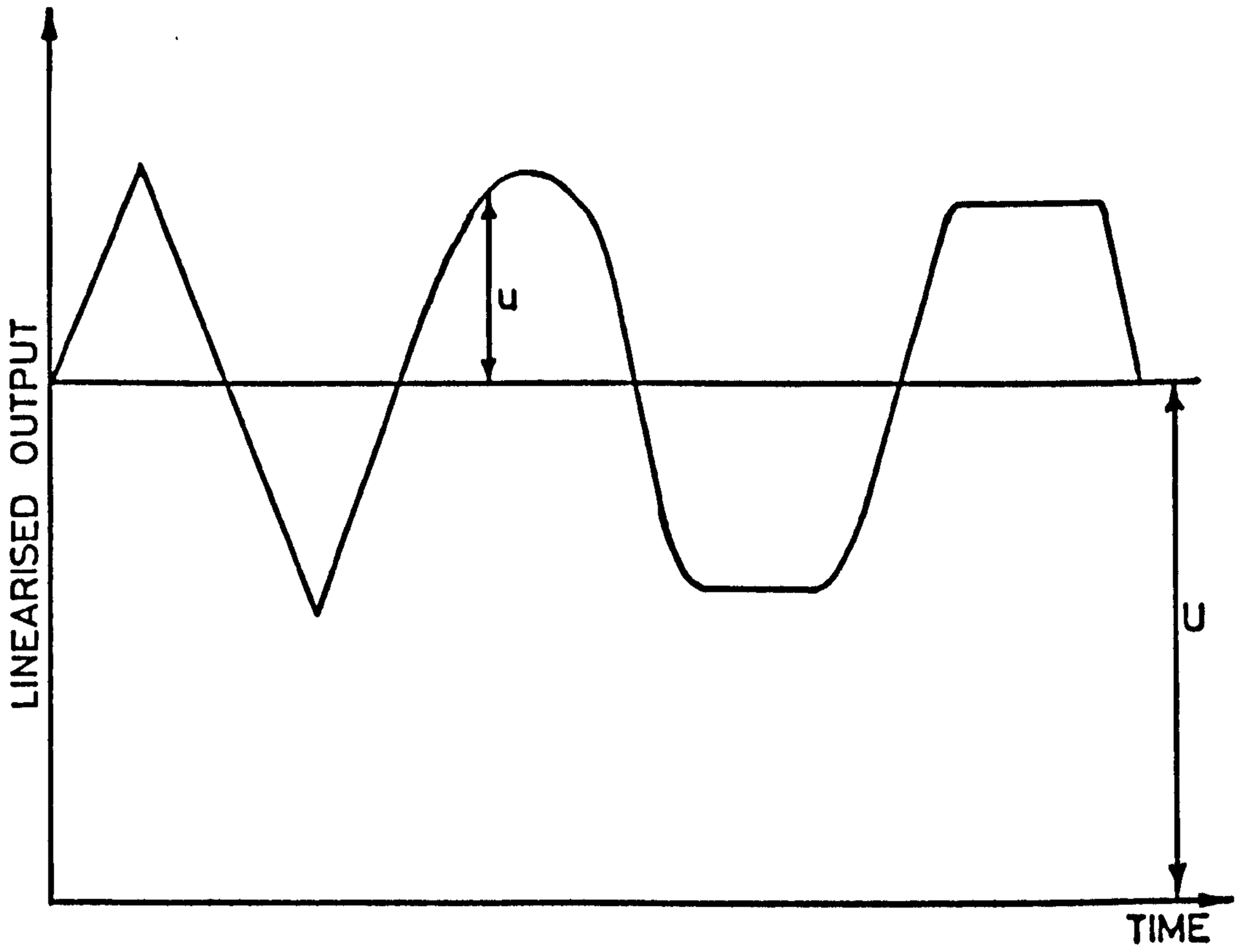

(a) CONVENTIONAL RAW SIGNAL

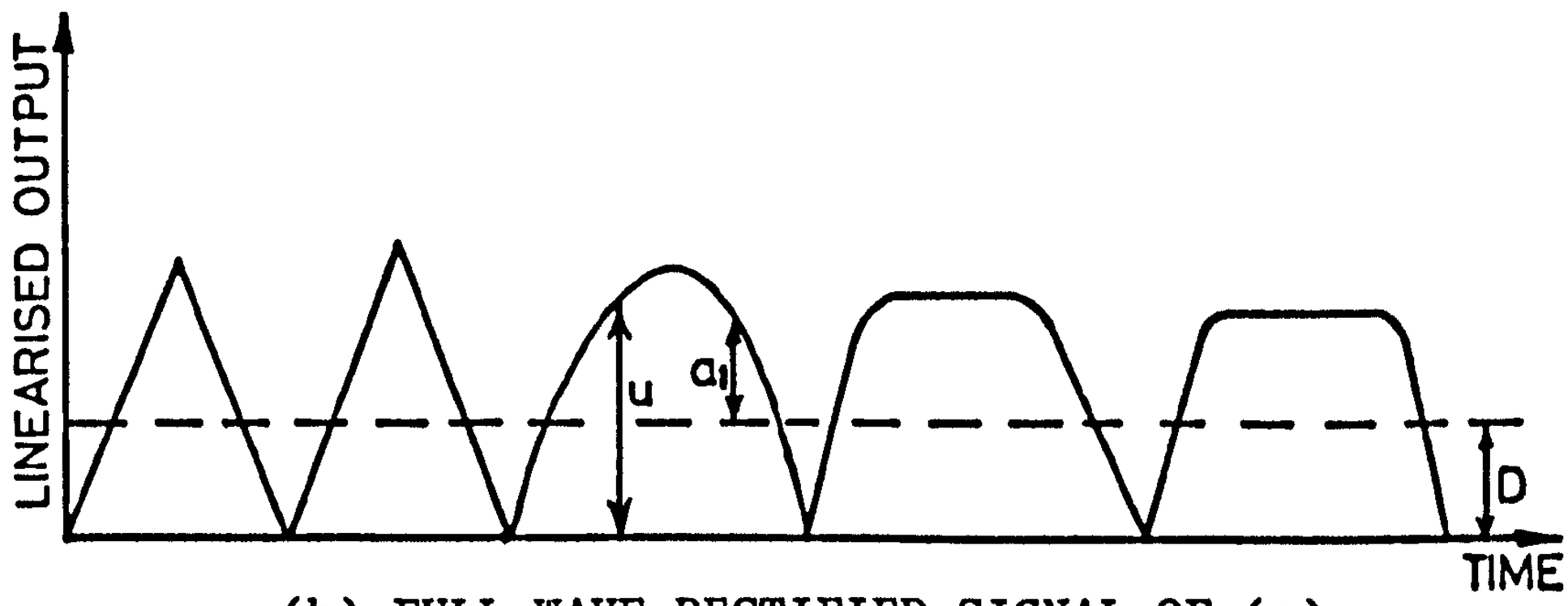

(b) FULL WAVE RECTIFIED SIGNAL OF (a)
BY HOT WIRE BUT WITH NO MEAN FLOW

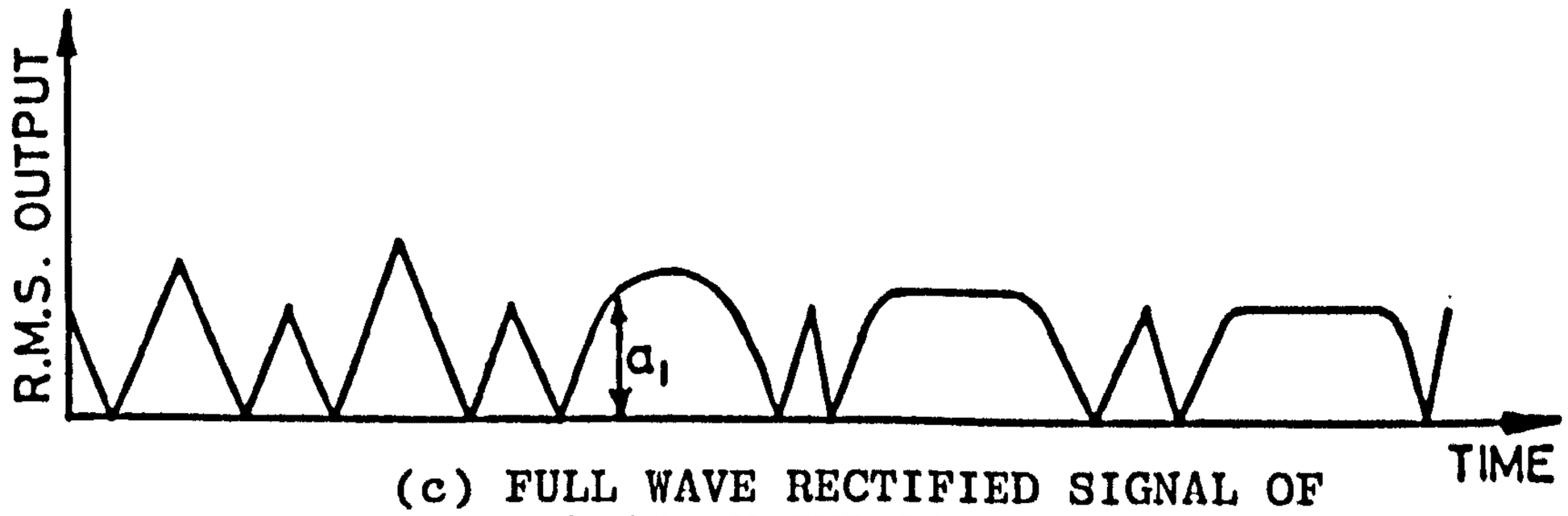

(c) FULL WAVE RECTIFIED SIGNAL OF
(b) ABOUT THE PSEUDO (D)

FIG.3.12 RECTIFICATION OF HOT WIRE SIGNALS

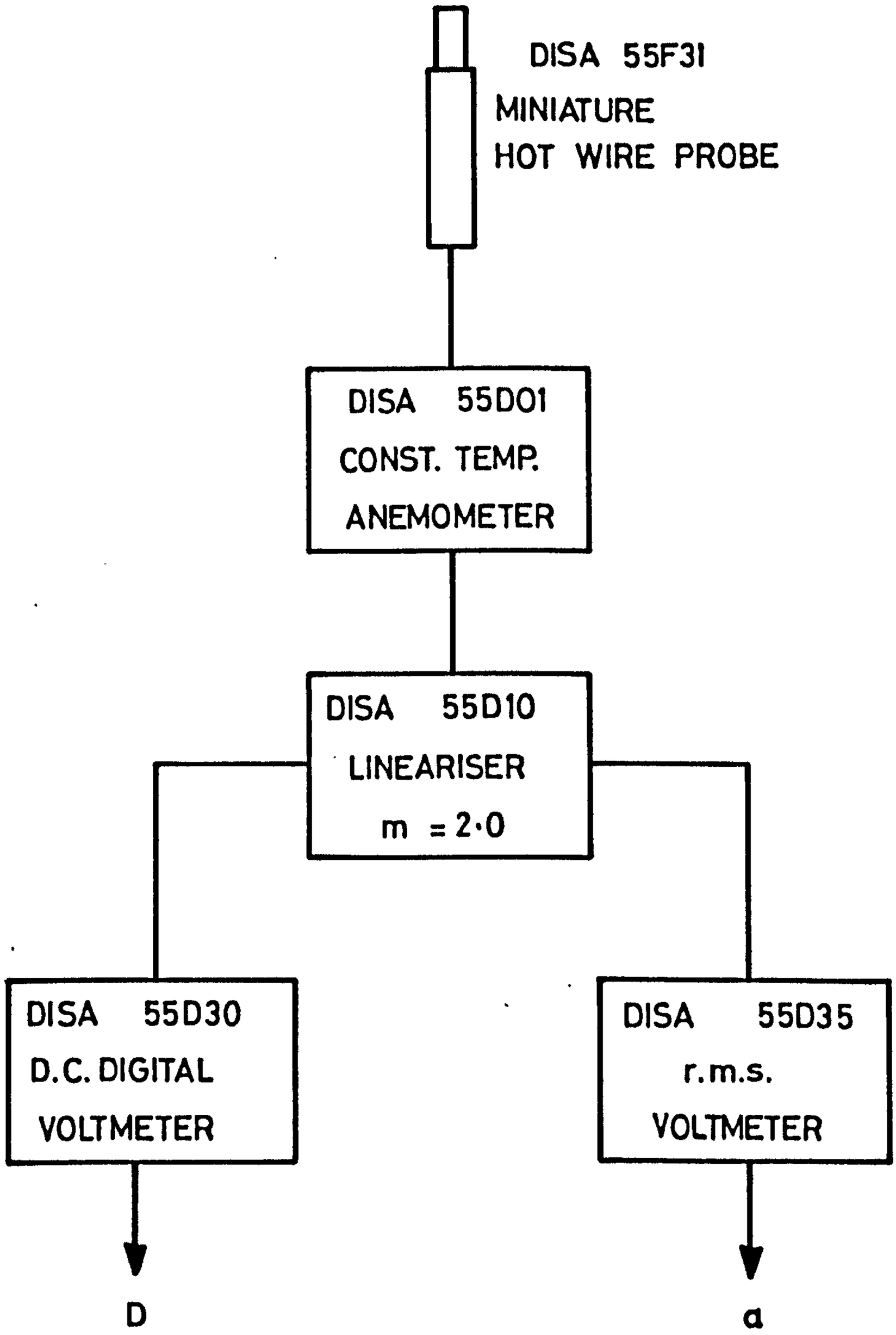

FIG. 3.13 EXPERIMENTAL ARRANGEMENT FOR THE MEASUREMENT OF r.m.s. TURBULENT VELOCITY

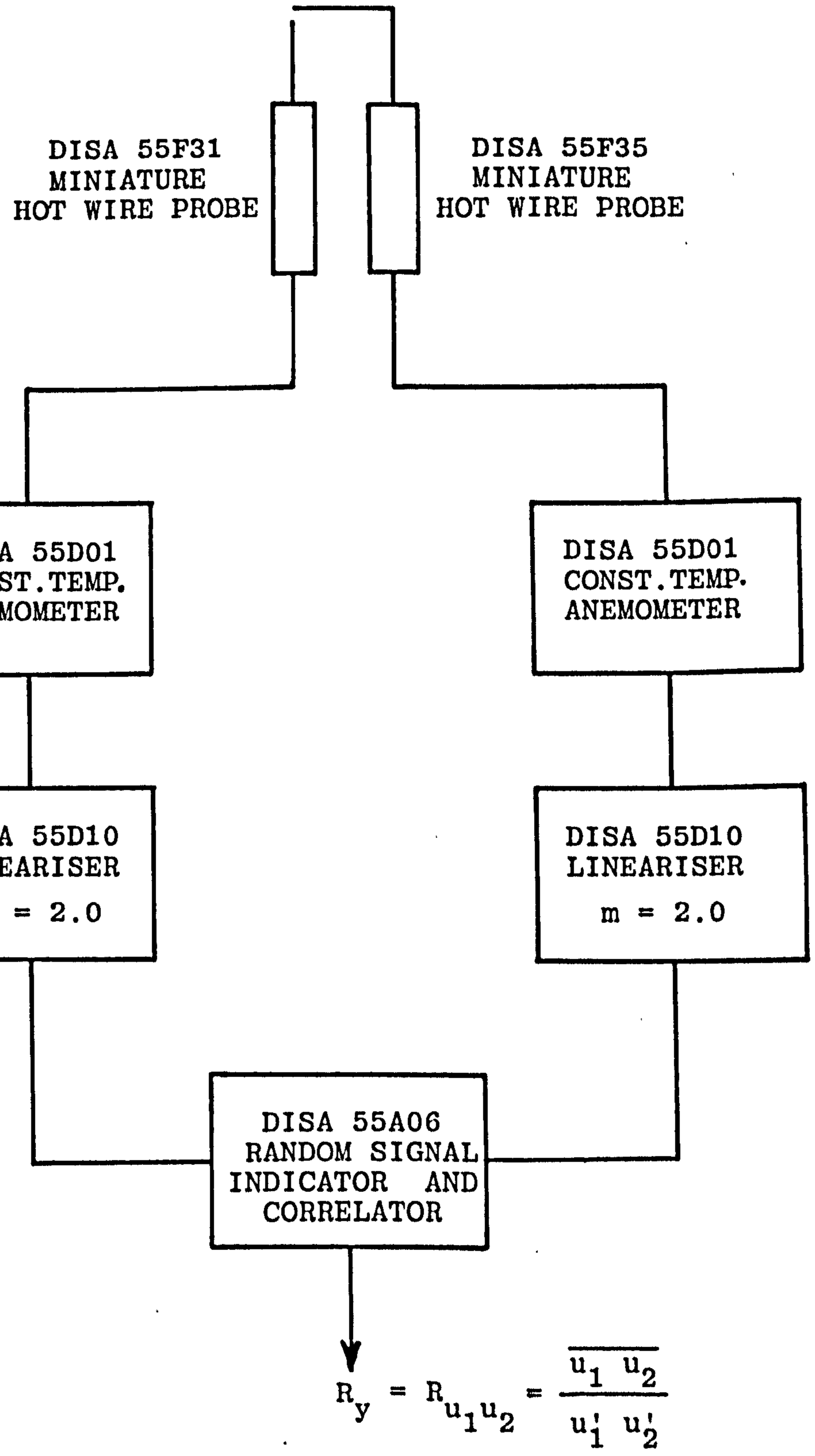

FIG.3.14 EXPERIMENTAL ARRANGEMENT FOR THE MEASUREMENT OF THE INTEGRAL SCALE OF TURBULENCE BY TWO POINT CORRELATION METHOD

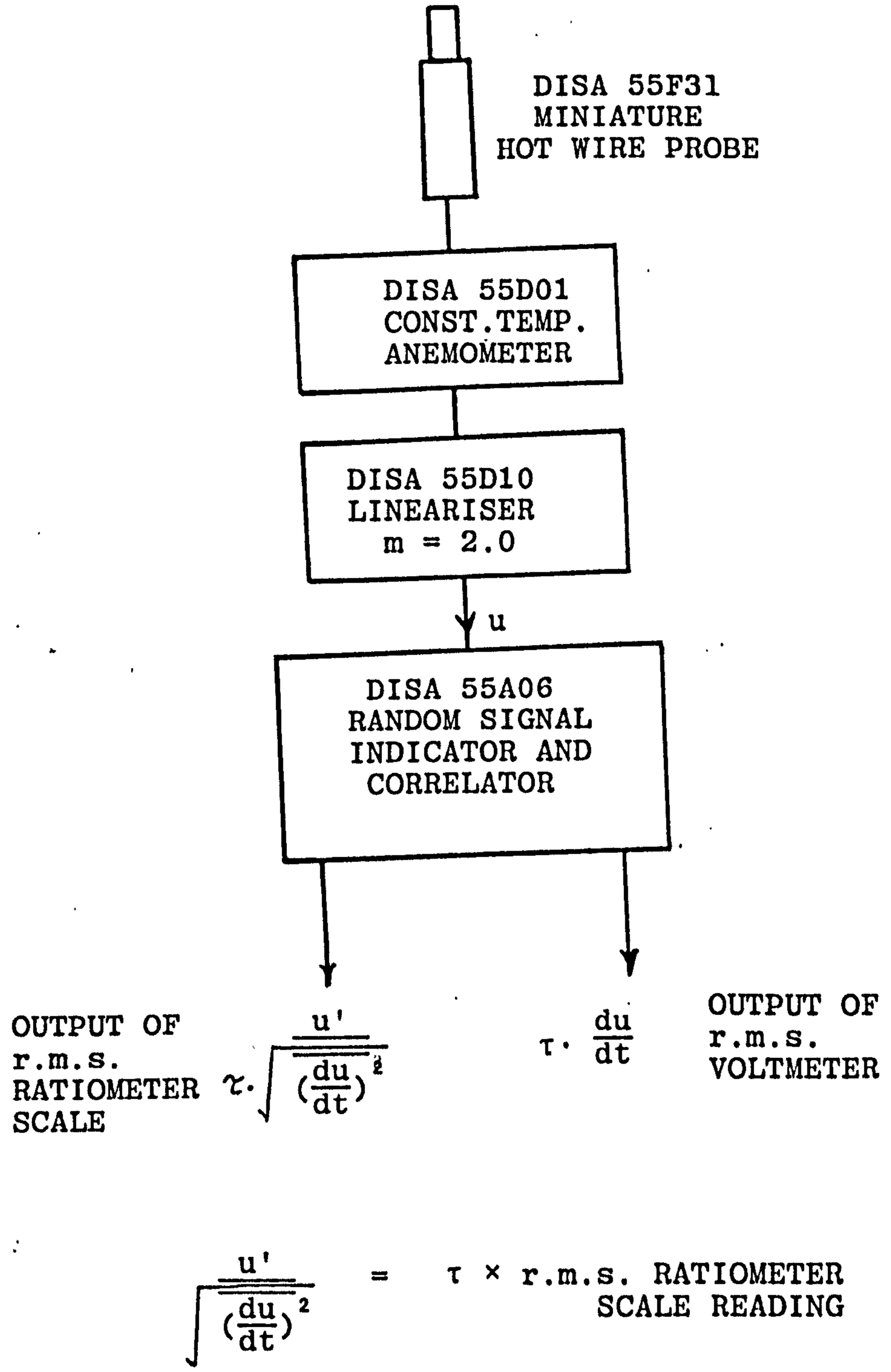

$$\sqrt{\frac{u'}{(\frac{du}{dt})^2}} = \tau \times \text{r.m.s. RATIOMETER SCALE READING}$$

FIG.3.15 EXPERIMENTAL ARRANGEMENT FOR OBTAINING THE FIRST TIME DIFFERENTIAL OF THE VELOCITY SIGNAL AND MEASURING THE VALUE of $\sqrt{\frac{u'}{(\frac{du}{dt})^2}}$

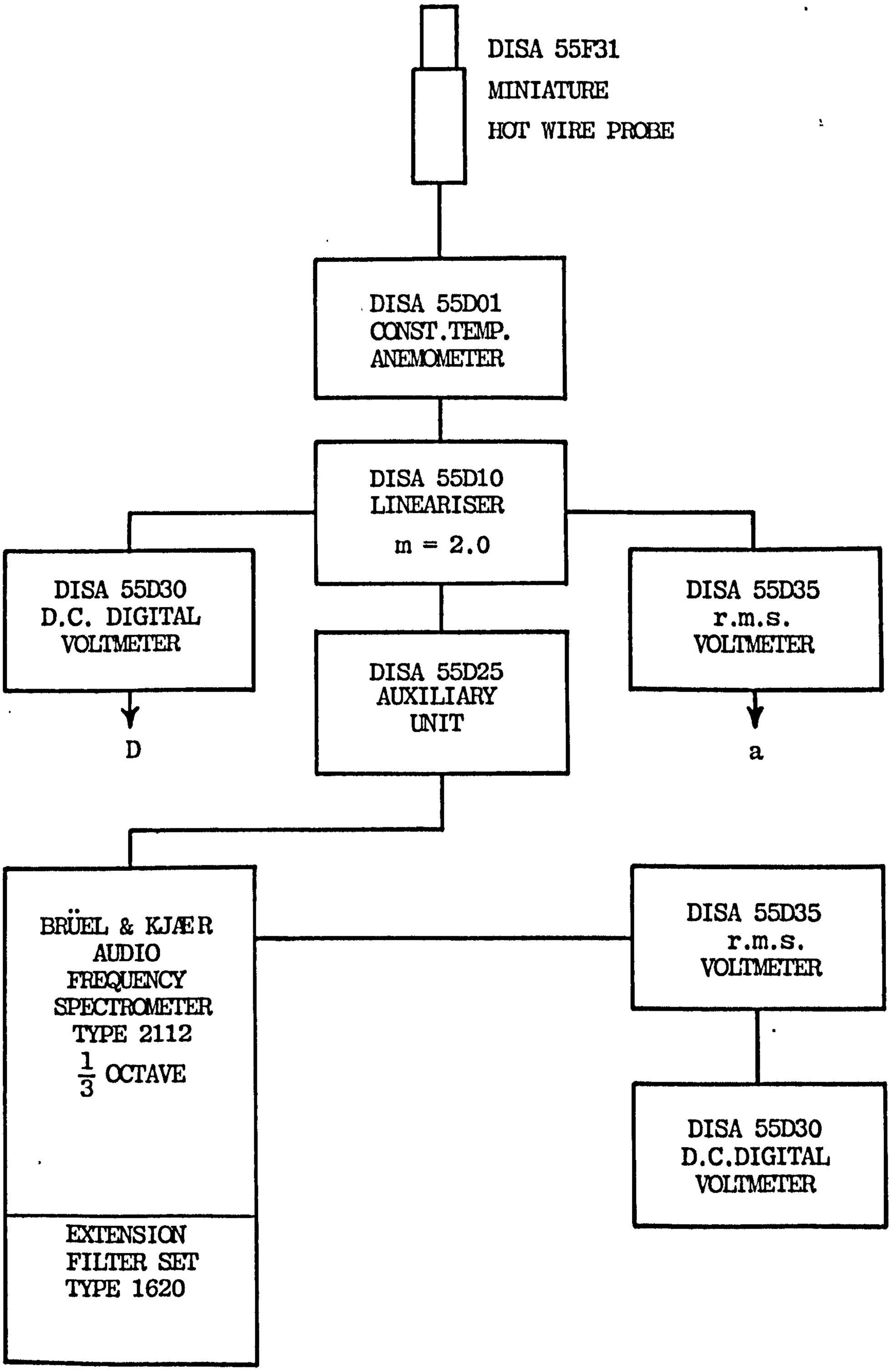

FIG.3.16 EXPERIMENTAL ARRANGEMENT FOR THE MEASUREMENT OF THE INTEGRAL AND TAYLOR SCALES OF TURBULENCE BY SPECTRUM METHOD

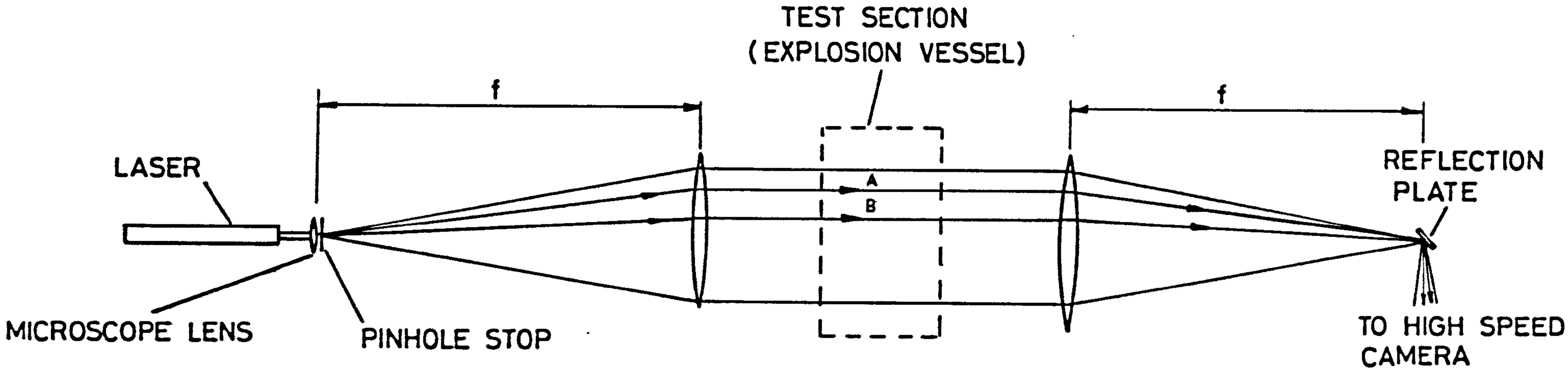

FIG.3.17 REFLECTION PLATE INTERFEROMETER

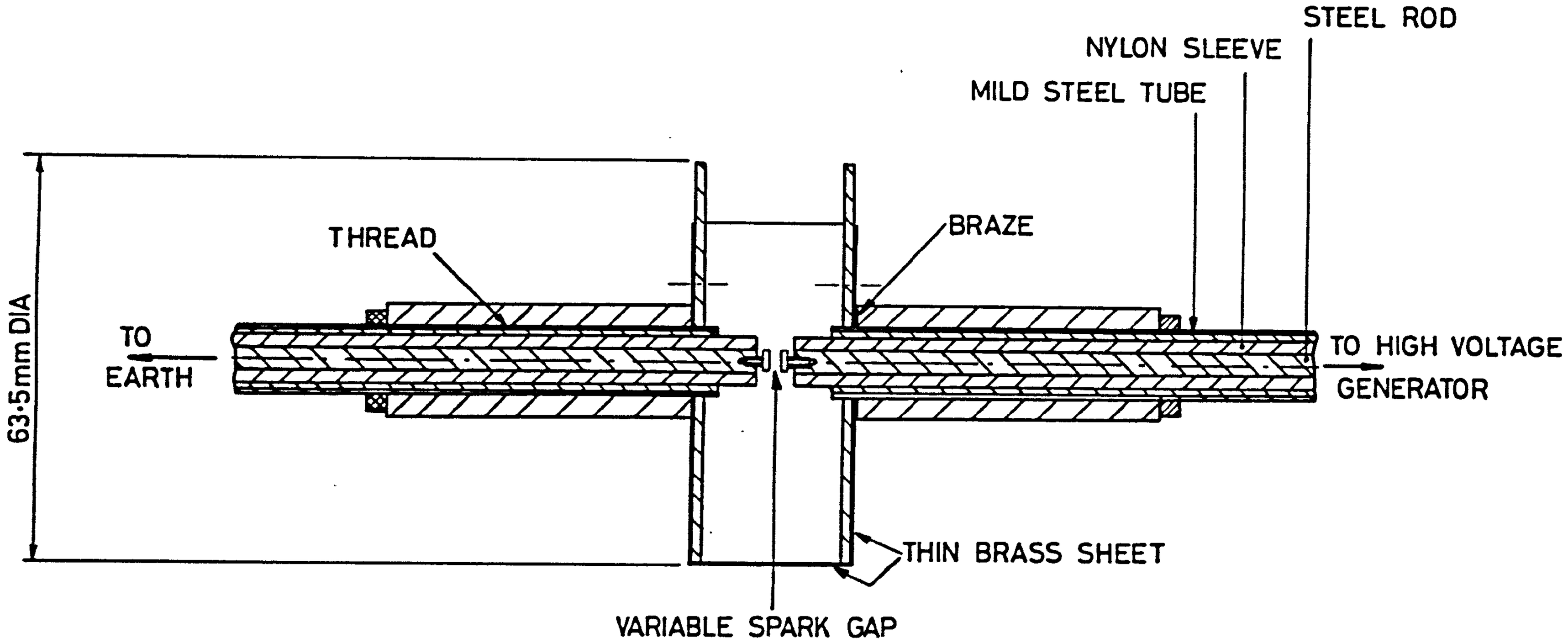

FIG.3.18 ARRANGEMENT OF THE TWO VARIABLE DISTANCE DISCS WITH A VARIABLE SPARK GAP (TULIP A)

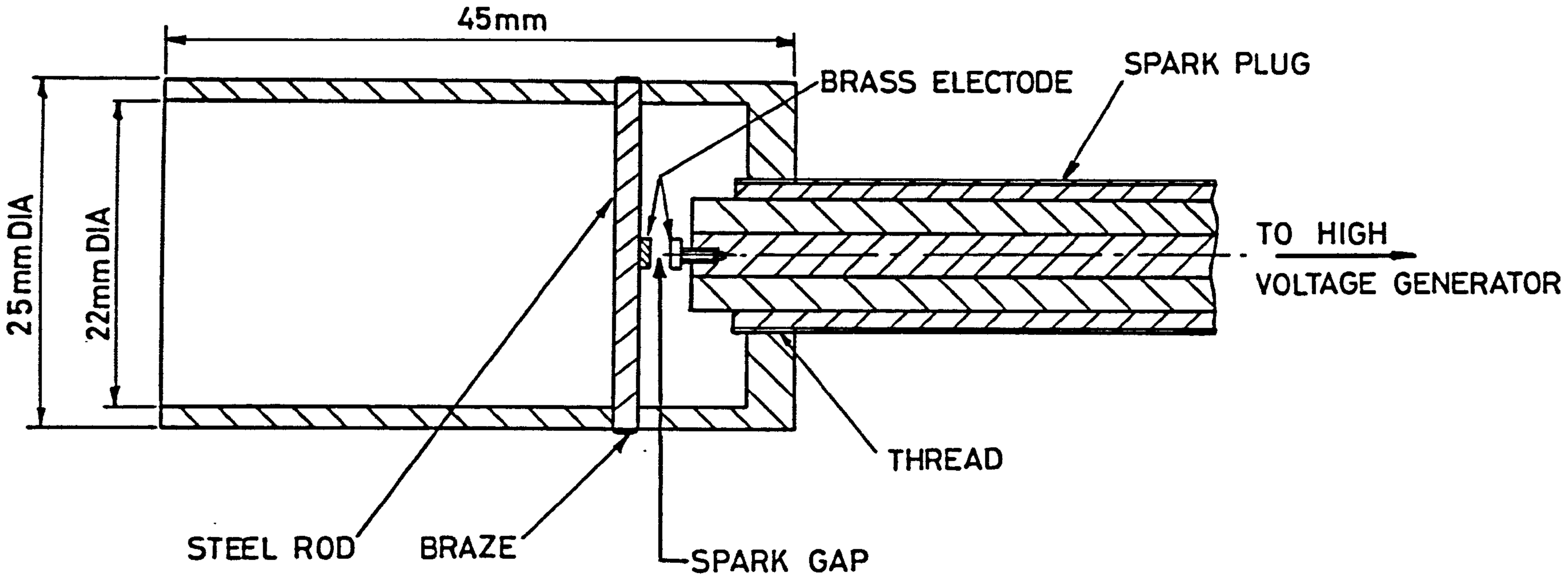

FIG.3.19 ARRANGEMENT OF TULIP B CONNECTED TO THE SPARK PLUG

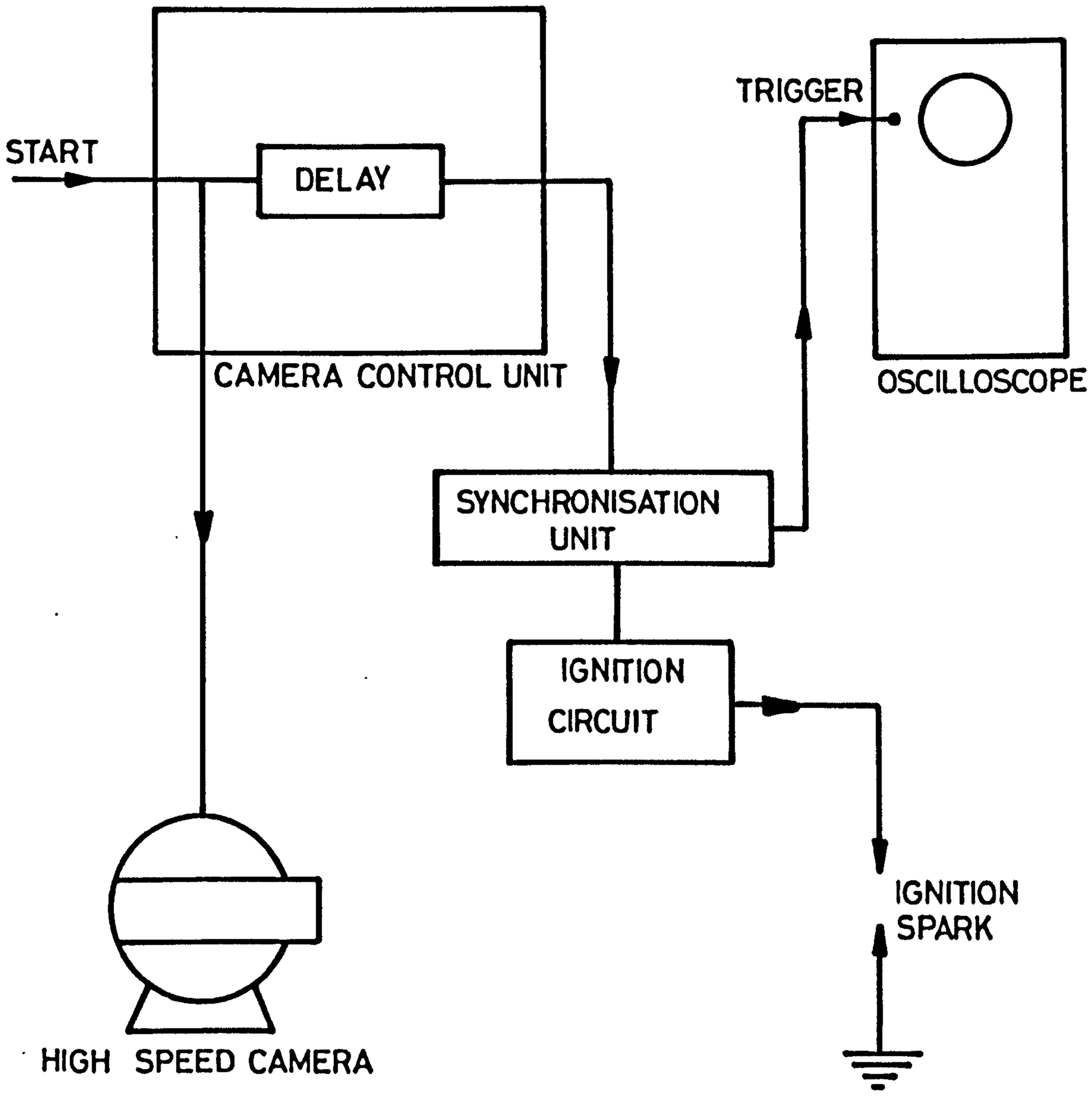

FIG. 3. 20 TRIGGER SYSTEM FROM CAMERA CONTROL UNIT

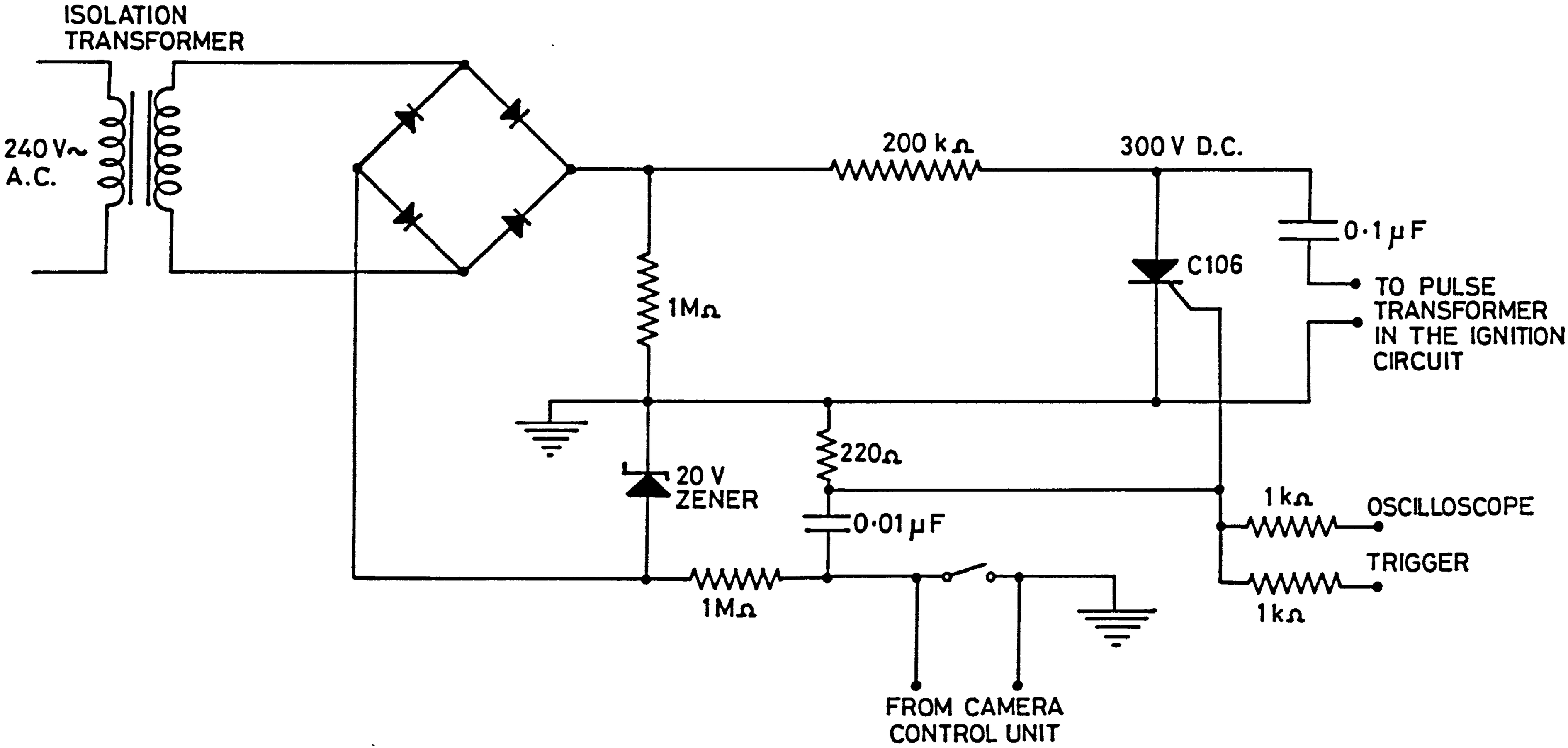

FIG. 3.21 IGNITION CIRCUIT AND OSCILLOSCOPE TRIGGER CIRCUIT

CHAPTER 4

EXPERIMENTAL RESULTS

CHAPTER 4

EXPERIMENTAL RESULTS

4.1 INTRODUCTION

In order to develop theories of turbulent combustion it is necessary to have accurate measurements of such parameters as burning velocity and propagation limits and a knowledge of how they correlate with turbulent and chemical parameters.

This Chapter describes the experimental investigation of turbulent flame structure and its propagation. Measurements are reported of cold gas turbulent parameters for both air and a range of hydrogen-air mixtures at atmospheric and subatmospheric pressures. Also reported are results on the effect of turbulence on ignition, propagation limits, and turbulent quenching of propagating kernels of methane-air and hydrogen-air mixtures. From these results physical pictures emerge which enhance the understanding of turbulent reacting flows and these are discussed further in Chapter 5.

4.2 THE STRUCTURE OF TURBULENCE IN THE EXPLOSION VESSEL

The vessel turbulence was produced by four identical high speed fans, running at the same speed, and driven by one horsepower d.c. motors (Figs. 3.1 and 3.3). Such a system has the advantages of producing a significant volume of gas with uniform, isotropic turbulence, at values of turbulent Reynolds number comparable to those achieved in practical combustion chamber (1,2).

Andrews (3) showed that in the present vessel the turbulence is isotropic up to a radius of at least 75 mm for all fan speeds. He (3) investigated the variation of u' with radial distance at various fan speeds, in both horizontal and vertical directions and concluded that a volume with a constant value of u' existed at the centre of the vessel. This volume decreased as the fan speed increased, but even at the highest fan speed was sufficiently large for the valid determination of burning velocity.

4.2.1 R.M.S. Turbulent Velocity

Measurements of r.m.s. turbulent velocity, u', were made in gases at room temperature. A variety of mixtures, with different values of kinematic viscosity, ν, were used in the calibration. For an anemometer wire at the centre of the vessel, the variations of u' obtained from Eqs. (3.5) and (3.8) with fan speed are shown by the

full line in Fig. 4.1. These were the same for air at both one and a third of an atmosphere, and for hydrogen-nitrogen mixtures with 20%, 30% and 40% of hydrogen at one atmosphere pressure.

Andrews (3) and Lwakabamba (4) measured variations of u' with fan speed for the same vessel and fans, but no allowance was made for the effect of hot wire rectification. Accordingly, u' was based only on the a.c. component, a, in Eq. (3.5). The results so obtained and reported by Lwakabamba (4) are shown by the broken line in Fig. 4.1. Clearly, their neglect of rectification effects resulted in an underestimation of u'.

Semenov (2) in his analysis of fan turbulence in closed vessels, studied the effect of pressure. Measurements were made in air and in hydrogen at pressures ranging from 0.13 to 1 atmosphere. The r.m.s. turbulent velocity, u', was measured by a hot wire anemometer. These measurements showed u' to have but slight dependence on pressure for a given fan speed, and are in line with the present results.

4.2.2 Length Scales

The integral scales, L, were measured for air at atmospheric and at a third of an atmosphere pressure, and also for hydrogen-nitrogen mixtures at atmospheric pressure, by the two point velocity correlation technique, described in Section 3.3.3.1. Figure 4.2 shows the variation

of the correlation function, R_y, with wire separation distance, y, for various fan speeds. It can be seen that the correlation function is not greatly affected by fan speed. Graphical integration of the correlation curve yielded the value of integral scale, L.

This variation of L with fan speed is shown by the full line in Fig. 4.3. This curve was the same for both air and the mixture of 40% H_2 at atmospheric pressure and also for air at a third of this pressure. Thus the value of L appears to be independent of kinematic viscosity, ν.

Semenov (2) also made measurements in air and hydrogen at pressures from 0.13 to 1 atmosphere. The r.m.s. turbulent velocity, u', was measured by hot wire anemometer, whilst the turbulent diffusivity, ε, was derived from the heat flux from a hot body and the temperature gradient. The Lagrangian scale, L', was calculated from the expression

$$\varepsilon = u' L' \qquad (4.1)$$

These measurements showed the Lagrangian scale to vary with $(\text{pressure})^{-0.4}$ and to be slightly dependent on the molecular properties of the gas. Figure 4.3 shows no such effects on the value of L.

It is not surprising that the value of L has but slight dependence on fan speed (2,5). The fans principally produce turbulence by eddies shed from the blade edges and the dimensions of the eddies are mainly a function of

fan blade geometry. Thus, the only means for achieving a significant variation of L would appear to be through the use of fans of different blade geometry.

With a value of ν of 15.74×10^{-6} m^2 sec^{-1} for air and 24.06×10^{-6} m^2 sec^{-1} for the 40% H_2-60% N_2 mixture, which was computed from the programme given in Appendix 1, values of R_L were obtained for different fan speeds, and these are shown in Fig. 4.4.

The Taylor microscale, λ, was obtained by fitting a parabola through the peak region of the two point correlation curve. The parabola also passed through the maximum value, as shown in Fig. 4.5. The variation of λ with fan speed is shown in Fig. 4.6.

The variations with fan speed of time length scales, obtained by Andrews (3) from autocorrelation measurements, are shown in Fig. 4.7 for L_t and Figs. 4.8 and 4.9 for λ_t. As discussed in Chapter 3, values of L and λ were obtained by multiplying these values by the velocity u', measured in the present work and such values are shown in Figs. 4.3 and 4.6, respectively.

The normalised power spectral density function, F(n), versus central frequency, n, was obtained, as described in Chapter 3 and the results are shown for different fan speeds in Figs. 4.10 and 4.11. Also shown in Fig. 4.10 is a line of -5/3 slope which represents the energy distribution predicted by Kolmogrov (6) from

dimensional analysis for the inertial subrange. Tennekes (7) has predicted a frequency distribution with this slope for isotropic turbulence in the absence of mean flow. Also shown in the figure is a line of -7 slope which represents the energy distribution predicted by Heisenberg (8) for the viscous dissipative régime. Figure 4.10 shows that the power spectral density measured in the present vessel has regions corresponding to these two power laws.

The values of length scales L and λ obtained from the distribution of power spectral density with frequency are plotted against fan speed in Figs. 4.3 and 4.6, respectively. It might be expected that both the auto-correlation and the power spectral density function methods would give the same values of length scales, since the power spectral density function and the autocorrelation function are Fourier transform pairs (9). Either can be obtained by transforming the other. Also both methods employed the assumption that U=u'. Figures 4.3 and 4.6 show that the values of L obtained from spectral analysis are higher than those obtained from autocorrelation measurements, but that the two sets of values of λ are in good agreement.

The creation of turbulence by fans in closed vessels has several advantages over its creation in continuous flow systems. On the other hand, some problems arise with the former method due to the rectification of the velocity fluctuations by the hot wire, as demonstrated in Chapter 3.

It might be expected that in the two point correlation method, the rectified electrical signals would not give the same correlation coefficient as would the associated values of velocity. Figure 3.12 shows the former to have a higher frequency than the latter. The rectification will reduce the correlation coefficient for the two signals, and hence the apparent integral length scale. On the other hand, the values of λ are based upon a small separation of the wires and the rectification of the two signals is relatively less important for these measurements.

Equation (3.5) shows, for the case of the full energy spectrum, the importance of the d.c. component contribution to the turbulent energy. In this case the d.c. component can be measured. However, when a spectral band energy is to be measured there are no means of obtaining the associated d.c. contribution. Because of this omission integral length scales, obtained by an extrapolation to zero frequency of the value of F(n) and the use of Eq. (3.18) will be too low, as pointed out by Semenov (2).

Ohta et al (5) in their studies on a fan-stirred bomb attempted to overcome these difficulties by the use of an electronic circuit to reverse the polarity of the linearised output signal each time it reached a zero velocity value. In this way the signal was de-rectified. These workers reported values of L, but not the method of measurement.

The use of three different techniques for the measurement of L, reveals limitations in all of them, primarily because of problems arising from rectification of the anemometer signal. It is probable that all values are too low and the present results lead to the further researches of McMahon (10) in this measurement problem. Figure 4.6 reveals a greater agreement in values of λ obtained by the different techniques. There appears to be no problem in obtaining accurate values of u'.

4.3 THE MEASUREMENT OF TURBULENT BURNING VELOCITY

A photograph of a typical approach of two turbulent flame kernels is shown in Fig. 4.12; there was not much flattening of the kernels as they approached each other, in comparison with that shown in Fig. 4.13 for the laminar case. This was in line with the fact that although the flame speed increased with the turbulence, the gas velocity did not increase to the same extent (1).

Values of u_t were obtained by measuring the separation distance between those segments of the kernels which approached each other along a common normal. This has been described in detail by Andrews and Bradley (11). A typical plot of kernel separation distance against time is shown in Fig. 4.14 for a 30% H_2-air mixture at 2000 r.p.m. The rate of decrease of this distance with respect to time at the instant just before contact is equal to twice the burning velocity, u_t. Andrews and Bradley (11) reported that one of the difficulties of this technique

was that of spark synchronisation. However, because of the increase in ignition delay time with fan speed, even though the flame speed increased differences in timing of the two sparks were relatively unimportant and the ignition circuit gave a sufficiently short time interval between the two sparks.

For the reasons given in Chapter 1 measurements were required at high values of u_ℓ. They were made over the range of 15% to 40% hydrogen-air mixtures at an initial pressure of one atmosphere. The results are given in Table 4.1. Values of u_ℓ for H_2-air were taken from Andrews and Bradley (11) and these reached a maximum of 3.48 m sec^{-1} for 40% H_2-air.

With the objective of attempting to obtain the greatest generality for any theories or empirical expressions for turbulent burning, some 10% CH_4-air explosions were carried out at subatmospheric pressures of 0.25 and 0.5 atmosphere. These results also are given in Table 4.1. Values of u_ℓ again were taken from Andrews and Bradley (11).

The pressure records in all cases confirmed that burning velocity measurements were made before there was significant increase in pressure. In the case of H_2-air mixtures low amplitude high frequency oscillations were observed on the pressure records in the range of 30% to 40% H_2.

4.4 THE EFFECT OF TURBULENCE ON IGNITION AND PROPAGATION LIMITS

Although near-limit mixtures of gaseous fuels and air could be ignited successfully under laminar conditions, this becomes more difficult under turbulent conditions (12-17). The régime of ignitability between the lean and rich limits narrowed as the fan speed increased. The influence of turbulence upon spark ignition was the subject of parallel research by McMahon (10). The concern of the present writer was to ascertain whether flame propagation limits existed and, if they did, to define them quantitatively. Because ignition became more difficult with increase in turbulence, the tulips, described in Chapter 3 were used to initiate ignition in a region of low turbulence. The flame emerged from the open end of the tulip into the region of maximum turbulence and high speed photography and pressure measurements were used to ascertain whether or not the flame could propagate in this region. In this way ignition and flame propagation limits were uncoupled.

The variable energy, variable frequency ignition circuit, unit (B), described in Section 3.2.1.2 was used throughout this investigation. Stored spark energies of 3 and 12 joules were used for various types of explosions, with 12 joules for most of the work.

Spark gaps were varied between 0.36 mm and 0.76 mm, with preference for the latter in most of the experiments.

Spark gaps less than 0.36 mm were liable to electrical leakage across the gap whilst for those greater than approximately 1 mm, electrical breakdown was not possible at the maximum available voltage of 2 KV.

Measurements were made with both methane and hydrogen-air mixtures. First, a set of experiments were carried out with tulip A and a variable distance between the two discs, in order to obtain a critical distance. Too large distance between the discs could allow excessive turbulence around the spark plug and thus prevent ignition, whilst too small a distance could give rise to thermal quenching by the walls. The results are given in Table 4.2. A distance of 22 mm was found to be suitable and for this reason the diameter of tulip B was 22 mm.

The lean and rich flammability limits for methane-air are shown in Fig. 4.15 and the conditions in Table 4.3. It is seen how an increase in fan speed, narrows slightly the lean limit but more markedly decreases the rich limit. However, the rich data of runs 2 and 3 show that an increase in the stored spark energy, from 3J to 12J, extends the limits. The rich data for runs 1 and 5 reveal a similar extension, as shown from the two lines on Fig.4.15, when the flame is allowed first to develop under the less turbulent conditions between the discs, before emerging into the fully turbulent region. Slight widening of the limits was observed when the spark gap was increased from 0.36 mm to 0.76 mm. These results are based upon an 80 per cent probability of

ignition and a minimum of 20 sparks at each set of conditions.

Table 4.4 gives the lean flammability limits for hydrogen-air mixtures. These were only obtained for high fan speeds.

4.5 HIGH SPEED PHOTOGRPAHY OF LIMIT FLAMES

The tulip B was used with a 0.76 mm spark gap and stored energies of 3 and 12 J in photographic studies of flame quenching at high tubulence levels. The schlieren interferometery technique was used, since it was found to give a better definition of the flame front than that obtained with the knife edge technique. The fan ran at the highest possible speed of 3,500 r.p.m. The Hitachi camera was used with a speed of 3,000 frames per second, which corresponds to an effective shutter exposure time, of 66.67 μ sec (with the film exposed for one fifth of the running time).

Prints from high speed film of methane-air explosions are shown in Figs. 4.16 to 4.21. The outside diameter of the tulip, visible on the photographs, is 25 mm. Figures 4.16 to 4.21 are three quarters full size. Frames (a) on each figure are for a 13.04% methane-air mixture, the flame of which was just capable of complete propagation at this fan speed. Frames (b) are for a 13.13%

methane-air mixture, the flame of which was incapable of complete propagation and consequently quenched. The nominal spark energy for frames (a) and (b) was 12 J. Frames (c) are for a 13.18% methane-air mixture, giving a quenched flame, from a stored energy of 3 J.

The quoted time is that which elapsed from the time at which the flame emerged from the tulip. Figures 4.16 to 4.18 for times of .07, .27, and .67 m sec, respectively show the initial stages of propagation as the flame moves into the fully turbulent region, and the propagating kernels are very much the same, over the same time interval. Figures 4.19 (a) and 4.20 (a) show a propagating flame at times of 1.20 and 1.53 m sec, respectively, with which it is instructive to compare the non-propagating flame of Figs. 4.19 (b) and 4.20 (b), over the same range of time. In Fig. 4.21 (b) the extinction of the flame becomes clear and the burnt became mixed with the unburnt gases by the action of the turbulence.

Group (c) of the prints is shown for comparison with group (b). Both show quenching flames, but the former with lower spark energies. A change in the spark energy from 12 to 3 J, has had no apparent effect on the quenching mechanism. This is particularly clear from a comparison of Fig. 4.20 (b) and (c).

It was hoped to estimate the effect of turbulence on the ignition delay from the films both with tulip A, without a shield, and in the absence of a tulip but this

attempt was unsuccessful due to the short time resolution of the camera.

4.6 THE STRUCTURE OF TURBULENT FLAMES

4.6.1 Optical Studies of Turbulent Flames

In the present study the Fastax camera was used with framing speeds of between 3,000 and 6,500 frames sec^{-1}. The higher framing speeds were used for the mixtures of higher burning velocity at high levels of turbulence. The Hitachi camera also was employed at a framing speed of 3,000 frames sec^{-1}, for slow methane-air mixtures close to the propagation limit. The P.C.D. 'X-Y' Digital Data Reader was used in measurements of the films.

Some prints at the flame front from the ciné films for 10% CH_4-air explosions obtained using the wire schlieren technique, are shown in Fig. 4.22 (a)-(c). These prints are taken from the Thesis of Lwakabamba (4). The corresponding values of fan speed and film exposure time are given in Table 4.5. The distance, along the vessel centreline diameter, between the spark plug and the hot wire probe, shown in these photographs, is 38.1 mm and Fig. 4.22 has a magnification of about 1.2. The wire diffraction schlieren interferometer technique was found to give good flame structure definition, which, of course, is dependent upon the existence of temperature gradients.

The photographs show clearly the dominance of a

large scale eddy structure up to a fan speed of approximately 1,500 r.p.m. for 10% CH_4-air mixture. Lwakabamba (4) has shown these eddies to have a size comparable to that of the integral scale of cold gas turbulence. As the speed of the fans was increased further, the small scale structure became more dominant. Chomiak (18) and Lwakabamba (4) have shown experimentally that these small eddies, or veins, have a size close to that of the Kolmogorov microscale.

Careful examination of the behaviour of the small eddies close to the edge of the flame front shows them, illustrated in Fig. 4.23, to appear as veins or tubes, which sometimes detached themselves from the surface of a large eddy. The differences in temperature between these veins and their environment were sufficient to enable them to be optically visualised.

Figure 4.23 (a)-(c) shows the typical behaviour of the veins, from appearance to disappearance, over several frames of the ciné film. Part (a) shows the movement of two veins, each at the edge of a flame front, as the two kernels approach each other, for a 20% H_2-air mixture at 2,000 r.p.m. Part (b) shows the movement of a vein at the edge of a flame front, for a 10% CH_4-air mixture at 1,500 r.p.m. Part (c) shows the movement of a vein with respect to a large cell, for 10% CH_4-air mixture at 3,000 r.p.m. This was also close to the edge of the flame front. The quoted time is that which elapsed from the time at which the vein first appeared. Also shown in part (b) of

the figure, is the movement of the flame front. This is not shown in parts (a) and (c) for reasons of clarity.

From Figs. 4.22 and 4.23 and the many other ciné films analysed, the following picture emerged of the behaviour of these veins:

(i) Long veins appeared with a length of usually eight to twelve times the diameter. The size remained unchanged during the apparent lifetime.

(ii) There was no appearance of flame propagation along either the length or the radius.

(iii) If these are dissipative eddies, as would be suggested by their association with the Kolmogorov microscale, then the temperature difference between them and their environment, which is necessary to render them visible, is perhaps maintained by continuing chemical reaction.

(iv) They move spatially with a velocity close to that of the gas velocity ahead of the flame front.

(v) Their number 'density' on the film increases with fan speed, for a given mixture.

4.6.1.1 Measurements of Apparent Small Eddy Lifetime

The apparent lifetime of the veins or small eddies, t_ξ, were obtained by identifying a certain small eddy close to the edge of the flame front and noting the number of

frames from its appearance to its disappearance. This range of frames was then converted to a time scale from the film speed. The whole procedure was repeated for a number of small eddies on each explosion film.

Figure 4.24 shows the mean apparent lifetime of the veins measured from the explosion films for the following mixtures:

13.11% CH_4-air at one atmosphere.

10% CH_4-air at 0.5 atmosphere.

20%, 30%, and 40% H_2-air at one atmosphere.

The figure shows that the lifetimes of the small eddies generally decrease, as the fan speed increases. There is also a general trend for the apparent lifetime to decrease as the laminar burning velocity increases. It was found for 40% H_2-air mixtures at a fan speed of 3,500 r.p.m., lifetime of the small eddies became small, and an edddy only appeared on a single frame. In this case the lifetime was taken to be that corresponding to the half-frame time. Values of u_ℓ in the figure were taken from Andrews and Bradley (11,19).

4.6.1.2 Measurements of Small Eddy Density

Figure 4.22 (a)-(c) shows that the number of small eddies increases with fan speed. The number density of these eddies, Y, should roughly correspond to the area occupied by these eddies. Hence, the number of discrete

small eddies per square inch was counted by eye, on the screen of the Reader, close to the flame front and at different positions within a single frame of film. This was repeated for different frames and average values were obtained to give the points plotted in Fig. 4.25. Measurements were made for 20%, 30%, and 40% H_2-air mixtures at atmospheric pressure with different fan speeds, and the results, together with those obtained by Lwakabamba (4) for a 10% CH_4-air mixture, are shown in the figure. The values have been normalised by dividing them by the number density for a fan speed of 5,000 r.p.m. and a 10% CH_4-air mixture. Figure 4.25 shows the variation of normalised small eddy density with laminar burning velocity. This shows that there is a general trend for Y to be reduced as the laminar burning velocity increases. The four mixtures investigated covered a wide range of u_ℓ values and yet showed similar results. Values of u_ℓ given in the figure were taken from Andrews and Bradley (11).

4.6.2 Ionisation Fluctuations in Turbulent Flames

Some diagnosis of the turbulence of the hot flame gases was obtained from the chemi-ionisation of the gases and the use of an electrostatic probe. The probe used in the present study was designed by Andrews (3). The fluctuations in the ionisation current to a negatively based electrostatic probe were measured as the turbulent flame swept across the probe. This probe was a platinum-40% rhodium cylinder of 0.2 mm diameter and 8 mm long,

whilst the other electrode consisted of a long stainless steel wire, 1 mm diameter, with a surface area greater than that of the negative electrode. There was always a sufficiency of electrons around the larger electrode to ensure that electron flux was not current limiting and that the current measured by the circuit was the positive ion current to the negative probe. The measuring probe was positioned 44 mm from the spark gap and was designed to minimise electrical interferences. It was insulated completely from the vessel by mounting in a P.T.F.E. boss which was screwed into the vessel. A constant voltage difference of 4.5 was maintained across the electrodes and current-time characteristics were displayed on oscilloscopes and photographed with an oscilloscope camera.

Two ion current temporal fluctuations are shown as the top traces in Fig. 4.26 (a) and (b) for 10% CH_4-air mixture. The lower traces are those of pressure, obtained as described in Chapter 3. It is the early stage of combustion, before significant increase of pressure, with which the present study is concerned. It is seen that higher frequency current fluctuations are superimposed upon the surge of ionisation associated with the arrival of the flame front. These are probably associated with the small scale eddies. Just as differences in temperature between these eddies and their immediate environment are sufficient to enable them to be optically visualised, so differences in ionisation enable small eddies to be registered by ionisation current fluctuations.

From the many ionisation probe records that had been obtained it was seen that, for the same fan speed, the number of high frequency ripples varied significantly from record to record. This is indicative of the random intermittent character of the dissipative eddies. In general, the number of high frequency peaks increased with fan speed. The same conclusions have also been reported previously by Andrews (3) and Lwakabamba (4).

TABLE 4.1 Experimental Results of Turbulent Burning Velocity

Fan Speed r.p.m. / U_t msec^{-1}	15% H_2 u_ℓ=1.01msec^{-1}	20% H_2 u_ℓ=1.56msec^{-1}	30% H_2 u_ℓ=2.78msec^{-1}	40% H_2 u_ℓ=3.48msec^{-1}	10% CH_4 0.50 atm. u_ℓ=0.63msec^{-1}	10% CH_4 0.25 atm. u_ℓ=0.90msec^{-1}
250		2.60	3.80	4.68		
500	2.75	3.60	5.20	5.75	1.58	1.625
1000		5.10	6.60	7.29		
1500		5.90	7.40	8.10		
2000		6.50	8.10	8.85		
2500		7.20	9.13	9.70		
3000		7.85	9.63	10.60		
3500		8.60	10.40	11.30		

TABLE 4.2 Results of Thermal Quenching in Mathane-Air

Fan Speed r.p.m.	Distance apart of two discs (Tulip A) mm	Mixture strength % Methane	Observed Thermal Quenching
Laminar	10 without shield	13.56	Yes
2000	10 without shield	13.56	Yes
Laminar	10 without shield	13.34	Yes
2000	10 without shield	13.34	Yes
Laminar	17 shielded	13.06	No
3500	17 shielded	13.07	Yes
3500	17 shielded	12.98	Yes
3500	17 shielded	12.90	Yes

TABLE 4.3 Conditions for Fig. 4.15

Run	Tulip A	Stored Energy Joules	Spark Gap mm	Disc Distance Apart mm
1	-	12	0.76	-
2	without shield	3	0.76	22
3	without shield	12	0.76	22
4	shielded	12	0.36	22
5	shielded	12	0.76	22
6	shielded	12	0.76	22

N.B.: Run 5 - Rich limit

Run 6 - Lean limit

TABLE 4.4 Propagation Limits of Hydrogen-Air Mixtures

Fan Speed r.p.m.	Tulip	Stored Energy Joules	Spark Gap mm	% H_2
2500	B	12	0.76	7.05
3500	B	12	0.76	7.08

TABLE 4.5 Conditions for Fig. 4.22 (a)-(c)

Figure	Fan Speed r.p.m.	Exposure Time μ sec
4.22 (a)	500	107
4.22 (b)	1500	97
4.22 (c)	3500	92

4.7 NOMENCLATURE

a	a.c. voltage component, Eq. (3.4)
F(n)	normalised power spectral density function
L	integral scale of turbulence
L'	Lagrangian integral scale of turbulence
L_t	integral time scale
n	frequency
R_L	$\frac{u'L}{\nu}$
R_y	the correlation coefficient between velocity at two points a distance y apart
t'_ξ	apparent small eddy, or veins, lifetime
u'	r.m.s. turbulent velocity
u_ℓ	laminar burning velocity
u_t	turbulent burning velocity
U	mean flow velocity
y	separation distance
Y	small eddy, or veins, density
ε	turbulent diffusivity
λ	Taylor microscale of turbulence
λ_t	Taylor micro time scale
ν	kinematic viscosity

4.8 REFERENCES

1. G.E. ANDREWS, D. BRADLEY and S.B. LWAKABAMBA, Measurement of turbulent burning velocity for large turbulent Reynolds numbers, Fifteenth Symposium (International) on Combustion, The Combustion Institute: Pittsburgh, 655 (1975).

2. E.S. SEMENOV, Measurement of turbulence characteristics in a closed volume with artificial turbulence, Combustion, Explosion and Shock Waves 1, 57 (1965).

3. G.E. ANDREWS, Laminar and turbulent flame propagation, Ph.D. thesis, Dept. Mechanical Engineering, Univ. Leeds (1972).

4. S.B. LWAKABAMBA, Turbulent flame propagation in closed vessels, Ph.D. thesis, Dept. Mechanical Engineering, Univ. Leeds (1975).

5. Y. OHTA, K. SHIMOYAMA and S. OHIGASHI, Vaporization and combustion of single liquid fuel droplets in a turbulent environment, Bulletin of the JSME 18, 47 (1975).

6. A.N. KOLMOGOROV, The local structure of turbulence in incompressible viscous fluid for very large Reynolds numbers, C. R. Acad. Sci. URSS 30, 301 (1941).

7. H. TENNEKES, Eulerian and Lagrangian time microscales in isotropic turbulence, J. Fluid Mech. 67, 561 (1975).

8. W. HEISENBERG, On the theory of statistical and isotropic turbulence, Proc. Roy. Soc. (London) Ser. A, 195 (1948-49).

9. J.O. HINZE, Turbulence - An introduction to its mechanism and theory, McGraw-Hill, New York (1959).

10. M. McMAHON, The influence of turbulence upon spark ignition, Ph.D. thesis, Dept. Mechanical Engineering, Univ. Leeds (1979).

11. G.E. ANDREWS and D. BRADLEY, Determination of burning velocity by double ignition in a closed vessel, Combustion and Flame 20, 77 (1973).

12. R.V. WHEELER, The ignition of turbulent explosive mixtures by electric sparks, J. Fuel 14, 147 (1935).

13. E.S. STARKMAN, L.P. HAXBY and A.G. CATTENEO, A study of free flames in turbulent streams, Fourth Symposium (International) on Combustion, p. 670, Williams and Wilkins: Baltimore (1953).

14. V.P. KARPOV and A.S. SOKOLIK, Ignition limits in turbulent gas mixtures, Doklady Akad. Nauk SSSR, 141, 393 (1961). (English Translation: Proc. Acad. Sci. USSR, Phys. Chem. Sec. 141, 866 (1961).)

15. S.A. GOLDENBERG and V.N. PELEVIN, The effect of turbulence in a combustible gas mixture flow on ignition, Izv. Akad. Nauk SSSR, Mekhanika Mashinostroenie No. 4, 112 (1963).

16. J.A. BOLT and D.L. HARRINGTON, The effects of mixture motion upon the lean limit and combustion of spark-ignited mixtures, SAE paper No. 670467 (1967).

17. K. IINUMA, A study of turbulent flame propagation in closed vessels, Automobile Exhaust Clarification Study Group, Japan, March 1977.

18. J. CHOMIAK, A possible mechanism of turbulent flames at high Reynolds number, Combustion and Flame 15, 319 (1970).

19. G.E. ANDREWS and D. BRADLEY, Limits of flammability and natural convection for methane-air mixtures, Fourteenth Symposium (International) on Combustion, The Combustion Institute: Pittsburgh, 1119 (1973).

SYMBOL	MIXTURE	PRESS.(ATM.)	$(m^2 sec^{-1})x10^6$
⊙	AIR	1	15.74
X	AIR	1/3	47.22
●	20% H_2—N_2	1	18.95
⊗	30% H_2—N_2	1	21.22
△	40% H_2-N_2	1	24.06

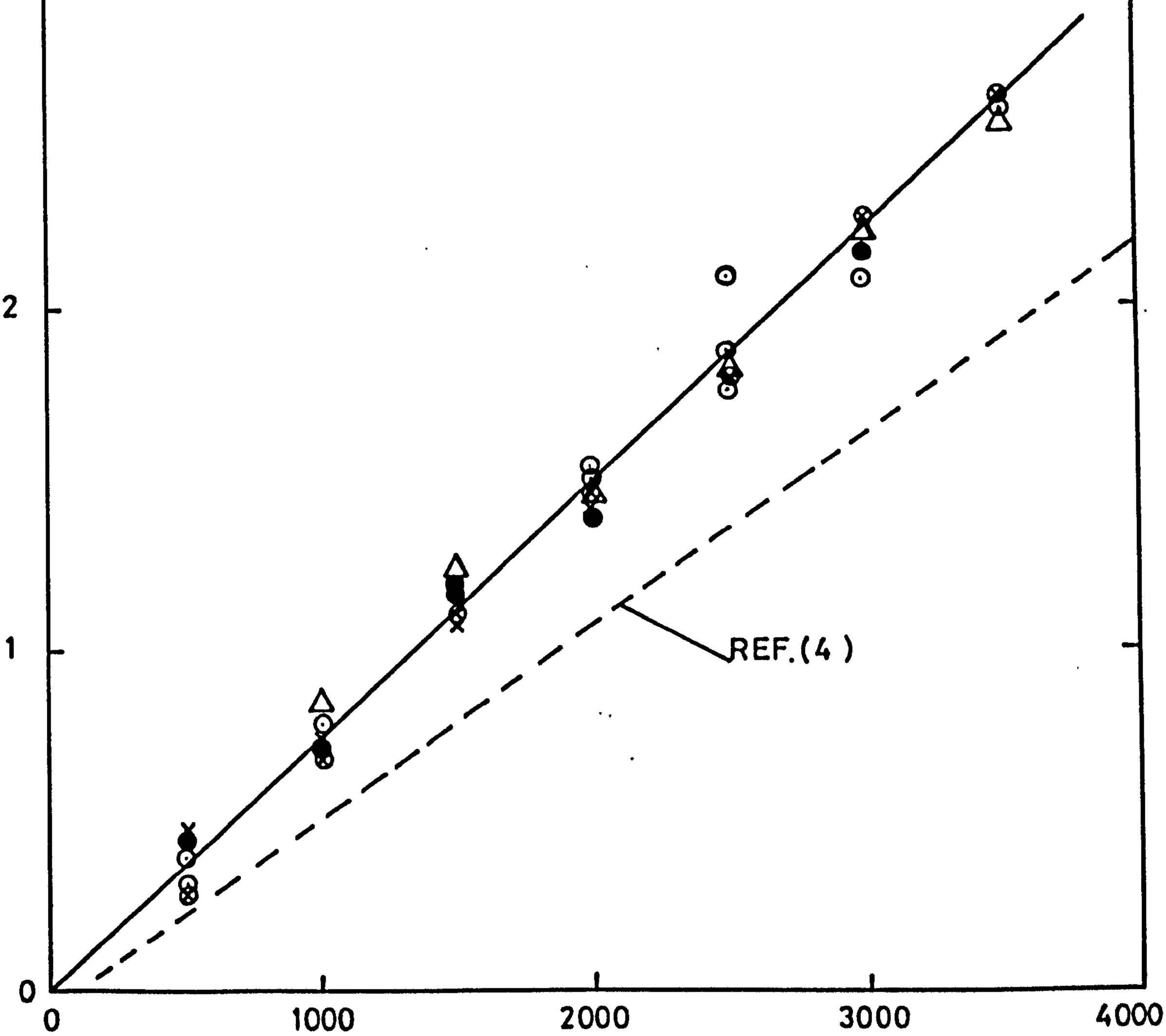

FIG. 4.1 VARIATION OF R.M.S. TURBULENT VELOCITY, u', WITH FAN SPEED FOR DIFFERENT MIXTURE AND PRESSURES

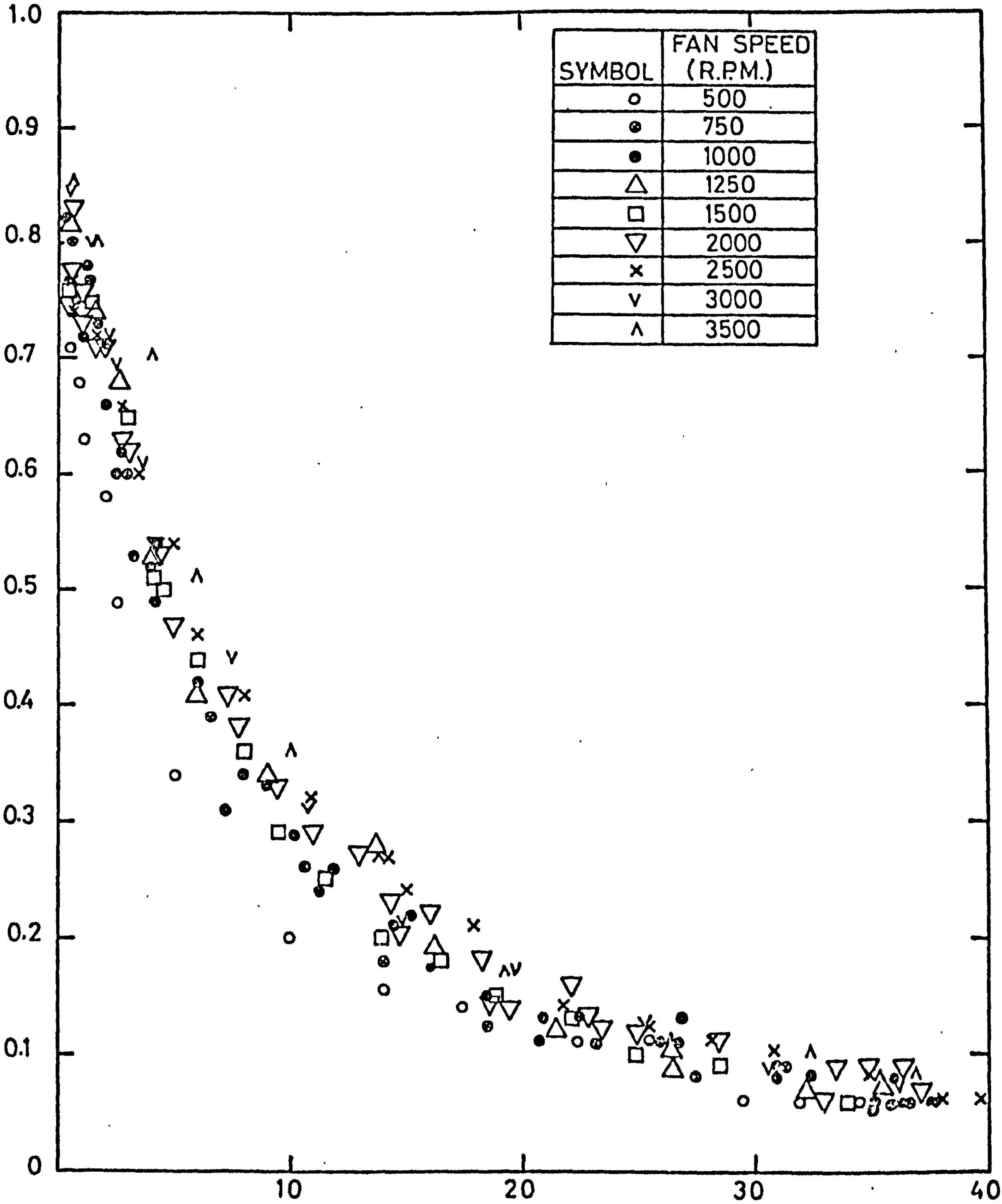

FIG.4.2 TWO WIRE VELOCITY CORRELATION COEFFICIENT AGAINST SEPARATION DISTANCE

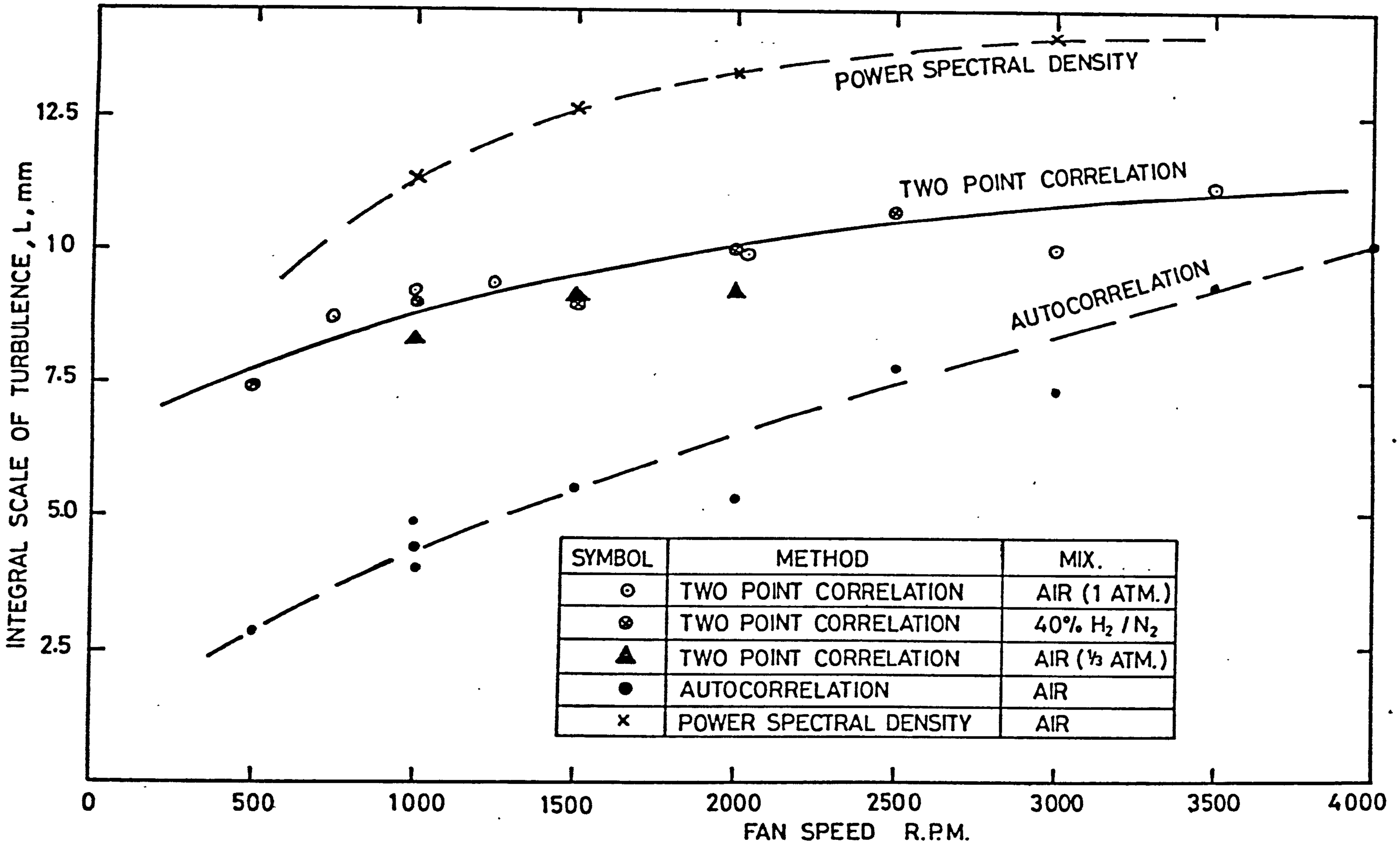

FIG.4.3 VARIATION OF INTEGRAL SCALE OF TURBULENCE WITH FAN SPEED BY DIFFERENT METHODS

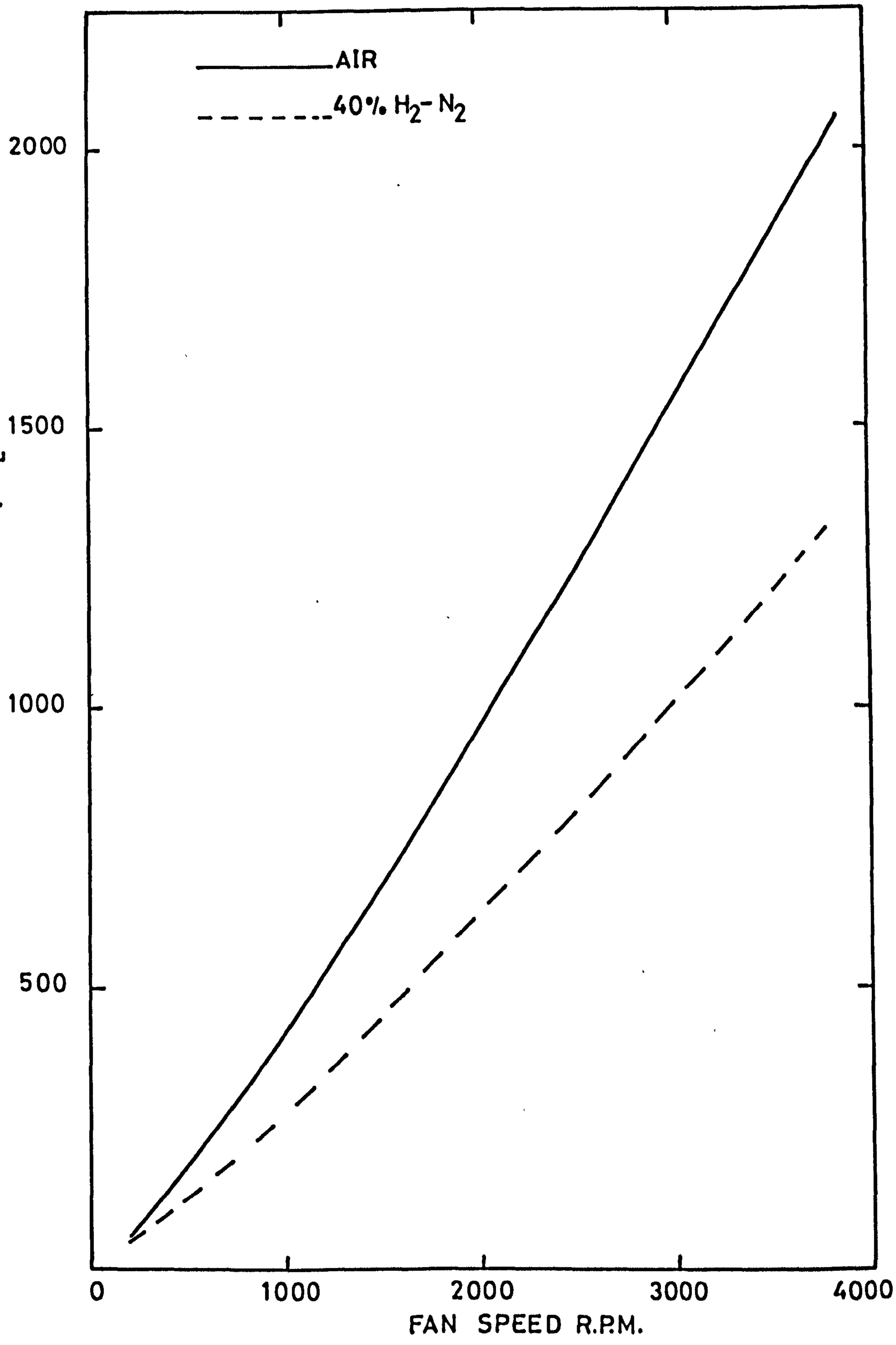

FIG. 4.4 VARIATION OF TURBULENT REYNOLDS NUMBER WITH FAN SPEED

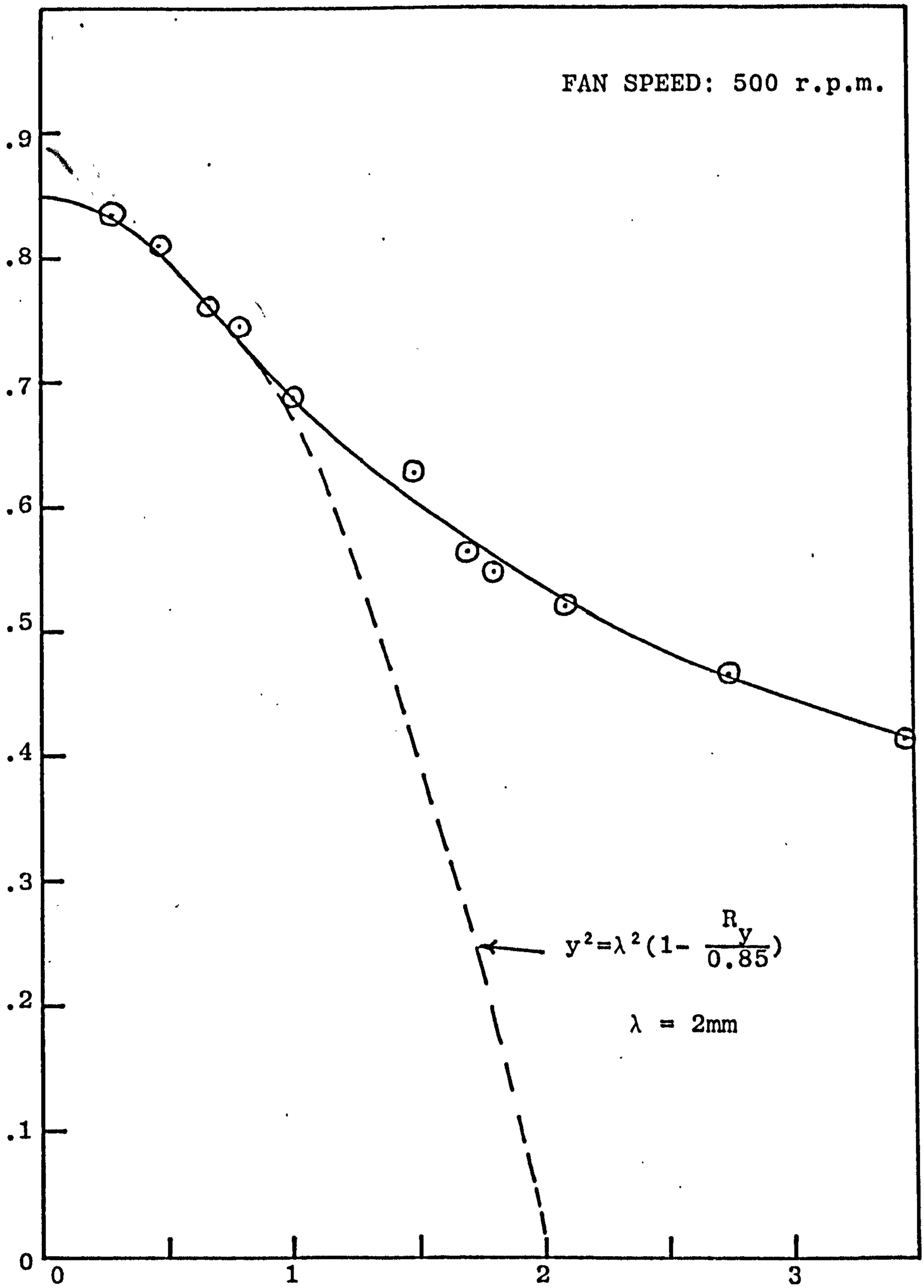

FIG.4.5 DETERMINATION OF TAYLOR MICROSCALE BY FITTING A PARABOLA METHOD

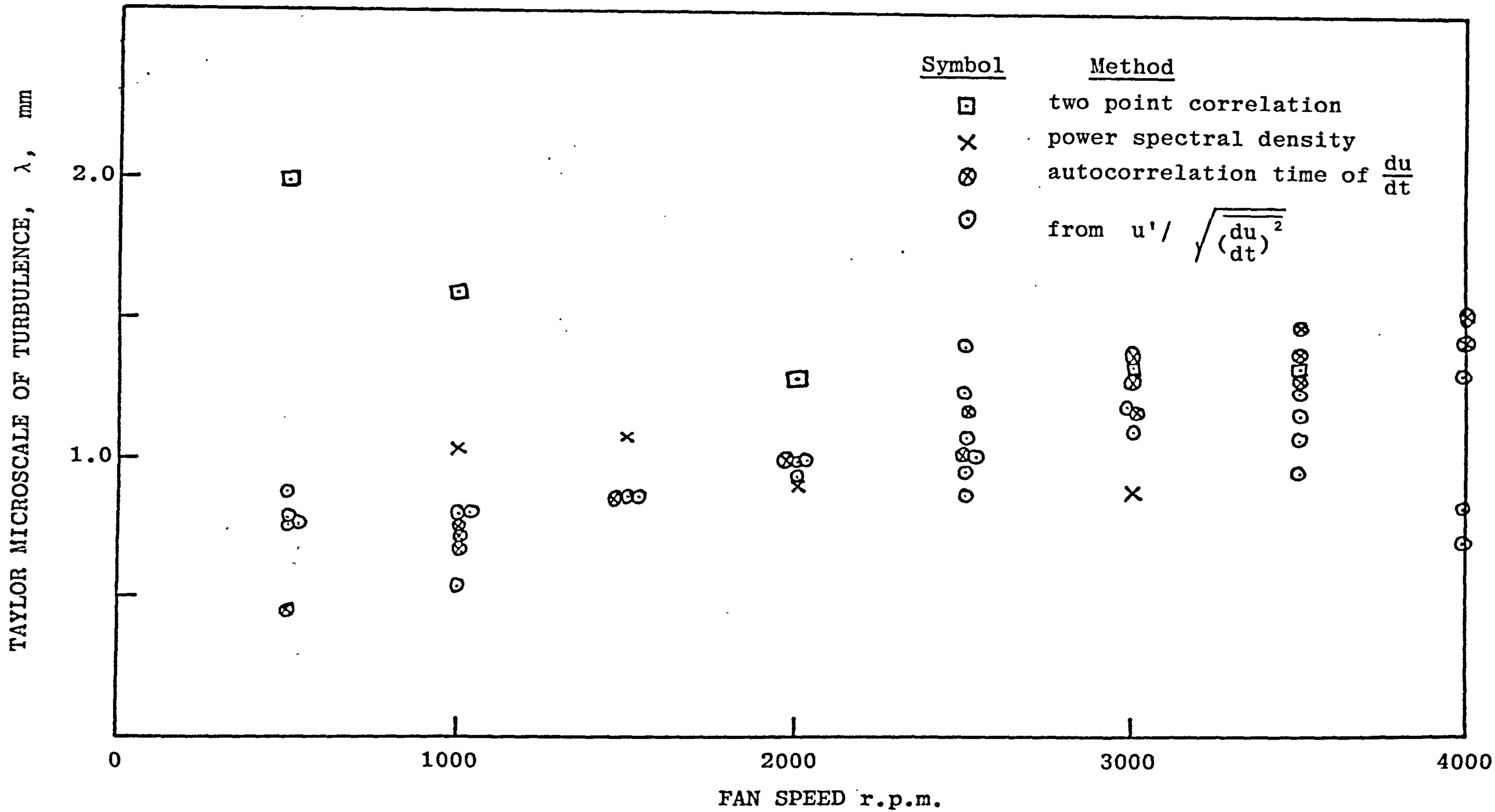

FIG.4.6 VARIATION OF TAYLOR MICROSCALE WITH FAN SPEED BY DIFFERENT METHODS

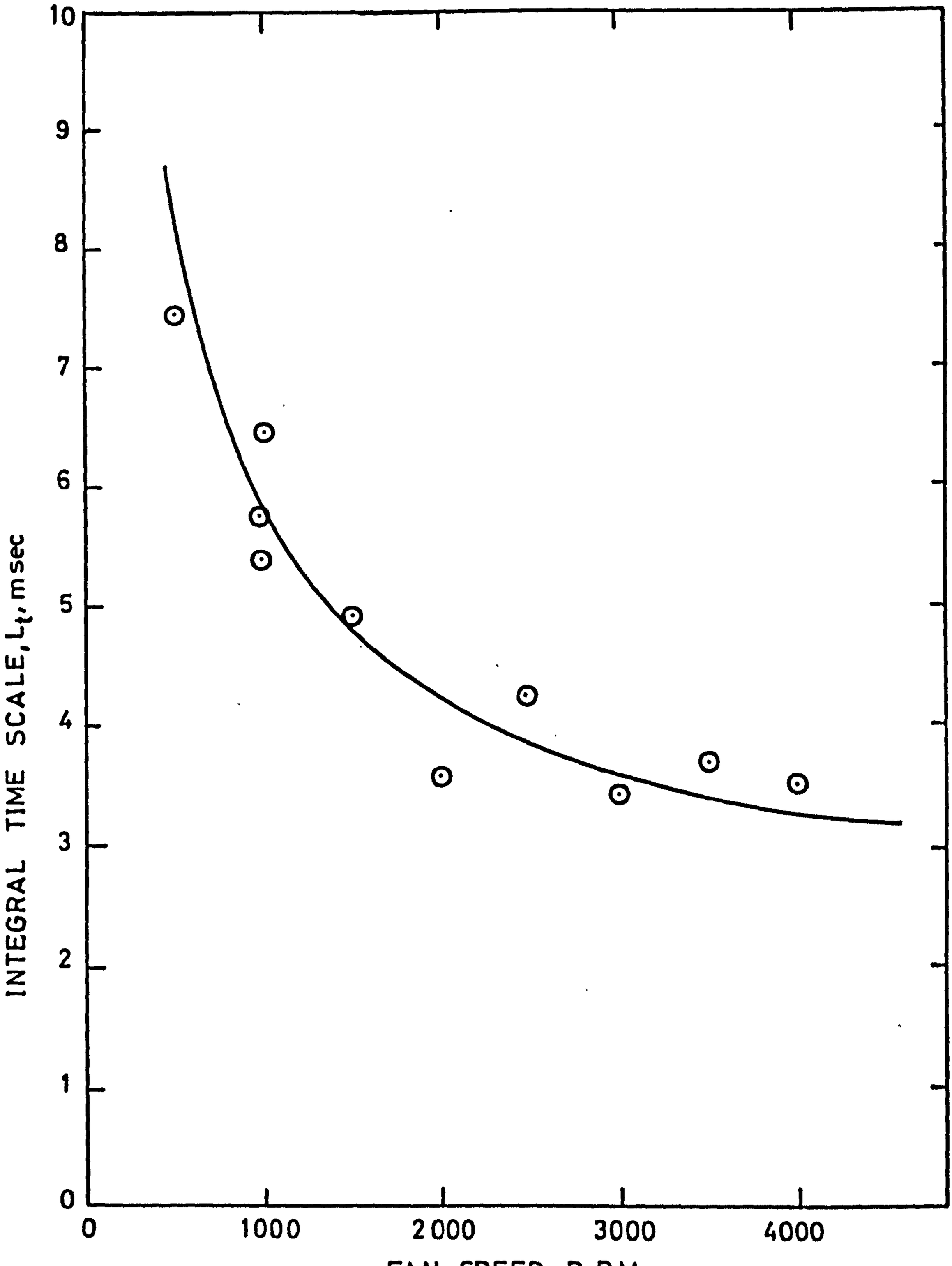

FIG. 4.7 VARIATION OF INTEGRAL TIME SCALE WITH FAN SPEED

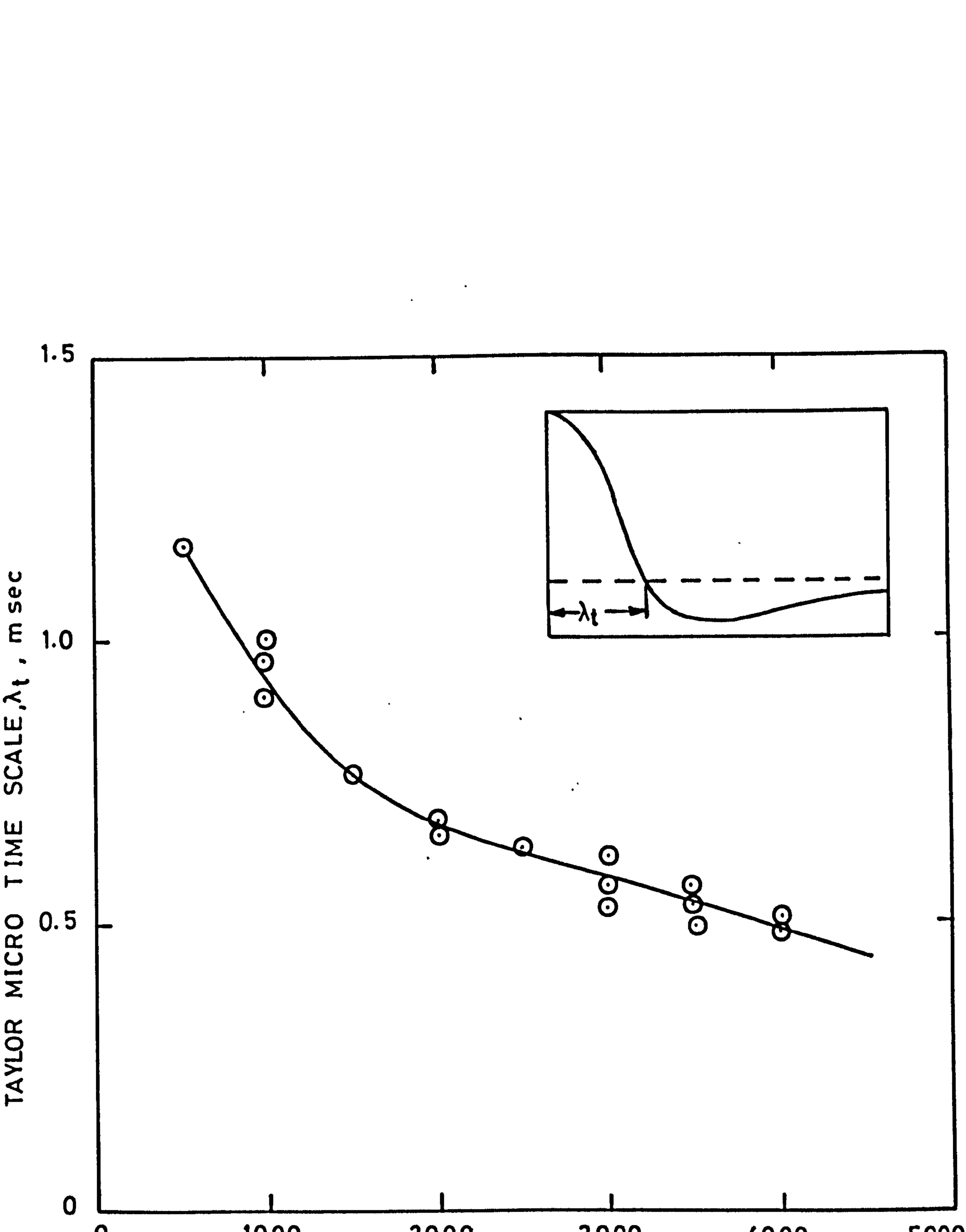

FIG.4.8 VARIATION OF TAYLOR MICRO TIME SCALE FOR $\frac{du}{dt}$ WITH FAN SPEED

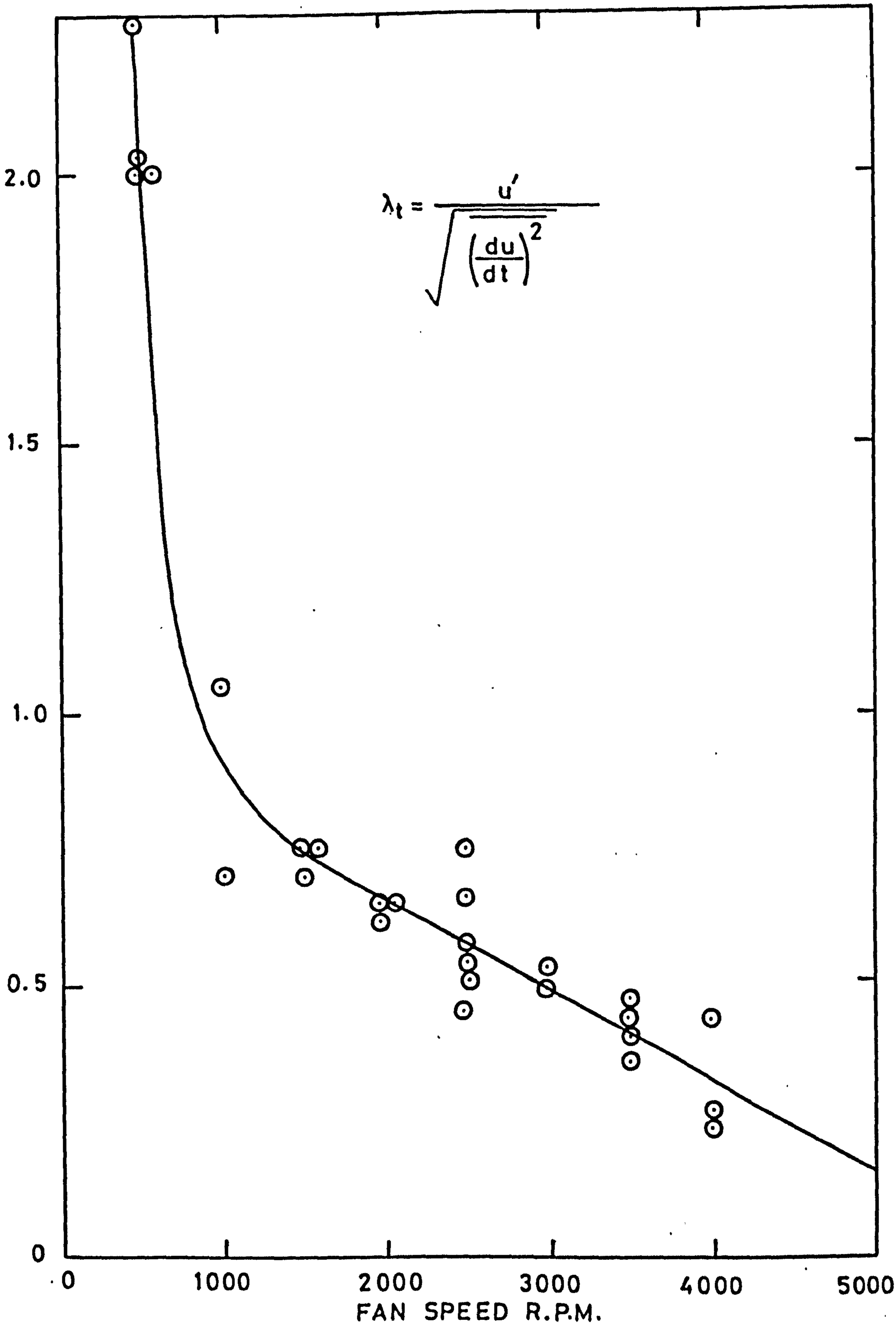

FIG.4.9 VARIATION OF TAYLOR MICRO TIME SCALE WITH FAN SPEED

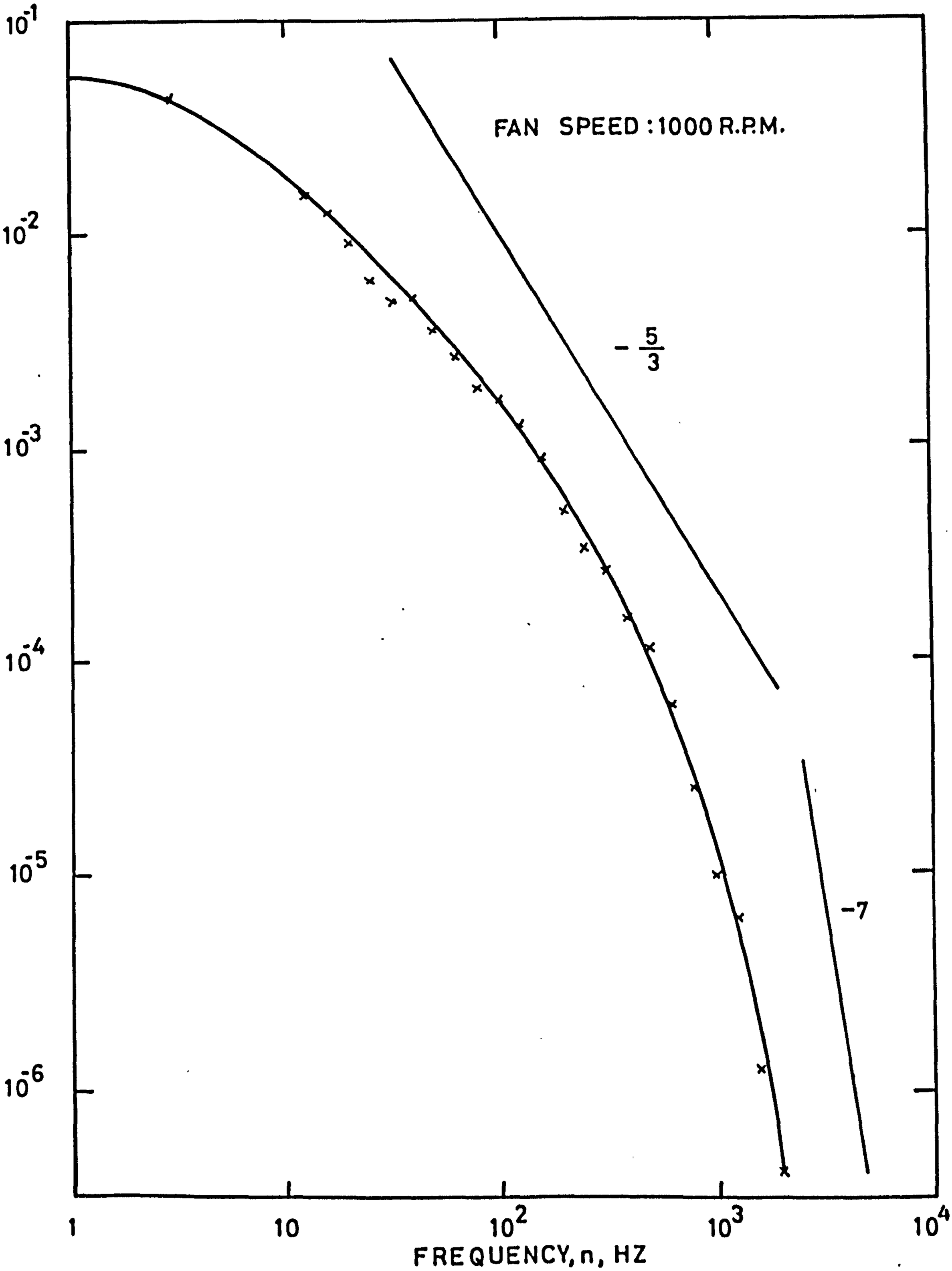

FIG. 4.10 VARIATION OF NORMALISED SPECTRAL DENCITY WITH FREQUENCY (1000 R.P.M.)

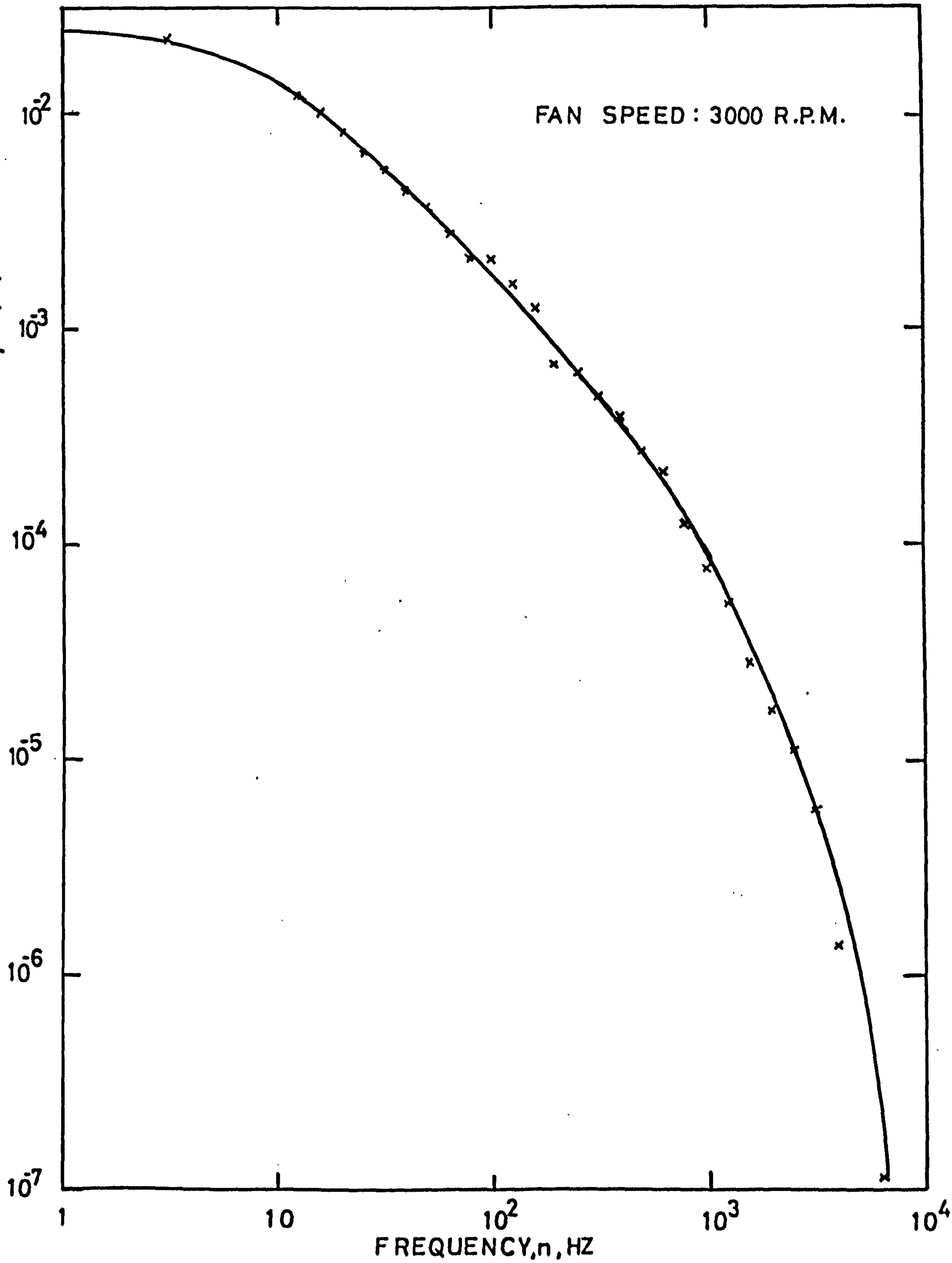

FIG. 4.11 VARIATION OF NORMALISED POWER SPECTAL DENSITY WITH FREQUENCY (3000 R.P.M.)

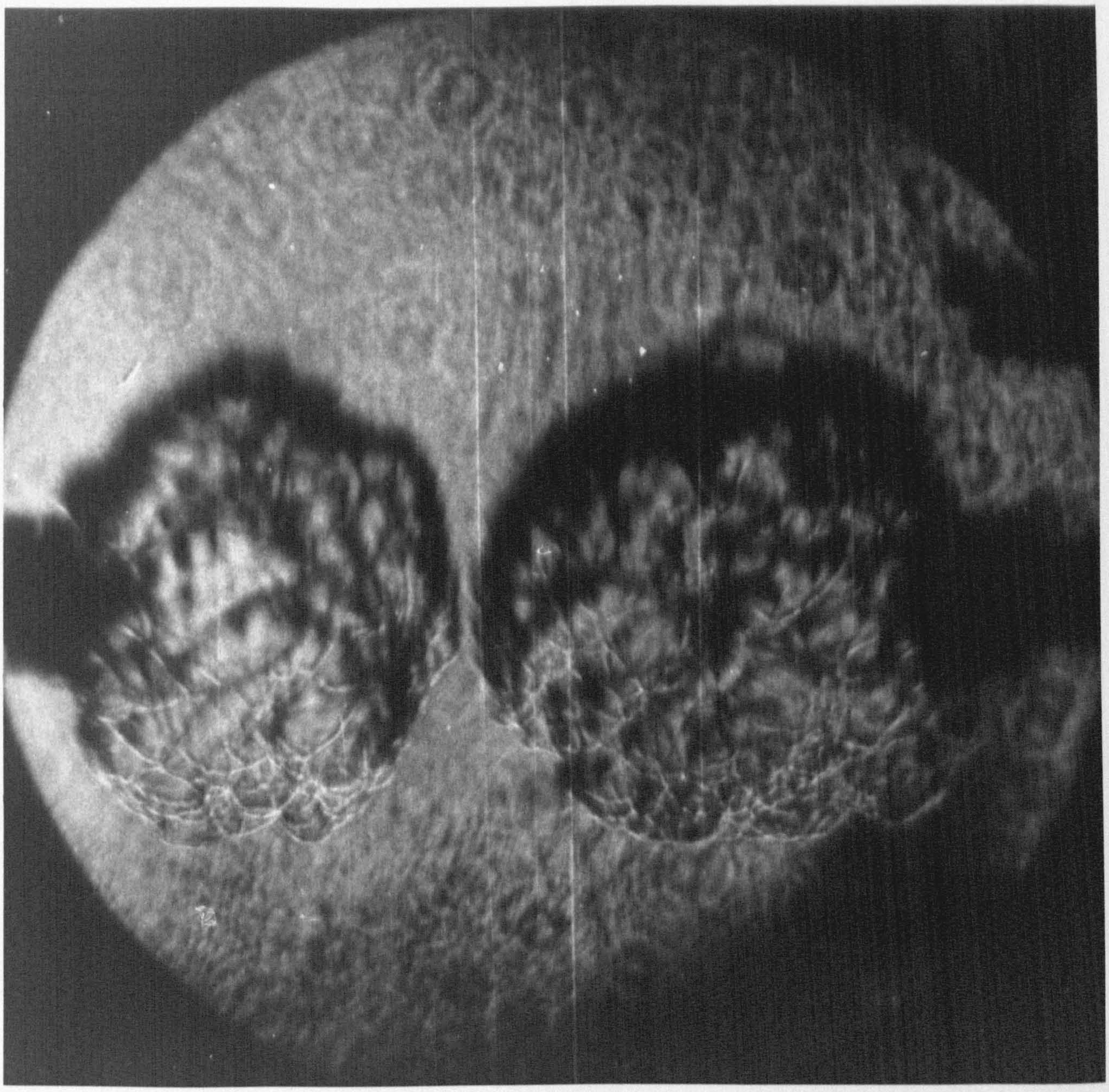

FIG. 4.12 1500 r.p.m., KNIFE EDGE SCHLIEREN, 20% H_2-AIR

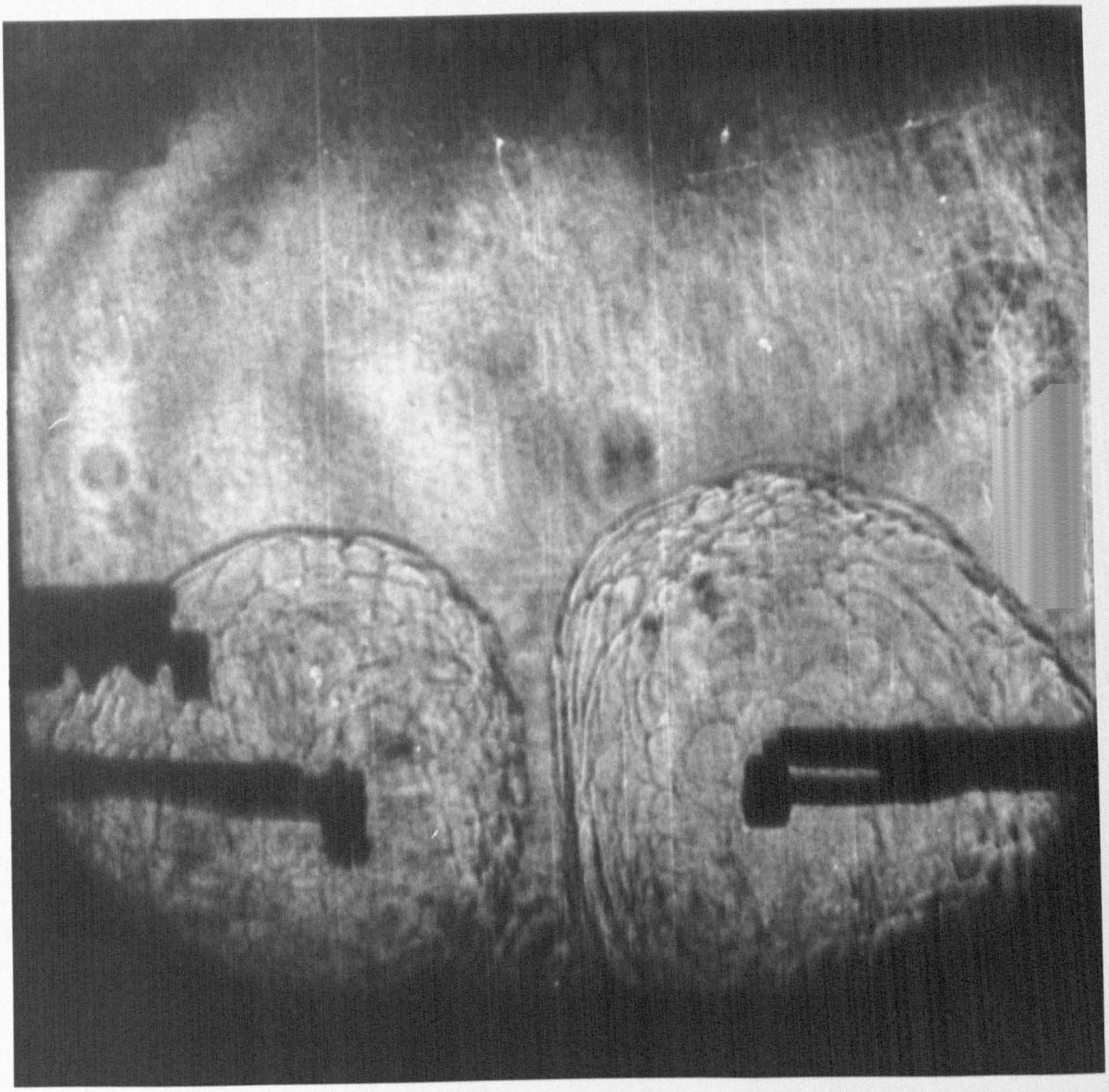

FIG. 4.13 LAMINAR, KNIFE EDGE SCHLIEREN, 20% H_2-AIR

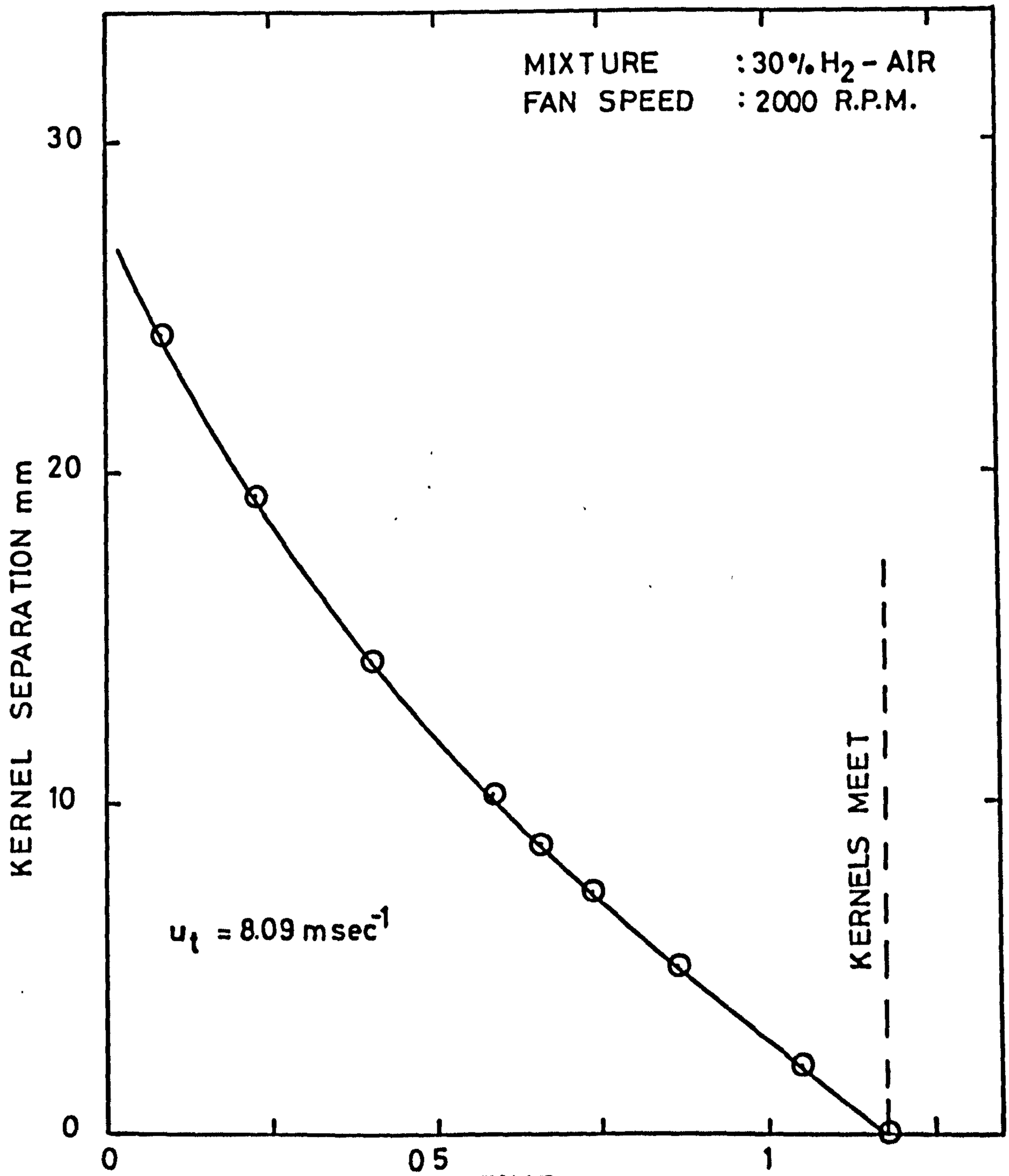

FIG. 4.14 VARIATION OF KERNEL SEPARATION DISTANCE WITH TIME

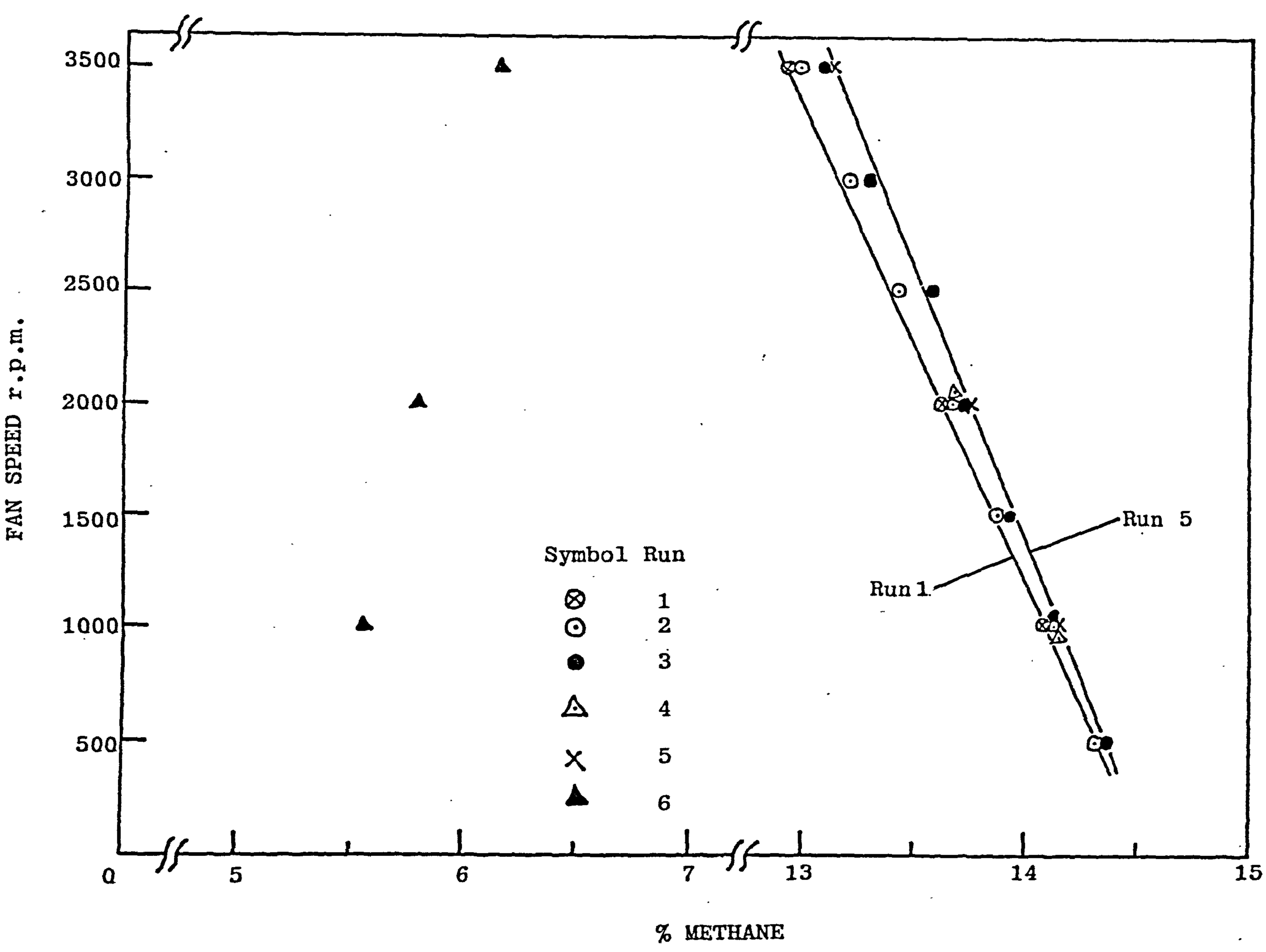

FIG.4.15 FLAMMABILITY LIMITS FOR METHANE-AIR AT ATMOSPHERIC PRESSURE AND TEMPERATURE

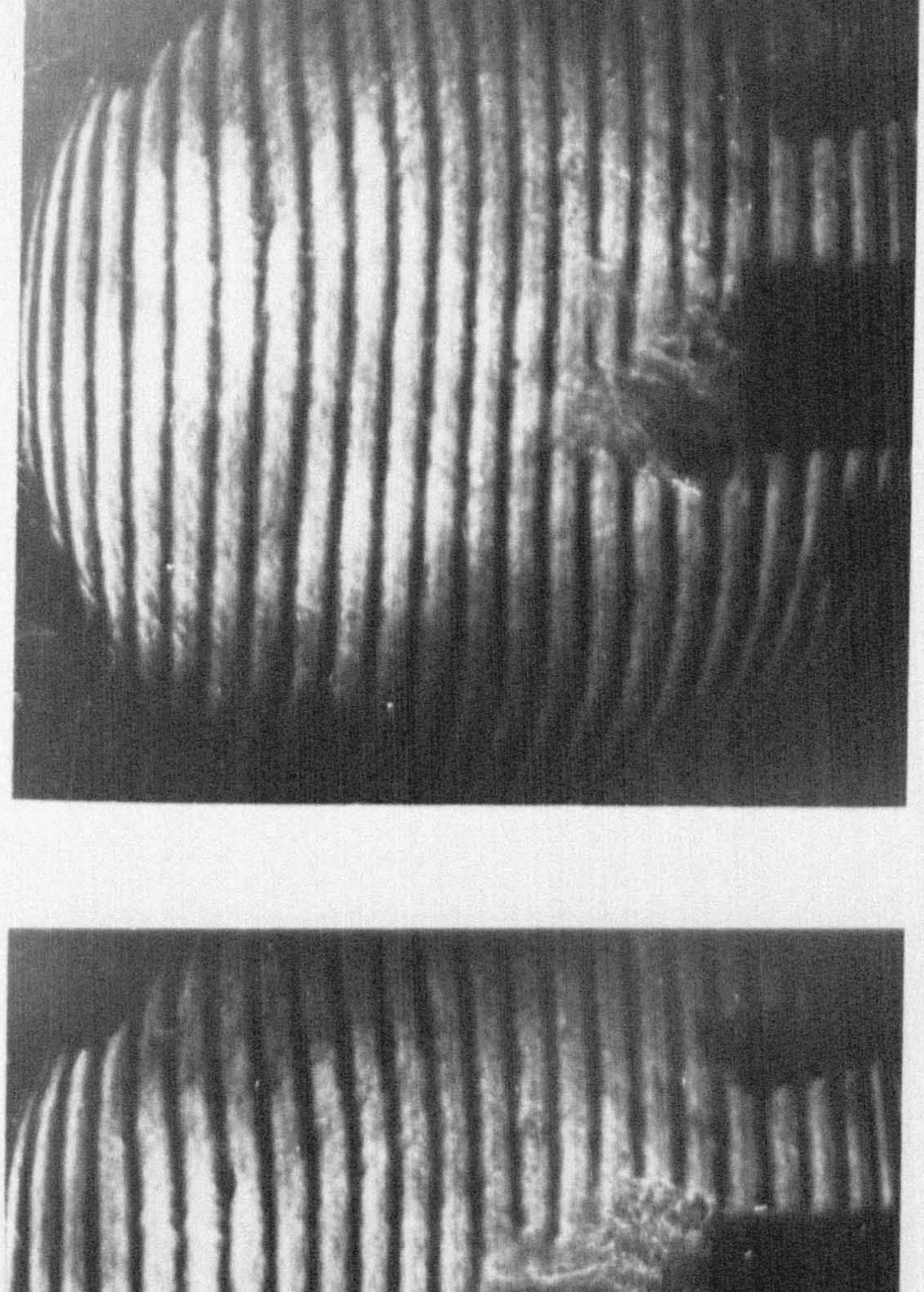

(a)

13.04% CH_4-AIR
12 J
(COMPLETE
PROPAGATION)

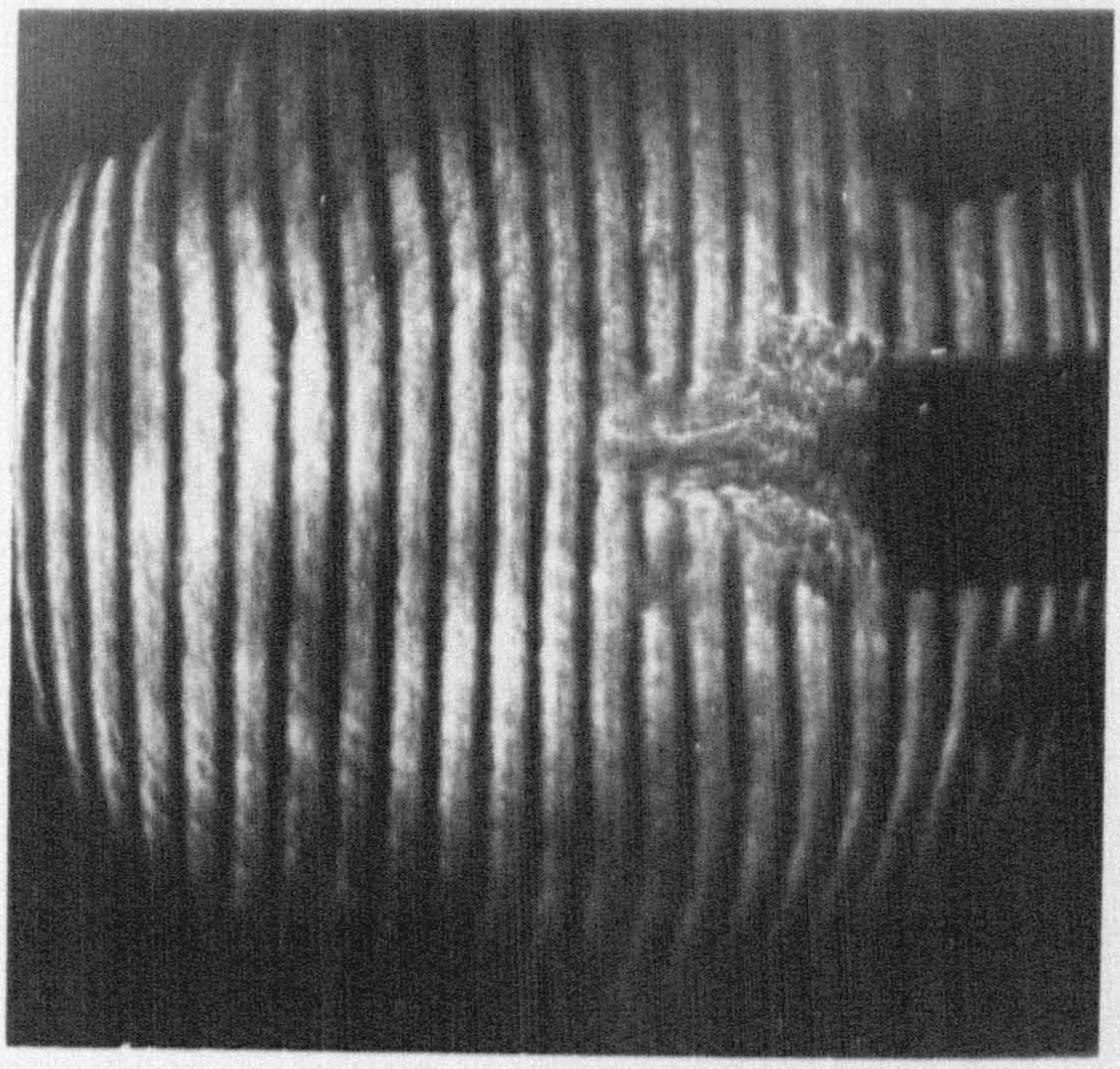

(b)

13.13% CH_4-AIR
12 J
(PARTIAL
PROPAGATION)

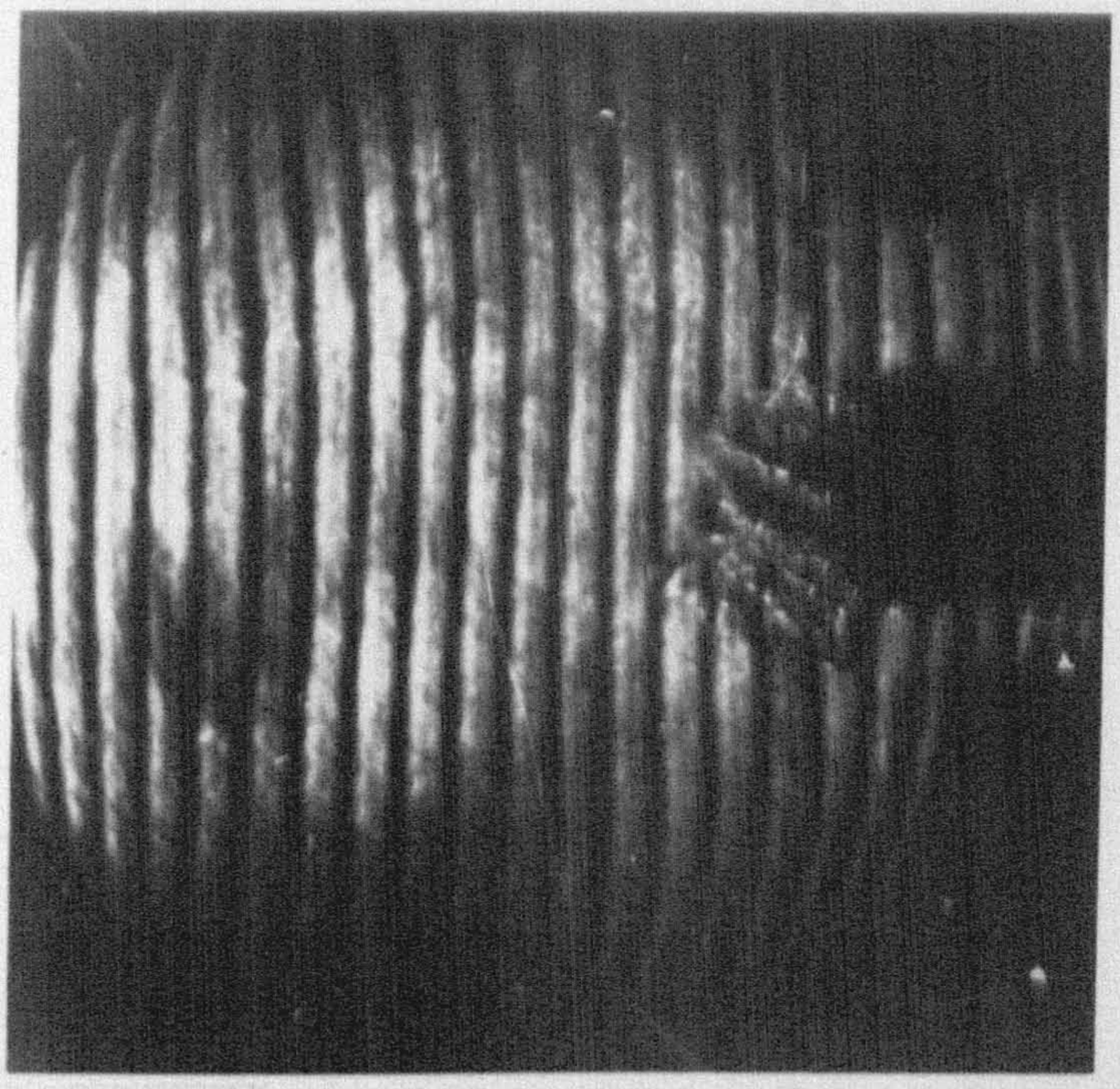

(c)

13.18% CH_4-AIR
3 J
(PARTIAL
PROPAGATION)

FIG. 4.16 NEAR-PROPAGATION LIMIT FLAMES, TIME FROM LEAVING TULIP = .07 m sec

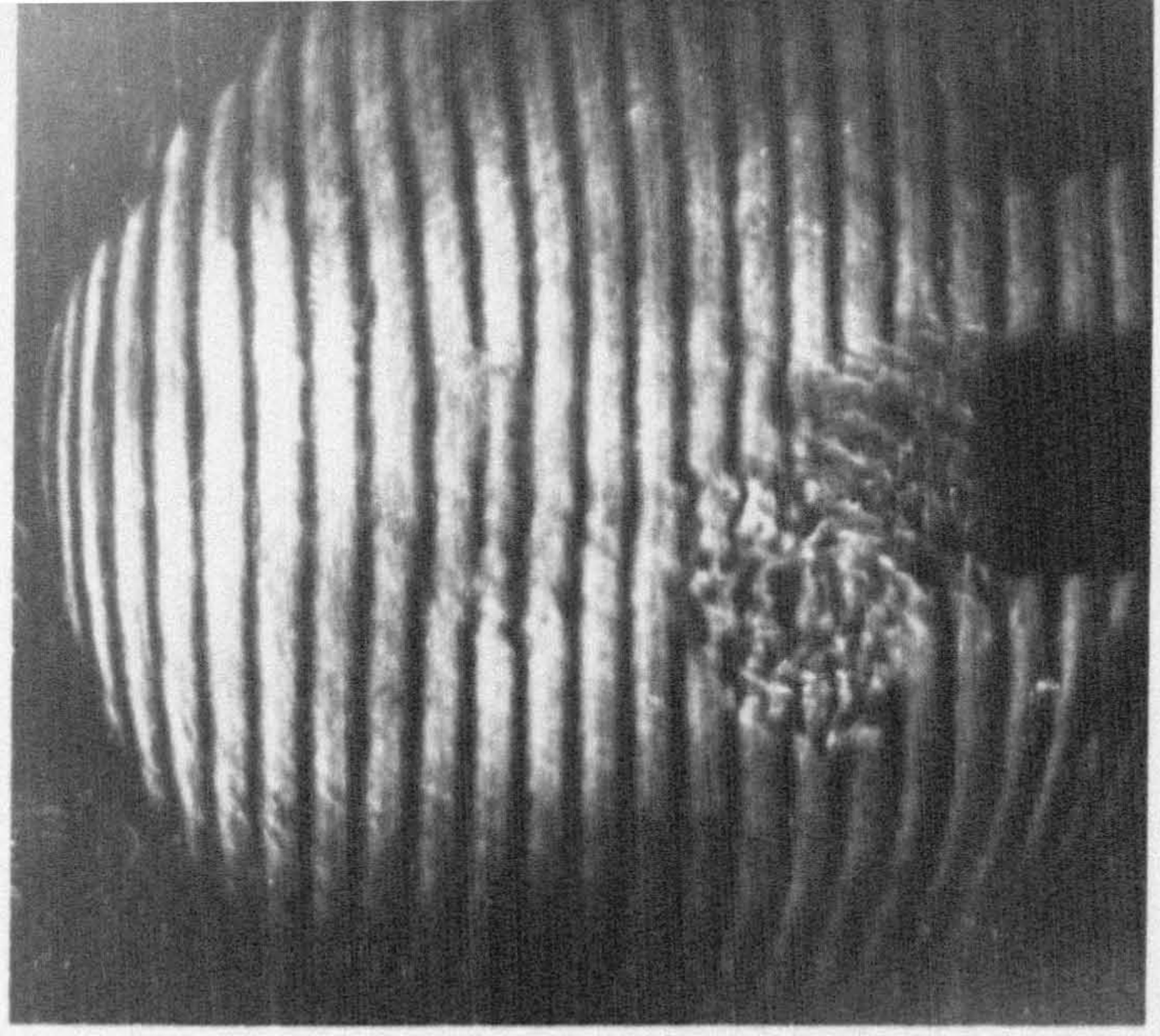

(a)

13.04% CH_4-AIR
12 J
(COMPLETE
PROPAGATION)

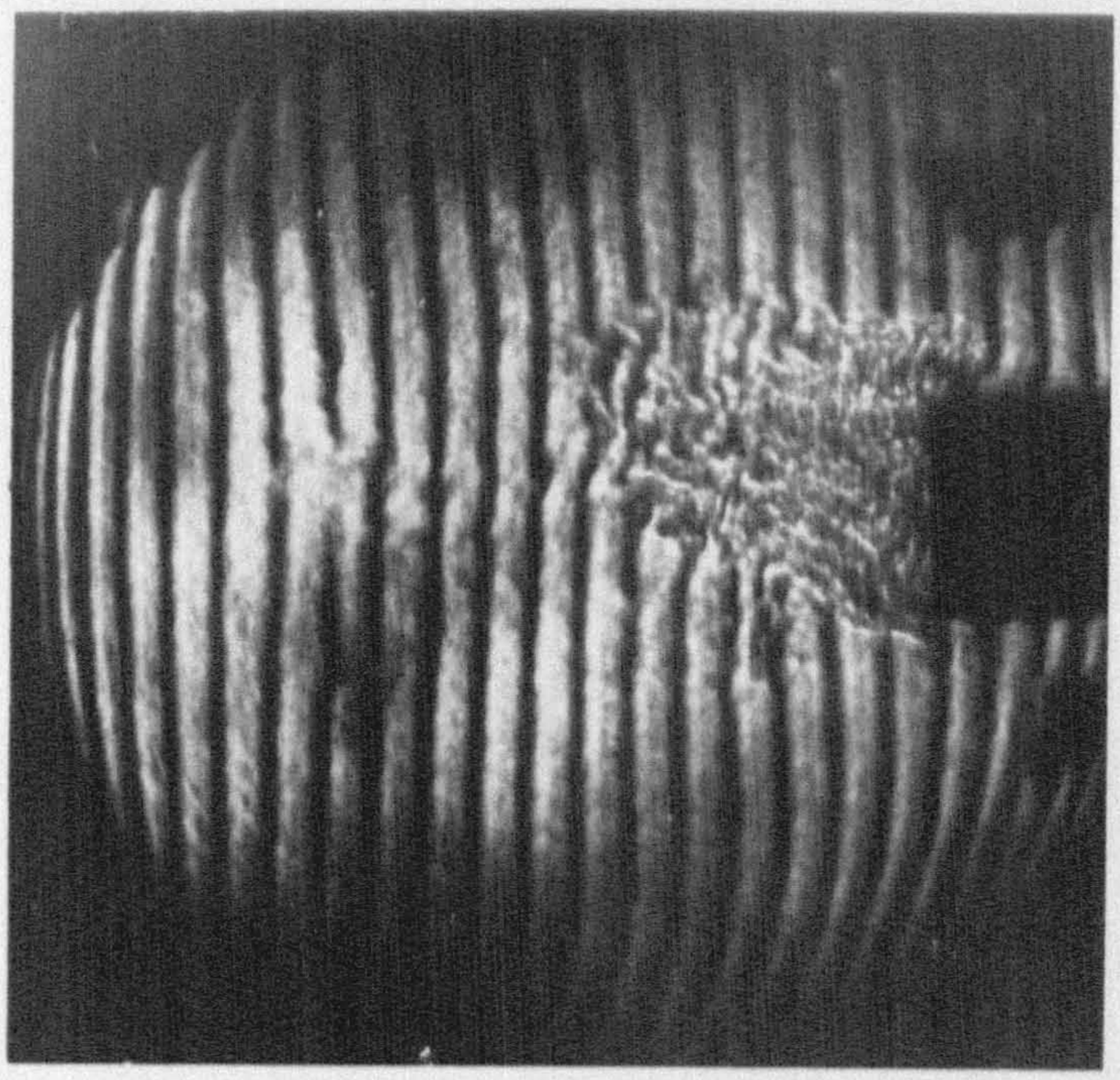

(b)

13.13% CH_4-AIR
12 J
(PARTIAL
PROPAGATION)

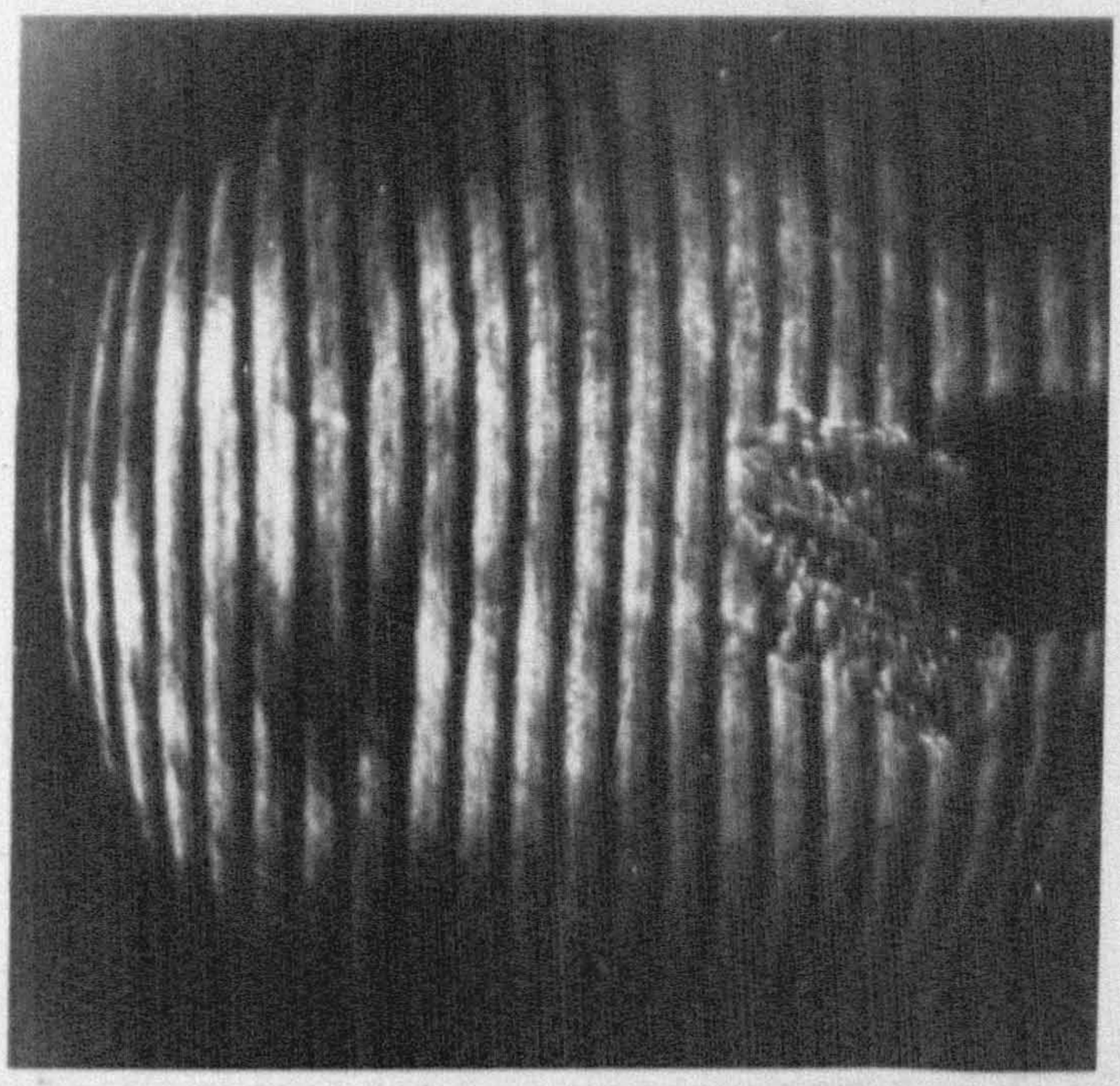

(c)

13.18% CH_4-AIR
3 J
(PARTIAL
PROPAGATION)

FIG. 4.17 NEAR-PROPAGATION LIMIT FLAMES, TIME FROM LEAVING TULIP = .27 m sec

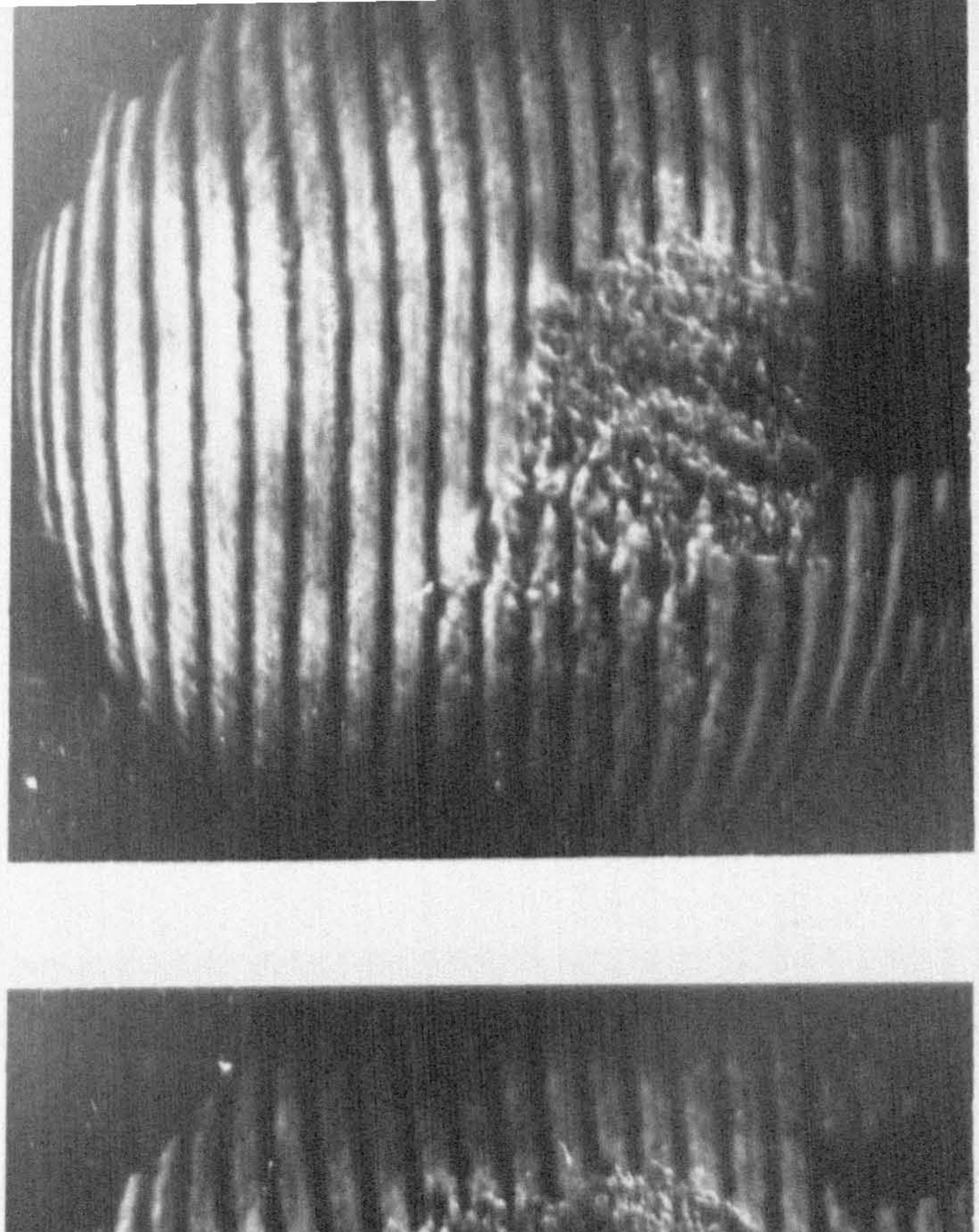

(a)

13.04% CH_4-AIR
12 J
(COMPLETE
PROPAGATION)

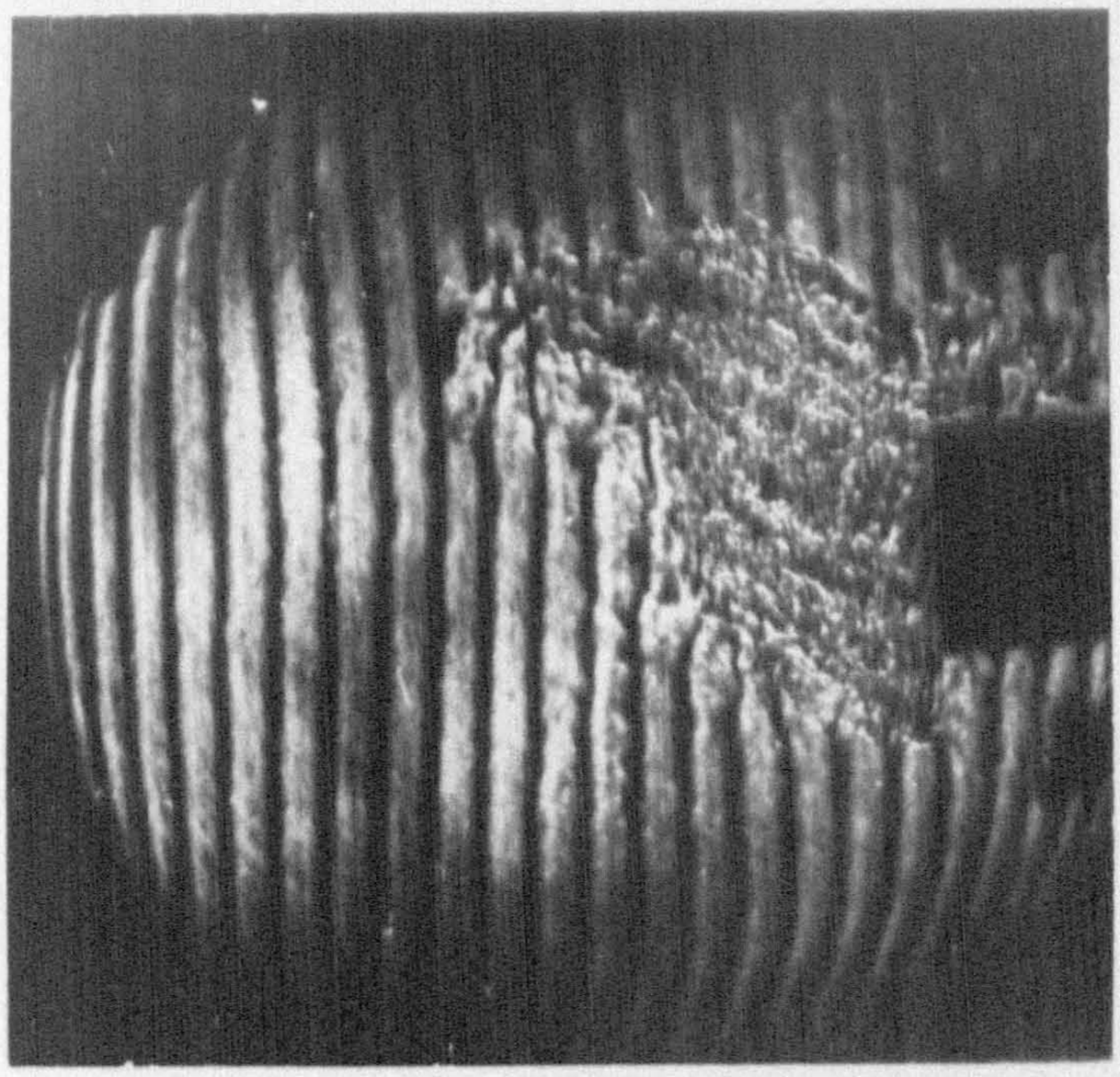

(b)

13.13% CH_4-AIR
12 J
(PARTIAL
PROPAGATION)

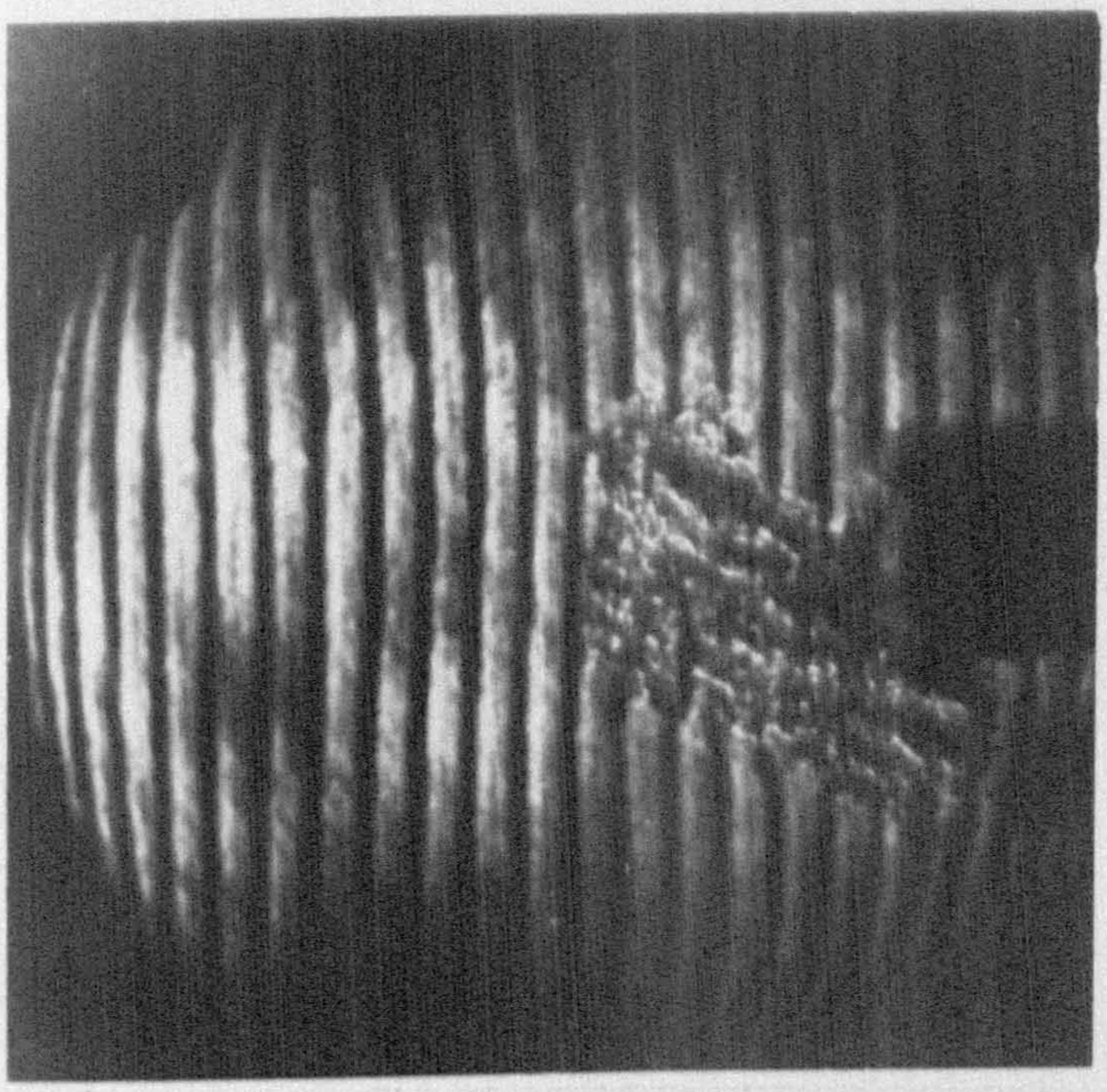

(c)

13.18% CH_4-AIR
3 J
(PARTIAL
PROPAGATION)

FIG. 4.18 NEAR-PROPAGATION LIMIT FLAMES, TIME FROM LEAVING TULIP = .67 m sec

(a)

13.04% CH_4-AIR
12 J
(COMPLETE
PROPAGATION)

(b)

13.13% CH_4-AIR
12 J
(PARTIAL
PROPAGATION)

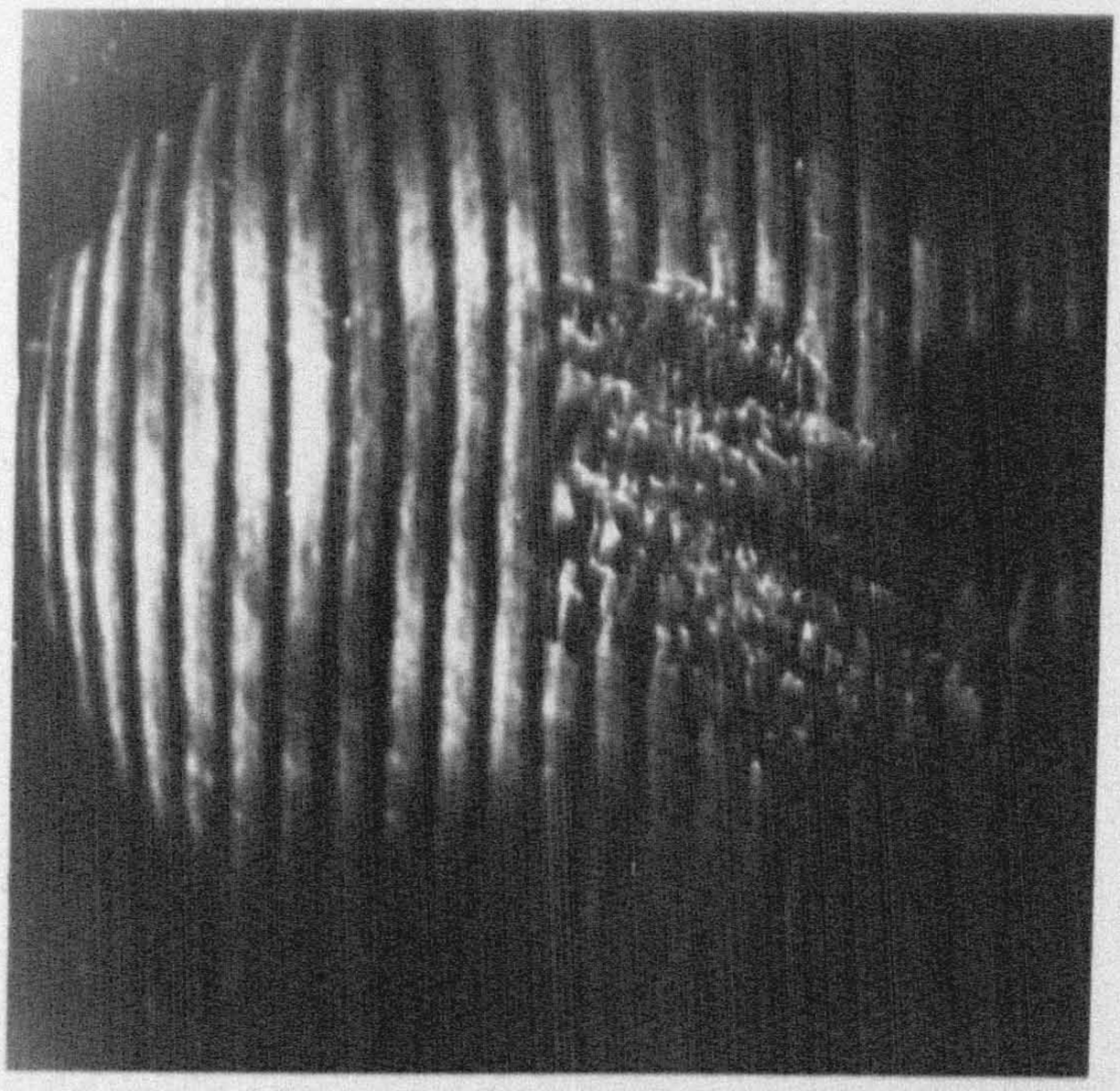

(c)

13.18% CH_4-AIR
3 J
(PARTIAL
PROPAGATION)

FIG. 4.19 NEAR-PROPAGATION LIMIT FLAMES, TIME FROM LEAVING TULIP = 1.20 m sec

(a)
13.04% CH_4-AIR
12 J
(COMPLETE
PROPAGATION)

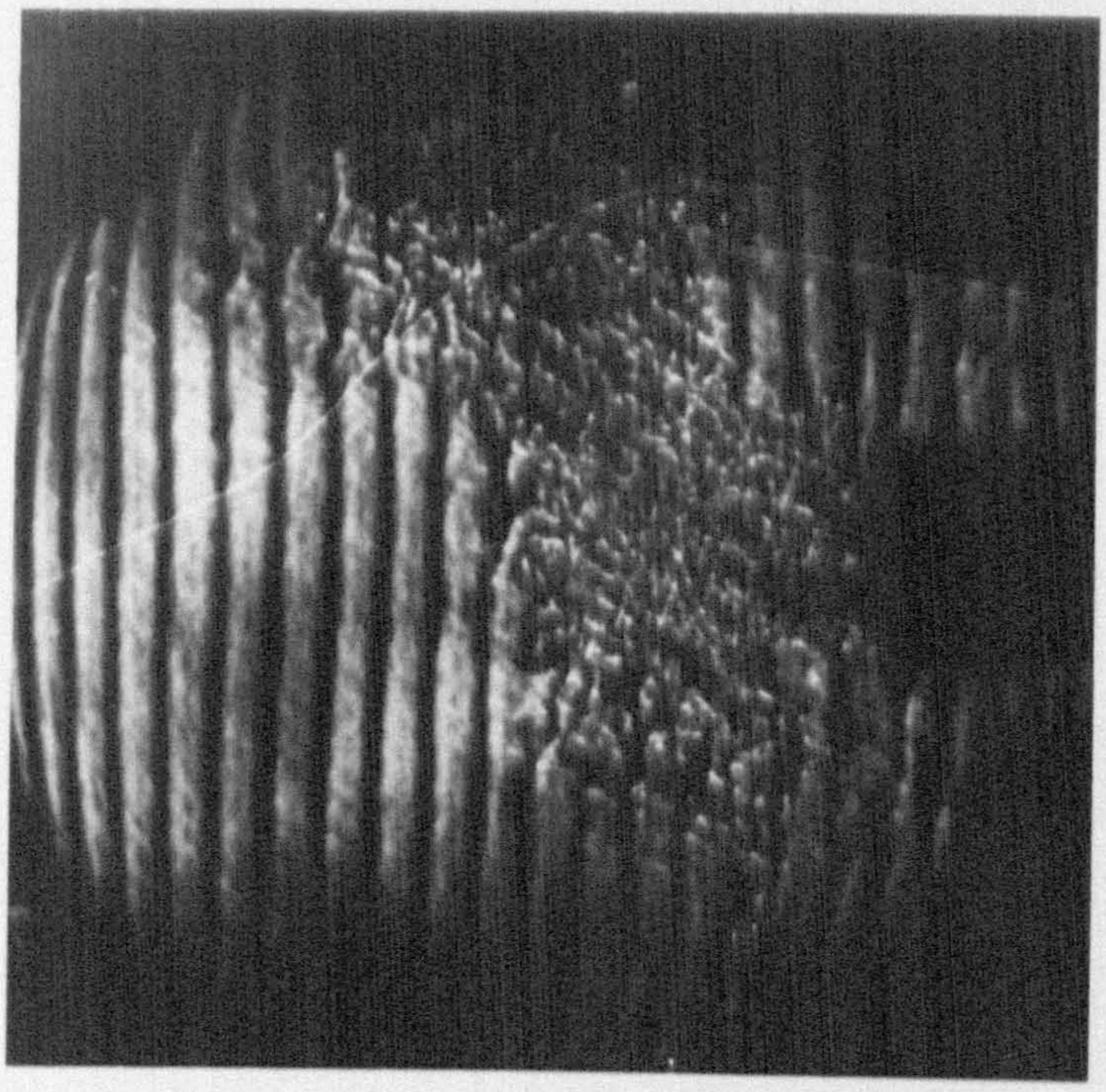

(b)
13.13% CH_4-AIR
12 J
(PARTIAL
PROPAGATION)

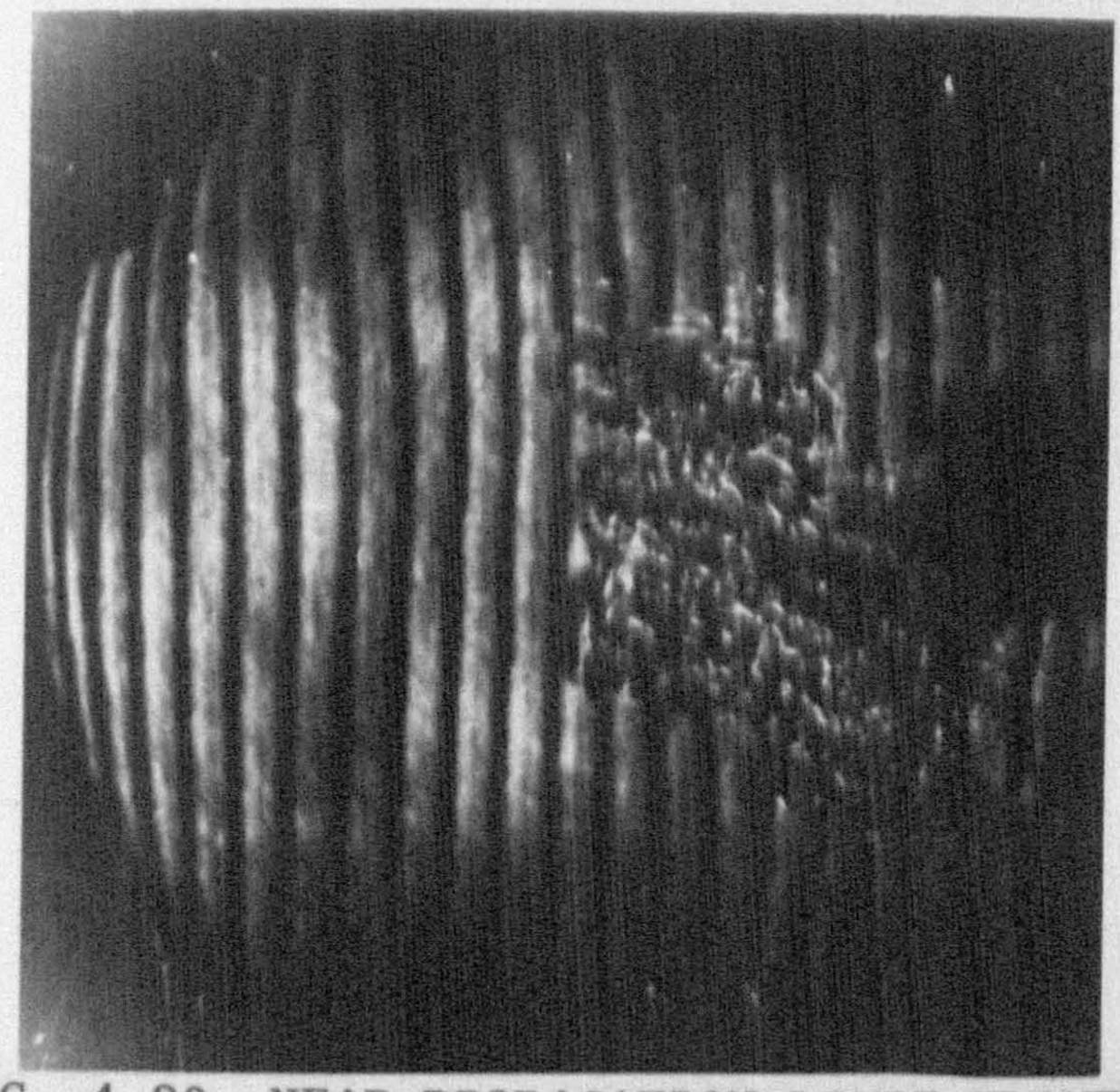

(c)
13.18% CH_4-AIR
3 J
(PARTIAL
PROPAGATION)

FIG. 4.20 NEAR-PROPAGATION LIMIT FLAMES, TIME FROM LEAVING TULIP = 1.53 m sec

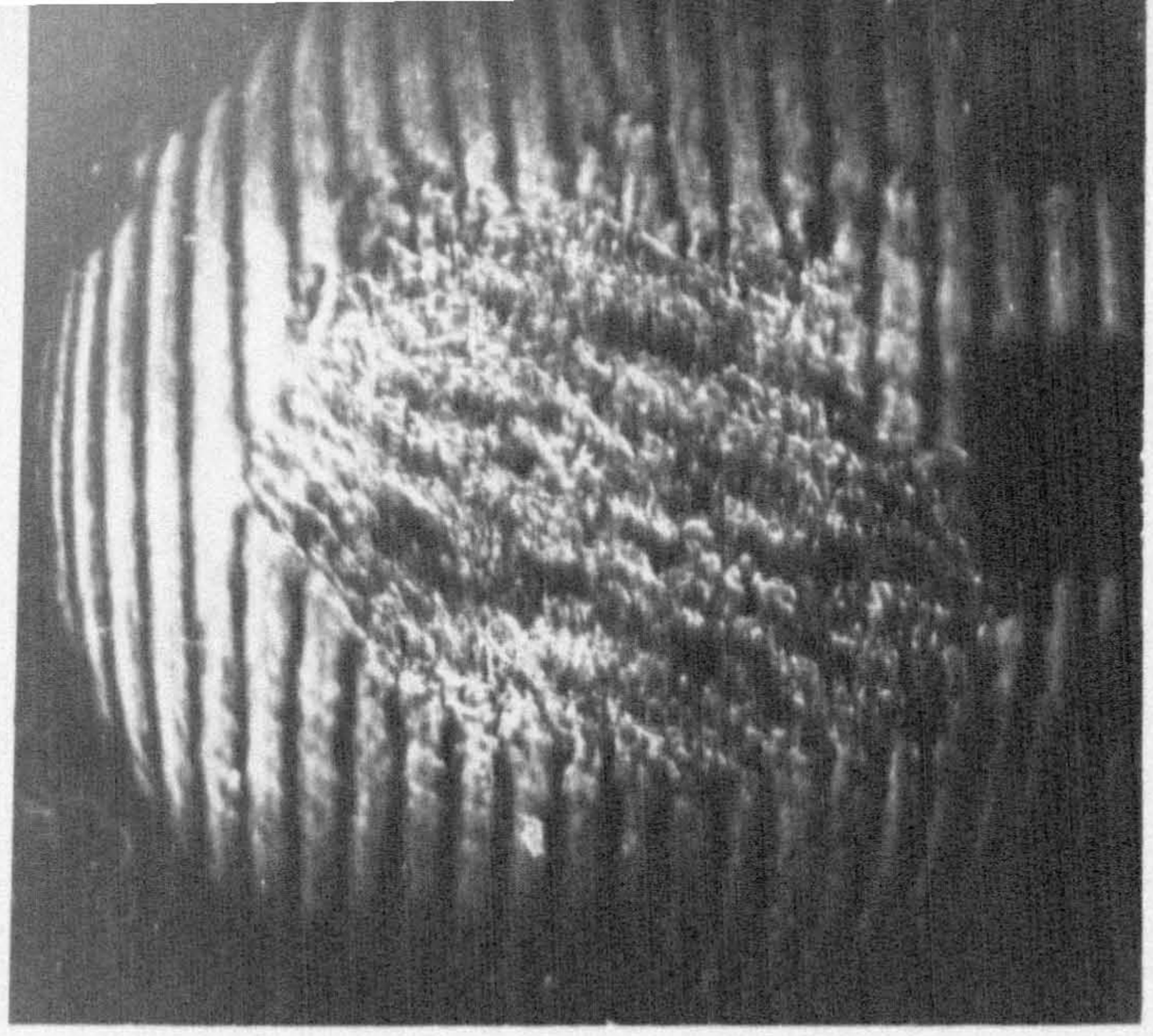

(a)

13.04% CH_4-AIR
12 J
(COMPLETE
PROPAGATION)

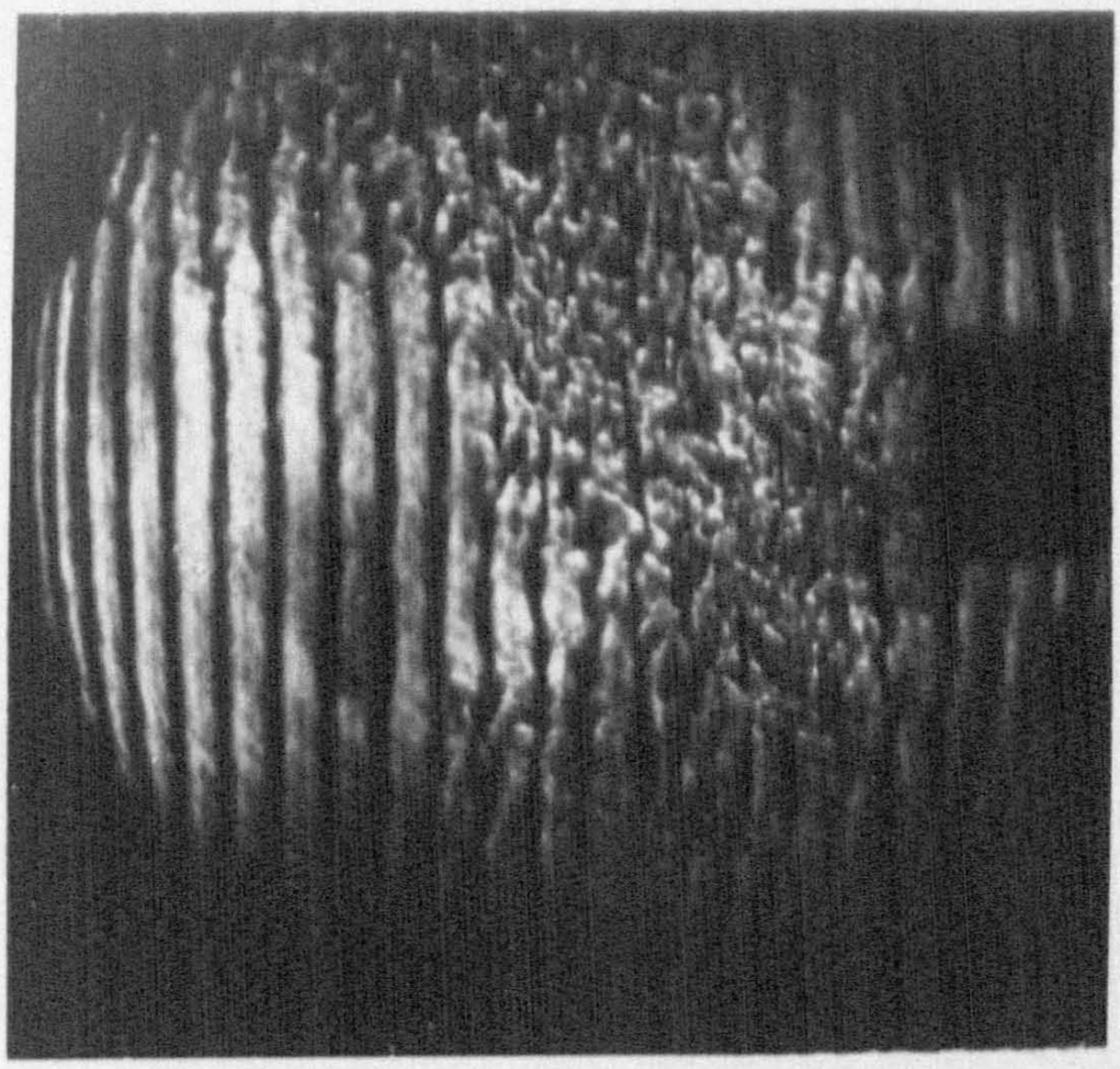

(b)

13.13% CH_4-AIR
12 J
(PARTIAL
PROPAGATION)

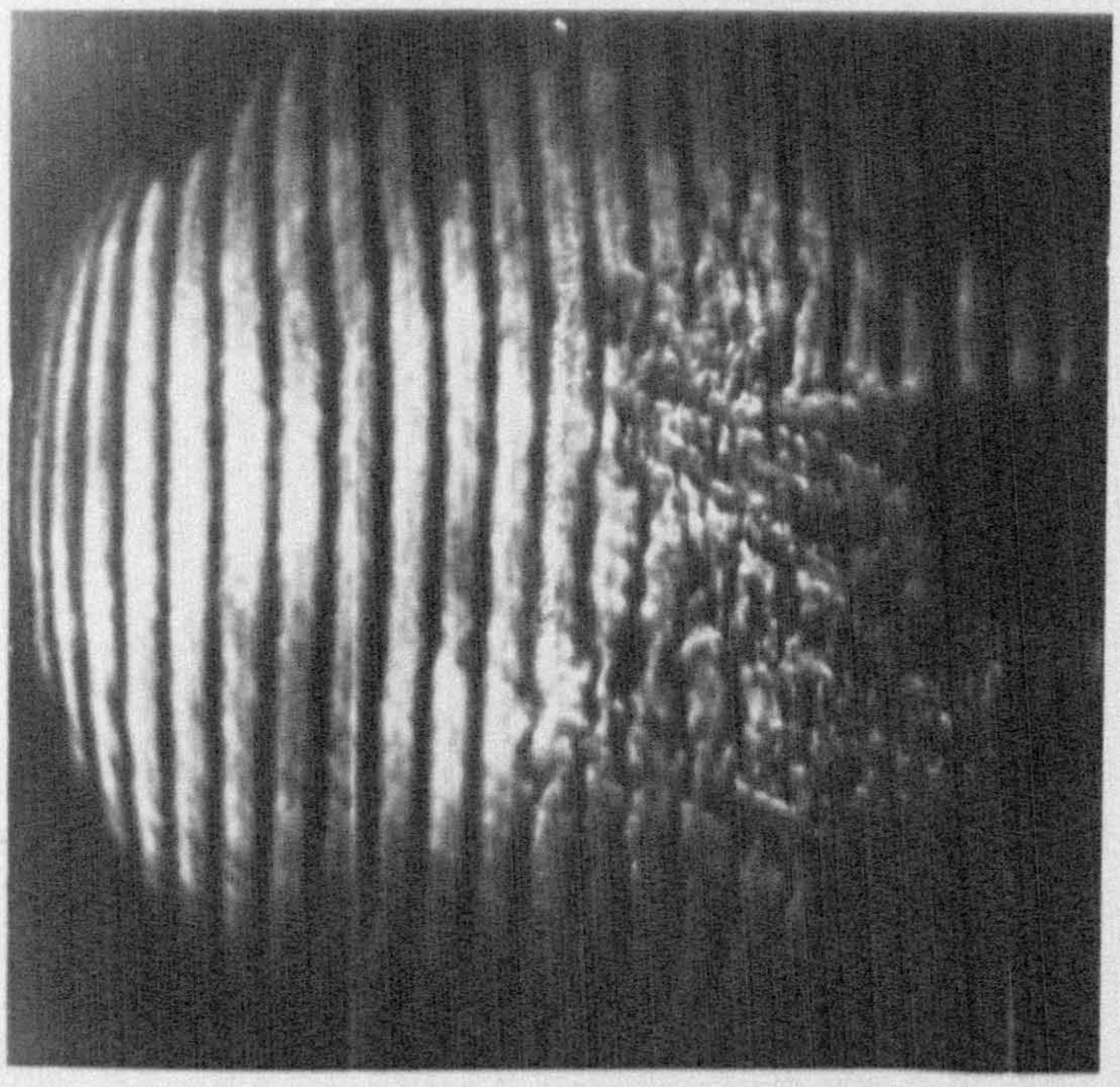

(c)

13.18% CH_4-AIR
3 J
(PARTIAL
PROPAGATION)

FIG. 4.21 NEAR-PROPAGATION LIMIT FLAMES, TIME FROM LEAVING TULIP = 2.47 m sec

FIG. 4.22 WIRE SCHLIEREN, 10% CH_4-AIR

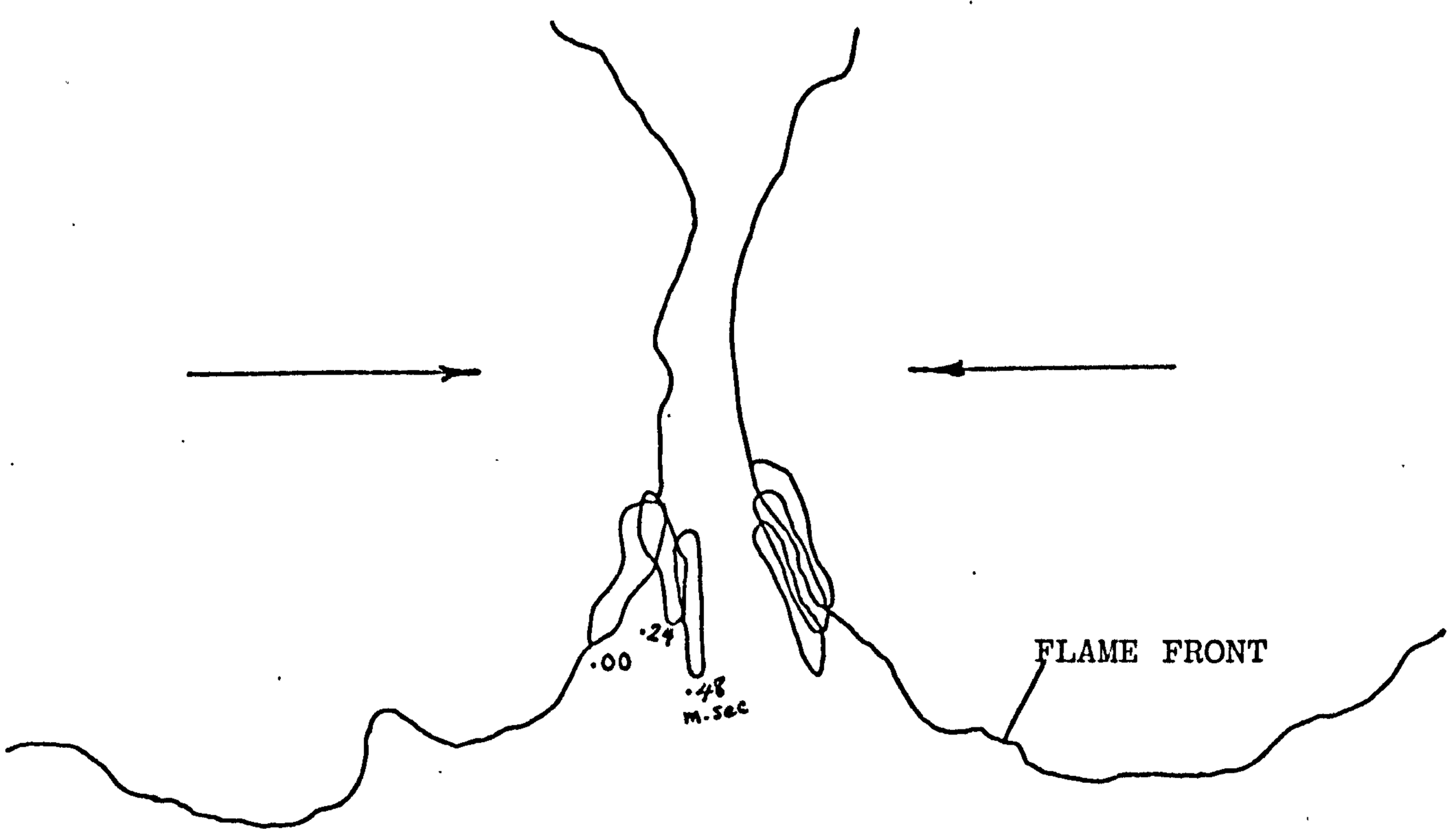

(a) DOUBLE KERNEL - 20% H_2-AIR, 2000 r.p.m.

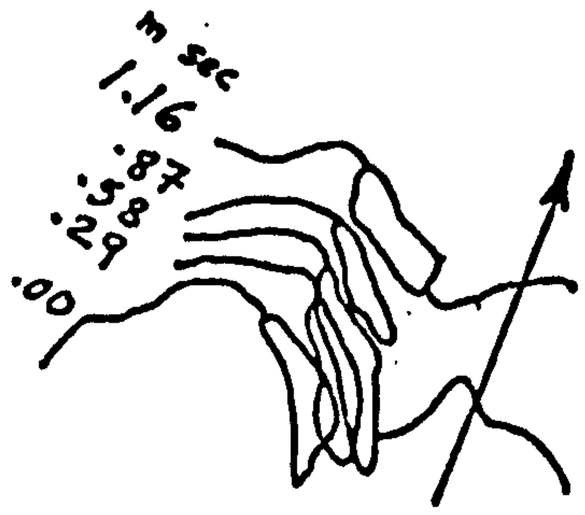

(b) MOVEMENT OF SMALL EDDY AT THE EDGE OF A FLAME FRONT
10% CH_4-AIR, 1500 r.p.m.

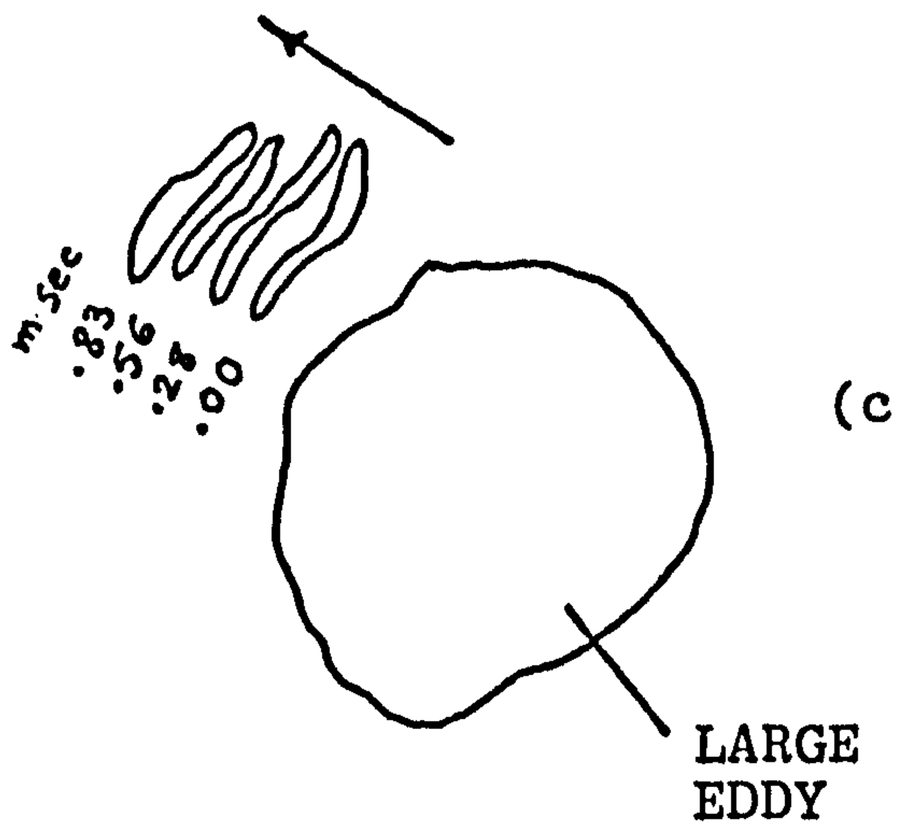

(c) MOVEMENT OF A VEIN WITH RESPECT TO LARGE EDDY
10% CH_4-AIR, 3000 r.p.m.

FIG.4.23 TYPICAL BEHAVIOUR OF SMALL EDDIES (OR VEINS) AS SHOWN BY EXPLOSION FILMS

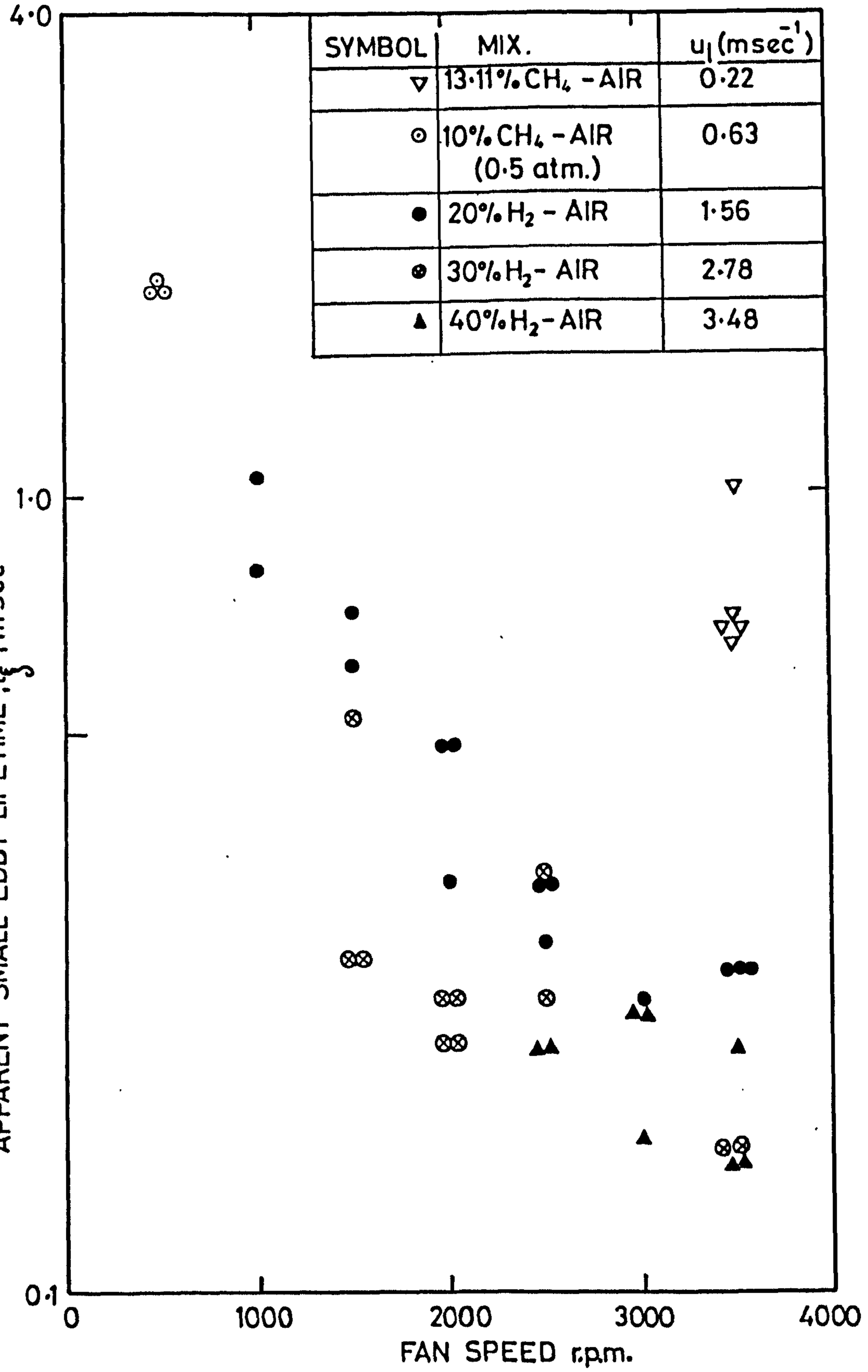

FIG. 4.24 VARIATION OF APPARENT SMALL EDDY LIFETIME WITH FAN SPEEDS FOR DIFFERENT MIXTURES

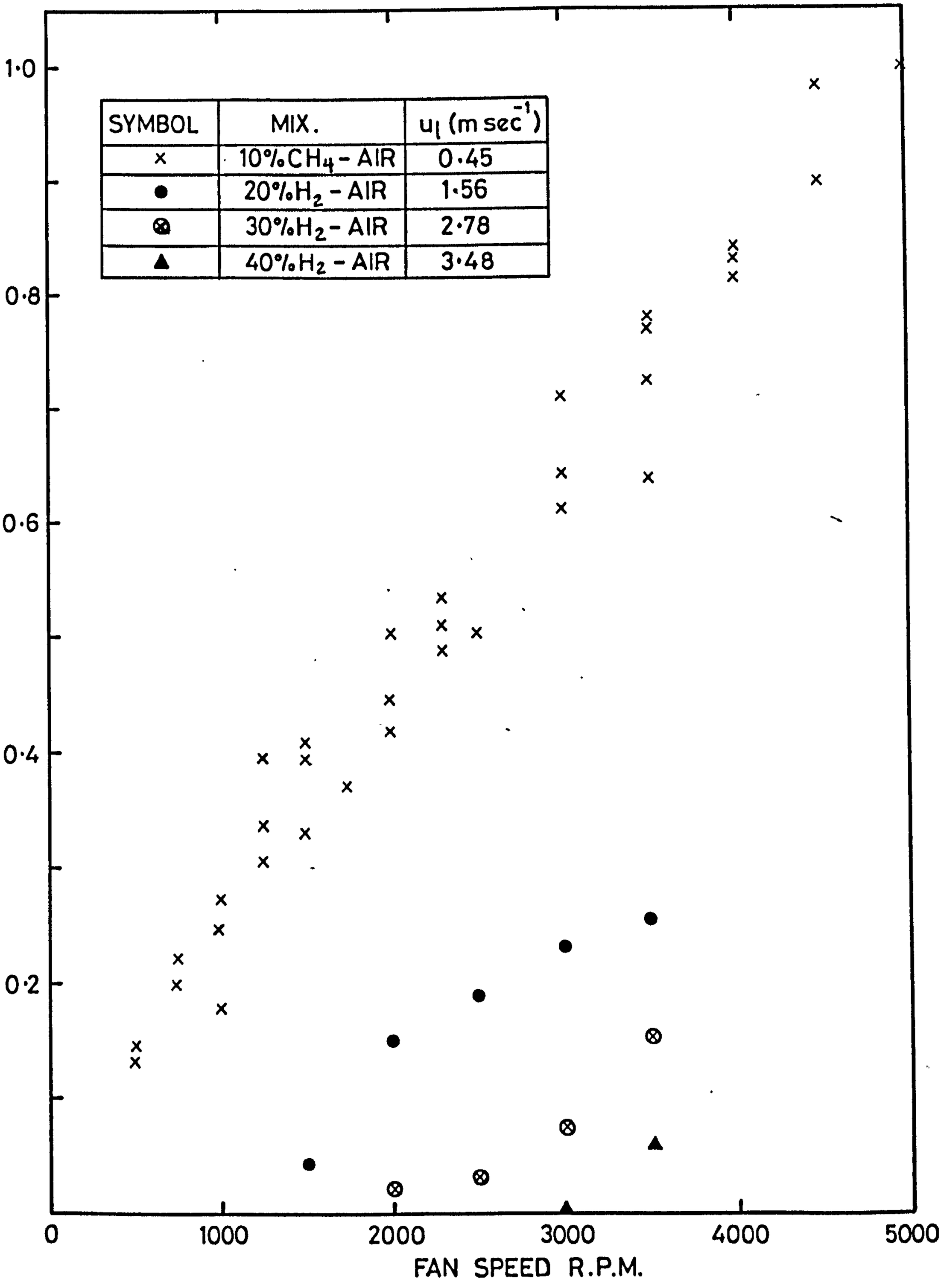

FIG. 4.25 VARIATION OF SMALL EDDIES DENSITY WITH FAN SPEED FOR DIFFERENT MIXTURES

ION GAUGE
1v / DIV
PRESSURE
50mv / DIV

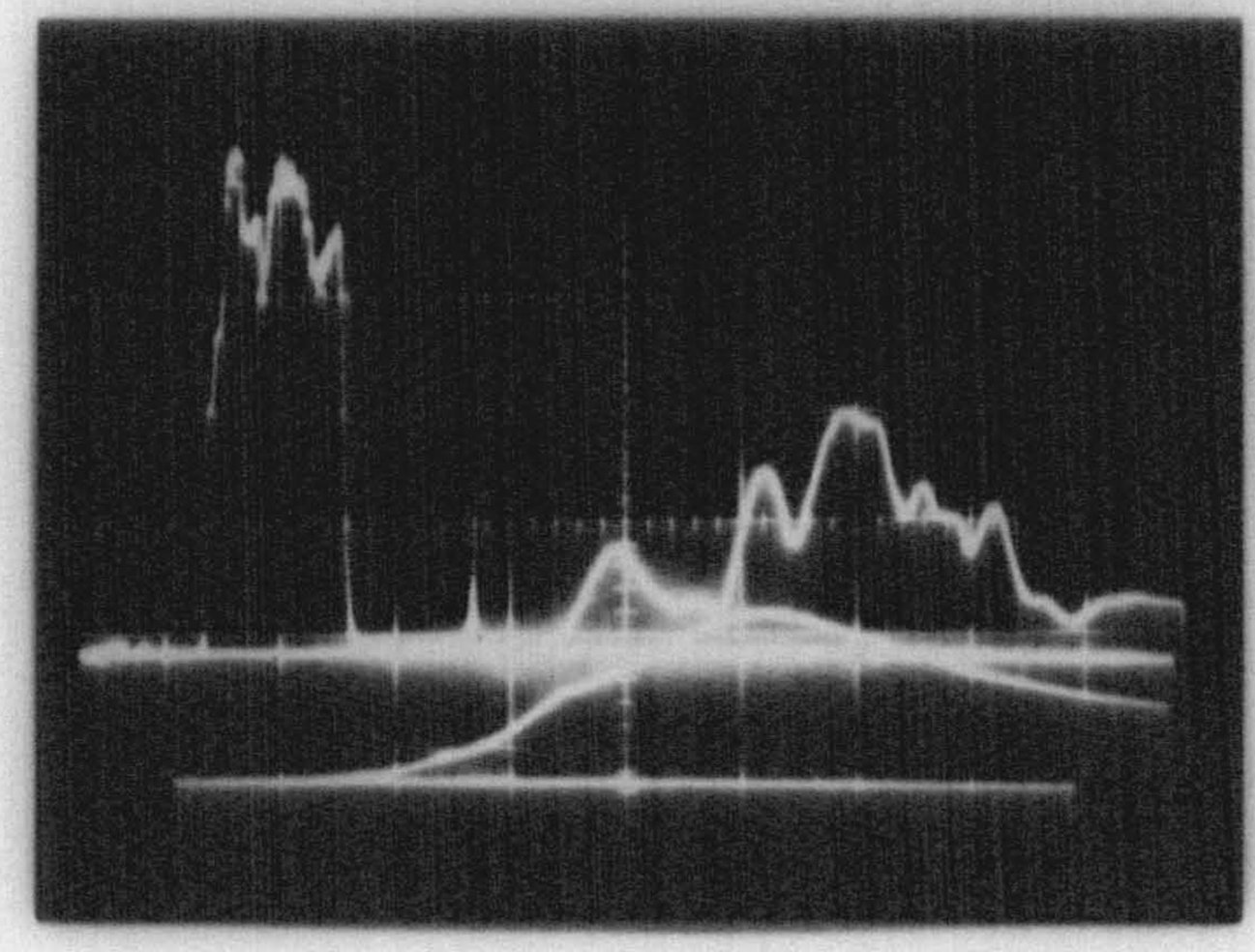

1000 rpm

(a)

10ms / DIV

ION GAUGE
0·5v / DIV
PRESSURE
50mv / DIV

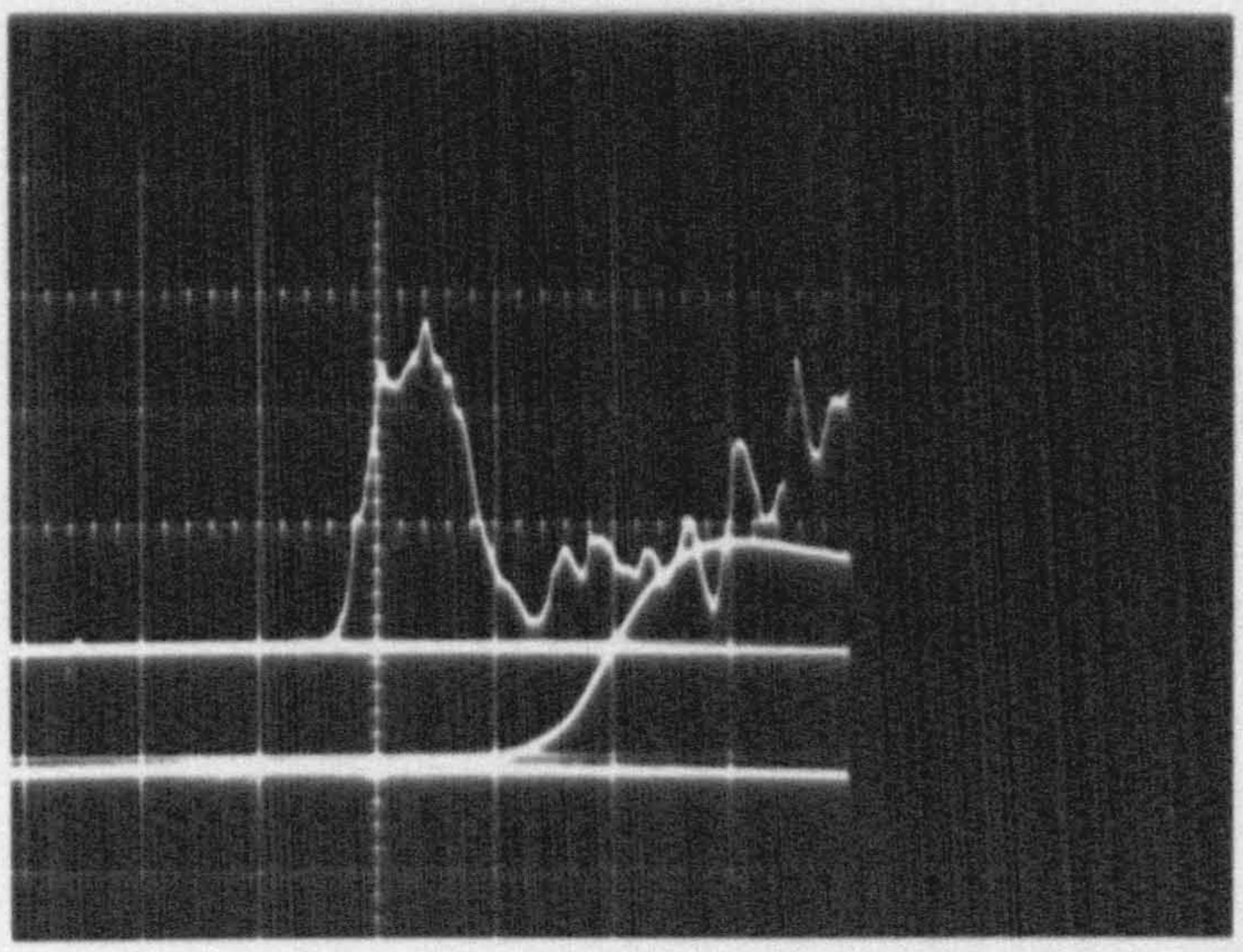

3000 rpm

(b)

5ms / DIV

FIG·4·26 IONISATION AND PRESSURE VARIATION THROUGHOUT THE 10% CH_4 - AIR EXPLOSION

CHAPTER 5

DISCUSSION OF TURBULENT FLAME PROPAGATION MEASUREMENTS

5.1 INTRODUCTION

The need to utilise the data and understand the mechanism of turbulent flame propagation has led to various proposed correlations of u_t, u_ℓ and turbulence parameters.

The experimental data of Chapter 4 and those of previous workers were plotted in a variety of ways to seek a satisfactory correlation. The best presentation seems to be one in which u_t/u_ℓ is plotted against u_ℓ/u' for different values of turbulent Reynolds number, R_L. Because any correlations which might be proposed should be valid for any system, irrespective of how the turbulence was produced, all known reasonably reliable data, drawn from a variety of rigs, are plotted alongside the data of Chapter 4. This has involved the correlation of several hundred experimental points and, where the required parameters had not been measured directly, the best possible estimation of their values. The problem is further complicated by the difficulties of measuring u_ℓ and u_t accurately and by certain arbitrariness in derivations of turbulent length scales.

5.2 CORRELATION OF TURBULENT BURNING VELOCITY DATA

5.2.1 Present Work

The results of Chapter 4 (Table 4.1) are given in Table 5.1, for hydrogen-air mixtures, and Table 5.2 for methane-air mixtures at subatmospheric pressures. These

are reproduced as functions of u_ℓ/u' and R_L. Values of u' and L at the corresponding fan speeds were drawn from the full line curves in Figs. 4.1 and 4.3, respectively, whilst values of the kinematic viscosity, ν, were computed from the programme given in Appendix 1. These results also are shown in graphs of u_t/u_ℓ, plotted against u_ℓ/u', for different ranges of R_L in Figs. 5.1 to 5.15.

Alongside the present experimental points, are those of previous workers, which are summarised in Table 5.3. These cover a wide range of burning conditions, mixture compositions and turbulent parameters. The "best" curves were drawn through the points by eye with some regard being paid to the possible accuracy of the measurements although, because of the variety of measured parameters involved, a satisfactory error analysis for each point was not possible.

The present work extended the range of experimental investigations on premixed turbulent combustion, with an approximately three-fold increase in maximum values of u_ℓ/u' over previously measured values, up to values of R_L in the region of 1500. Values of u_ℓ for H_2-air were taken from Andrews and Bradley (32) and these reached a maximum of 3.48 m sec^{-1} for 40% H_2. The values of u_ℓ for 10% CH_4-air at subatmospheric pressures were taken from the same reference and these reached a maximum of 0.90 m sec^{-1} at 0.25 atm. The use of H_2 made possible the attainment of values of u_ℓ/u' as high as 17.40, at a

value of R_L of 59. The lowest value of u_ℓ/u' was 0.60 at a peak value of R_L of 1522.

5.2.2 Previous Work

Reference to Table 5.3 shows that experimentalists have recognised the importance of measuring u' in cold flow, but often the turbulent length scale has not been measured and the importance of kinematic viscosity has been unrecognised, despite the fact that its value is the determining factor for small eddy size. Few workers have presented data that are complete enough for the proposed correlation. An alternative method of deriving R_L therefore was adopted for circular tube and flat slot burners. Experimental measurements of turbulent length scales and r.m.s. turbulent velocities in non-reacting flows at the centre line in tubes and between parallel plates have been reviewed in Chapter 2 and values of R_L, with L measured in the transverse direction, were correlated with the flow Reynolds numbers, Re and Re_p for tubes and plates, respectively.

One of the problems with such burners is that u' and L vary across the burner. Powe et al (36,37) have measured the variations of these parameters across a pipe and Laufer (38) has measured them between parallel plates. It is clear that there is an associated variation in R_L. In the present work the values of these at the plane half-way between the centre axis and the walls were estimated,

because flame measurements have been associated with this region. Such estimates are not facilitated by the increasing departure from isotropic turbulence and the lack of length scale data as the walls are approached. Further complications might arise from the generation of turbulence by the gases discharging from the burner, but any such effect upon the unburnt gases has been neglected.

Experimental measurements of r.m.s. turbulent velocity by hot wire anemometer in non-reacing flows across tube diameter, have been measured by other workers (36,39-43). Figure 5.16 shows the variation with Re of the ratio of the r.m.s. turbulent velocity for the radial direction to the mean centre line axial velocity, u'/U , at half radius of the tube. The relationship is expressed by

$$\frac{u'}{U} = 0.1676\ (Re)^{-0.119} \qquad (5.1)$$

Similarly Fig. 5.17 shows the variation of this ratio at half-way between the centre plane and a plate with Re_p based upon the distance apart of the plates. The relationship is expressed by

$$\frac{u'}{U} = 0.1151\ (Re_p)^{-0.118} \qquad (5.2)$$

Because of the lack of data for L remote from the centre line of the tube, it was not possible to obtain directly the variation of L or R_L with Re . In this case, the isotropic relationship between ε/ν and R_L ,

given by Eq. (2.20) was adopted, together with the Richardt expression for the variation of ε/ν with Re across the tube diameter, Eq. (2.3). The assumption of the validity of Eq. (2.20) at half radius is discussed in Appendix 2.

At half radius of the tube, Eq.(2.3) yields

$$\varepsilon/\nu = 0.0075\ (Re)^{7/8} \qquad (5.3)$$

From Eqs. (2.20)and (5.3)

$$R_L = 2.182 \times 10^{-6}\ (Re)^{1.563} \qquad (5.4)$$

for $100 < R_L < 3000$

There are no measurements to check the applicability of this equation at values of R_L greater than 3000, but it was extrapolated to a value of 7700.

For parallel plates, Laufer's measurements of L and u' in a channel were used to obtain R_L and these are shown in Fig. 5.18. To extend the range of Re_p, Eq. (2.20) was applied to the measurements of ε/ν of Shrowed and Wortz (48) and Page et al (49), to obtain the corresponding values of R_L. These also are shown in Fig.5.18. The relationship is expressed by

$$R_L = 6.121 \times 10^{-6}\ (Re_p)^{1.593} \qquad (5.5)$$

for $10 < R_L < 1000$

Again this equation was extrapolated to values of R_L up to 10,500.

Where it was necessary to estimate the value of L in a grid-generated turbulence the data of Ref.50 were utilised in the form

$$\frac{L_y}{b} = 0.115 \left(\frac{x}{b}\right)^{0.452} \qquad (5.6)$$

where

x = distance downstream from mid-plane of screen,

b = bar width,

L_y = length scale transverse to direction of flow (x).

Previous burning velocity measurements made in the present bomb and reported by Andrews, Bradley and Lwakabamba (25) employed CH_4-air and C_2H_4-air mixtures. These measurements were used in the present correlations but with revised values of u' and L , obtained from the measurements given in Chapter 4.

The curves in Figs. 5.1 to 5.15 clearly indicate the influence of both u_ℓ/u' and R_L upon the ratio u_t/u_ℓ . The best curves through the experimental points are collected together in Fig. 5.19 for R_L up to 3000, when Eqs. (5.4) and (5.5) are most valid. Bearing in mind all the difficulties in accurately measuring burning velocities and turbulent parameters, the exhibited correlations are significant. Practical combustors operate at the highest values of R_L and with u_ℓ/u' in the region of 0.1 (51). Figure 5.19 shows that this is a régime where an increase in turbulence can increase u_t

appreciably, although this may be accompanied by increasingly difficult ignition and stability, as discussed in Section 5.3.1.

It has been suggested (51,84,85,124-126) that as the turbulence level is increased, so turbulent flame propagation is increased through the agency of small scale dissipative isotropic eddies at the Kolmogorov, high frequency end of the turbulence spectrum. At high turbulence levels a laminar flame mechanism is unlikely and both energy and mass transport probably occur principally through small scale eddy mixing within a relatively thick flame zone. If it is assumed that turbulent predominates over molecular transport, with but small changes in chemical kinetics, a relationship can be derived between u_t/u_ℓ and the turbulent transport number, ε/ν, where ε is the eddy diffusivity. The treatment of Spalding (52,53) in deriving an analytical expression for u_ℓ may be followed, but with turbulent transport coefficients replacing those of molecular transport. For constant transport parameters and specific heats, and with turbulent Lewis number of unity, this leads to

$$\frac{u_t}{u_\ell} = \left(\frac{\varepsilon}{\nu} Pr\right)^{\frac{1}{2}} \qquad (5.7)$$

where Pr is the Prandtl number. This assumes that the area under the chemical heat release rate versus reactedness curve, and the shape of the curve, are

unchanged by turbulence. Correlation of the available experimental data given in Chapter 2, suggests that for isotropic turbulence, the turbulent transport number and turbulent Reynolds number are related by Eq.(2.20).

Equation (5.7) essentially is obtained from an analogy between small eddy and molecular transport, but this has many deficiencies. In the limit, as turbulence intensity, u', infinite or u_t/u' and u_ℓ/u' tend towards zero, Eq. (5.7) is most valid.

Theoretical values of u_t/u_ℓ were found from Eqs. (2.20) and (5.7), for different values of R_L, with Pr = 0.7. The two equations give

$$\frac{u_t}{u_\ell} = 2.787\ (R_L)^{0.28} \qquad (5.8)$$

for $R_L > 100$ and $u_\ell/u' \to 0$

Values of u_t/u_ℓ obtained from Eq. (5.8) have been marked by an asterisk, for the mid range values of R_L, on Figs. 5.1 to 5.15, for u_ℓ/u' equal to zero. The agreement with the curves through the experimental points is fair. It will be noticed from Figs. 5.1 to 5.3 that the point derived from Eq. (5.8) becomes significantly less than experimental values at values of R_L above 3000. As u_ℓ/u' tends to larger values, so molecular transport processes overwhelm those of turbulent transport and, in the limit, with u_ℓ/u' infinite, u_t/u_ℓ is unity. Figures 5.5 to 5.15

show this trend. The decrease of u_t/u_ℓ between these two limits is discussed theoretically in Chapter 6.

Examination of the data of Figs. 5.1 to 5.15, for any effect of flame confinement, showed there to be no observable effect even when the flame was confined in a duct with a width as low as twice burner diameter. However, when the duct width was equal to the burner diameter, as in Ref.19, higher values of u_t/u_ℓ were observed. Possibly this is explained by the additional production of turbulence through shear stresses. The figures also show that this effect is reduced as the turbulence level increases as might be expected.

5.2.3 Dependence of u_t on Pressure and Temperature

Many practical turbulent combustion devices operate at pressures and temperatures other than ambient. Thus the effect of these parameters on u_t is important and the results of several investigations on this are listed in Table 5.4.

In the course of the present work it was decided to investigate the correlation of u_t/u_ℓ at subatmospheric pressures. This necessitated the calibration of the present vessel, by measuring u' and L, at low pressures and the results are discussed in Chapter 4. Measurements were made of u_t at 0.25 and 0.50 atmosphere using 10% CH_4-air mixtures. The two results obtained are given

in Table 5.2 and are shown in Fig. 5.13 for 0.50 atm. and Fig. 5.14 for 0.25 atm. They show good correlation with other measurements made at ambient pressures. Measurements of u_t have been made by other workers in mixtures at non-ambient pressures and temperatures and are included in Table 5.3 and shown in Figs. 5.3 to 5.14. Again, these support the proposed correlations.

5.3 RÉGIMES OF COMBUSTION

Since Damköhler's (1) use of the ratio of integral scale of turbulence to laminar flame thickness as a criterion of mode of flame propagation various dimensionless parameters have been suggested as bounds to define régimes. The different criteria, in the form of values for a dimensionless parameter Γ, which have been used to define régimes of wrinkled and non-wrinkled turbulent flames are listed in Table 5.5. A wrinkled flame can be regarded as a continuous, yet irregular, laminar flame surface. Where $\Gamma << 1$ then the wrinkled laminar flame model is applicable and where $\Gamma >> 1$, the flame front is no longer represented by a continuous wrinkled laminar-type flame. Table 5.5 also shows these criteria after transformations in terms of the parameters u_ℓ/u' and R_L. The equations used to do this are listed in the last column.

Three criteria are now briefly outlined. First, that given by Kovasznay (70), assumes that locally only the

rate of deformation controls the break-up of the flame front. The dimensionless parameter, Γ, is then proportional to the velocity gradient in the cold turbulent flow divided by a velocity gradient in the laminar flame. This is given (70) in the form

$$\Gamma = \frac{u'}{\lambda} \cdot \frac{\delta_\ell}{u_\ell} \tag{5.9}$$

where λ is the Taylor microscale of turbulence and δ_ℓ is the laminar flame thickness given by (87)

$$\delta_\ell = \frac{\nu}{u_\ell . Pr} \tag{5.10}$$

where Pr is the Prandtl number, assumed to be 0.7 in the present analysis. Kovasznay suggested that high values of Γ will give continuous combustion zones, and low values a wrinkled laminar flame, whilst cross-over occurs where Γ is in the region of unity. Introduce Eqs. (2.18) and (5.10) into Eq. (5.9) and the condition $\Gamma < 1$ leads to

$$\frac{u_\ell}{u'} > 0.468\ R_L^{-0.25} \tag{5.11}$$

Equality of the two terms is indicated by the dotted curve A in Fig.5.20. To the right of this curve $\lambda > \delta_\ell$, and to the left $\lambda < \delta_\ell$.

Kovasznay also proposed to investigate available experimental information by plotting

$$\frac{\text{apparent turbulent flame speed}}{\text{laminar flame speed}} = f(\Gamma)$$

to see whether a good correlation is obtained. He argued that the r.m.s. turbulent velocity was not sufficient to characterize turbulent agitation but that the microscale was equally important.

Second, Klimov's criterion (74,75) is that Γ is the product of the highest significant strain rate with the residence time in the flame. This takes the form

$$\Gamma = \frac{u'}{L} \cdot \frac{\delta_\ell}{u_\ell} \qquad (5.12)$$

Klimov argued that when $\Gamma << 1$ the turbulent flame is a distorted laminar flame front, and the probability of damping of sections of the flame front is low; that when $\Gamma >> 1$ 'volume' combustion predominates, and the probability of the existence of laminar fronts is low, the transition region corresponds to $\Gamma \sim 1$. From Eq.(5.10), the condition $\Gamma << 1$ leads to

$$\frac{u_\ell}{u'} >> 1.195 \quad R_L^{-0.5} \qquad (5.13)$$

Equality of the two terms is indicated by the chain curve B in Fig.5.20. To the right of this curve $L > \delta_\ell$, and to the left $L < \delta_\ell$.

Third, Williams' criterion (86) is that a wrinkled laminar flame structure can exist when the laminar flame thickness is much smaller than the Kolmogorov microscale of turbulence, η. The latter is given in isotropic turbulence by (51)

$$\eta = \lambda\, 15^{-0.25}\ R_\lambda^{-0.5} \qquad (5.14)$$

From Eqs.(2.18),(5.10) and (5.14) this criterion leads to

$$\frac{u_\ell}{u'} >> 1.102\ R_L^{-0.25} \qquad (5.15)$$

Equality of the two terms is indicated by the dashed curve C in Fig.5.20. To the right of this curve $\eta > \delta_\ell$ and to the left $\eta < \delta_\ell$.

A wrinkled laminar flame structure would occur only significantly to the right of this curve. The curve, however, does not delineate two distinctively different flame structures.

Other workers have proposed other criteria and these are listed in Table 5.5. Among them are Sokolik's (72) and Talantov's (73) amendment of Klimov's criterion. More recently, Chomiak (84,85) used the model of intermittency proposed by Tennekes (109), to suggest an intermittent fine flame structure at values of $R_\lambda > 100$, where $R_\lambda = \frac{u'\lambda}{\nu}$. At higher values of R_λ , Chomiak argued that any continuous flame sheet would be disrupted.

Since the publication by Andrews, Bradley and Lwakabamba (51) of a review of theories of turbulent burning velocity, Ballal and Lefebvre (24) have examined experimentally the influence of turbulence intensity and length scale on burning velocity and flame structure. They used premixed propane-air mixtures at atmospheric pressure. From analysis

of their results, they presented a three-region model for turbulent burning.

Unfortunately, the agreement between the present results and the algebraic expressions of Ballal and Lefebvre is not good, as is shown from consideration of their three-regions.

Region 1: $u' < 2\, u_\ell$ and the Kolmogorov microscale, η, greater than the laminar flame thickness, δ_ℓ. They argued that in this region, the burning velocity is increased due to the effect of turbulence in wrinkling the flame and thereby extending its surface area. If the condition $\eta > \delta_\ell$ is considered, then this is the region to the right of the dashed curve C in Fig.5.20. Reference 24 gives for this region (after a correction to the published expression by the authors (88))

$$\left(\frac{u_t}{u_\ell}\right)^2 = 1 + 0.03 \left(\frac{u'L}{u_\ell \delta_\ell}\right)^2 \qquad (5.16)$$

With the expression for δ_ℓ given by Eq.(5.10) this becomes

$$\left(\frac{u_t}{u_\ell}\right)^2 = 1 + 0.03 \left(R_L\, Pr\right)^2 \qquad (5.17)$$

This expression shows no dependence upon u_ℓ/u'. The experimental results for hydrogen-air flames show that even when R_L is large, $u_t/u_\ell \to 1$ as $u_\ell/u' \to \infty$. For example, measurements, reported in Table 5.1, show that with $R_L = 1005$, and $u_\ell/u' = 1.56$ then $u_t/u_\ell = 3.05$. On the other hand, Eq. (5.17) gives u_t/u_ℓ, for this value of R_L and with Pr = 0.7, the impossibly high value of 122.

Region 3: $u' > 2\, u_\ell$ and Kolmogorov microscale less than the laminar flame thickness. They argued that in this region the combustion zone may be regarded as a fairly thick matrix of burned gases interspersed with eddies of unburned mixtures, and the combustion is sustained almost solely by the reactions taking place at the interfaces formed between the combustion products and the eddies of fresh mixture. If the condition $\eta < \delta_\ell$ is considered, then this is the region to the left of the dashed curve C in Fig.5.20. Reference 24 gives for this region

$$\frac{u_t}{u_\ell} = 0.5 \left(\frac{u'\delta_\ell}{u_\ell\, \eta}\right) \tag{5.18}$$

From the expressions given in Eqs. (2.16), (2.18) and (5.14) it readily can be shown that $\eta \alpha L\, R_L^{-\frac{3}{4}}$. If this is combined with the expression given by Eq. (5.10) for δ_ℓ, then

$$\frac{\delta_\ell}{\eta} \alpha \frac{u'}{u_\ell}\; R_L^{-\frac{1}{4}} \tag{5.19}$$

Substitution of Eq.(5.19) in Eq.(5.18) gives

$$\frac{u_t}{u_\ell} \alpha \left(\frac{u'}{u_\ell}\right)^2\; R_L^{-\frac{1}{4}} \tag{5.20}$$

and u_t/u_ℓ would decrease with increase of R_L at constant value of u_ℓ/u'. This is contrary to the results summarised by the curves in Fig.5.19.

Region 2: $u' \simeq 2\, u_\ell$ and $\eta \simeq \delta_\ell$. The authors argued

that this region lies between regions 1 and 3 and the fresh mixture contains eddies which are both larger and smaller than the thickness of the flame. They argued that in this region, two different mechanisms for augmenting the surface area of the flame operate simultaneously.

(i) The flame front is wrinkled by all eddies larger than its own thickness.

(ii) The area of interface between combustion products and fresh mixture is significantly increased by the eddies entrained between the inner and outer boundaries of the flame zone.

If the condition $\eta \simeq \delta_l$ is considered, then this is the region indicated by the dashed curve C in Fig.5.20. Reference 24 gives for this region

$$u_t = 2\ u' \tag{5.21}$$

and in a dimensionless form this becomes

$$\frac{u_t}{u_l} = 2\ \left(\frac{u_l}{u'}\right)^{-1} \tag{5.22}$$

This expression shows no dependence upon R_L. This is contrary to the results summarised by the curves in Fig.5.19.

In Chapter 2, the measured length scales of Ballal and Lefebvre (24) were discussed and shown in Fig.2.10. They indicate a poor correlation of L and λ, contrary to what would be expected in isotropic turbulence. Errors

in length scale measurements might explain the discrepancies between their results and those of the present study.

5.3.1 Effect of Turbulence upon Flammability Limits

Table 5.6 shows that the effects of turbulence on ignition and flammability limits have received only limited experimental attention. Historically the investigations of Wheeler (89) are significant, because of the conclusions concerning the effect of turbulence on flame propagation. He realised that turbulence did not necessarily increase the burning velocity of all flames by the same relative amount. He also reported the first observations of turbulent quenching of an initially propagating flame, a phenomenon, he concluded, that would occur first in those mixtures with lower burning velocity.

Most quantitative investigations have been into the effect of turbulence on minimum ignition energies and all show these to increase with turbulence intensity. Most practical systems ulilise energies much greater than the minimum ignition energy but an increase in turbulence can result in an ignition failure.

Spark ignition of a mixture is a form of thermal explosion, and critical conditions for its occurrence exist when the rate of heat liberation from the reaction in the spark kernel becomes equal to the energy loss from the surface.

The effect of turbulence parameters on flammability limits have never been quantitatively investigated, apart from the investigation of Karpov and Sokolik (97). Andrews and Bradley (106) showed that the actual measurement of laminar flammability limits was difficult and that under certain circumstances gas mixtures could exhibit limits, whereas in an infinite enclosure a flame could propagate. Hence true flammability limits which are independent of the ignition source and the enclosure are difficult, if not impossible, to measure. Fig.4.15 shows how an increased level of turbulence narrows slightly the lean limits of flammability, whilst the effect is more marked at the rich limits. This is in line with the results obtained by Karpov and Sokolik (97) in experiments in a nearly spherical vessel equipped with four stirrers driven by electric motors, by Wakisaka et al (102) in a two-stroke cycle gasoline engine, and by Hamamoto et al (105) in an L-head single cylinder engine burning propane.

The results of Fig.4.15 and Table 4.4 are expressed in terms of the dimensionless parameters employed for burning velocity correlations in Fig.5.19. Values of u_l were taken from Ref. 106 for methane-air mixtures and from an extrapolation of the data of Ref. 32 for hydrogen-air mixtures. Values of ν, for determining R_L, were computed with the programme given in Appendix 1. Figures 5.21 and 5.22 show that the flammability limits could be correlated in terms of these parameters. Indeed correlation of flammability limits in this way is not entirely satisfactory

because of the limited knowledge and accuracy of near-limit burning velocities.

Karlovitz (107,108) argued that if

$$\frac{\delta_\ell}{u_\ell} \cdot \frac{u'}{L} > 1$$

the heat of the combustion wave is rapidly scattered and the flame is likely to be quenched. With the expression given by Eq.(5.10) for δ_ℓ, this condition leads to

$$\frac{u_\ell}{u'} < 1.195 \; R_L^{-0.5} \qquad (5.23)$$

Equality of the two terms is indicated by the dashed curve in Fig.5.21 and the dashed line in Fig.5.22. This is almost parallel to the present experimental results but with lower flammability limits.

The only known investigations of the effect of turbulence parameters on the flammability limits in the literature, are those of Karpov and Sokolik (97) in a stirred bomb. They investigated the effect of u' and spark energy upon such limits; which were shown to be narrowed by an increase in u' . A twenty-fold increase in spark energy extended the limits of propane-air mixtures at atmospheric pressure.

Figure 5.22 shows that burning was possible with other fuels and in other apparatus, to the left of the presently observed flammability limits. This suggests that in no way do these limits represent universal limits.

An explanation of the discrepancies between the results of the present work and those of others lies in the limited size of the present vessel. Perhaps limit flames had not become fully developed and therefore quenched, whereas in a larger vessel if a critical flame diameter had been attained, propagation might have been possible. This question is touched upon theoretically in the next Chapter.

5.4 SMALL EDDY STRUCTURE

An attempt was made to relate régimes of combustion to flame structure from the available photographic evidence.

The first photographic studies of turbulent flames were simple time-averaged photographs of the luminous flame (110). The only relevant information these yield is the time-averaged flame brush thickness, which has always been found to be greater than that of a laminar flame. The most useful photographic technique is that of short duration exposure or spark photography. This technique attempts to freeze the fluctuations, so that the instantaneous distribution of optical inhomogeneities within the turbulent flame brush can be examined.

Both shadow (111,112) and schlieren (71,113-117) instantaneous photography has been used to examine the structure of turbulent flames. The instantaneous structure revealed is qualitatively similar for a wide variety of conditions and consists of a randomly distorted discontinuous 'optical surface' within the turbulent flame brush. Particle

track studies (17,118) indicate that the instantaneous form of the reaction zone is similar to that revealed by the spark schlieren photographs. Karlovitz et al (3) and many other workers (17,114-118) assumed that the optical inhomogeneity detected by the instantaneous schlieren photographs is a laminar flame reaction zone. However, Dubrovskaya et al (119) using 5 μ sec. spark schlieren photography, have found that the thin surface of flame, characteristic of laminar flame, was completely absent from photographs and the observed reaction zone was much thicker.

Summerfield et al (120,121) obtained spark shadow photographs of the reaction zone of mild turbulent flames. The time resolution was sufficient to freeze any wrinkled laminar flame that might have been present. The pictures, which are similar to other short duration photographs, were interpreted as indicating a highly granular flame zone, with many cell size irregularities as small as 1mm and possibly smaller. This observation was thought to be inexplicable on the basis of a mildly fluctuating laminar flame structure.

The optical inhomogeneities were attributed to statistical fluctuations of temperature and composition. In their tests the turbulent burning velocity was less than six times the laminar burning velocity and these conditions would lie within the wrinkled flame régime of Fig.5.20.

More recently, Chomiak (85) has obtained spark shadow photographs of exposure time about 10 μ sec., of a turbulent flame at high turbulence levels. These photographs

showed a distinct structure of width approximately equal to the Kolmogorov microscale and which Chomiak assumes to be a vortex tube. This was thought to illustrate that turbulent burning zones at high levels of turbulence consist of strong, loose vortex tubes in which the chemical reaction occurs. Ono et al (122) have obtained schlieren photographs of a high tubulent flames. They showed that the mean size of wrinkling of the flame front is close to the corresponding integral scale of cold turbulence, a result which had been obtained previously by Lwakabamba (123) in his studies at Leeds.

Instantaneous schlieren photography records the sharp changes in refractive index gradient caused by combustion. The schlieren photographs of turbulent flames, obtained in the present study, enable the nature of the reaction zone to be examined, as described in Chapter 4.

The curves A,B,C of Fig.5.20 do not delineate two distinctively different flame structures. Schlieren photographs of flames were compared for two régimes in Fig.5.20. At high values of R_L with hydrocarbon-air flame values of u_ℓ/u' in the vicinity of 0.1, a pronounced small scale structure was in evidence, in addition to the macro-structure, as shown in Fig.4.22(c). For a 20% H_2-air flame with R_L = 1522 and u_ℓ/u' = 0.6, which point lies to the right of the dashed curve C in Fig.5.20, a small scale structure also was revealed. At comparable values of R_L, but with hydrogen-air flames with values of u_ℓ/u' greater

than unity, only the macro-structure was in evidence. The appearance now was that of a wrinkled laminar flame. Reference to Fig.5.20 shows such a flame to be in the régime where this structure might be expected. The present evidence suggests the wrinkled flame régime occurs for $u_\ell/u' > 1$.

Outside the régime of the wrinkled laminar flame, the dissipative eddies, that have been observed photographically, very probably play an active role in flame propagation. If this is so, the apparent lifetime of these small eddies might be expected to be of the order of the cold Kolmogorov time scale, t_η .

5.4.1 Apparent Small Eddy Lifetime

The apparent lifetime of the small eddies or veins, t_ξ , shown in Fig.4.24, together with those measured by Lwakabamba (123) in the present vessel for 10% CH_4-air and 5.77% C_2H_4-air mixtures are plotted in Fig.5.23. In line with the correlations of burning velocity these are expressed in dimensionless form, with t_ξ/t_η plotted against $\eta/u_\ell t_\eta$. For isotropic turbulence t_η is given by (51)

$$t_\eta = 15^{-0.5} \frac{\lambda}{u'} \qquad (5.24)$$

Equations (2.16) and (5.24) yield

$$t_\eta = 1.681 \frac{L}{u'} R_L^{-0.5} \qquad (5.25)$$

The time, η/u_ℓ , is a notional chemical lifetime for the small eddies and is the time a laminar flame would take to propagate across a vortex tube of diameter η .

The small eddies which were observed photographically might consist of already burnt or of chemically reacting gas. Dissipation along a vortex tube ultimately will reduce the temperature gradients and eventually it will cease to be visible.

The value of t_ξ will be a function, not only of the eddy lifetime, but also of its temperature history and the sensitivity of the measuring system. When initiation of chemical reaction occurs, there might be an associated induction period, during which the vortex tube is invisible. When a chemical lifetime is longer than the eddy lifetime, the continuing reaction might render the eddy visible for a longer period. In these ways there might be a secondary influence of chemical lifetime upon the apparent lifetime.

These considerations receive support from Fig.5.23, which indicates that small eddies are visible for a period of time most probably in the range of values of t_ξ/t_η between 0.5 and 1.5. The secondary influence of chemistry might be discerned in some tendency for the value of t_ξ/t_η to be small or large in concert with that of $\eta/u_\ell t_\eta$. But although the photographic technique reveals apparent eddy lifetimes to be close to Kolmogorov times, it cannot yield accurate values of their chemical lifetimes.

The distribution of experimental measurements in Fig.5.23 suggests that lifetimes would be described more accurately by probability distribution functions (pdfs). Furthermore, such functions should also be a function of the reactedness. The present photographic measurements are based upon the eddies at the kernel edge, where the value of the mean reactedness is low.

It has been pointed out in Chapter 4 that for hydrogen-air mixtures the number of frames upon which a small eddy appeared was small when compared with hydrocarbon-air mixtures. An eddy might appear only on a single frame for a 40% H_2-air mixture with a fan speed of 3,5000 r.p.m., whilst for a 10% CH_4-air mixture at the same speed, an eddy might appear on five frames. Accordingly, the measurements in hydrogen-air mixtures are less accurate than in hydrocarbon-air mixtures,

5.4.2 Small Eddy Density

The measured normalised photographic densities of the small eddies, Y, which were reported previously in Fig.4.25, are reproduced as functions of R_L and u_ℓ/u', in Fig.5.24. Dashed curves at approximately constant values of Y have been drawn through the experimental points.

Figure 5.24 shows clearly that these curves are parallel to curve C in Fig.5.20. Values of Y increase either by a decrease in u_ℓ for a given turbulence level or by an increase in turbulence for a given mixture, with the

former exerting a greater influence. The figure clearly shows that an increase in turbulence, increases the number of small eddies with an associated increase in u_t. The quantitative measurements of the optical density of such eddies confirm the importance of small eddy burning as curve C is approached.

TABLE 5.1 Experimental Results of Present Work with H_2-air Mixtures

Fan Speed r.p.m.	15% H_2 u_ℓ=1.01 m sec^{-1}			20% H_2 u_ℓ=1.56 m sec^{-1}			30% H_2 u_ℓ=2.78 m sec^{-1}			40% H_2 u_ℓ=3.48 m sec^{-1}		
	$\frac{u_t}{u_\ell}$	$\frac{u_\ell}{u'}$	R_L	$\frac{u_t}{u_\ell}$	$\frac{u_\ell}{u'}$	R_L	$\frac{u_t}{u_\ell}$	$\frac{u_\ell}{u'}$	R_L	$\frac{u_t}{u_\ell}$	$\frac{u_\ell}{u'}$	R_L
250				1.67	7.80	75	1.37	13.92	67	1.35	17.40	59
500	2.72	2.66	163	2.31	4.11	154	1.87	7.33	138	1.69	9.16	122
1000				3.27	2.08	348	2.37	3.71	311	2.09	4.64	274
1500				3.78	1.38	567	2.66	2.46	507	2.33	3.08	447
2000				4.17	1.04	799	2.91	1.86	713	2.54	2.32	629
2500				4.62	0.84	1030	3.28	1.50	920	2.79	1.87	811
3000				5.03	0.70	1276	3.46	1.25	1139	3.05	1.56	1005
3500				5.51	0.60	1522	3.74	1.07	1359	3.25	1.34	1198

TABLE 5.2 Experimental Results of Present Work with 10% CH_4 - air Mixtures at Low Pressures

Fan Speed r.p.m.	10% CH_4 0.50 atm. u_ℓ = 0.63 m sec^{-1}			10% CH_4 0.25 atm. u_ℓ = 0.9 m sec^{-1}		
	$\frac{u_t}{u_\ell}$	$\frac{u_\ell}{u'}$	R_L	$\frac{u_t}{u_\ell}$	$\frac{u_\ell}{u'}$	R_L
500	2.51	1.66	92	1.81	2.37	46

TABLE 5.3 Turbulent Burning Velocity Data of Previous Workers

Author	Ref.	Mixture	P (Atmos)	T (^{o}C)	ν ($m^2 s^{-1} \times 10^{-6}$)	u_ℓ ($m\,s^{-1}$)	u_ℓ Ref.	u' ($m\,s^{-1}$)	L (mm)	Method
Damköhler	1	Propane-O_2	1	25	11.6-13.2	1.27-2.90	1	Eq.(5.1), 1.12-4.17	Eq.(5.4), R_L	Tube, inner cone area.
Williams et al	2	City Gas-Air	1	25	16.0	.24-.35	2	Given, $\frac{u'}{U}$ = 2.3%	Measured, 3.18	Nozzle,grid, inner flame area.
Karlovitz et al	3	2 mixtures	1	25	15.879	.45, 1.75	3, 28	Measured, .4-6.5	Eq.(5.4), R_L	Tube, inner angle, $\frac{r}{R} \lesssim 0.7$.
Karlovitz	4	Methane-Air	1	25	15.879	0.45	28	Measured, .09-3.5	Measured, .5-3.0	Tube, inner angle.
Wohl and Shore	5	2 mixtures	1	25	15.70	.12 - .4	5	Given,Refs. 29,30 $\frac{u'}{U}$ = 0.9% - 13.3%	Given,Ref. 31, .22 - 1.64	Tube, total area of maximum luminosity.
Wagner	6	3 mixtures	1	25	≈ 15.0	.36 - 1.24	6	Given, $\frac{u'}{U}$ = 2% - 4.9%	Eq.(5.4), R_L	Tube, mean flame-surface area .
Richmond et al	7	Methane-Air	1	25	15.89	.45	28	Measured, .04 - .37	Eq.(5.4), R_L	Tube, "V" flame, angle.

TABLE 5.3 (cont.)

Author	Ref.	Mixture	P (Atmos)	T (^{o}C)	ν ($m^2 s^{-1} \times 10^{-6}$)	u_ℓ ($m\ s^{-1}$)	u_ℓ Ref.	u' ($m\ s^{-1}$)	L (mm)	Method
Khramtsov	8	Propane-Air	0.1-0.6	20	26.22 - 157.32	$.46\ P^{-0.5}$, .59 - 1.45	32, 33	Given, 2.8 - 5.0	Measured, 2.8	Tube, grid, inner area.
Karpov et al Semenov Sokolik et al	9 10 11	9 mixtures	1	25	13.6-95.3	.29-1.4	9, 11	Measured, .8 - 8.4	Measured, 2.3 - 4.8	Bomb, fan, expansion ratio.
Kozachenko	12, 13	Benzene-Air	1	167 - 197	29.62 - 33.17	.69 - .79	12, 34	Given, $\frac{u'}{U}$ = 5% - 15%	Eq.(5.6) 1.54-3.30	Duct, grid, inner area.
Rasbash and Rogowski	14	Pentane-Air	1	25	≃ 15.0	.442	14	Eq.(5.1), .201-1.38	Eq.(5.4), R_L	Tube, Pressure and ionisation gauges, curve extrapolated to give $\frac{U}{U_o}$ = 2.5 at R_e = 2.500, $\frac{u_t}{u_\ell} = \frac{U}{U_o} \times \frac{1}{2.5}$.
Petrov and Talantov	15	Benzene-Air	1	100	23.2	.2 - .6	15	Measured, 1.3 - 16	Eq.(5.6), 2.67-3.90	Pipe, grid, inner area.
Kozachenko	16	Benzene-Air	1	17-227	15.27 - 36.55	.46 - .96	16, 34	Given, $\frac{u'}{U}$ = 5%	Eq.(5.4), R_L	Duct, inner area.

TABLE 5.3 (cont.)

Author	Ref.	Mixture	P (Atmos)	T (^{o}C)	ν ($m^2 s^{-1} \times 10^{-6}$)	u_ℓ ($m\ s^{-1}$)	u_ℓ Ref.	u' ($m\ s^{-1}$)	L (mm)	Method
Grover et al	17	Methane-Air	1	25	15.89	.32	17	Given, Ref. 31, .19-.65	Given, Ref. 31, 0.76 - 1.27	Tube, grid, total area.
Kuznetsov and Malanov	18	Propane-Air	1	25	14.72	.28 - .46	34	Given, .7 - 3.22	Eq. (5.4) R_L	Square tube, "V" flame, gas velocity angle.
Kozachenko and Kuznetsov	19	Propane-Air	1	25	14.37-14.85	.27 - .46	34	Measured, .3 - 11.0	Eqs. (5.2), (5.5), R_L	Slot burner, inner area.
Kozachenko and Kuznetsov	19	Hydrogen-Air	1	25	17.83-20.75	.66-2.42	32	Measured, .4 - 11.6	Eqs. (5.2), (5.5), R_L	Slot burner, inner area.
Zotin and Talantov	20	Gasoline-Air	1	150-550	28.1 - 87.5	.8 - 2.92	35	Eq. (5.1), 1.47 - 4.86	Eq. (5.4), R_L	Tube, inner area.
Zotin and Talantov	21	Gasoline-Air	1	150-350	28.1 - 55.8	.5 - 1.65	35	Measured, 1.0 - 8.0	Eq. (5.4), R_L	Tube, inner area.
Vinckier and Van Tiggelen	22	6 mixtures	1	25	15.01-16.07	.89-1.98	22	Measured, 1.06-5.70	Measured, .55 - 1.64	Opposed flow, flame position.

TABLE 5.3 (cont.)

Author	Ref.	Mixture	P (Atmos)	T (^{o}C)	ν ($m^2 s^{-1} \times 10^{-6}$)	u_ℓ ($m\ s^{-1}$)	u_ℓ Ref.	u' ($m\ s^{-1}$)	L (mm)	Method
Putnam and Giammar	23	Methane-Air	1	25	15.7	.337	23	Given, .007-.70	Given, 1.21-62.48	Bomb, grid, time-average-pressure-rise history of spherically expanding flame.
Ballal and Lefebvre	24	Propane-Air	1	25	14.72	.45	24	Measured, .25 - 3.84	Measured. .56 - 5.08	Square tube, grid, "V" flame, angle.
Andrews et al	25	2 mixtures	1	25	15.83-15.94	.15 - .79	25	Measured, (Chapter 4 this thesis), .38 - 2.98	Measured, (Chapter 4 this thesis) 7.7-11.25	Bomb, fan, double kernel.
Singh	26, 27	Methane-Air	1	286.2 - 310.2	47.23-50.54	10+.000371 (T+273), .337	28	Measured, 7.53-15.37	Measured, 3	Square tube, pressure distribution along the axis of the combustion chamber, using indirect method.

TABLE 5.4 Effect of Pressure and Temperature on u_t

Author	Ref.	Mixture	Method	Pressure Range (atmos)	Pressure Law	Temperature Range	Temperature Law
Fine	54	Propane-O_2-N_2 Hydrogen-air	Tube burner, annular pilot, pipe turbulence, very low turbulence intensity. Mean flame area.	0.26-0.8	$\frac{u_t}{u_\ell} \alpha P^{0.3}$		
Goldenberg and Pelevin	55-57	Gasoline-air	Burner, annular pilot flame. Inner apex cone angle	0.13-1.0	$u_t \alpha P^{-0.25}$ $u_\ell \alpha P^{-0.25}$ mass vel.const. $u_t \alpha P^{0.5}$ const.flow vel.		
Sokolik and Karpov	58	Propane-air Hydrogen-air	Bomb, four symmetrical fans. Flame radius and pressure time records.			1600-2500°K	$u_t \alpha P^{2.5}$ u' const.
Kramtsov	8,59	Propane-air	Burner,grid turbulence. Flame area.	0.1-0.6	u_t=9.5 $P^{0.4}$ u' variable u_t=8.3 $P^{0.12}$ u' const.	300-600°K	$u_t = \beta T^{0.25}$ where $\beta = f(P)$

TABLE 5.4 (cont.)

Author	Ref.	Mixture	Method	Pressure Range (atmos)	Pressure Law	Temperature Range	Temperature Law
Dorashenko and Nikitski	60	Benzene-air	Tube burner, grid turbulence. Flame area.	0.2-1.0	$u_t \propto P^{0.5}$ $u_l \propto P^{-0.25}$	$\frac{T}{To} = 1 \rightarrow 1.55$ $To = 373^{o}K$	$\frac{u_t}{(u_t)_{To}} = 0.67 + 0.33 \frac{T}{To}$
Karpov and Sokolik	61	Propane-air	Bomb, four symmetrical fans. Flame radius and pressure time records.	0.2-1.8	$u_t \propto P^{0.3}$ $u_l \propto P^{-0.05}$ u' const.		
Talantov	62		Theoretical analysis.		$u_t \propto P^{0.15}$		$u_t \propto T^{0.4}$
Povinelli and Fuhs	63	Propane-air	Flat flame burner, grid turbulence.	0.169-1.0	As P increases $\frac{u_t}{u_l}$ decreases.		
Yermolayev and Talantov	64, 65	Gasoline-air	'V' burner, grid turbulence. Area. Pilot flame.	0.35-1.4	$\frac{u_t}{u_{to}} \propto \left(\frac{P}{Po}\right)^{0.2}$		

TABLE 5.4 (cont.)

Author	Ref.	Mixture	Method	Pressure Range (atmos)	Pressure Law	Temperature Range	Temperature Law
Zotin and Talantov	20, 65	Gasoline-air	Burner, annular pilot, grid turbulence. Area			150-600°C	$\frac{u_t}{u_{to}} \propto \left(\frac{T}{To}\right)^{0.65}$
Golubev et al	66	Gasoline-air	Square tube burner, pipe and grid turbulence. Flame position.	0.2-4.5	$u_t \propto P^{(-0.09)-(+0.2)}$ u' variable		
Chomiak	67		Theoretical analysis.		$u_t \propto P^{(0.15-0.35)}$		$u_t \propto T^{(2.1-2.6)}$

TABLE 5.5 Wrinkled Laminar Flame Criteria

Author	Ref.	Dimensionless Parameter, Γ, in Original Reference	Derived $\Gamma << 1$ in u_ℓ/u' and R_L Form	Equations used in Derivation
Damköhler Schelkin	1 68	$\Gamma = \frac{\delta_\ell}{L}$	$\frac{u_\ell}{u'} << 1.429\ R_L^{-1}$	$\delta_\ell = \frac{\nu}{u_\ell \cdot Pr}$; $Pr = 0.7$
Richardson	69	$\Gamma = \frac{L}{L_t} \frac{1}{(u' u_\ell)^{\frac{1}{2}}}$ where L_t = integral time scale of turbulence $\frac{L}{L_t} \simeq u'$ $\therefore\ \Gamma \simeq (\frac{u'}{u_\ell})^{\frac{1}{2}}$	$\frac{u_\ell}{u'} >> 1$	
Kovasznay	70	$\Gamma = \frac{\text{typical velocity gradient in approaching cold flow}}{\text{typical velocity gradient in laminar flame}}$ $= \frac{u'}{\lambda} \frac{\delta_\ell}{u_\ell}$ where λ = Taylor microscale	$\frac{u_\ell}{u'} > 0.468\ R_L^{-0.25}$	$\delta_\ell = \frac{\nu}{u_\ell \cdot Pr}$; $Pr = 0.7$, $R_\lambda = 6.5\ R_L^{0.5}$

TABLE 5.5 (Cont.)

Author	Ref.	Dimensionless Parameter, Γ, in Original Reference	Derived $\Gamma \ll 1$ in u_ℓ/u' and R_L Form	Equations used in Derivation
Wohl et al	71	$\Gamma = \frac{\text{mean chemical reaction time}}{\text{mean lifetime of an eddy}} = \left(\frac{\delta_\ell}{u_\ell}\frac{T_u}{\bar{T}}\right) \cdot \frac{u'}{L'}$ where $\bar{T} = \frac{T_b - T_u}{2}$; T_u = temperature of unburnt gas; T_b = temperature of burnt gas; L' = Lagrangian scale of turbulence		
Sokolik	72	$\Gamma = \frac{u'}{L} \cdot \frac{\delta_\ell}{u}$ where u is the mean velocity of gas flow in the flame; $u \simeq \frac{u_\ell(1+\rho_u/\rho_b)}{2}$; where ρ_u = density of unburnt gas; ρ_b = density of burnt gas $\Gamma \simeq \frac{u'}{L} \cdot \frac{2\,\delta_\ell}{u_\ell(1+\rho_u/\rho_b)}$		

TABLE 5.5 (Cont.)

Author	Ref.	Dimensionless Parameter, Γ, in Original Reference	Derived $\Gamma \ll 1$ in u_ℓ/u' and R_L Form	Equations used in Derivation
Talantov	73	$\Gamma = \frac{\text{chemical reaction time in a laminar flame}}{\text{residence time in turbulent combustion zone}} = (\frac{\delta_\ell}{L}) \cdot (\frac{u'}{u_\ell}) \cdot \frac{1}{\ell n(1+u'/u_\ell)}$	$R_L > 1.429 \ (\frac{u'}{u_\ell})^2 \cdot \frac{1}{\ell n(1+u'/u_\ell)}$	$\delta_\ell = \frac{\nu}{u_\ell \cdot Pr}$; $Pr = 0.7$
Klimov	74, 75	$\Gamma = S \frac{\delta_\ell}{u_\ell} \simeq \frac{u'}{u_\ell} \frac{\delta_\ell}{L}$ where S is the relative rate of change of the area of a surface element of the flame; $S \simeq \frac{u'}{L}$	$\frac{u_\ell}{u'} >> 1.195 \ R_L^{-0.5}$	$\delta_\ell = \frac{\nu}{u_\ell . Pr}$; $Pr = 0.7$
Ippolitov Bhaduri Bhaduri et al	76 77-80 81	$\Gamma = \frac{\varepsilon}{U.d} = \frac{u'\ell}{U\ d}$ where U = flow velocity, ℓ = mixing length; d = duct diameter	$R_L < 6.172 \times 10^{-35}$	$\frac{\varepsilon}{\nu} = 11 \ R_L^{0.56}$, $R_L = 1.67 \times 10^{-6} \ Re^{1.57}$
Sanematsu	82	$= \frac{u'}{u_\ell} \cdot \frac{L}{b} \cdot \phi^n$ where b = screen mesh diameter; ϕ = equivalence ratio; n = constant		

TABLE 5.5 (Cont.)

Author	Ref.	Dimensionless Parameter, Γ, in Original Reference	Derived $\Gamma << 1$ in u_ℓ/u' and R_L Form	Equations used in Derivation
Williams	83	$\Gamma = (\frac{D}{\delta_\ell z})^{\overline{u'Y'}} \simeq \frac{L}{\delta_\ell}(\frac{D}{2u'L})^{\frac{1}{2}}$ where D = multi-component diffusion coefficient and kinematic viscosity; Y' = species fluctuations; $\overline{u'Y'} = f(u', L)$		
Chomiak	84, 85	$R_\lambda < 100$ where $R_\lambda = \frac{u'\lambda}{\nu}$	$R_L < 237$	$R_\lambda = 6.5\ R_L^{0.5}$
Putnam and Giammar	23	$\Gamma' = \frac{u'}{L}\frac{u_\ell}{\delta_\ell}$ N.B. (not dimensionless)		
Williams	86	$\Gamma = \frac{\delta_\ell}{\eta}$ where η = Kolmogorov microscale	$\frac{u_\ell}{u'} >> 1.102\ R_L^{-0.25}$	$\eta = \lambda 15^{-0.25}\ R_\lambda^{-0.5}$, $\delta_\ell = \frac{\nu}{u_\ell . Pr}$; Pr = 0.7, $R_\lambda = 6.5\ R_L^{0.5}$

TABLE 5.6 Investigations into the Effect of Turbulence on Ignition and Flammability Limits

Author	Ref.	Details of Ignition Investigations	Details of Flammability Investigations
Wheeler	89	Bomb, Fan turbulence. At constant ignition energy, increase of fan speed can cause a mixture, which when quiescent is easily flammable, not to ignite.	Increase in fan speed narrowed the limits of flammability and made near limit flames propagate faster with much greater rates of pressure rise.
Wheeler	90	Bomb, Fan turbulence. Increase of minimum ignition energy as fan speed is increased.	
Swett and Doulon	91	Spark ignition in a stream of gas, grid turbulence. Minimum ignition energy and ignition lag increase with both scale and intensity of turbulence.	
Starkman et al	93	Flame propagation from a spark in a gas flow along a tube, pipe turbulence. Ignition energy kept constant.	Rich limit continually decreased as turbulence increased; weak limit first extended then decreased steadily.
Olsen and Gayhart	94, 95	Incipient flame kernel propagation from a spark in a turbulent flow. Turbulent quenching of the ignited kernels observed.	

TABLE 5.6 (Cont.)

Author	Ref.	Details of Ignition Investigations	Details of Flammability Investigations
Karpov and Sokolik	97	Bomb, Fan turbulence. Increase of minimum ignition energy as turbulence intensity increased.	Flammability limits came closer together as turbulence is increased. Limits also close as spark energy is reduced.
Goldenburg and Pelevin	98	Flow through heated tube, grid turbulence. Turbulence increases the ignition temperature.	
Saima	99	Spark ignition in a stream of gas, grid turbulence. Minimum ignition energy and ignition lag increase with both scale and intensity of turbulence.	
Bolt and Harrington	100	Bomb, Fan turbulence. At constant ignition energy, increase of mixture velocity at the spark gap due to increased fan speed, caused very lean mixtures not to ignite.	With increased mixture velocity relative to spark plug, lean limit of ignition became richer. Increase in mixture velocity greatly increased rate of pressure rise of near limit flames.
De Soete	101	Spark ignition in a stream of gas, grid turbulence. Minimum ignition energy increased, critical ignition diameter increased.	
Wakisaka et al	102	Two-stroke cycle gasoline engine. Quenching effect of the spark plug electrodes was slight in rich, but remarkable in lean mixture.	Lean limit did not differ so much from that in quiescent mixtures. Rich limit narrower than in quiescent mixtures. Both limits narrowed by increase in engine speed.

TABLE 5.6 (Cont.)

Author	Ref.	Details of Ignition Investigations	Details of Flammability Investigations
Karim et al	103	Flame propagation from a spark through a stratified mixture along a tube, pipe turbulence. Ignition energy kept constant.	Limits of ignition narrowed progressively as flow Reynolds number increased.
Iinuma	104	Bomb, grid tubulence. In an extremely lean or rich mixture, flame growth in the earlier period of propagation is prevented by an excessive turbulence.	
Belles	92	Flame tube, axial rotor. Ignition carried out in a section where the gas remained quiescent.	For quiescent and low rotor speed the limit remained constant but weakened at high speed. Turbulence only reduced the lower limit.
Palmer and Tonkin	96	Flame propagation from a spark in a gas flowing along a tube, pipe turbulence.	Both limits were initially extended particularly at the upper limit, then contracted to the same level as for quiescent conditions at highly turbulent flows.
Hamamoto et al	105	L-head single cylinder engine. Ignition energy kept constant.	Increasing engine speed narrowed slightly the lean limits, whilst decreasing considerably the rich limit.

5.5 NOMENCLATURE

b	screen mesh diameter, Eq.(5.6)
d	pipe diameter
D	multi-component diffusion coefficient and kinematic viscosity, Table 5.5
ℓ	mixing length
L	integral scale of turbulence
L_t	integral time scale
L_y	integral scale of turbulence in the radial direction
L'	Lagrangian integral scale of turbulence
n	constant, Table 5.5
P	pressure
P_o	initial pressure
Pr	Prandtl number
Re	pipe flow Reynolds number = $\frac{Ud}{\nu}$
Re_p	channel flow Reynolds number based upon the distance apart of the plates
R_L	$\frac{u'L}{\nu}$
R_λ	$\frac{u'\lambda}{\nu}$
t_ξ	apparent small scale, or veins, lifetime
t_η	Kolmogorov time scale, Eq.(5.24)
T	temperature
T_b	temperature of burnt gas
T_o	initial temperature

T_u temperature of unburnt gas

u_ℓ laminar burning velocity

u_t turbulent burning velocity

u' r.m.s. turbulent velocity

U mean flow velocity

x distance down stream from mid-plane of screen, Eq. (5.6)

Y small eddy, or veins, density

Y' species fluctuations, Table 5.5

δ_ℓ laminar flame thickness, Eq. (5.10)

ε turbulent diffusivity

η Kolmogorov microscale, Eq. (5.14)

λ Taylor microscale of turbulence

ν kinematic viscosity

ρ_b density of burnt gas

ρ_u density of unburnt gas

ε/ν turbulent transport number, Eq. (2.20)

ϕ equivalence ratio $= \dfrac{\text{actual fuel-air ratio}}{\text{stoichiometric fuel-air ratio}}$

5.6 REFERENCES

1. G.DAMKÖHLER, The effect of turbulence on the flame velocity in gas mixtures, Zeitschrift fur Elektrochemie und Angewandte Physikalische Chemie 46, 601 (1940). (English Translation: NACA TM 1112 (1947).)

2. G.C.WILLIAMS, H.C.HOTTEL and A.C.SCURLOCK, Flame stabilisation and propagation in high velocity gas streams, Third Symposium (International) on Combustion, p.21, Williams and Wilkins: Baltimore (1949).

3. B.KARLOVITZ, D.W.DENNISTON and F.E.Wells, Investigation of turbulent flames, J.Chem.Phys. 19, 541 (1951).

4. B. KARLOVITZ, A turbulent flame theory derived from experiments, Selected Combustion Problems, AGARD p.248, Butterworths (1954).

5. K.WOHL and L.SHORE, Experiments with butane-air and methane-air flames, Ind.Eng.Chem. 47, 828 (1955).

6. P.WAGNER, Burning velocities of various premixed turbulent propane flames on open burners, NACA TN 3575 (1955).

7. J.K.RICHMOND, J.M.SINGER, E.B.COOK, J.R.OXENDINE, J.GRUMER and D.S.BURGESS, Turbulent burning velocities of natural gas-air flames with pipe-flow turbulence, Sixth Symposium (International) on Combustion, p.303, Reinhold: New York (1957).

8. V.A.KRAMTSOV, Investigation of pressure effect on the parameters of turbulence and on turbulent burning, Seventh Symposium (International) on Combustion, p.609, Butterworths: London (1959).

9. V.P.KARPOV, E.S.SEMENOV and A.S.SOKOLIK, Turbulent combustion in an enclosed space, Dokl.Akad.Nauk, SSSR 128, 1220 (1959). (English Translation: Proc. Acad. Sci. USSR, Phys. Chem. Sec. 128, 871 (1959).)

10. E.S.SEMENOV, Measurement of Turbulence characteristics in a closed volume with artificial turbulence, Combustion, Explosion and Shock Waves 1, 57 (1965).

11. A.S.SOKOLIK, V.P.KARPOV and E.S.SEMENOV, Turbulent combustion of gases, Fizika Goveniga i Vzryva 3, 61 (1967). (English Translation: Combustion, Explosion and Shock Waves 3, 36 (1967).)

12. L.S.KOZACHENKO, The Combustion of gasoline - air mixtures in turbulent flow, The Third All-Union Congress on Combustion Theory Vol.1, Flame propagation and detonation in gas mixtures, p.126, Moscow (1960).

13. L.S.KOZACHENKO, Combustion of gasoline - aire mixtures in turbulent flow, Izv. Akad. Nauk SSSR, Otd. Khim. Nauk No.1, 45 (1960). (English Translation: Bull.Acad.Sci.USSR, Div.Chem.Sci. No.1, 37 (1960).)

14. D.J.RASBASH and Z.W.ROGOWSKI, Gaseous explosions in vented ducts, Combustion and Flame 4, 301 (1960).

15. E.A.PETROV and A.V.TALANTOV, Investigation of basic characteristics of combustion of a homogeneous mixture of an open turbulent stream, Izv.Vyssh. Uchebn.Zaved.Aviat.Tekn. No.3, 91 (1959). (English Translation: ARS J.31, 408 (1961).)

16. L.S.KOZACHENKO, The combustion mechanism and burning velocity in a turbulent flow, Eighth Symposium (International) on Combustion, p.567, Williams and Wilkins: Baltimore (1962).

17. J.H.GROVER, E.N.FALES and A.C.SCURLOCK, Turbulent flame studies in a two-dimensional open burner, Ninth Symposium (International) on Combustion, p.21, Academic Press: New York (1963).

18. I.L.KUZNETSOV and M.D.MALANOV, Measuring the turbulent velocity of flame propagation by the inverse-cone method, Prik.Mek.Tek.Fiz. Vol.4 (1964). (English Translation: FTD-HT-66-261 p.256 (1967).)

19. L.S.KOZACHENKO and I.L.KUZNETSOV, Burning velocity in a turbulent stream of homogeneous mixture, Combustion, Explosion and Shock Waves 1, 22 (1965).

20. V.K.ZOTIN and A.V.TALANTOV, Influence of initial temperature on the propagation velocity of a flame in a turbulent flow of a homogeneous mixture, Izv.Vyssh.Uchebn.Zaved.Aviat.Tekn. No.1, 115 (1966). (English Translation: Soviet Aeronautics 9, 60 (1968).)

21. V.K.ZOTIN and A.V.TALANTOV, Relations for the flame propagation rate in turbulent flow of a homogeneous mixture, Izv.Vyssh.Uchebn.Zaved.Aviat.Tekn. No.3, 98 (1966). (English Translation: Soviet Aeronautics, p.54 (1968).)

22. J.VINCKIER and A.VAN TIGGELEN, Structure and burning velocity of turbulent premixed flames, Combustion and Flame 12, 561 (1968).

23. A.A.PUTNAM and R.D.GIAMMAR, The effect of grid-generated turbulence on flame propagation velocity for premixed natural-gas flames, Phase Report, Research Project BR-3-5, Battelle, Columbus Laboratories, Columbus, Ohio, February 1972.

24. D.R.BALLAL and A.H.LEFEBVRE, The structure and propagation of turbulent flames, Proc.Roy.Soc.344A, 217 (1975). With values of L, as corrected by the authors (Private communication - see Chapter 2).

25. G.E.ANDREWS, D.BRADLEY and S.B.LWAKABAMBA, Measurement of turbulent burning velocity for large turbulent Reynolds numbers, Fifteenth Symposium (International) on Combustion, The Combusion Institute: Pittsburgh, 655 (1975).

26. V.P.SINGH, A study of turbulent flames stabilized in a high velocity, high-temperature flow, Combustion Science and Technology 11, 181 (1975).

27. V.P.SINGH, Evolution de la flamme turbulente dans un foyer air-methane, Deuxieme Symposium Europeen sur la Combustion, Section Francaise du (Combustion Institute: Pittsburgh, p.557 (1975).

28. G.E.ANDREWS and D.BRADLEY, The burning velocity of methane-air mixtures, Combustion and Flame 19, 275 (1972).

29. T.VON KÁRMÁN, Some remarks on the statistical theory of turbulence, Proc.Fifth International Congress Appl. Mechanics, Cambridge, Mass., p.347 (1938).

30. L.F.G.SIMMONS and C.SALTER, Experimental investigation and analysis of the velocity variations in turbulent flow, Proc.Roy.Soc. (London) Ser.A, 145, 212 (1934).

31. H.L.DRYDEN, A review of the statistical theory of turbulence, Q.App.Maths. 1, 7 (1943).

32. G.E.ANDREWS and D.BRADLEY, Determination of burning velocity by double ignition in a closed vessel, Combustion and Flame 20, 77 (1973).

33. R.LINDOW, Eine verbesserte brennermethode zur bestimmung der laminaren flammengeschwindigkeiten von brenngas/luft-gemischen, Brennst.Wärme Kraft 20, 8 (1968).

34. G.J.GIBBS and H.F.CALCOTE, Effect of molecular structure on burning velocity, J.Chem.Eng.Data 4, 226 (1959).

35. N.N.INOZEMTSEV, Izv.Vyssh.Uchebn.Zaved.Aviat.Tekn.4, 72 (1958).

36. H.W.TOWNES, J.L.GOW, R.E.POWE and N.WEBER, Turbulent flow in smooth and rough pipes, Trans.Am. Soc.Mech.Engrs 94, 353 (1972). (Series D, Journal of Basic Engineering.)

37. R.E.POWE and H.W.TOWNES, Turbulence structure for fully developed flow in rough pipes, Trans.Am.Soc. Mech.Engrs 95, 255 (1973). (Series I, Journal of Fluid Engineering.)

38. J.LAUFER, Investigation of turbulent flow in a two-dimensional channel, NACA Rep.1053 (1951). (Supersedes NACA TN 2123, 1950.)

39. J.LAUFER, The structure of turbulence in fully developed pipe flow, NACA, Report 1174 (1954).

40. W.R.MICKELSEN, An experimental comparison of Lagrangian and Eulerian correlation coefficients in homogeneous isotropic turbulence, NACA TN 3570 (1955).

41. L.V.BALDWIN and T.J.WALSH, Turbulent diffusion in the core of fully developed pipe flow, A.I.Ch.E.Jl.7, 53 (1961).

42. C.J.LAWN, The determination of the rate of dissipation in turbulent pipe flow, J.Fluid Mech. 48, 477 (1971).

43. J.M.ROBERTSON, J.H.BURKHART and J.D.MARTIN, Study of turbulent flow in rough pipes, University of Ill., Theoretical and Applied Mechanics Rep. No.279, Urbana (1965).

44. J.A.CLARK, A study of incompressible turbulent boundary layers in channel flow, Trans.Am.Soc.Mech. Engrs 90, 455 (1968). (Series D, Journal of Basic Engineering.)

45. A.K.M.F.HUSSAIN and W.C.REYNOLDS, The mechanics of a perturbation wave in turbulent shear flow, FM-6. Mechanical Engineering Dept., Stanford University, May 1970.

46. A.K.M.F.HUSSAIN and W.C.REYNOLDS, Measurements in fully developed turbulent channel flow, Trans.Am.Soc. Mech.Engrs 97, 568 (1975). (Series I, Journal of Fluids Engineering.)

47. M.ACHARYA and W.C.REYNOLDS, Measurements and prediction of a fully developed turbulent channel flow with imposed controlled oscillations, TF-8, Mechanical Engineering Dept., Stanford University, May 1975.

48. T.K.SHERWOOD and B.B.WOERTZ, Mass transfer between phases - role of eddy diffusion, Ind.Engng Chem. 31, 1034 (1939).

49. F.PAGE, W.H.CORCORAN, W.G.SCHLINGER and B.H.SAGE, Temperature and velocity distributions in uniform flow between parallel plates, Ind. Engng Chem. 44, 419 (1952).

50. W.D.BAINES and G.E.PETERSON, An investigation of flow through screens, Trans.Am.Soc.Mech.Engrs 73, 467 (1951).

51. G.E.ANDREWS, D.BRADLEY and S.B.LWAKABAMBA, Turbulence and turbulent flame propagation - a critical appraisal, Combustion and Flame 24, 285 (1975).

52. D.B.SPALDING, One-dimensional laminar flame theory for temperature explicit reaction rates, Combustion and Flame 1, 296 (1957).

53. D.B.SPALDING, Predicting the laminar flame speed in gases with temperature - explicit reaction rates, Combustion and Flame 1, 287 (1957).

54. B.FINE, Effect of pressure on turbulent burning velocity, Combustion and Flame 2, 109 (1958).

55. S.A.GOLDENBERG, Influence of the lower pressure on the diffusion of the flame and the zone of burning in the turbulent flow, In: "Combustion at reduced pressures and some problems on stabilising the flame in single phase and two phase systems", Izd-vo AN SSSR, p.24, Moscow (1960).

56. S.A.GOLDENBERG and V.S.PELEVIN, Effect of pressure on the speed of flame propagation in a turbulent stream, Izv.Akad.Nauk SSSR, Otd.Tekhn.Nauk, Energetika i Automatika No.2, 26 (1959). (English Translation: ARS J. 29, 765 (1959).)

57. S.A.GOLDENBERG and V.S.PELEVIN, Influence of pressure on rate of flame propagation in turbulent flow, Seventh Symposium (International) on Combustion, p.590, Butterworths: London (1959).

58. A.S.SOKOLIK and Y.P.KARPOV, The effects of temperature and laminar velocity on the rate of turbulent combustion, Doklady Akad.Nauk.SSSR 129, 168 (1959). (English Translation: Proc.Acad.Sci. USSR, Phys.Chem.Sec., Vol.129 Nos. 1-6 (1959).)

59. V.A.KRAMTSOV, Researches on the influence of pressure on the turbulence parameters and on turbulent burning, In: "Combustion at reduced pressures and some problems on stabilising the flame in single phase and two phase systems", Izd-vo AN SSSR, p.43, Moscow (1960).

60. V.E.DORASHENKO and A.I.NIKITSKI, Researches into the influence of parameters of mixing on the characteristic pressures of turbulent burning, Ibid. p.3.

61. V.P.KARPOV and A.S.SOKOLIK, The effect of pressure on the rate of laminar and turbulent combustion, Doklady Akad.Nauk SSSR 132, 1341 (1960). (English Translation: Proc.Acad.Sci.USSR, Phys.Chem.Sec. 132, 531 (1960).)

62. A.V.TALANTOV, Analysis of operation of simplest ramjet combustion chamber under flying conditions, Izv.Vyssh.Uchebn.Zaved.Aviat.Tekn. No.2, 122 (1959). (English Translation: ARS J.30, 379 (1960).)

63. L.A.POVINELLI and A.E.FUHS, The spectral theory of turbulent flame propagation, Eighth Symposium (International) on Combustion, p.554, Williams and Wilkins: Baltimore (1962).

64. V.M.YERMOLAYEV and A.V.TALANTOV, Study of effect of pressure on flame propagation velocity in a turbulent flow in a uniform mixture, Izv.Vyssh. Uchebn.Zaved.Aviat.Tekn. No.4, 82 (1961).

65. A.V.TALANTOV, Research on combustion in flow, I.V.U.Z. Aviatsionnaya Tekhnika (1967). (English Translation: FTD-MT-24-209-68.)

66. V.V.GOLUBEV, V.M.YANKOVSKII, V.F.POSTNOV and A.V.TALANTOV, Influence of pressure on flame propagation velocity in turbulent stream, Izv. Vyssh.Uchebn.Zaved.Aviat.Tekn. Vol.16, No.2, 77 (1973). (English Translation: Soviet Aeronautics Vol.16, No.2, 64 (1973).)

67. J.CHOMIAK, Dissipation fluctuations and the structure and propagation of turbulent flames in premixed gases at high Reynolds numbers, Sixteenth Symposium (International) on Combustion, The Combustion Institute: Pittsburgh, 1665 (1977).

68. K.I.SHCHELKIN, On combustion in turbulent flow, Zh.Eksp. i Teoret. Fiz.13, 520 (1943). (English Translation: NACA TM 1110 (1947).)

69. J.M.RICHARDSON, Mathematical theory of turbulent flames, Proc.Gas Dynamics Symposium on Aerothermochemistry, Northwestern Univ., Illinois (1956).

70. L.S.G.KOVASZNAY, A comment on turbulent combustion, Jet Propulsion 26, 485 (1956).

71. K.WOHL et al , On the structure of turbulent flames, Sixth Symposium (International) on Combustion, p.333, Reinhold: New York (1957).

72. A.S.SOKOLIK, Self-ignition, flames and detonation in gases, Izdate'stvo Akademii Nauk SSSR, Moskva (1960). (English Translation: IPST, Jerusalem (1963).)

73. A.V.TALANTOV, On the mechanism of combustion in the turbulent flow of a well-mixed mixture, Izv.Vyssh. Uchebn.Zaved.Aviat.Tekn. No.3, 92 (1963). (English Translation: JPRS: 22, 703, p.128-139 (1964) OTS: 64 - 21268.)

74. A.M.KLIMOV, Zh.Prikl.Mekh. i Tekhn. Fiz.3, 49 (1963).

75. A.M.KLIMOV, The mechanism of turbulent combustion, Teoriya i Praktika Szhiganiya Gaza Izd-vo "NEDRA" Leningrad p.167-172 (1967). (English Translation FTD-HT-23-1407-68.)

76. A.S.IPPOLITOV, Speed of propagation of a flame front in a turbulent air-dust torch, Inzh.Fiz.Zh. 7, 28 (1964).

77. D.BHADURI, Evaluation of flame speed in turbulent flow, Indian J. Tech. 3, 308 (1965).

78. D.BHADURI, Mechanism of turbulent combustion, Indian J. Tech. 6, 187 (1968).

79. D.BHADURI, Effect of turbulence on premixed gaseous flames, CMERI Report No. B6 (1968).

80. D.BHADURI, Turbulent flame propagation; comment on Sanematsu's correlation, Combustion and Flame 15, 79 (1970).

81. D.BHADURI, P.BASU and S.DASGUPTA, Combustion in premixed turbulent flows, Mechanical Engineering Bulletin 3, 77 (1970).

82. H.S.SANEMATSU, Turbulent flame propagation parameter, Combustion and Flame 13, 91 (1969).

83. F.A.WILLIAMS, An approach to turbulent flame theory, J.Fluid Mech. 40, 401 (1970).

84. J.CHOMIAK, Turbulent fluctuations of energy dissipation and the flame front structure at high Reynolds numbers, Fluid Dynamic Transactions 5, 47 (1971).

85. J.CHOMIAK, A possible mechanism of turbulent flames at high Reynolds number, Combustion and Flame 15, 319 (1970).

86. F.A.WILLIAMS, A review of some theoretical considerations of turbulent flame structure, in Analytical and numerical methods for investigation of flow fields with chemical reactions, especially related to combustion AGARD,Conference Proceedings No.164, p.II 1-1 (1975).

87. A.G.GAYDON and H.G.WOLFHARD, Flames: their structure, radiation and temperature, Chapman and Hall, London, p.112 (1970).

88. D.R.BALLAL, Private Communication, 13th February 1976.

89. R.V.WHEELER, The inflammation of mixtures of ethane and air in a closed vessel: the effects of turbulence, J.Chem.Soc.115, 81 (1919).

90. R.V.WHEELER, The ignition of turbulent explosive mixtures by electric sparks, Fuel 14, 147 (1935).

91. C.C.SWETT and R.H.DOULON, Spark ignition of flowing gases III. Effect of turbulence promoter on energy required to ignite a propane-air mixture, NACA RME52J28 (1953).

92. F.E.BELLES, A preliminary investigation of propane-air flames, NACA RM E50J10a (1950).

93. E.S.STARKMAN, L.P.HAXBY and A.G.CATTENEO, A study of free flames in turbulent streams, Fourth Symposium (International) on Combustion, p.670, Williams and Wilkins: Baltimore (1953).

94. H.L.OLSEN and E.L.GAYHART, Effect of turbulence on incipient flame propagation, J.Chem.Phys. 25, 402 (1955).

95. H.L.OLSEN and E.L.GAYHART, Incipient flame propagation in a turbulent stream, Jet Propulsion 25, 276 (1955).

96. K.N,PALMER and P.S.TONKIN, The flammability limits of moving mixtures of propane and air, J.Appl.Chem. 11, 5 (1961).

97. V.P.KARPOV and A.S.SOKOLIK, Ignition limits in turbulent gas mixtures, Doklady Akad.Nauk SSSR 141, 393 (1961). (English Translation: Proc.Acad.Sci. USSR, Phys.Chem.Sec.141, 866 (1961).)

98. S.A.GOLDENBERG and V.N.PELEVIN, The effect of turbulence in a combustible gas mixture flow on ignition, Izv.Akad.Nauk SSSR, Mekhanika Mashinostroenie No.4, 112 (1963).

99. A.SAIMA, Spark ignition of turbulent mixture, Report of the Research Institute of Tech., Nihon Univ.No.9, p.571 (1966).

100. J.A.BOLT and D.L.HARRINGTON, The effects of mixture motion upon the lean limit and combustion of spark-ignited mixtures, SAE paper No.670467 (1967).

101. G.G.DE SOETE, The influence of isotropic turbulence on the critical ignition energy, Thirteenth Symposium (International) on Combustion, p.669, The Combustion Institute: Pittsburgh (1971).

102. T.WAKISAKA, Y.HAMAMOTO, S.OHIGASHI, T.NABARI and M.HOSOI, Limits of flame propagation in two-stroke cycle gasoline engines, Bulletin of the JSME 19, 1204 (1976).

103. G.A.KARIM, P.TSANG, G.S.SARPAL and O.BUDR, A fundamental study into flame propagation through stratified mixtures, Conference on Stratified Charge Engines, The Institute of Mechanical Engineers, paper No. C255/76, 23-25 November 1976.

104. K.IINUMA, A study of turbulent flame propagation in closed vessels, Automobile Exhaust Clarification Study Group, Japan, March 1977.

105. Y.HAMAMOTO, T.Wakisaka and S.OHIGASHI, Limits of flame propagation in spark iginition engines-behaviour of flames and exhaust emissions, Sixteenth International Congress of FISITA, Tokyo, 16-21 May 1976.

106. G.E.ANDREWS and D.BRADLEY, Limits of flammability and natural convection for methane-air mixtures, Fourteenth Symposium (International) on Combustion, The Combustion Institute: Pittsburgh, 1119 (1973).

107. B.KARLOVITZ, The growth and burn-out of flame surface in a turbulent stream, Seventh Symposium (International) on Combustion, Butterworth: London, 604 (1959).

108. B.KARLOVITZ, Flow phenomena and flame technology, Chemical Engineering Progress 61, 56 (1965).

109. H.TENNEKES, Simple model for the small-scale structure of turbulence, The Physics of Fluids 11, 669 (1968).

110. L.M.BOLLINGER and D.T.WILLIAMS, Effect of Reynolds number in turbulent flow range on flame speeds of bunsen burner flames, NACA Rep. 932, 1949.

111. F.W.BOWDITCH, Some effects of turbulence on combustion, Fourth Symposium (International) on Combustion, p.674, The Williams and Wilkins Co., Baltimore (1953).

112. H.C.HOTTEL, G.C.WILLIAMS and R.S.LEVINE, The influence of isotropic turbulence on flame propagation, Fourth Symposium (International) on Combustion, p.636, The Williams and Wilkins Co., Baltimore (1953).

113. K.WOHL, L.SHORE, H.ROSENBERG and C.W.WEIL, The burning velocity of turbulent flames, Fourth Symposium (International) on Combustion, p.620, Williams and Wilkins, Baltimore (1953).

114. J.GRUMER, J.M.SINGER, K.RICHMOND and J.R.OXENDINE, Photographic studies of turbulent flame structure, Ind. and Eng.Chem. 49, 305 (1957).

115. M.D.FOX and J.WEINBERG, Optical methods for the study of flames in turbulent premixed gas streams, Br.J.App.Physics 11, 269 (1960).

116, M.D.FOX and J.WEINBERG, An experimental study of burner-stabilised turbulent flames in premixed reactants, Proc.Roy.Soc. A268, 222 (1962).

117, W.G.BERL, J.L.RICE and P.ROSEN, Flames in turbulent streams, Jet Propulsion 25, 341 (1955).

118. J.H.GROVER, E.N.FALES and A.C.SCURLOCK, Turbulent flame studies in a two-dimensional open burner, ARS J.29, 275 (1959).

119. O.N.DUBROVSKAYA, K.P.VLASOV and N.N.INOZEMTSEV, Investigation of the structure of turbulent flames, Izv.Akad,Nauk SSSR. Otdel Tekh.Nauk Energetika i Transport No.2, 214 (1963). (English Translation: Shell Translation No.1102.)

120. M.SUMMERFIELD, S.H.REITER, V.KEBELY and R.W.MASCOLO, The physical structure of turbulent flames, Jet Propulsion 24, 254 (1954).

121. M.SUMMERFIELD, S.H.REITER, V.KEBELY and R.W.MASCOLO, The structure and propagation mechanism of turbulent flames in high speed flow, Jet Propulsion 25, 377 (1955).

122. S.ONO, M.TSUGE, M.KURUSU and I.FUKUE, A study on the influences of the scale of turbulence on the burning rate in a vessel, Bulletin of the JSME 19, 547 (1976).

123. S.B.LWAKABAMBA, Turbulent flame propagation in closed vessels, Ph.D. thesis, Dept.Mechanical Engineering, Univ. Leeds (1975).

124, F.C.LOCKWOOD and A.O.O.ODIDI, Measurement of mean and fluctuating temperature and of ion concentration in round free-jet turbulent diffusion and premixed flames, Fifteenth Symposium (International) on Combustion, The Combustion Institute: Pittsburgh, 561 (1975).

125. BJØRN F. MAGNUSSEN, An investigation into the behavior of soot in a turbulent free jet C_2H_2-flame, Fifteenth Symposium (International) on Combustion, The Combustion Institute: Pittsburgh, 1415 (1975).

126. R.W.BILGER and R.E.BECK, Further experiments on turbulent jet diffusion flames, Fifteenth Symposium (International) on Combustion, The Combustion Institute: Pittsburgh, 541 (1975).

Key for Figs. (5.1) to (5.15) is given in Fig. (5.1).

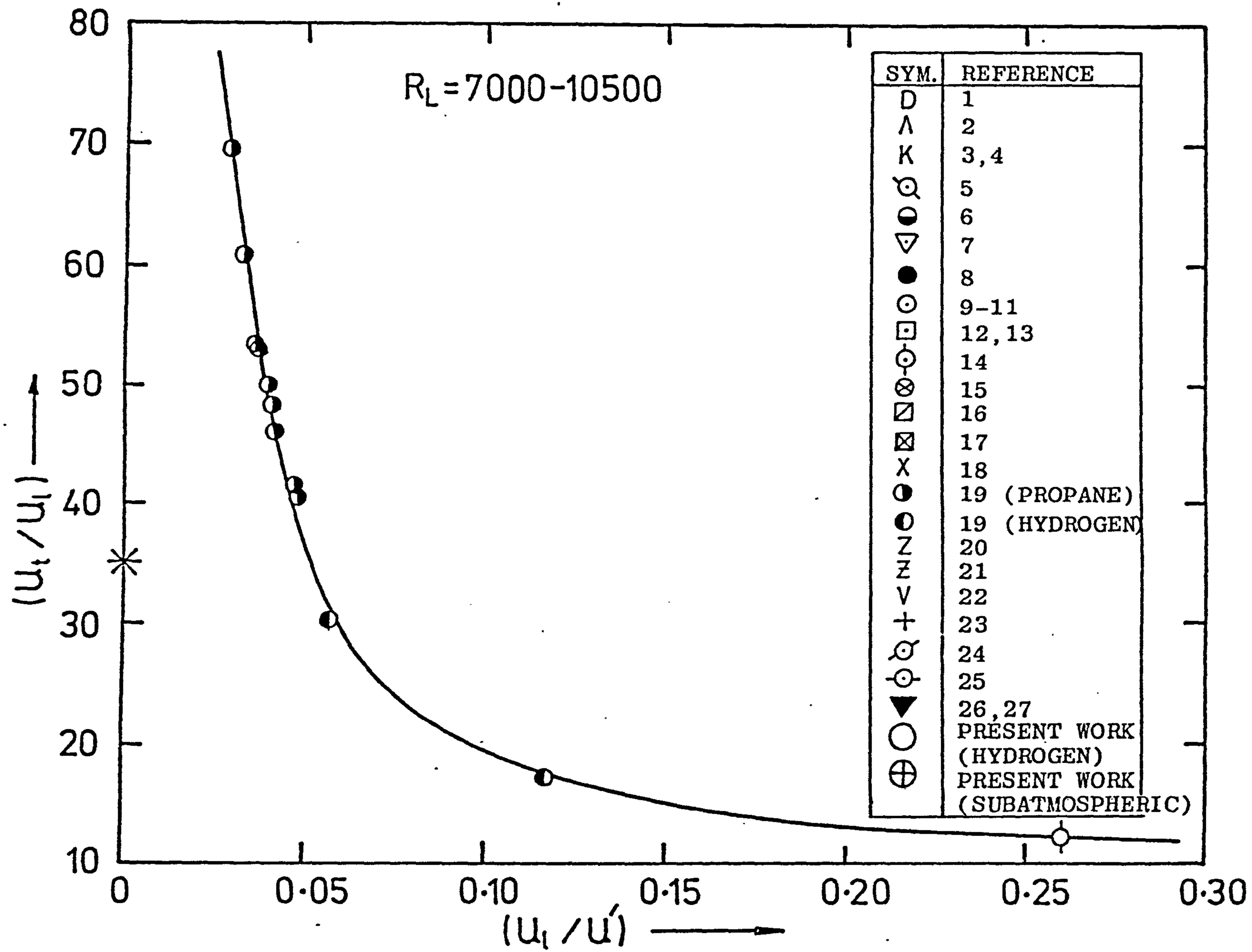

FIG.5.1 VARIATION OF u_t/u_ℓ WITH u_ℓ/u' , R_L = 7000-10500.
ASTERISKED POINT FROM EQ.(5.8)

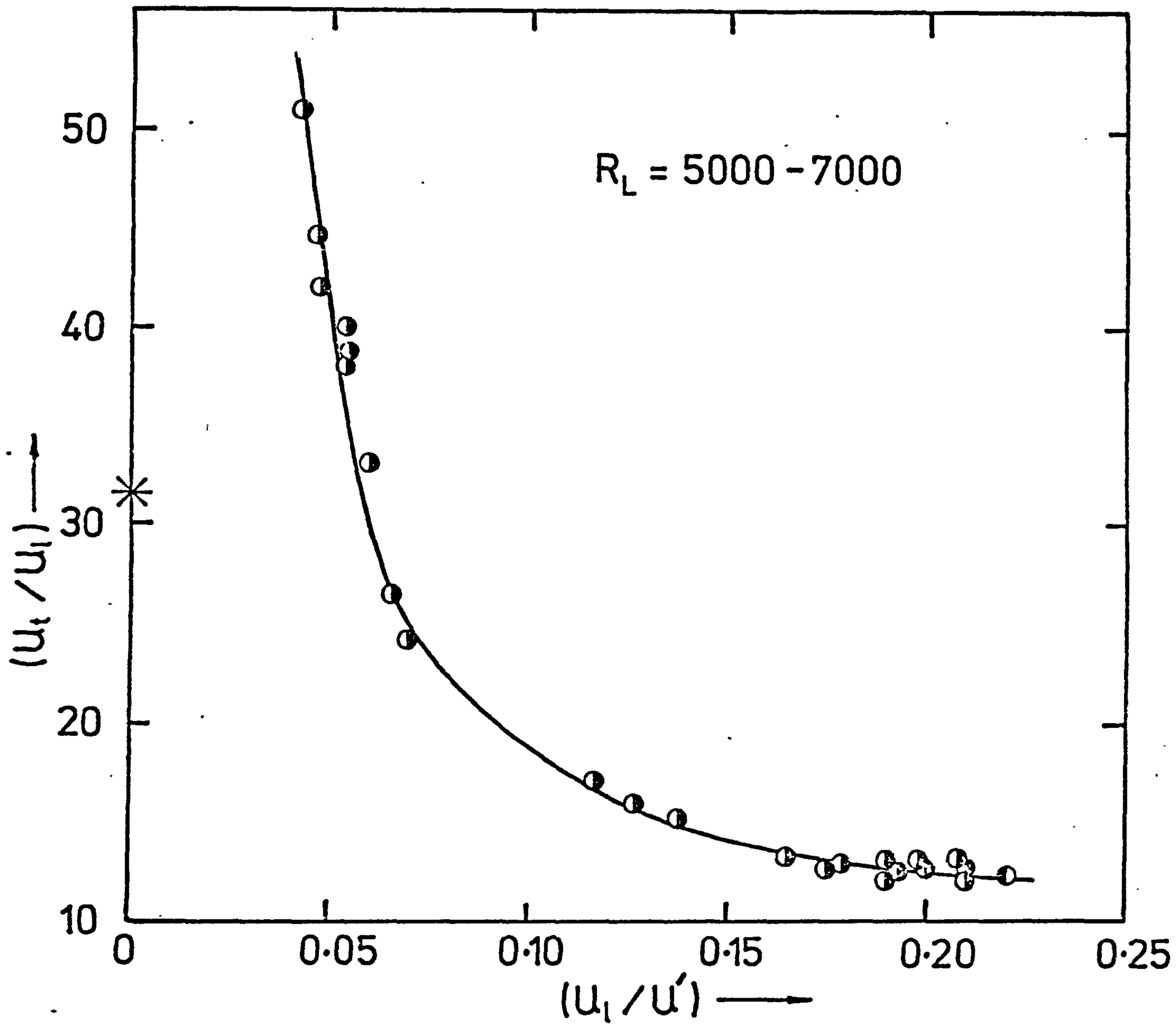

FIG.5.2 VARIATION OF u_t/u_ℓ with u_ℓ/u', R_L = 5000-7000
ASTERISKED POINT FROM EQ.(5.8)

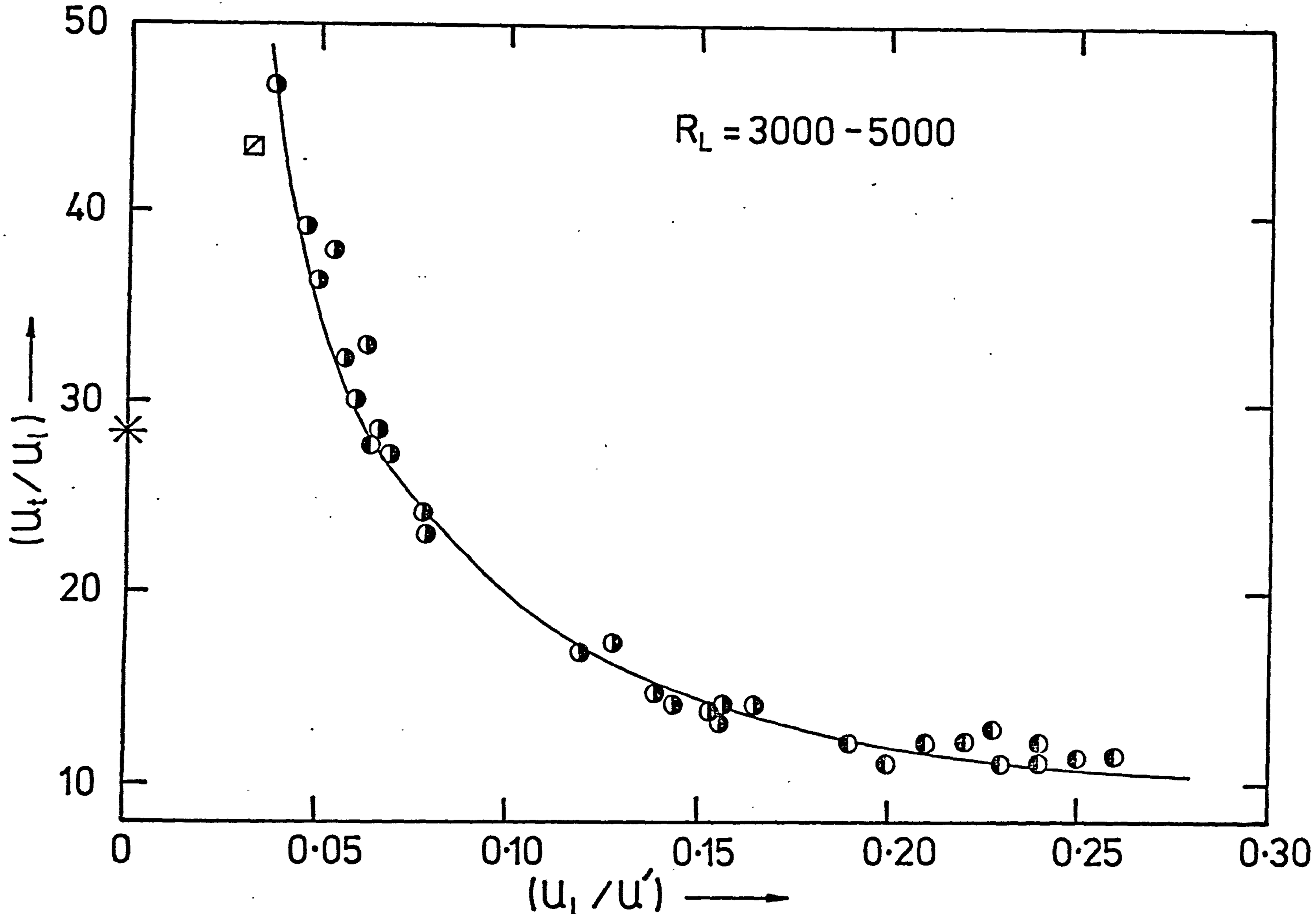

FIG.5.3 VARIATION OF u_t/u_ℓ WITH u_ℓ/u', R_L = 3000-5000. ASTERISKED POINT FROM EQ.(5.8)

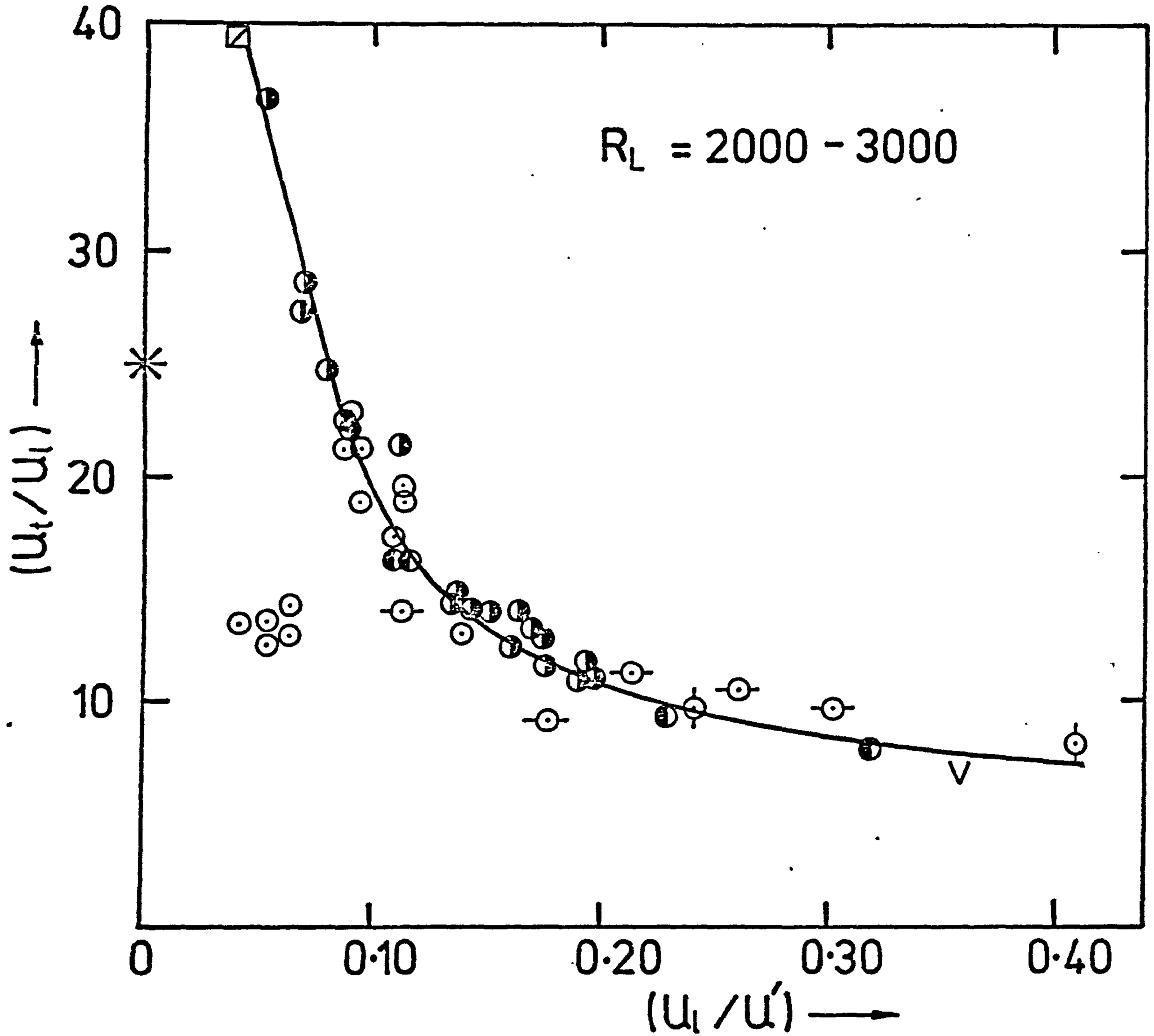

FIG.5.4 VARIATION OF u_t/u_ℓ with u_ℓ/u', R_L = 2000-3000. ASTERISKED POINT FROM EQ.(5.8)

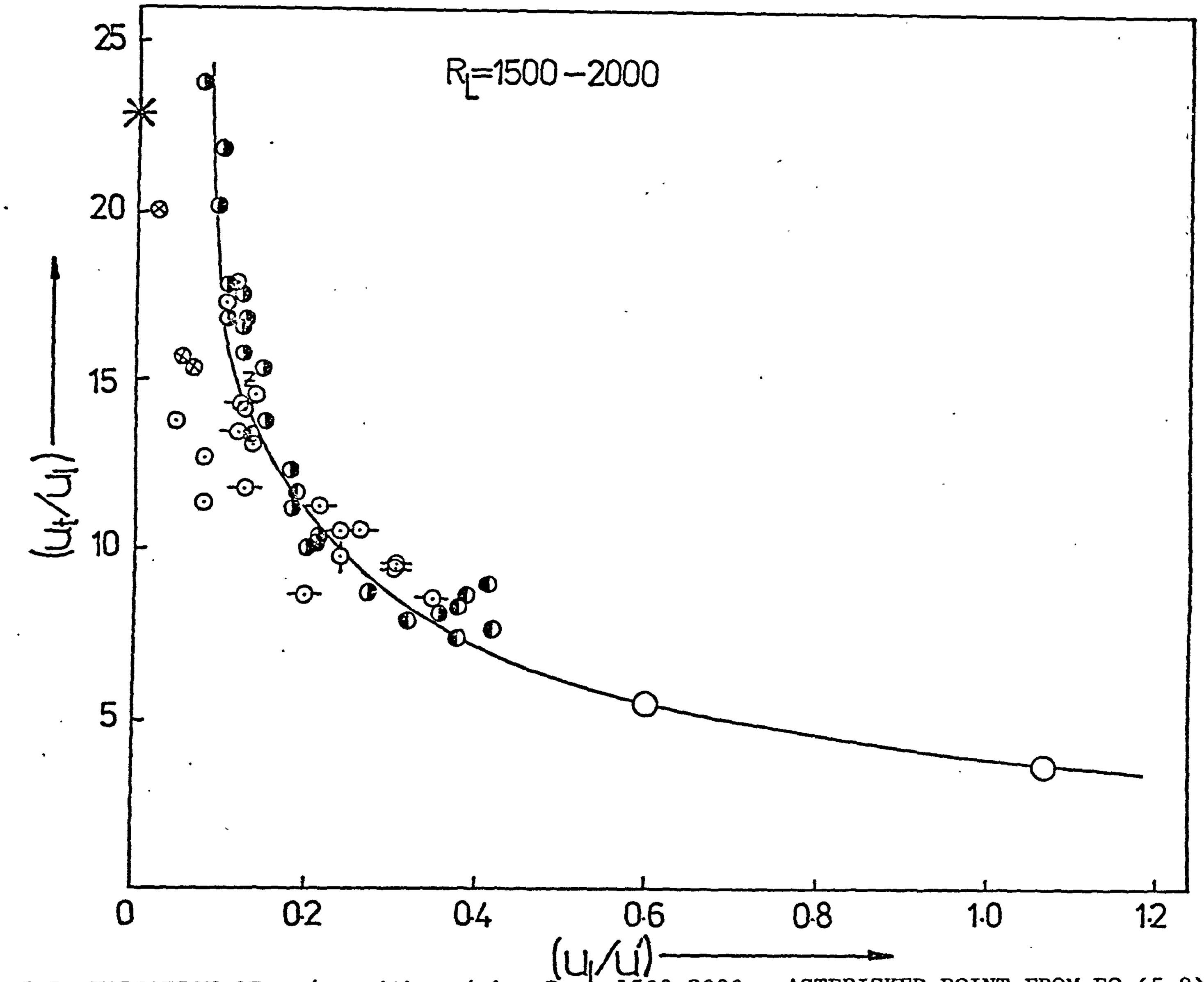

FIG.5.5 VARIATION OF u_t/u_ℓ with u_ℓ/u', R_L = 1500-2000. ASTERISKED POINT FROM EQ.(5.8)

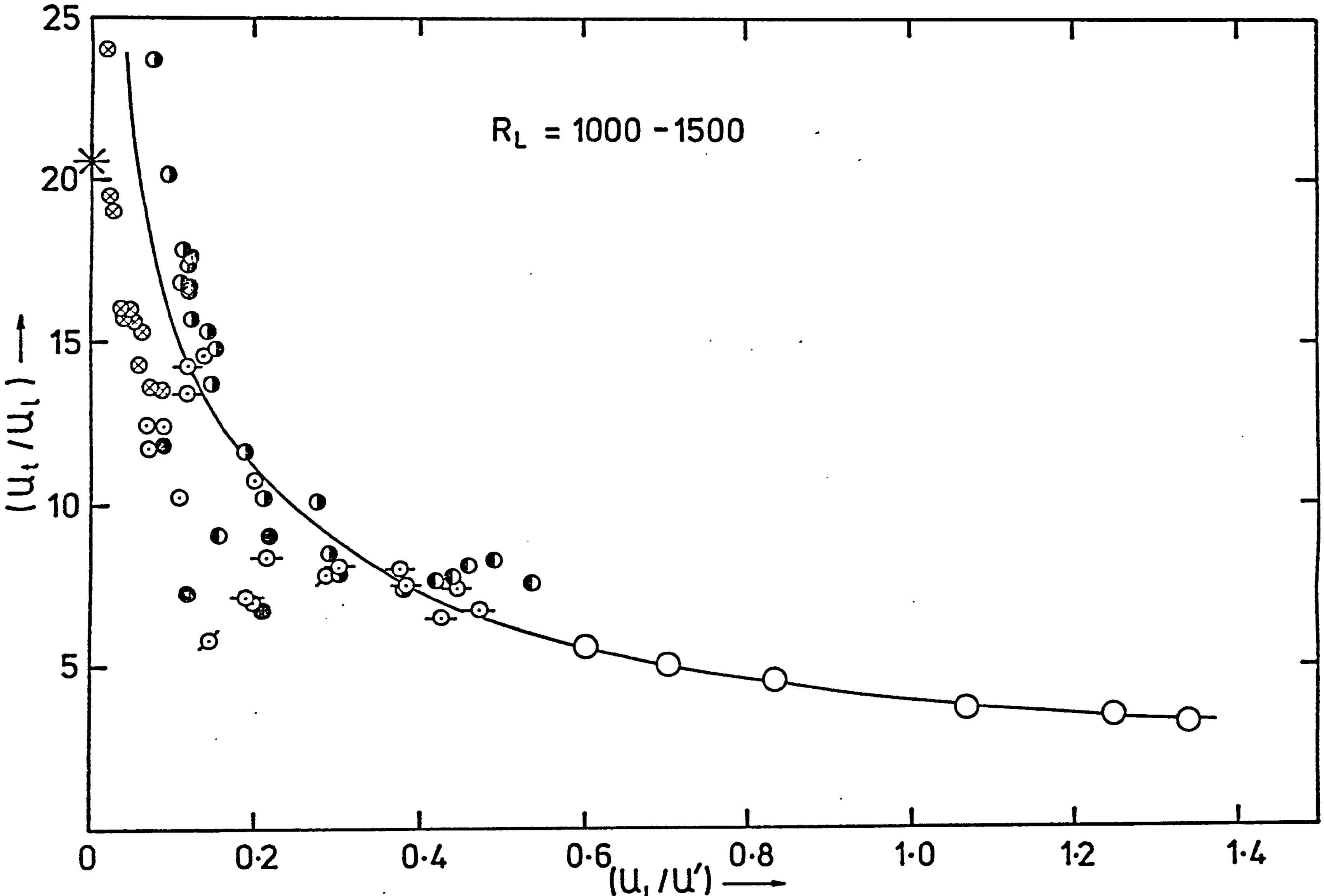

FIG.5.6 VARIATION OF u_t/u_ℓ WITH u_ℓ/u', R_L = 1000–1500. ASTERISKED POINT FROM EQ.(5.8)

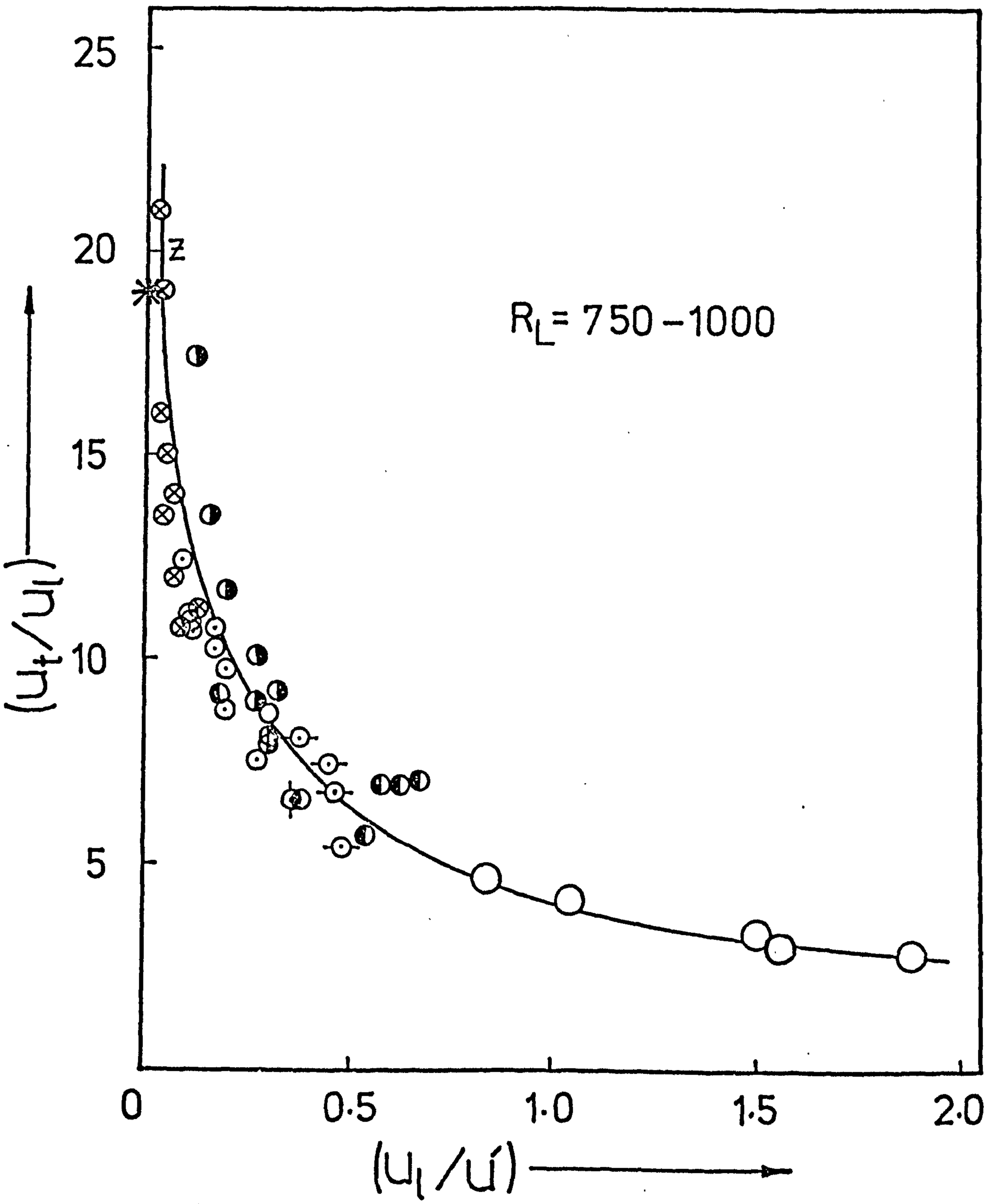

FIG. 5.7 VARIATION OF u_t/u_ℓ WITH u_ℓ/u', R_L = 750-1000. ASTERISKED POINT FROM EQ.(5.8)

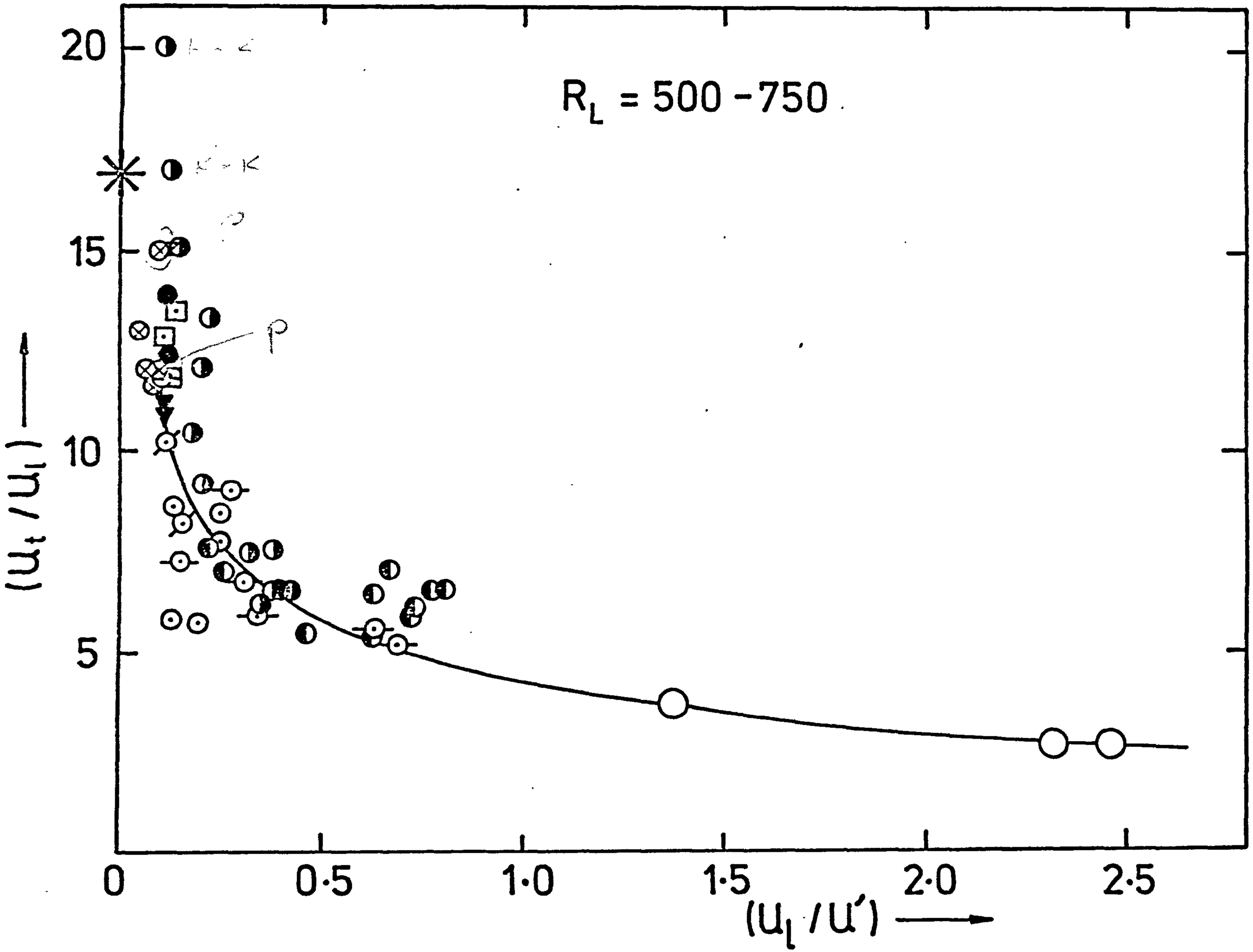

FIG. 5.8 VARIATION OF u_t/u_ℓ WITH u_ℓ/u', R_L = 500-750. ASTERISKED POINT FROM EQ.(5.8)

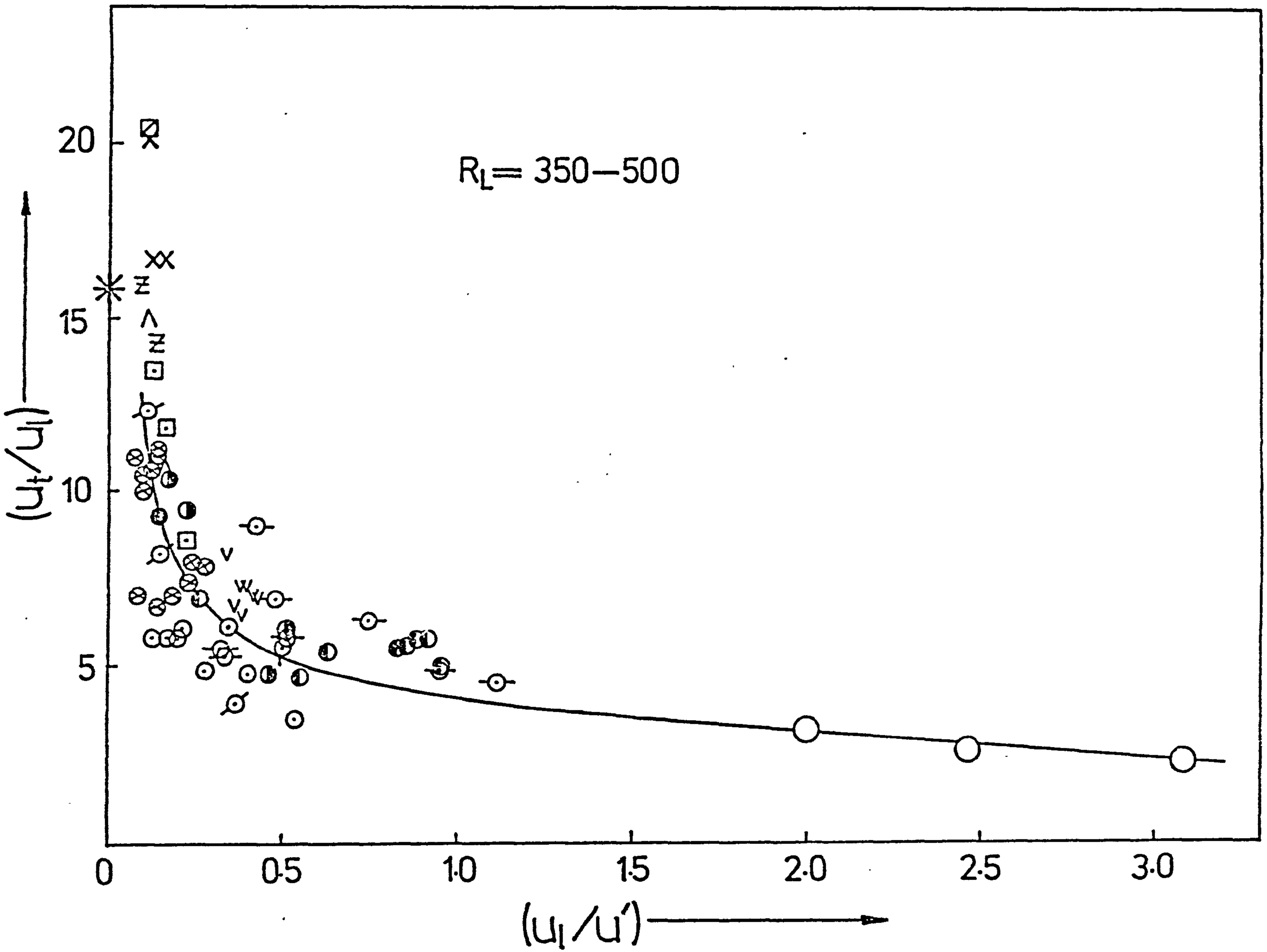

FIG. 5.9 VARIATION OF u_t/u_ℓ WITH u_ℓ/u', R_L = 350-500. ASTERISKED POINT FROM EQ.(5.8)

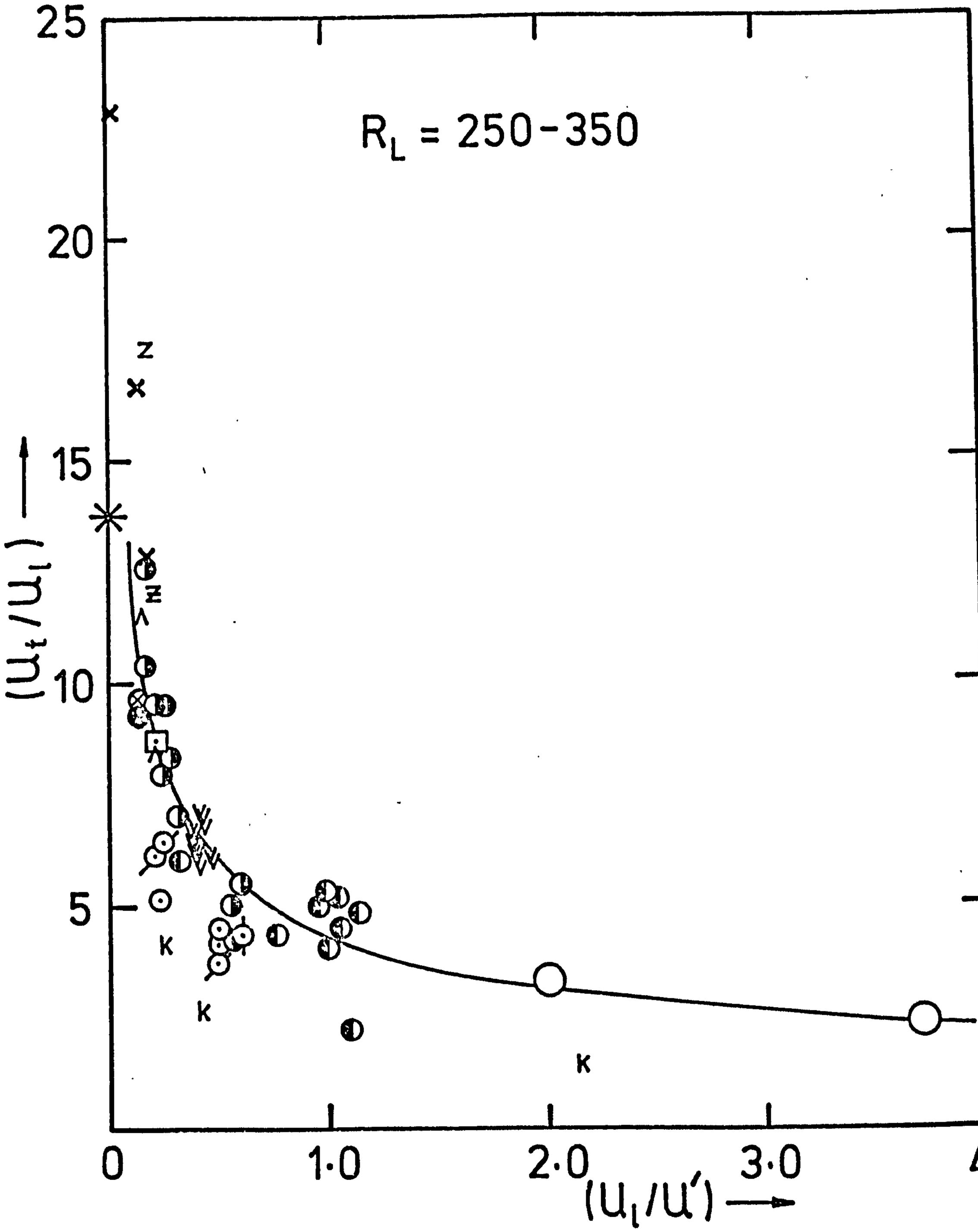

FIG. 5.10 VARIATION OF u_t/u_ℓ WITH u_ℓ/u', R_L = 250=350.
ASTERISKED POINT FROM EQ.(5.8)

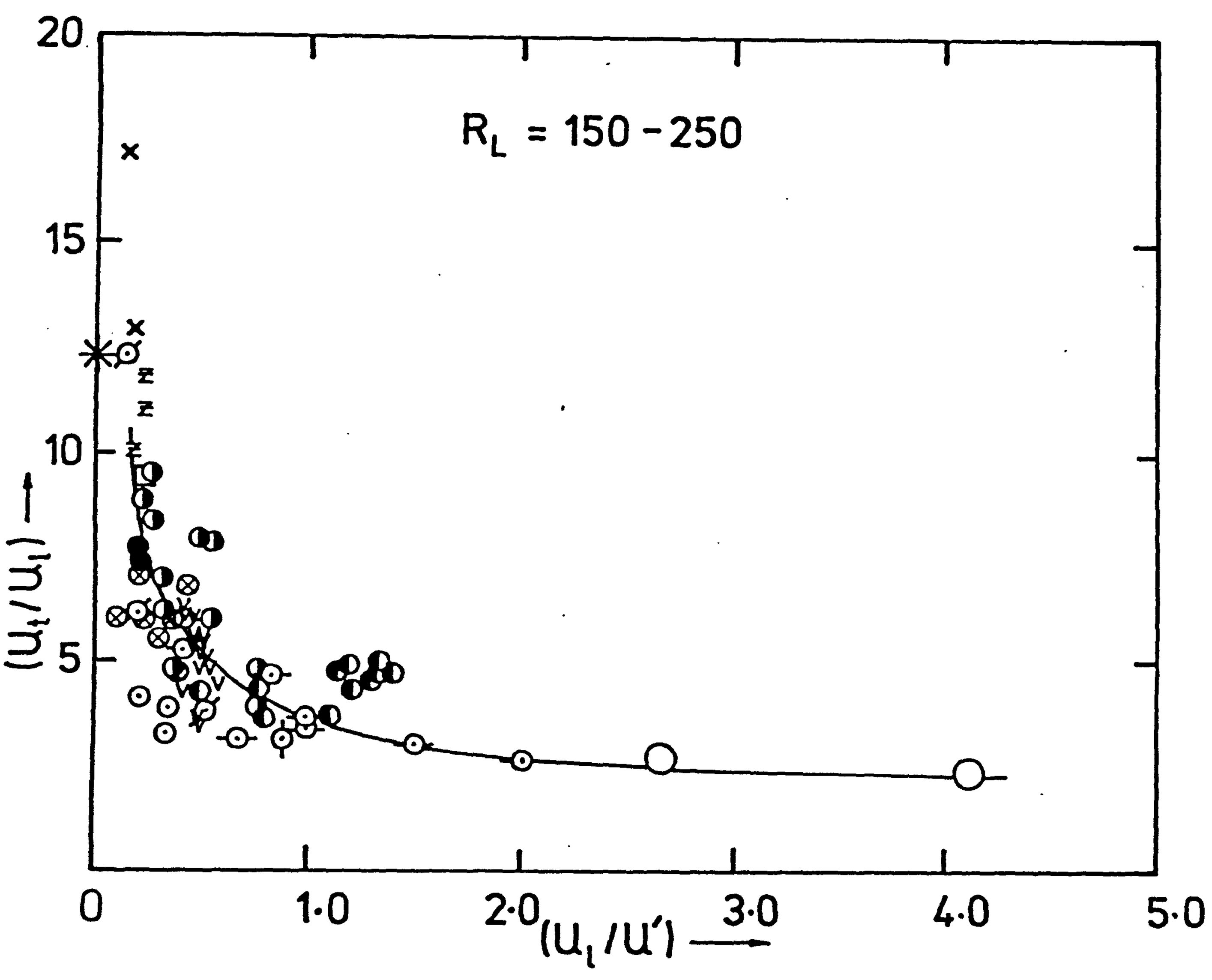

FIG. 5.11 VARIATION OF u_t/u_l WITH u_l/u', R_L = 150-250. ASTERISKED POINT FROM EQ.(5.8)

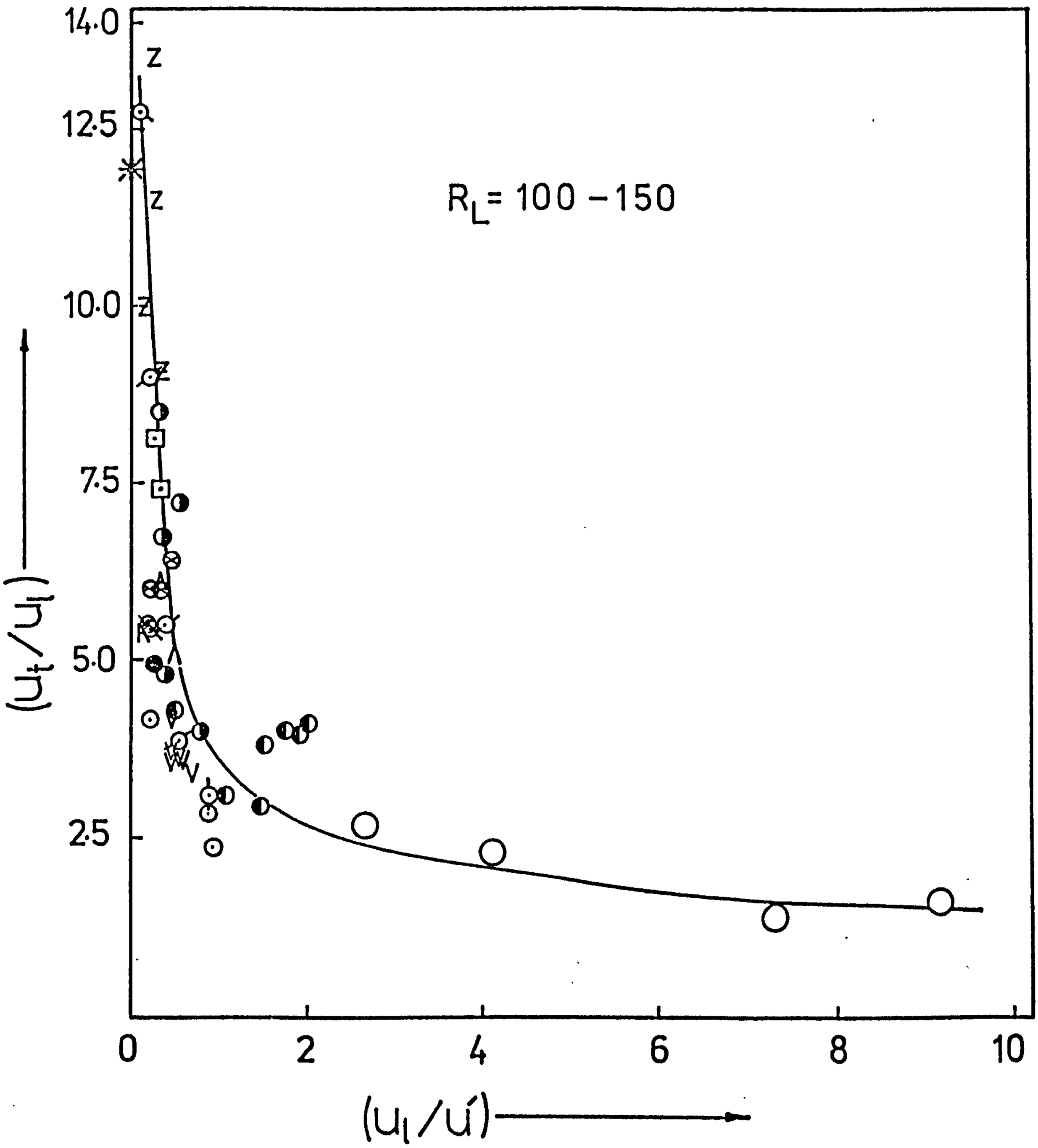

FIG. 5.12 VARIATION OF u_t/u_ℓ WITH u_ℓ/u', R_L = 100–150.
ASTERISKED POINT FROM EQ.(5.8)

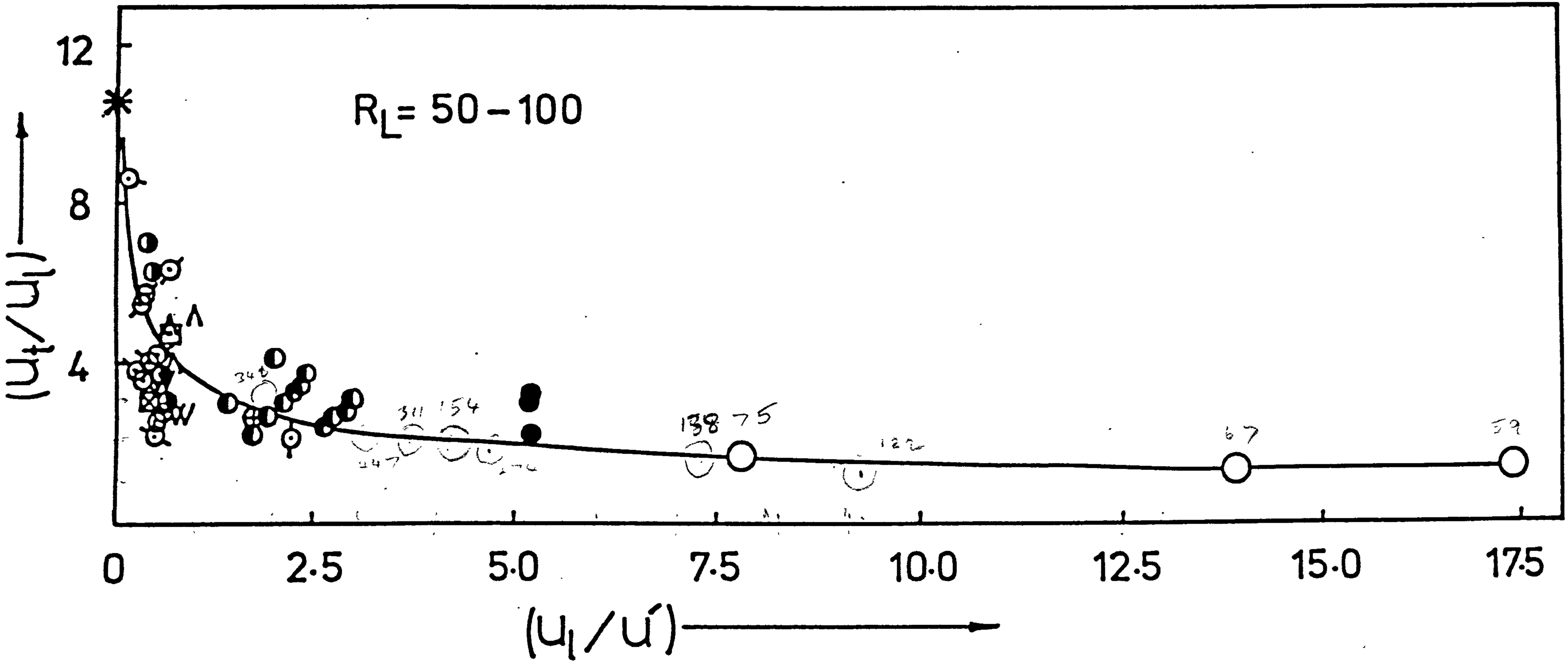

FIG. 5.13 VARIATION OF u_t/u_ℓ WITH u_ℓ/u', R_L = 50–100. ASTERISKED POINT FROM EQ.(5.8)

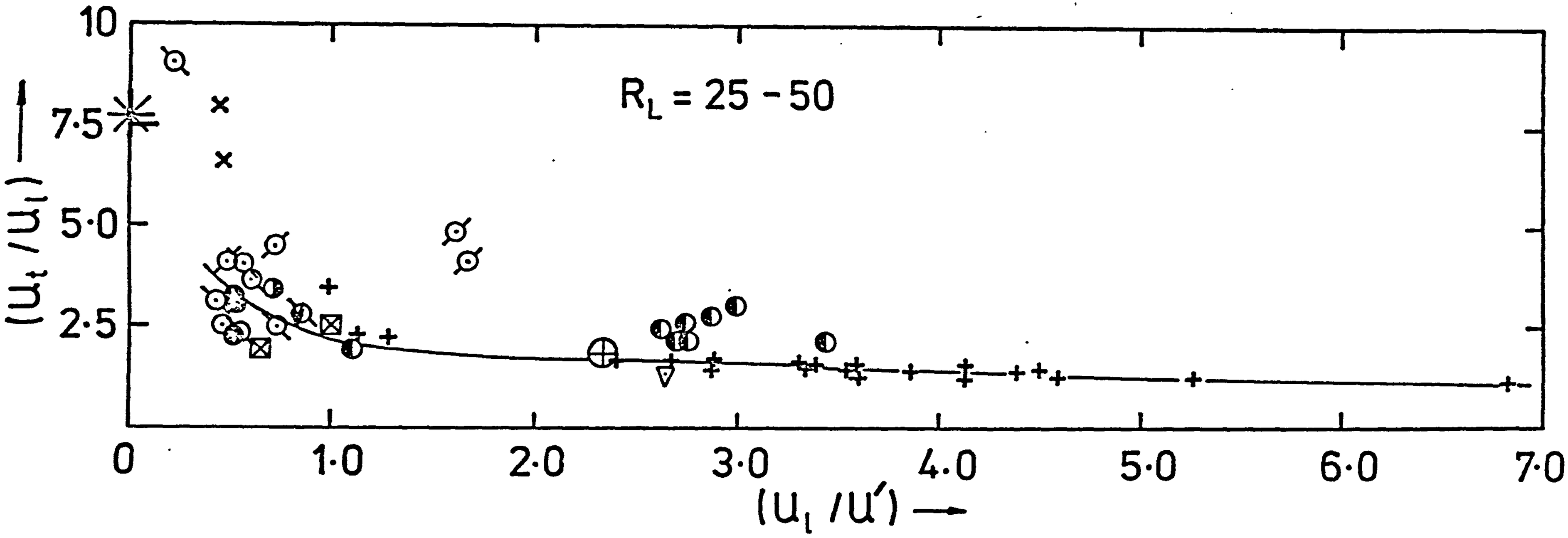

FIG. 5.14 VARIATION OF u_t/u_ℓ WITH u_ℓ/u', R_L = 25-50. ASTERISKED POINT FROM EQ.(5.8)

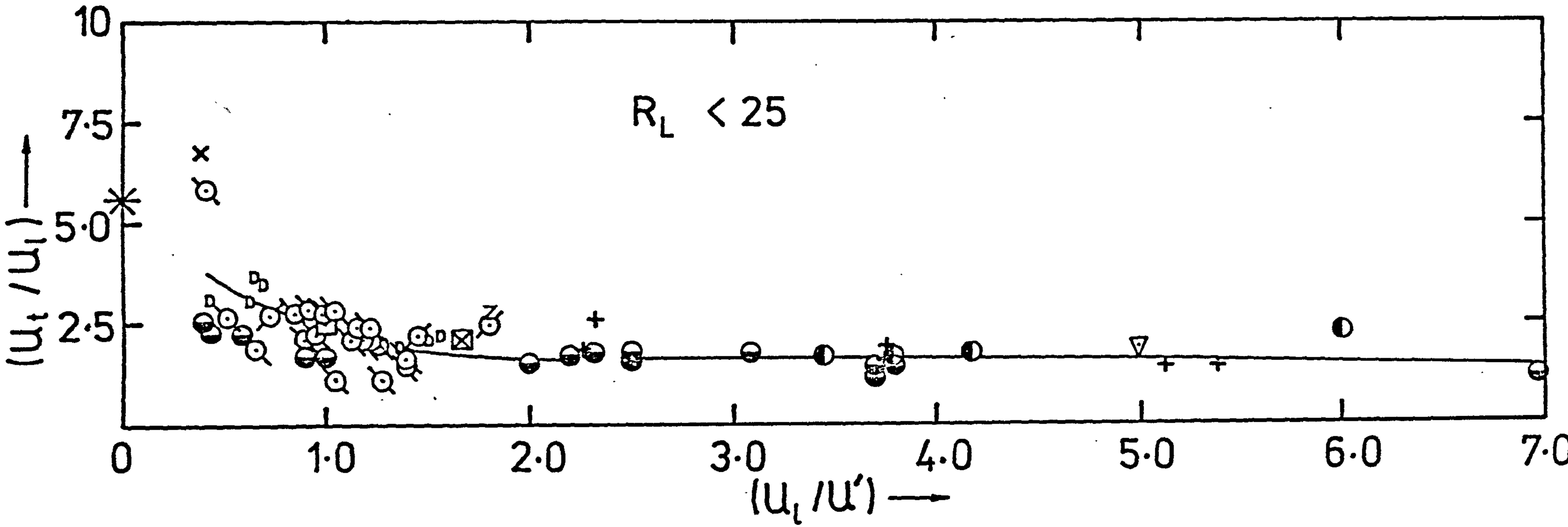

FIG. 5.15 VARIATION OF u_t/u_ℓ WITH u_ℓ/u', $R_L < 25$. ASTERISKED POINT FROM EQ.(5.8)

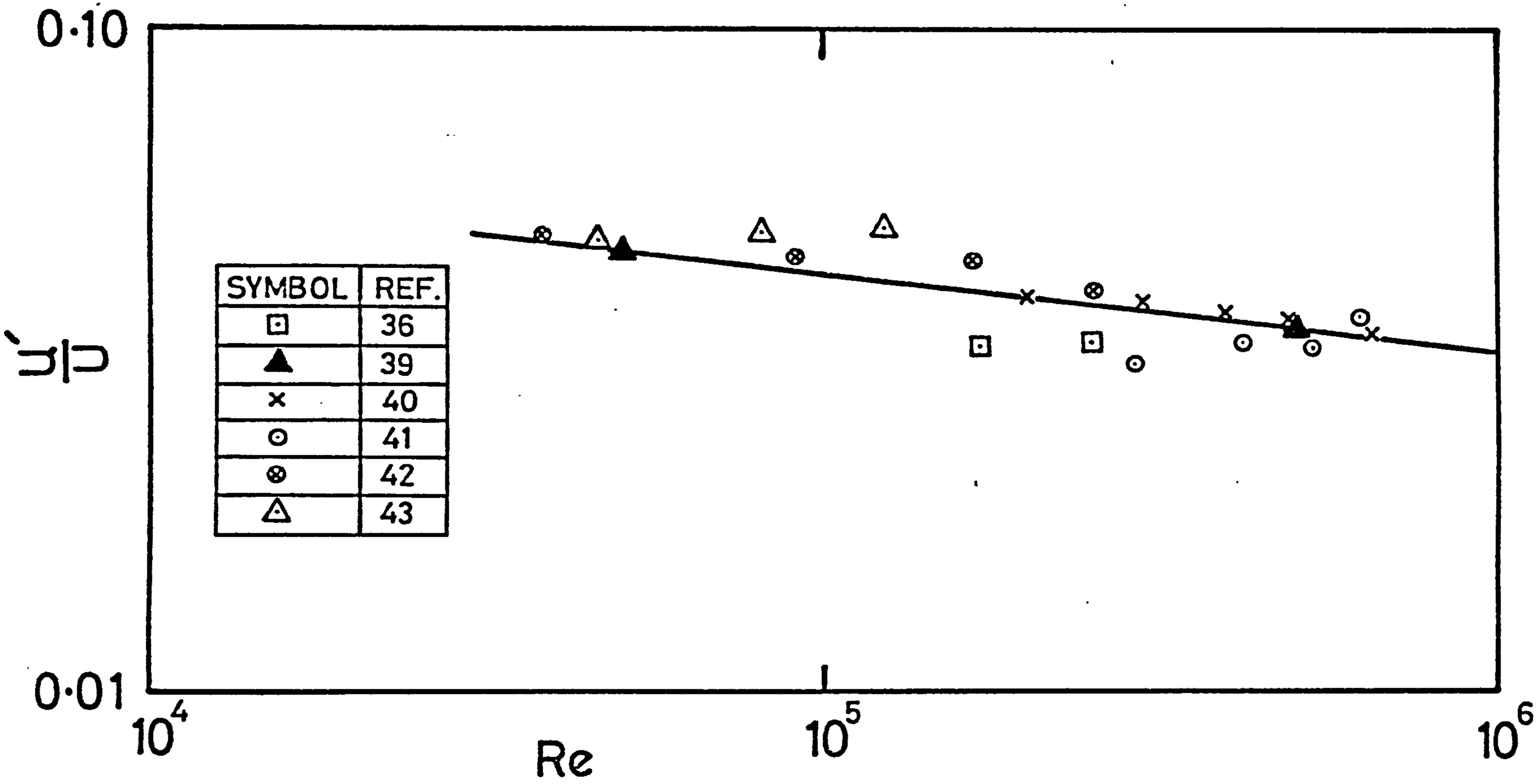

FIG.5.16 VARIATION OF RADIAL R.M.S. TURBULENT VELOCITY AT HALF RADIUS OF THE PIPE WITH PIPE FLOW REYNOLDS NUMBER

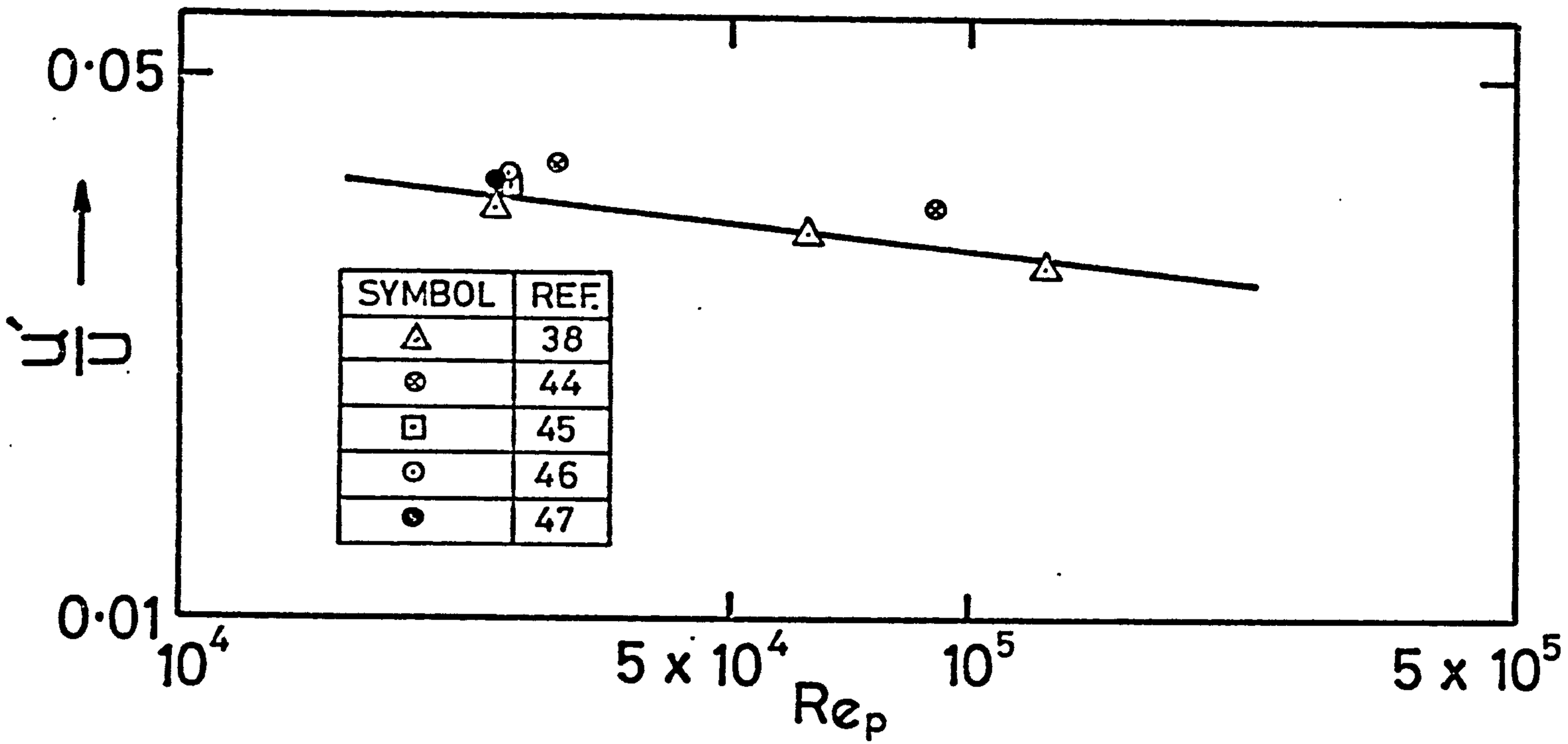

FIG.5.17 VARIATION OF RADIAL R.M.S. TURBULENT VELOCITY AT HALF-WAY BETWEEN THE CENTRE PLANE AND A PLATE WITH CHANNEL FLOW REYNOLDS NUMBER

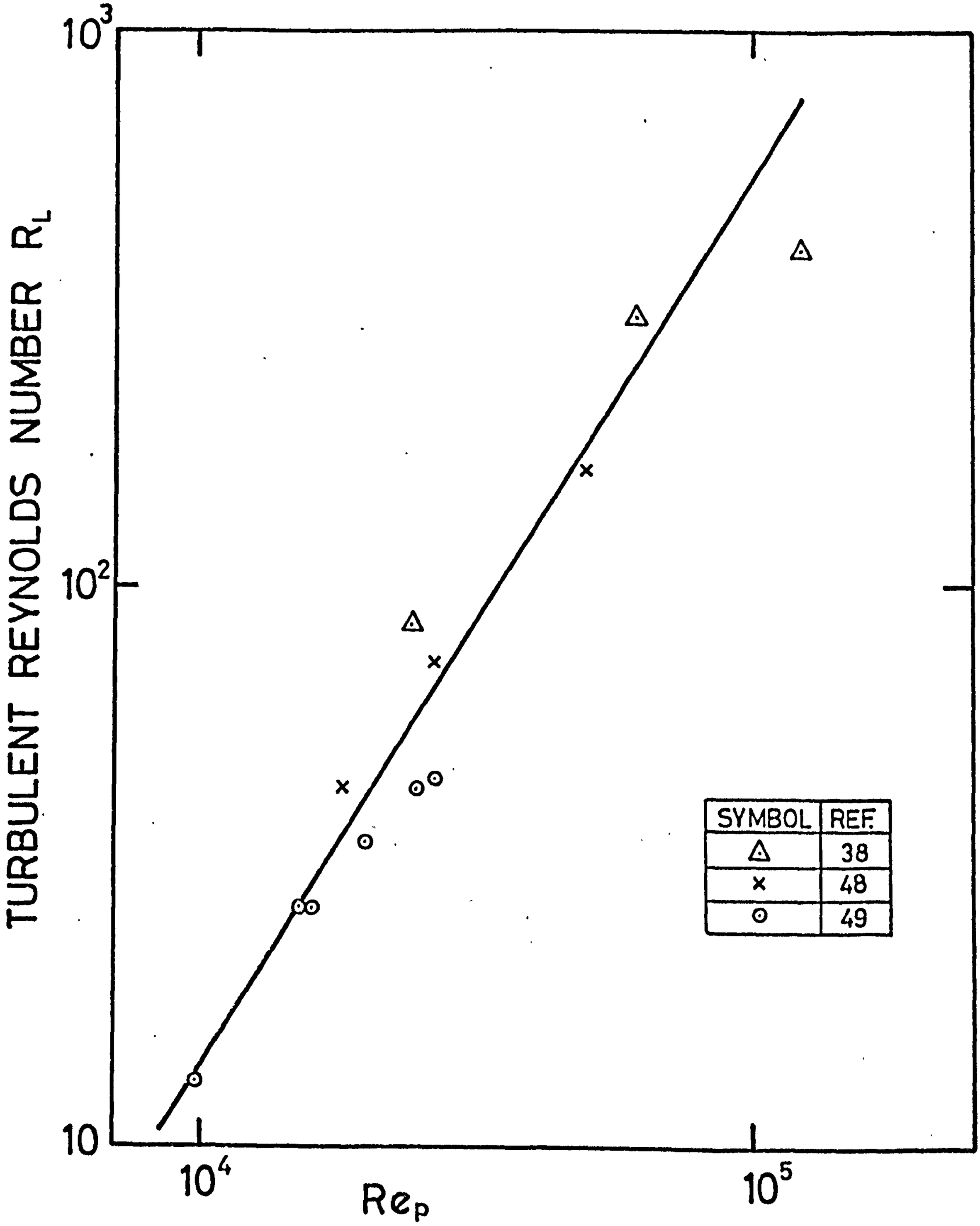

FIG.5.18 VARIATION OF RADIAL TURBULENT REYNOLDS NUMBER AT HALF-WAY BETWEEN THE CENTRE PLANE AND A PLATE WITH CHANNEL FLOW REYNOLDS NUMBER

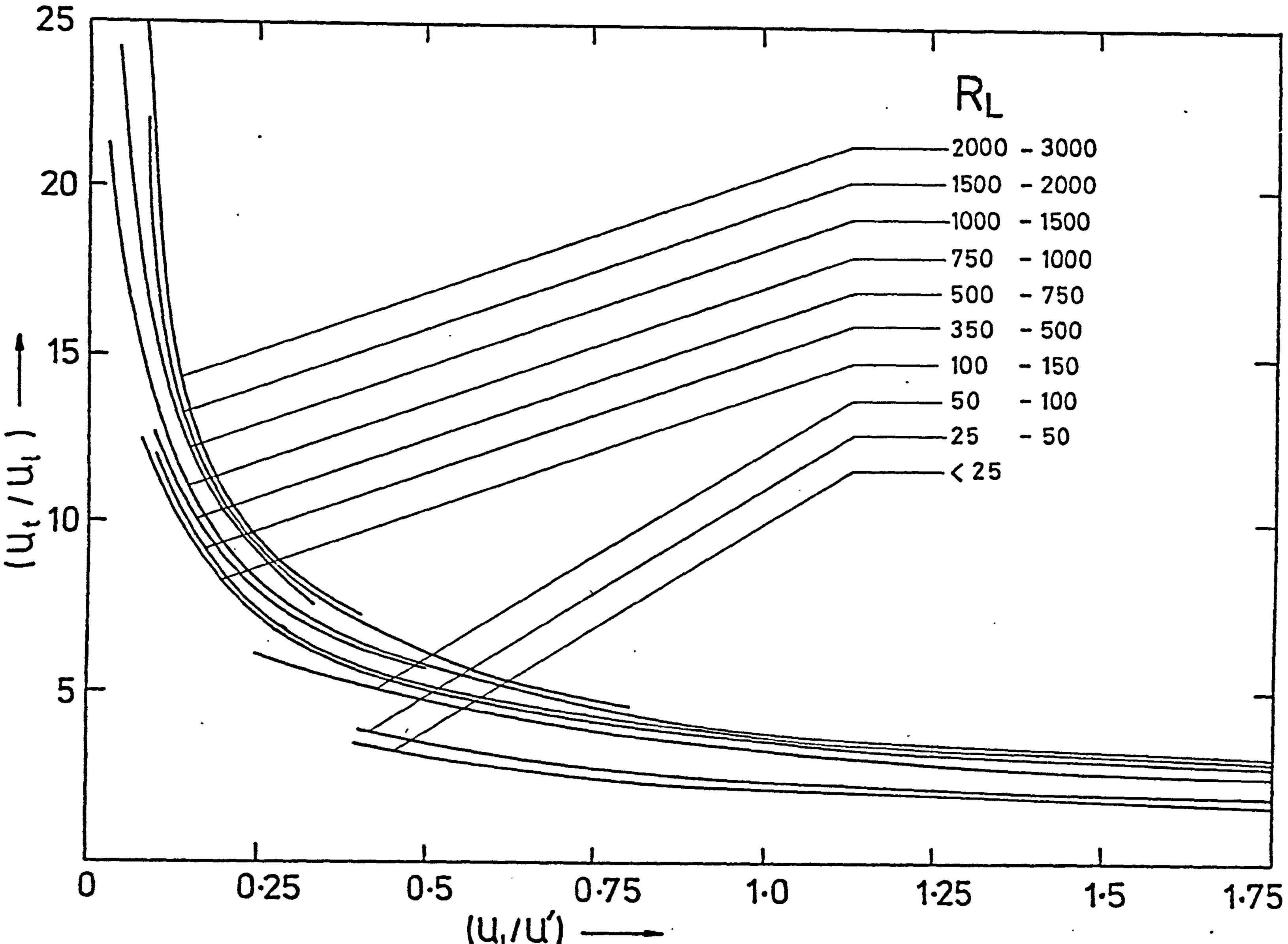

FIG.5.19 VARIATION OF u_t/u_ℓ WITH u_ℓ/u', FOR DIFFERENT VALUES OF R_L

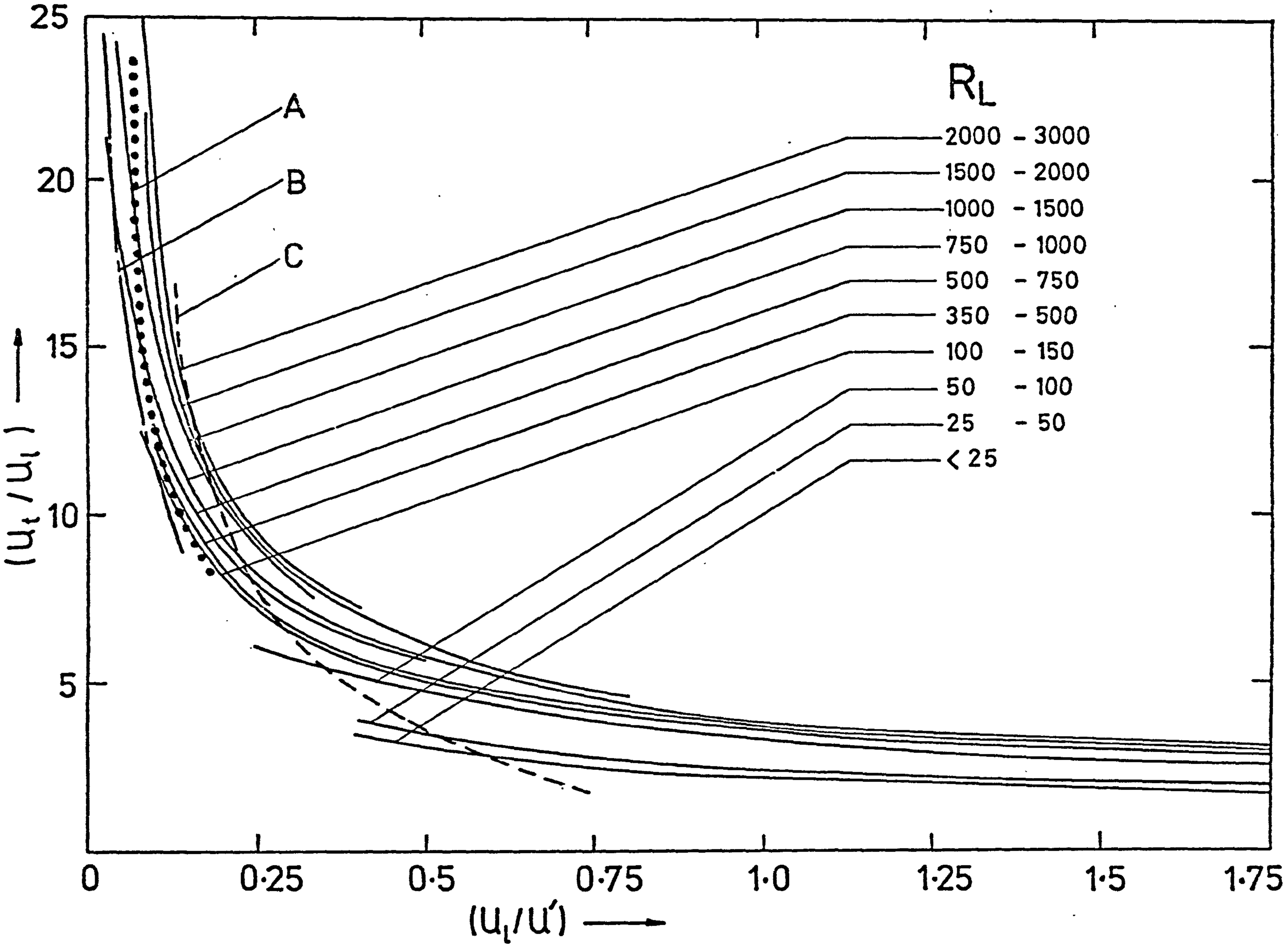

FIG. 5.20 RÉGIMES OF COMBUSTION

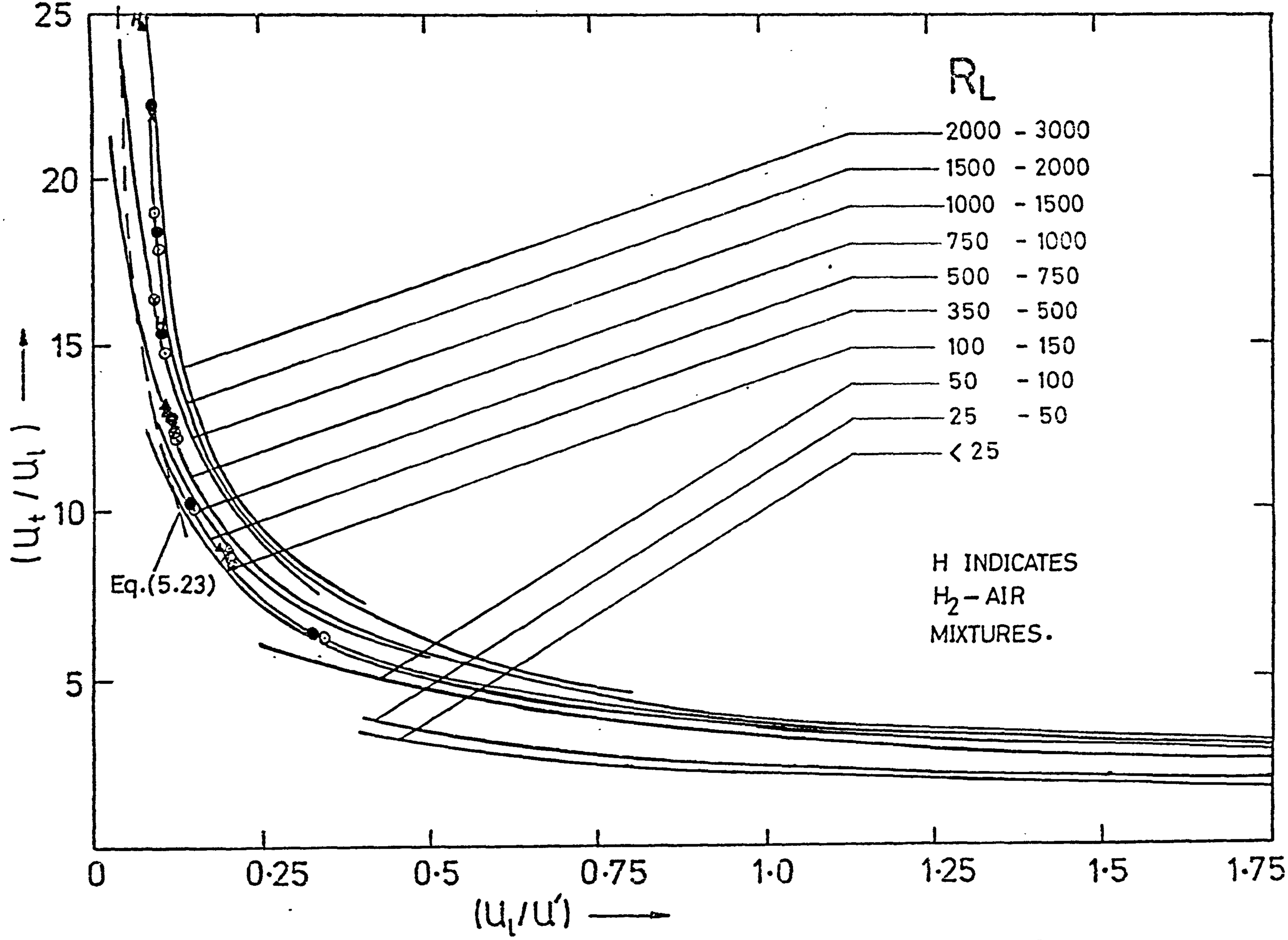

FIG. 5.21 PROPAGATION LIMITS AS PLOTTED ON FIG. 5.19 (FOR NOTATIONS SEE FIG. 4.15 & TABLE 4.3)

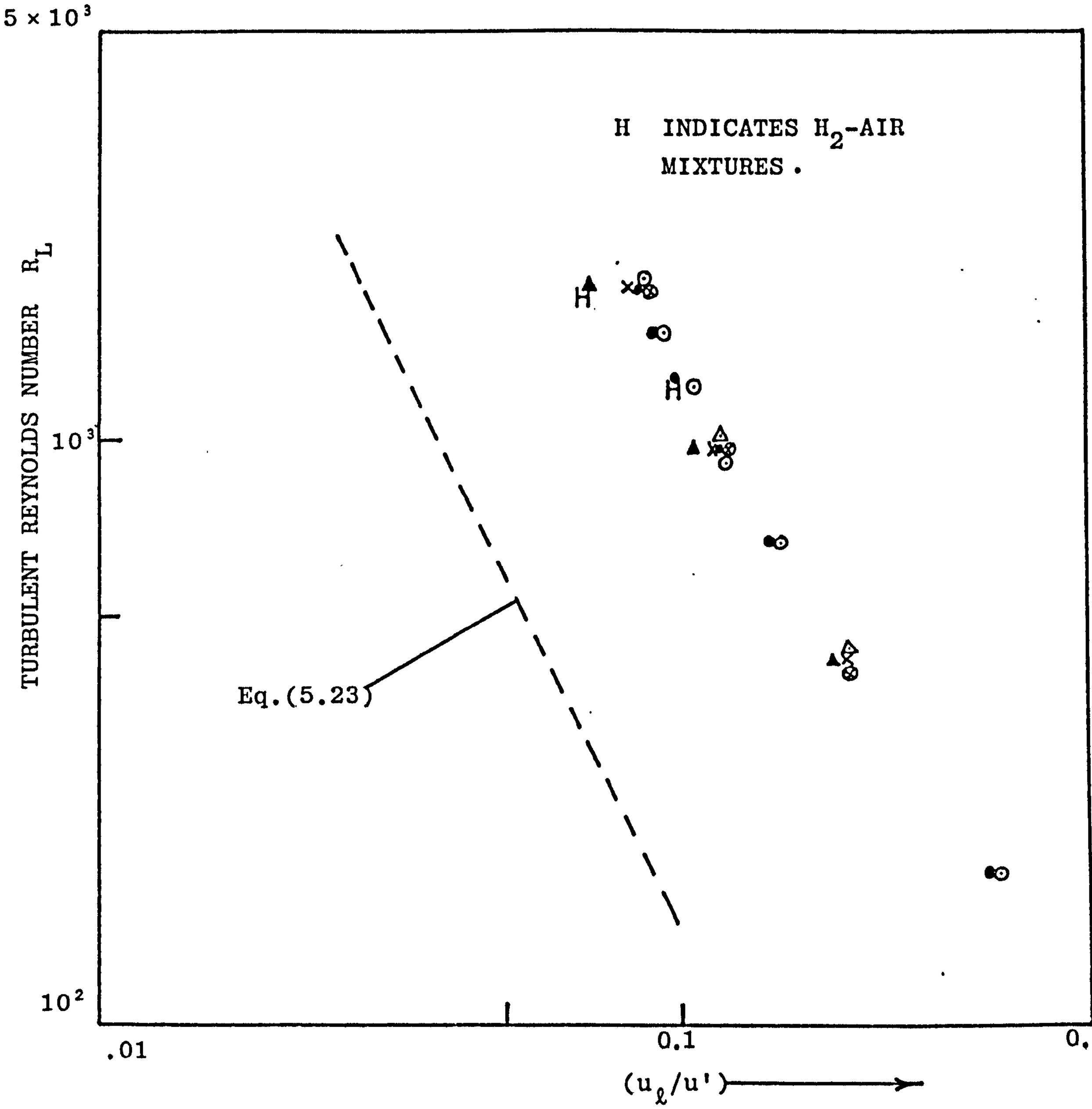

FIG.5.22 PROPAGATION LIMITS CORRELATION (FOR NOTATIONS SEE FIG.4.15 & TABLE 4.3)

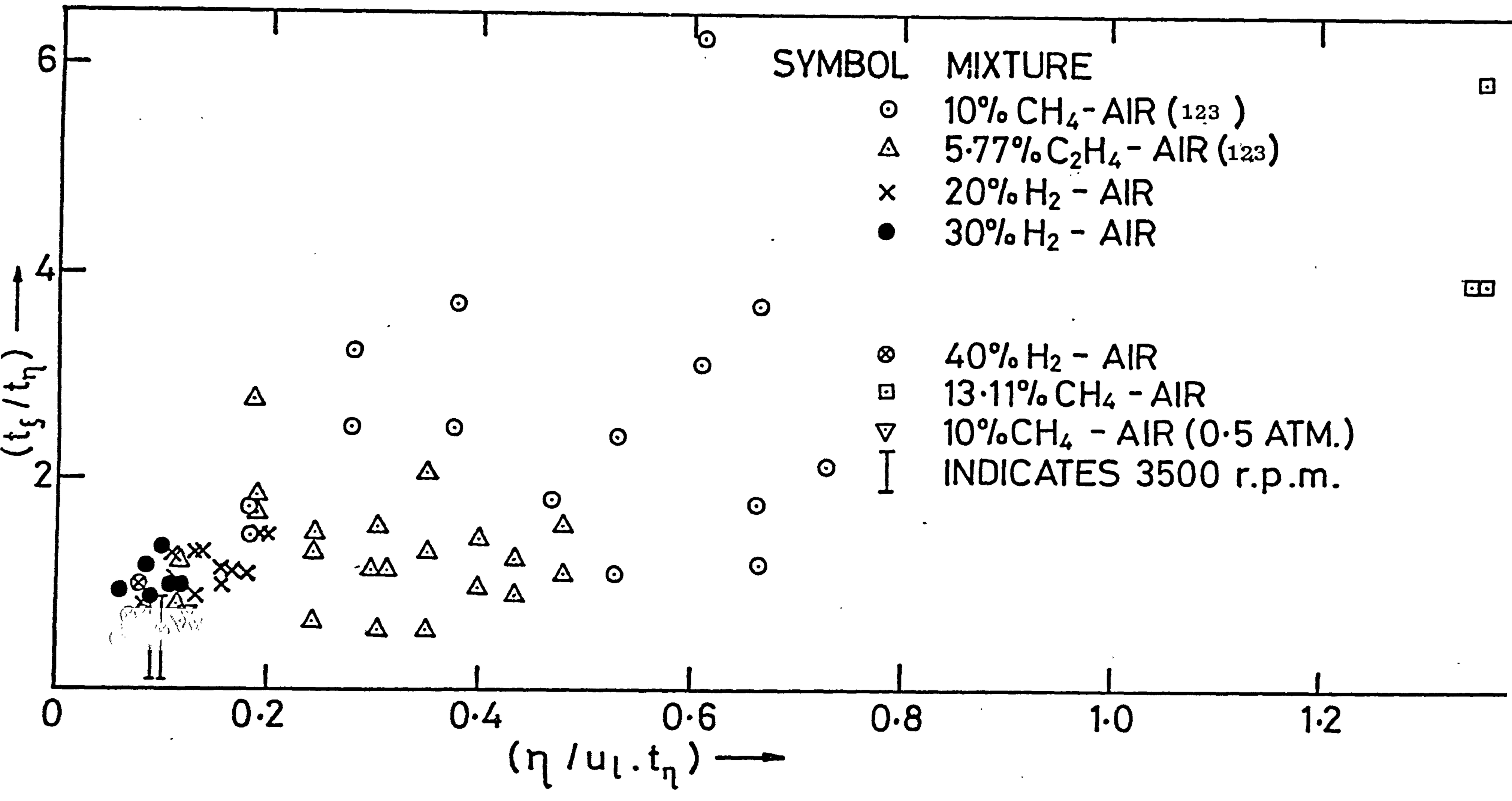

FIG.5.23 RELATIONSHIP OF MEASURED DIMENSIONLESS SMALL EDDY APPARENT LIFETIME, t_ξ/t_η, to $\eta/u_\ell\ t_\eta$

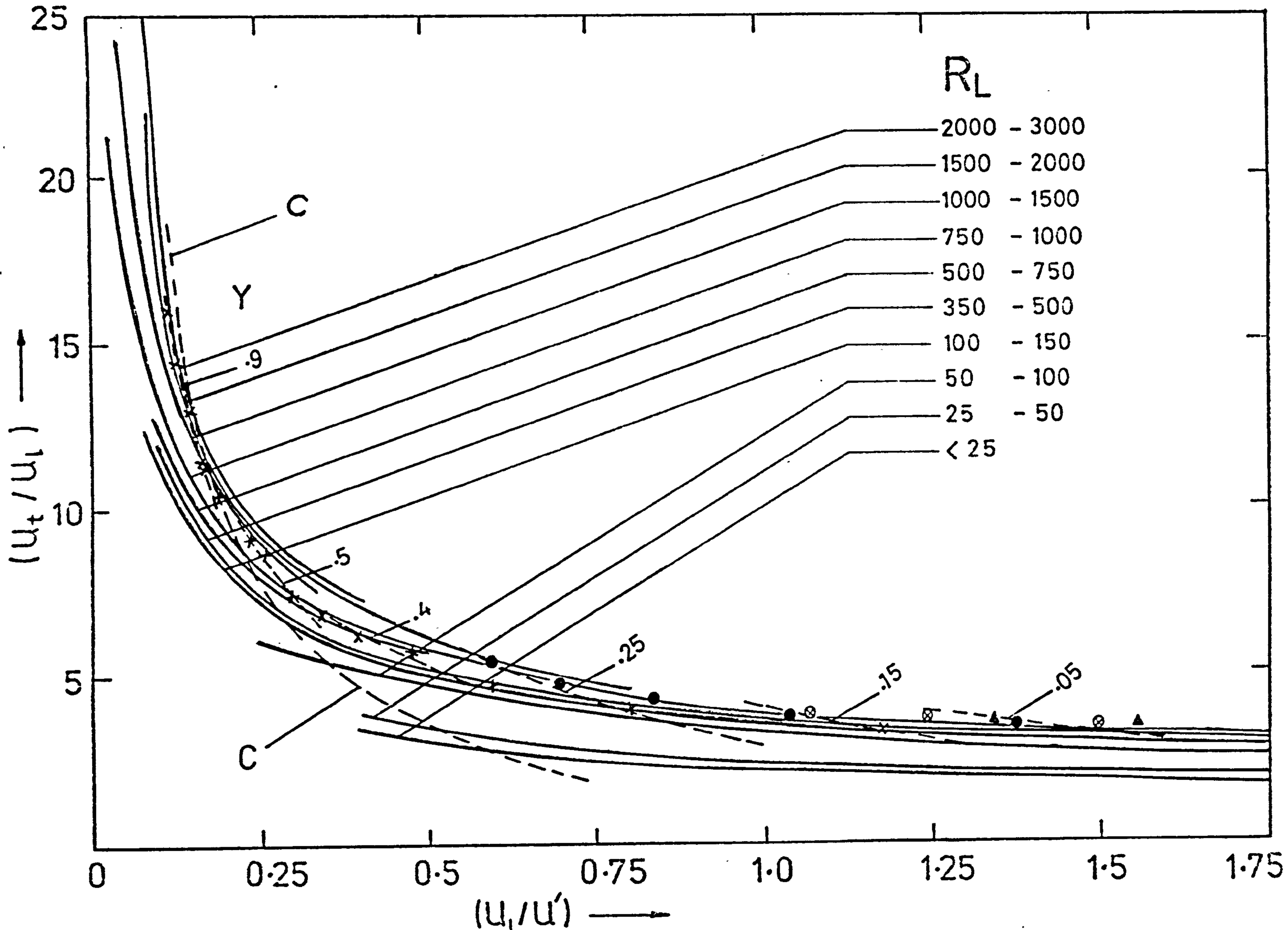

FIG.5.24 THE NORMALISED OPTICAL DENSITY OF SMALL EDDIES AS PLOTTED ON FIG. 5.19 (FOR NOTATIONS SEE FIG. 4.25)

CHAPTER 6

A TWO EDDY THEORY OF TURBULENT COMBUSTION

CHAPTER 6

A TWO EDDY THEORY OF TURBULENT COMBUSTION

6.1 INTRODUCTION

The wide range of turbulent combustion régimes, from the simple bunsen burner to the intensely turbulent combustion in a stirred reactor, makes any attempt at a unified theory of turbulent flame propagation and structure a prodigious task.

Existing theories for the prediction of turbulent burning velocity, u_t, all involve an assumption of a model of the turbulent flame structure; these various models have been reviewed in Ref.1. On the basis of the results presented in Chapter 4 and the available data on turbulent flame and turbulent flow structure, a two eddy theory of burning is postulated. Values of u_t/u_ℓ obtained from this are compared with experimental values of the ratio.

6.2 SMALL SCALE STRUCTURE

The flame photographs in the present study, and the measurements of them, revealed two markedly different categories of eddy size: large scale eddies with an

equivalent diameter close to that of the integral scale, L, and small scale eddies suggestive of elongated vortex tubes with a diameter close to that of the Kolmogorov microscale, η , The dashed curve C in Fig.5.20 defines the equality of η and the laminar flame thickness, δ_ℓ . To the left of the curve the former is less than the latter. Far to the right of the curve the photographs revealed that the large scale structure predominated, but that as the curve was approached and crossed, the small scale structure became more marked. This would appear to be a régime where small eddy burning predominated (1).

Experimental indications of the important role of small, intermittent, high frequency eddies in highly turbulent flames also comes from other photographs (2,3), measurements of light scattering from soot particles (4), current fluctuations from electrostatic probes (5-9) and fluctuations of chemiluminescent emission (6). More details of the small scale structure are given in Section 6.8.

6.3 A TWO EDDY THEORY OF BURNING

The turbulent structure suggested by the experimental evidence of the previous section accords with that suggested by Tennekes (10) and Kuo and Corrsin (11), in which dissipative eddies consist of vortex tubes, with a diameter of the order of η , and a spacing of the order of the Taylor microscale, λ. This fine scale structure is mutually interconnected with that of the large scale, the nature of which also progressively is being revealed (12-14).

That the rate of decay of large eddies is an important rate-determining step in an overall rate of chemical reaction in turbulent flow is embodied in the eddy break-up theory of Spalding (15) and the eddy dissipation model of Magnussen and Hjertager (16). The present theory considers the rates of decay of both large and small eddies in isotropic turbulence and the associated chemical reaction. Theoretical values of turbulent burning velocity are compared with those of experiment and the relevance of the theory to the experimentally observed flammability limits is discussed.

The two eddy theory of burning is based upon the following assumptions:

(i) Combustion occurs in two sizes of eddy; in large eddies of average lifetime, L/u', and in dissipative eddies of average lifetime equal to the Kolmogorov time scale, t_η .

(ii) All the matter in large eddies is used in the formation of dissipative eddies. Dissipation along vortex tubes, with the associated molecular transport, is a necessary condition for flame propagation.

(iii) Laminar flames propagate through large eddies. Dissipative eddies chemically react along the length of the vortex tubes, not necessarily through flame propagation, but by reactions associated with molecular dissipation.

(iv) An exponential probability distribution function (pdf) is assumed for eddy lifetimes (14), but at present a constant value is assumed for chemical lifetimes. Later developments might assign pdfs for chemical lifetimes which are a function of mean reactedness.

(v) All the various rate processes are conveniently based upon a common dimensionless time, $\tau \doteq u'^2 t/\nu$, where t is real time.

6.3.1 Large Eddies

The dimensionless mean lifetime of large eddies, τ_{dL}, becomes

$$\tau_{dL} = \frac{u'^2 L}{\nu u'} \doteq R_L \qquad (6.1)$$

The associated decay constant, κ_L, for the break-down of large to small eddies is the reciprocal of τ_{dL} and

$$\kappa_L = R_L^{-1} \qquad (6.2)$$

If there are n_L large eddies in unit volume, their decay rate is given by $\kappa_L n_L$.

Let p_L be the probable fraction of an eddy which burns during the eddy lifetime and V_L be the eddy volume. If r is the mean reactedness at a point in a flame, then $(1-r)$ is the mean fractional volume unreacted. The associated dimensionless volumetric rate of burning, B_L, becomes

$$B_L = \kappa_L n_L p_L V_L^{(1-r)} \tag{6.3}$$

This form of expression is adopted for both large and small eddies. This is because, for chemical reaction to be effective in flame propagation, it must be followed by the break up of the eddy and ultimately by the mixing of the molecules comprising it with those from other eddies.

Evaluation of p_L requires a dimensionless chemical lifetime, τ_{cL}, for a large eddy. Based upon laminar burning in such an eddy, with a chemical lifetime of L/u_ℓ,

$$\tau_{cL} = \frac{L}{u_\ell}\frac{u'^2}{\nu} = \frac{u'}{u_\ell} R_L \tag{6.4}$$

The fraction of an eddy which has reacted during an eddy lifetime of τ, $(\leq \tau_{cL})$, is τ/τ_{cL}. For $\tau > \tau_{cL}$ all the eddy will have been reacted. With a pdf for eddy lifetimes given by $\tau_{dL}^{-1} \exp(-\tau/\tau_{dL})$,

$$p_L = \int_0^{\tau_{cL}} \frac{\tau}{\tau_{cL}} \tau_{dL}^{-1} \exp(-\tau/\tau_{dL}) d\tau + \int_{\tau_{cL}}^{\infty} \tau_{dL}^{-1} \exp(-\tau/\tau_{dL})\, d\tau \tag{6.5}$$

Now

$$\int_0^{\tau_{cL}} \tau \exp(-\tau/\tau_{dL})\, d\tau$$

$$= \tau \int_0^{\tau_{cL}} \exp(-\tau/\tau_{dL})\, d\tau - \int_0^{\tau_{cL}} -\tau_{dL} \exp(-\tau/\tau_{dL})\, d\tau \tag{6.6}$$

$$= \left\{ \tau[-\tau_{dL} \exp(-\tau/\tau_{dL})] - \tau_{dL}^2 \exp(-\tau/\tau_{dL}) \right\}_0^{\tau_{cL}} \tag{6.7}$$

$$= \tau_{cL}\left[- \tau_{dL} \exp(-\tau_{cL}/\tau_{dL}) \right] -$$

$$\left[\tau_{dL}^{2} \exp(-\tau_{cL}/\tau_{dL}) - \tau_{dL}^{2} \right] \qquad (6.8)$$

Equations (6.5) to (6.8) yield

$$p_L = - \exp(-\tau_{cL}/\tau_{dL}) - (\tau_{dL}/\tau_{cL}) \exp(-\tau_{cL}/\tau_{dL})$$

$$+ (\tau_{dL}/\tau_{cL}) + \exp(-\tau_{cL}/\tau_{dL}) \qquad (6.9)$$

$$p_L = \left[1 - \exp(-\tau_{cL}/\tau_{dL}) \right] \tau_{dL}/\tau_{cL} \qquad (6.10)$$

It is assumed that n_L is related to the intermittency factor for large eddies, γ_L, by

$$n_L = \gamma_L/V_L \qquad (6.11)$$

Equations (6.1) to (6.11) yield

$$B_L = R_L^{-1} \gamma_L [1 - \exp(-u'/u_\ell)](1-r)u_\ell/u' \qquad (6.12)$$

6.3.2 Small Eddies

The dimensionless mean lifetime of small eddies, $\tau_{d\eta}$, becomes, from Eq. (5.25),

$$\tau_{d\eta} = \frac{u'^2}{\nu} t_\eta = 1.681 R_L^{0.5} \qquad (6.13)$$

The associated decay constant, κ_η, is the reciprocal of $\tau_{d\eta}$ and

$$\kappa_\eta = 0.595 R_L^{-0.5} \qquad (6.14)$$

The chemical reaction associated with vortex tube dissipation is of a different character from that in a large eddy and it is proposed that the chemical lifetime is given by $k\eta/u_\ell$, where k is of order unity. It can be shown from Eqs.(2.16) and (5.14) that

$$\eta = 1.297\ L\ R_L^{-0.75} \tag{6.15}$$

The dimensionless chemical lifetime, $\tau_{c\eta}$, is given by

$$\tau_{c\eta} = \frac{k\eta}{u_\ell}\frac{u'^2}{\nu} = 1.297kR_L^{0.25}\ u'/u_\ell \tag{6.16}$$

The dimensionless volumetric rate of burning, B_η , is given by

$$B_\eta = \kappa_\eta n_\eta p_\eta V_\eta (1-r) \tag{6.17}$$

in which n_η is the number of small eddies, or vortex tube elements, in unit volume, p_η is the probable fraction of an eddy which burns during the eddy lifetime and V_η is the eddy volume.

The evaluation of p_η follows along similar lines to that employed for p_L . It is first again assumed that the fraction burnt is linear with time up to the chemical lifetime, $\tau_{c\eta}$. This probably is less justifiable than in the case of large eddies, where a propagating laminar flame is assumed. The nature of chemical reaction along a vortex tube might be different and departures from linearity might be expected.

Two other alternatives were considered. The first, reported in Section 6.6, considers departures from linearity by the incorporation of a chemical delay time effect in an Arrhenius-type expression. The second, reported in Section 6.9, and considers a chemical lifetime based upon the properties of a laminar flame. The pdf for eddy life-time is given by $\tau_{d\eta}^{-1} \exp(-\tau/\tau_{d\eta})$ and, following Eqs.(6.5) to (6.10),

$$p_\eta = \int_0^{\tau_{c\eta}} \frac{\tau}{\tau_{c\eta}} \tau_{d\eta}^{-1} \exp(-\tau/\tau_{d\eta})\, d\tau + \int_{\tau_{c\eta}}^{\infty} \tau_{d\eta}^{-1} \exp(-\tau/\tau_{d\eta}) d\tau \tag{6.18}$$

Now

$$\int_0^{\tau_{c\eta}} \tau \exp(-\tau/\tau_{d\eta})\, d\tau$$

$$= \tau \int_0^{\tau_{c\eta}} \exp(-\tau/\tau_{d\eta})\, d\tau - \int_0^{\tau_{c\eta}} -\tau_{d\eta} \exp(-\tau/\tau_{d\eta})\, d\tau \tag{6.19}$$

$$= \left\{ \tau \left[-\tau_{d\eta} \exp(-\tau/\tau_{d\eta}) \right] + \tau_{d\eta}^2 \exp(-\tau/\tau_{d\eta}) \right\}_0^{\tau_{c\eta}} \tag{6.20}$$

$$= \tau_{c\eta} \left[-\tau_{d\eta} \exp(-\tau_{c\eta}/\tau_{d\eta}) \right] -$$

$$\left[\tau_{d\eta}^2 \exp(-\tau_{c\eta}/\tau_{d\eta}) - \tau_{d\eta}^2 \right] \tag{6.21}$$

Equations (6.18) to (6.21) yield

$$p_\eta = -\exp(-\tau_{c\eta}/\tau_{d\eta}) - (\tau_{d\eta}/\tau_{c\eta}) \exp(-\tau_{c\eta}/\tau_{d\eta})$$

$$+ (\tau_{d\eta}/\tau_{c\eta}) + \exp(-\tau_{c\eta}/\tau_{d\eta}) \tag{6.22}$$

$$p_\eta = [1 - \exp(-\tau_{c\eta}/\tau_{d\eta})]\ \tau_{d\eta}/\tau_{c\eta} \qquad (6.23)$$

and

$$n_\eta = \gamma_\eta/V_\eta \qquad (6.24)$$

,where γ_η is the intermittency factor for small eddies.

Equations (6.13) to (6.24) yield

$$B_\eta = 0.771R_L^{-0.25}\gamma_\eta[1-\exp(-0.771kR_L^{-0.25}u'/u_\ell)](1-r)u_\ell/ku' \qquad (6.25)$$

6.3.3 Comparative Burning Rates

To evaluate B_L and B_η both the "k" and intermittency factors must be known. Values of 0.5, 1 and 2 were assumed in turn for the former factor for three typical values of R_L of 1750, 875 and 425, whilst "k" was assumed to be unity for the other values of turbulent Reynolds number. Hot wire anemometers mounted in the explosion vessel by Andrews (7) gave signals at different fan speeds in cold calibrations. He analysed these to obtain values of intermittency factors at different frequences.

The intermittency factor is the fraction of time for which the flow is turbulent. Its value ranges from zero in a fully laminar flow, to unity in a fully turbulent flow. The intermittency circuit used by Andrews for such measurements was similar to that used by Corrsin and Kistler (17) and the same as that of Mobbs (18). It gave a zero output for non-turbulent and a constant value for turbulent flow. With the aid of an oscilloscope the circuit was

adjusted to obtain a regular intermittent train of pulses to a digital counter with a square wave input. The value of "γ" was obtained from the number of counts registered on the counter during a period of time which was related to the pulse signal frequency. The spectral analysis of the linearised hot wire signal was obtained using a Brüel and Kjaer audio frequency spectrometer, type 2112, with a filter band width of 1/3 octave, inserted between the lineariser and intermittency circuit.

The raw signal was assumed to give values of γ_L and its third time derivative to give values of γ_η. Values of the latter also were obtained by Lwakabamba (8) from photographic measurements of the frequency of the small eddies and hot wire measurements of intermittency in different frequency bands. It is postulated that these can be generalised to be unique functions of R_L and these are shown in Fig.6.1. The reported experimental data of γ_L and γ_η were limited to a maximum value of R_L of 2500, but these were extrapolated up to R_L values of 8750, as shown in Fig.6.1. In the present calculations, values of γ_η were drawn from the chain dotted curve for values of R_L up to 1250 and from the full and dashed curve for higher values of R_L, whilst values of γ_L were drawn from the full and dashed curve.

Reference to Eqs.(6.12) and (6.25) shows that an increase in R_L decreases the dimensionless rate of burning of small eddies less than it does that of large eddies.

This is because of the more rapid decay of the former, indicative of a more rapid mixing process. The rate of burning is limited by the intermittent turbulent structure, but an increase in R_L not only increases the relative rate of mixing, but also the value of γ_η.

The importance of the small eddy structure is shown in Figs.6.2 to 6.11, where values of the ratio B_η/B_L for "k" equal to unity and r equal to 0.95 are shown as a function of u_ℓ/u' for different values of R_L. The ratio increases with increase in R_L and decrease in u_ℓ/u' and can be more than 400.

6.4 TURBULENT QUENCHING OF FLAMES

It might be expected that as the probable fraction of an eddy which burns during an eddy lifetime, p_η, decreases, so the tendency of the flame to quench will increase. Equation (6.23) gives p_η and Eqs.(6.13) and (6.16) give

$$\frac{\tau_{d\eta}}{\tau_{c\eta}} = \frac{1.297}{k} \left(\frac{u_\ell}{u'}\right) R_L^{0.25} \qquad (6.26)$$

Thus the probable fraction burnt tends to decrease with a decrease in this ratio. Any increase in chemical lifetime relative to the eddy lifetime increases the difficulties of flame propagation and Eq.(6.26) shows this can be brought about by a decrease in the value of either u_ℓ/u' or R_L.

This is born out in Fig.6.12 by the curves of flammability limits for runs 5 and 6 (see Fig.4.15), which

coincide when plotted on the experimental burning velocity data, drawn from Fig.5.19, for five values of R_L . Theoretical values of p_η were calculated from this for "k" equal to unity and were found to range from 0.65 to 0.49 between values of R_L of 417 and 1823 respectively. Whether or not a flame quenches depends additionally upon the size of the flame kernel and its temperature, and this is supported by the experimental work reported in Chapter 4 with different spark energies and the shielded spark gap. It readily can be shown that the dotted curve in Fig.6.12, represents the equality $\tau_{c\eta} = k\tau_{d\eta}$. In addition, it also represents the condition of equality of η and laminar flame thickness if Pr is assumed to be unity. Then Eq.(5.15) yields

$$\frac{u_\ell}{u'} >> 0.771\ R_L^{-0.25} \qquad (6.27)$$

6.5 TURBULENT BURNING VELOCITIES

The two eddy theory of burning can yield an approximate expression for the turbulent burning velocity. In a Lagrangian sense, the total rate of burning, $(B_L + B_\eta)$, can be expressed as the rate of change of reactedness, r . For a one dimensional flame, neglecting diffusion,

$$\frac{Dr}{D\tau} = (B_L + B_\eta) \qquad (6.28)$$

or

$$\frac{Dr}{(1-r)} = \frac{(B_L + B_\eta)D\tau}{(1-r)} \qquad (6.29)$$

In the present simplified analysis $(B_L + B_\eta)(1-r)^{-1}$ is not a function of reactedness and the equation is readily integrated. In a more rigorous analysis this would not be so and pdfs would be assigned to chemical lifetimes for different values of r. Additionally, instead of cold flow turbulence parameters, allowance might be made for the effects of combustion upon these.

From Eq.(6.29), if τ_f is the dimensionless time for reactedness to progress from zero to a value of r_f, then

$$\tau_f = \left(\frac{1-r}{B_L+B_\eta}\right) \quad \ell n \left(\frac{1}{1-r_f}\right) \tag{6.30}$$

and this can be evaluated from Eqs.(6.12) and (6.25).

Values of τ readily can be transformed into real time by the relationship, $t = \tau\nu/u'^2$. Together with the two approximate expressions relating turbulent flame thickness,

$$\delta_t \sim \frac{\varepsilon}{u_t} \tag{6.31}$$

and

$$t_f \sim \frac{\delta_t}{u_t} \tag{6.32}$$

, where ε is the turbulent diffusivity, it follows that

$$\frac{u_t}{u_\ell} \sim \frac{u'}{u_\ell}\left(\frac{\varepsilon}{\nu\tau_f}\right)^{0.5} \tag{6.33}$$

and

$$\frac{\delta_t}{L} \sim \left(\frac{\varepsilon\tau_f}{\nu}\right)^{0.5} R_L^{-1} \tag{6.34}$$

The turbulent transport number, ε/ν, is related to the turbulent Reynolds number and, for isotropic turbulence, the proposed relationship is given by Eq.(2.20).

Values of u_t/u_ℓ were found from Eqs.(2.20), (6.12), (6.25), (6.30) and (6.33), with r_f equal to 0.95 and with the previously listed values of k and intermittency factors. The results are plotted in Figs.6.2 to 6.11, for values of turbulent Reynolds number from 8750 down to 300. For comparison are shown experimental values of u_t/u_ℓ, drawn from a variety of sources and previously given in Chapter 5. In the region of R_λ ($=u'\lambda/\nu$) equal to 100, the dissipative eddies first start to acquire a size significantly less than that of the large eddies (19), and it might be expected that at $R_\lambda < 100$ the large eddies are dissipating directly. Applying Eq.(2.18) to this condition gives $R_L < 237$, in which range the present theory will not be applicable.

Values of turbulent flame thickness in relation to the integral scale of turbulence, δ_t/L, and given by Eq.(6.34), also are presented in Figs.6.2 to 6.11, with k equal to unity. The near limit turbulent flames are those with high values of δ_t/L.

6.6 ARRHENIUS TYPE REACTION RATES WITHIN SMALL EDDIES

It was suggested in Section 6.3.2 that the nature of chemical reaction along a vortex tube might be different from that in a large eddy and departures from

linearity might be expected due to a chemical delay time. The temporal variation of the degree of reaction was assumed to be given by $\exp(-\tau_{c\eta}/\tau)$. The full line curve in Fig.6.13 shows the variation of this function with the dimensionless ratio $\tau/\tau_{c\eta}$. For mathematical convenience this function was approximated to the form given by the dashed straight lines in the figure. These comprise three régimes of $\tau/\tau_{c\eta}$: (0-0.22), (0.22-2.35), and (2.35-∞). Accordingly, in the second régime the fraction of an eddy which has reacted now is given, not by $\tau/\tau_{c\eta}$, but by $\frac{1}{2.13}\left(\frac{\tau}{\tau_{c\eta}} - 0.22\right)$. No reaction occurs up to a time of $0.22\,\tau_{c\eta}$. The probable fraction of an eddy which burns during an eddy lifetime, p_η, formerly given by Eq.(6.18) now becomes

$$p_\eta = \int_{0.22\tau_{c\eta}}^{2.35\tau_{c\eta}} \frac{1}{2.13}\left(\frac{\tau}{\tau_{c\eta}} - 0.22\right) \tau_{d\eta}^{-1} \exp(-\tau/\tau_{d\eta})\, d\tau + \int_{2.35\tau_{c\eta}}^{\infty} \tau_{d\eta}^{-1} \exp(-\tau/\tau_{d\eta}) d\tau \qquad (6.35)$$

$$p_\eta = \frac{1}{2.13\tau_{c\eta}\tau_{d\eta}} \int_{0.22\tau_{c\eta}}^{2.35\tau_{c\eta}} (\tau - 0.22\tau_{c\eta}) \exp(-\tau/\tau_{d\eta})\, d\tau + \exp(-\,2.35\,\tau_{c\eta}/\tau_{d\eta}) \qquad (6.36)$$

Now

$$\int_{0.22\tau_{cn}}^{2.35\tau_{cn}} (\tau-0.22\ \tau_{cn})\ \exp(-\tau/\tau_{dn})\ d\tau$$

$$= \Big\{\ \tau\ [-\ \tau_{dn}\ \exp(-\tau/\tau_{dn})] - \tau_{dn}^{2}\ \exp(-\tau/\tau_{dn})$$

$$+\ 0.22\ \tau_{cn}\ \tau_{dn}\ \exp(-\tau/\tau_{dn})\ \Big\}_{0.22\tau_{cn}}^{2.35\tau_{cn}} \qquad (6.37)$$

$$= 2.35\ \tau_{cn}\ [-\ \tau_{dn}\ \exp(-2.35\ \tau_{cn}/\tau_{dn})]$$

$$-\ \tau_{dn}^{2}\ \exp(-2.35\ \tau_{cn}/\tau_{dn})$$

$$+\ 0.22\ \tau_{cn}\ \tau_{dn}\ \exp(-2.35\ \tau_{cn}/\tau_{dn})$$

$$+\ \tau_{dn}^{2}\ \exp(-0.22\ \tau_{cn}/\tau_{dn}) \qquad (6.38)$$

Equations (6.35) to (6.38) yield

$$p_{\eta} = \frac{1}{2.13}\ [-\ 2.35\ \exp(-2.35\ \tau_{cn}/\tau_{dn})$$

$$-\ \frac{\tau_{dn}}{\tau_{cn}}\ \exp(-2.35\ \tau_{cn}/\tau_{dn}) + 0.22\ \exp(-2.35\ \tau_{cn}/\tau_{dn})$$

$$+\ \frac{\tau_{dn}}{\tau_{cn}}\ \exp(-0.22\ \tau_{cn}/\tau_{dn})] + \exp(-2.35\ \tau_{cn}/\tau_{dn}) \qquad (6.39)$$

$$p_{\eta} = \frac{1}{2.13}\ [\exp(-0.22\ \tau_{cn}/\tau_{dn}) - \exp(-2.35\ \tau_{cn}/\tau_{dn})]\ \tau_{dn}/\tau_{cn} \qquad (6.40)$$

Equations (6.13) to (6.17), (6.24) and (6.40) yield

$$B_\eta = 0.362\, R_L^{-0.25}\, \gamma_\eta \,[\exp(-0.170\, k\, R_L^{-0.25}\, u'/u_\ell) - \exp(-1.812\, k\, R_L^{-0.25}\, u'/u_\ell)]\, (1-r)\, u_\ell/k\, u' \qquad (6.41)$$

Values of the ratio B_η/B_L for "k" equal to unity and r equal to 0.95 are shown in Figs.6.14 to 6.16 as a function of u_ℓ/u' for three typical values of R_L, namely 8750, 1750 and 425, respectively. Again values of B_L were calculated from Eq.(6.12), whilst values of γ_L and γ_η were taken, as before, from Fig.6.1. Again the ratio B_η/B_L increases with an increase in R_L and a decrease in u_ℓ/u' and can attain a value of 150.

Evaluations of u_t/u_ℓ and δ_t/L also follow along similar lines to those of Section 6.5. With r_f equal to 0.95 and "k" equal to unity the results are given in Figs.6.14 to 6.16, for values of R_L of 8750, 1750 and 425, respectively. Experimental values of u_t/u_ℓ are also shown for comparison. Comparison of Figs.6.14 to 6.16 with Figs.6.2, 6.6 and 6.10 respectively, for $k = 1$, show the present values of u_t/u_ℓ, as well as those of B_η/B_L, to be less than the previous values, whilst values of δ_t/L are higher.

The present values of u_t/u_ℓ are a good deal less than those of experiments. That the introduction of a chemical delay time effect should reduce the u_t/u_ℓ

and B_η/B_L ratios is to be expected. However, comparisons with experimental values do not lend support to this possibility. Another possibility is discussed in Section 6.9.

6.7 NUMBER DENSITY OF DISSIPATIVE EDDIES

A theoretical basis is now considered for the measured normalised number density of the small eddies, Y, reported in Chapter 4 and shown in Figs. 4.25 and also 5.24. These small eddies always were measured in comparable zones at the edge of the ball of flame gases and hence covering the reaction zone. It is to be expected that the number of eddies photographed would be proportional to the film exposure time. The measurements of Lwakabamba (8) were taken at different camera speeds from those in the present study of 3000 frames sec^{-1}. Accordingly, all measurements were corrected to a standard camera speed by multiplying each result by the ratio of the camera speed to 3000.

It also might be expected that the number of small eddies photographed would be directly related to their volume concentration. Furthermore, the shorter their lifetime the more we might expect to record, in so far as some might disappear during the exposure time and others appear. A longer chemical lifetime also would tend to render more eddies visible. Combining all these effects we might postulate that the number of eddies recorded at a given camera speed, y, is such that

$$y \alpha \text{ fractional volume occupied by small eddies} \times \frac{\tau_{c\eta}}{\tau_{d\eta}} \qquad (6.42)$$

Equations (6.11) and (6.24) give

$$\text{fractional volume occupied by small eddies} = \frac{n_\eta V_\eta}{n_L V_L} = \frac{\gamma_\eta}{\gamma_L} \qquad (6.43)$$

Substitution of Eqs. (6.26) and (6.43) into Eq. (6.42) leads to

$$y \alpha \frac{k}{1.297} \left(\frac{\gamma_\eta}{\gamma_L}\right) \left(\frac{u'}{u_\ell}\right) R_L^{-0.25} \qquad (6.44)$$

Values of the ratio γ_η/γ_L were drawn from Fig.6.1. The value of the right hand side of this equation was divided by the corresponding value for measurements at 5000 r.p.m. fan speed and a value of u_ℓ/u' equal to 0.12. The quotient now can be compared with the measured normalised number density, Y, of Chapter 4 and this is done in Fig.6.17. Semi-theoretical normalised values for two values of R_L are shown by the two curves, whilst experimental points are shown for four ranges of R_L.

The general forms of the semi-theoretical and experimental values of Y are in agreement, but the former values show a somewhat greater dependence upon R_L. On the other hand, when the experimental measurements of

Fig.4.25 are plotted on Fig.5.24, an opposite effect of R_L on Y is in evidence.

In the present analysis, intermittency factors γ_L and γ_η were employed and values were obtained from the measurements of Andrews (7) and Lwakabamba (8). It would, of course, be more satisfactory if an attempt at a theoretical analysis was not based on measured quantities. Moreover, the intermittency factors measured by hot wire anemometry are difficult to interpret physically. So far, it has been assumed that γ_η is a measure of the fractional volume occupied by the small eddies. An alternative possibility is that it is more indicative of their number density. In the next Section a more fundamental analysis of the volume occupied by small eddies is attempted.

6.8 SOME FUNDAMENTALS OF SMALL SCALE STRUCTURE

The experimental observation of intermittency led Townsend (20) to postulate a turbulence structure in which small scale eddies might be represented as a random tangle of vortex sheets (locally parallel vortex lines). Corrsin (21) suggested that the vortex sheets have a thickness of the order of the Kolmogorov microscale, η, and a spacing of the order of the integral scale, L, and that these dissipative regions occupy a volume fraction of order η/L. This with Eq.(6.15) leads to a fractional volume occupied

$$\text{by small eddies} \doteq 1.297\, R_L^{-0.75} \qquad (6.45)$$

Saffman (22) made an approximate heuristic analysis of the dissipation of energy in which the existence of concentrated sheets and tubes of vorticity was assumed and also that the turbulent energy was dissipated in these regions of large vorticity. According to Saffman the thickness of the sheets, or the radius of the tubes, both have a characteristic length scale, δ , which can be shown to be somewhat less than the Taylor microscale, λ . In the case of sheets the proportion of the volume occupied by them is shown by Saffman to be $(\delta/L)^{\frac{1}{2}}$. In the case of tubes this becomes δ/L. Such sheets, or tubes, are formed in a primary cascade.

Saffman postulated that the somewhat organised sheets and tubes are unstable and degenerate into smaller scale motions. For example it is known that curved vortex sheets may develop Taylor-Görtler instabilities and tubes develop Taylor-Couette instabilities, in both of which a stable secondary motion ensues. This has a cellular structure of size approximately, δ . Saffman shows that boundary layers exist at the cell edges and that the fractional volume of the sheets and tubes occupied by these regions of concentrated vorticity is η/δ . It is shown that the dissipation in this secondary cascade is consistent with values of Kolmogorov microscales, and η is the Kolmogorov microscale of turbulence. The fractional volume occupied by these strongly dissipative regions in the case of sheets $= (\frac{\delta}{L})^{\frac{1}{2}} \frac{\eta}{\delta} = \frac{\eta}{(L\delta)^{\frac{1}{2}}}$. Saffman shows that δ is given by

$$\delta = \left(\frac{\nu L}{u'}\right)^{\frac{1}{2}} \tag{6.46}$$

Comparison of Eqs. (2.16) and (6.46) leads to

$$\delta = 0.154\ \lambda \tag{6.47}$$

Equations (2.16), (6.15) and (6.47) give a fractional volume of sheets

$$= 1.297\ \ R_L^{-0.5} \tag{6.48}$$

In the case of tubes the fractional volume occupied by them $= \frac{\delta}{L}\ \frac{\eta}{\delta} = \eta/L$ and this leads to the same expression, Eq.(6.45), as that of Corrsin for dissipative sheets.

Tennekes (10) has suggested that dissipative eddies consist of vortex tubes with a diameter of the order of the Kolmogorov microscale and a spacing of the order of the Taylor microscale, λ , and these vortex tubes occupy a volume fraction η^2/λ^2 . From Eqs. (2.16) and (6.15) this leads to a fractional value

$$= 3.962 \times 10^{-2}\ \ R_L^{-0.5} \tag{6.49}$$

More recently, Kuo and Corrsin (11) have attempted to identify experimentally the geometric character of the regions of random fine structure. They tentatively concluded that these regions are more likely to be rod-like than blob-like or slab-like. They suggested that random, slightly "stringy" structures might overlap each other. The average linear dimensions of these fine structure regions is considerably larger than the turbulent fine structure within them.

All the theoretical predictions of the fractional volume occupied by the small strongly dissipative regions and given by Eqs. (6.45), (6.48) and (6.49), show this fractional volume to decrease as R_L increases. So far, in the present study, this volume has been taken to be γ_η/γ_L and Fig.6.1 shows this ratio to increase as R_L increases.

Numerical values of small eddy fractional volume calculated from Eqs. (6.45), (6.48) and (6.49) for two typical values of R_L are given in Table 6.1. This shows that the fractional volume calculated from these equations might be less than 1%, whilst there can be a 30 fold variation in the value given by the different expressions.

Assume, following Tennekes, that the length of vortex tubes is proportional to λ, then the volume and surface area of a dissipative vortex tube V_η and A_η may be expressed, respectively, as

$$V_\eta = \frac{\pi}{4} \eta^2 \lambda \qquad (6.50)$$

$$A_\eta = \pi \eta \lambda \qquad (6.51)$$

Equations (6.50) and (6.51) lead to

$$A_\eta = 4 \frac{V_\eta}{\eta} \qquad (6.52)$$

If n_η vortex tubes are contained within unit volume, then the total surface area, $A_{\eta t}$, obtained by multiplying both sides of Eq. (6.52) by n_η, becomes

$$A_{\eta t} = \frac{4\ n_\eta\ V_\eta}{\eta} \qquad (6.53)$$

where $n_\eta\ V_\eta$ is the total fractional volume occupied by these vortex tubes. This is given by Tennekes as Eq.(6.49). Equations (6.15), (6.49) and (6.53) lead to

$$A_{\eta t} \propto \frac{1}{L}\ R_L^{0.25} \qquad (6.54)$$

The same form is obtained from Saffman for a sheet structure, whereas Corrsin and Saffman, for a tubular structure, give

$$A_{\eta t} \propto \frac{1}{L} \qquad (6.55)$$

,with no R_L dependency.

Thus for a given volume of reactants, Eq.(6.54) shows that the total surface area of the dissipative eddies increases with R_L. If burning is associated simply with the surface area of dissipative eddies, then the increased rate of burning due to increased turbulence might be explained by this equation.

6.9 BURNING WITH CHEMICAL LIFETIME = $c\ \delta_\ell/u_\ell$ IN SMALL EDDIES

In a theory of turbulent burning it is more satisfactory to invoke a theoretical expression for the fractional volume occupied by small eddies than to derive this volume from experimental measurements. If the fractional volume given by Tennekes, Eq.(6.49), is substituted into Eq.(6.17) in place of the intermittency factor, γ_η, Eq.(6.25) becomes

$$B_\eta = 0.031 \quad R_L^{-0.75} \left[1-\exp(-0.771\, k\, R_L^{-0.25}\ u'/u_\ell)\right]$$

$$(1-r)\ u_\ell/k\, u' \qquad (6.56)$$

Values of u_t/u_ℓ were obtained along similar lines to those of Section 6.3 but now with the aid of Eq.(6.56). Values of k were taken to be equal to 0.5 and 1.0, $n_L V_L$ to be unity and r_f to be 0.95. Values of u_t/u_ℓ were calculated for two values of R_L for a range of u_ℓ/u' values and these are given in Table 6.2.

These results show u_t/u_ℓ to increase with a decrease in both u_ℓ/u' and R_L. The former dependence, unlike the latter, is in agreement with experimental observations. Table 6.2 also shows theoretical values of u_t/u_ℓ to be smaller than those of experiment.

Examination of the theoretical expressions reveals the main source of the inverse R_L dependence to lie in the use of η in the expression for the chemical lifetime of small eddies, $k\eta/u_\ell$, (see Eq.(6.15)). This leads to a consideration of other alternatives. Instead of a lifetime based upon laminar flame propagation across a vortex tube, one based upon the molecular processes of the laminar flame might be employed . In such a flame, the chemical lifetime might be expressed by $c\ \delta_\ell/u_\ell$, where c is of order unity. If the time through the reaction zone is considered, and not that through the preheat zone, the value of c might be assigned a value in the region of 0.25. The dimensionless chemical lifetime, $\tau_{c\eta}$, becomes

$$\tau_{cn} = c \frac{\delta_\ell}{u_\ell} \frac{u'^2}{\nu} \qquad (6.57)$$

Substitution of Eq.(5.10) into Eq. (6.57) leads to

$$\tau_{cn} = \frac{c}{Pr} \left(\frac{u'}{u_\ell}\right)^2 \qquad (6.58)$$

where Pr is the Prandtl number. Equations (6.13), (6.14), (6.17), (6.23), (6.49) and (6.58) yield a value for the dimensionless volumetric rate of burning, B_η, given by

$$B_\eta = 0.040\ Pr\ R_L^{-0.5} \left[1-\exp\left(-\frac{0.595}{Pr}\ c\ R_L^{-0.5}\ (u'/u_\ell)^2\right)\right]$$

$$\frac{(1-r)}{c}\ (u_\ell/u')^2 \qquad (6.59)$$

Values of u_t/u_ℓ were obtained again by adopting similar procedures to those of Section 6.3 but now with the aid of Eq.(6.59). Values of c were taken to be equal to 0.25 and 1.0, $n_L V_L$ to be unity, Pr to be 0.7 and r_f to be 0.95. Values of u_t/u_ℓ were calculated for two values of R_L for a range of u_ℓ/u' values and these are given in Table 6.3.

These results again agree with the observed experimental dependence of u_t/u_ℓ upon u_ℓ/u'. However, the theoretical dependence on R_L appears to be still slightly opposite to that observed experimentally, but it is improved over that given in the previous approach (Eq.(6.56) and Table 6.2). Table 6.3 also shows theoretical values of u_t/u_ℓ which are smaller than those of experiment.

A search for other sources which might yield the experimentally observed dependence of u_t/u_ℓ upon R_L, led to a reconsideration of the relationship between ϵ_y/ν and R_{Ly}, discussed in Chapter 2 and given by Eq.(2.20). Very recently, Smith (23) has suggested that at very high turbulent Reynolds numbers, such as occur in atmospheric turbulence, the relationship is

$$\frac{\epsilon_y}{\nu} = 0.438\ R_{Ly} \tag{6.60}$$

A possible interpretation of Fig.2.4 is that L_y/d is independent of Re (24) for $R_L > 280$ and

$$\frac{L_y}{d} = 0.08 \tag{6.61}$$

Equations (2.4), (2.9) and (6.61) lead to

$$\frac{\epsilon_y}{\nu} = 0.75\ R_{Ly}^{0.95} \tag{6.62}$$

for $R_{Ly} > 280$. This equation is similar to Eq.(6.60) and probably should replace Eq.(2.20) at high R_L values.

Equation (6.62) might be rewritten in the form

$$\frac{\epsilon}{\nu} = a\ R_L^{0.95} \tag{6.63}$$

and the fractional volume occupied by the small eddies in the form

$$= b\ R_L^{-0.5} \tag{6.64}$$

Using Eq.(6.64) for γ_η, the expression for B_η becomes

$$B_\eta = b\ Pr\ R_L^{-0.5}\ \left[1-\exp\left(-\frac{0.595}{Pr}\ c\ R_L^{-0.5}\ (u'/u_\ell)^2\right)\right]$$

$$\frac{(1-r)}{c}\ (u_\ell/u')^2 \qquad (6.65)$$

Neglecting B_L in comparison to B_η in Eqs.(6.28) to (6.30) and applying Eqs. (6.63) and (6.65), Eq.(6.33) becomes

$$\frac{u_t}{u_\ell} = \frac{\left(\frac{Pr}{c}\ .\ ab\right)^{0.5}}{\ell n\ \left(\frac{1}{1-r_f}\right)}\ R_L^{0.225}\ \left[1-\exp\left(-\frac{0.595}{Pr}\ c\ R_L^{-0.5}\ (u'/u_\ell)^2\right)\right]^{0.5}\ (u_\ell/u') \qquad (6.66)$$

With Pr assumed to be 0.7, r_f to be equal to 0.95 and c to be equal to 0.25, a value of a b equal to 33 in Eq. (6.66) was found to give values of u_t/u_ℓ in good agreement with experiment. The results are plotted in Figs. 6.18 to 6.21, for values of turbulent Reynolds number of 8750, 2500, 1750 and 425 respectively. For comparison are shown experimental values of u_t/u_ℓ. Figure 6.22 shows theoretical and experimental values of u_t/u_ℓ over a wide range of R_L, for values of u_ℓ/u' equal to 0.1 and 0.2.

The theoretical predictions are in satisfactory agreement with experimental values. Figure 6.22 shows the experimental measurements of u_t/u_ℓ to show no dependence on R_L for values of $R_L > 4000$, for both values of u_ℓ/u'. When u_ℓ/u' is equal to 0.2 there is little theoretical dependence of u_t/u_ℓ upon R_L throughout the full range of

values of R_L . It would appear that accurate measurements of u_t, u' and L are needed at $R_L > 4000$ in order to check these findings.

For an optimised value of 33 for the product 'ab' in Eq.(6.66), if 'a' is assigned the value of 0.75 in accordance with Eq. (6.62), then the constant 'b' of Eq. (6.64) must take the value of 44. Table 6.1 shows that it is Eq.(6.48) that yields the highest fractional volume of small dissipative eddies and the value of 44 might be compared with that of 1.297 in this equation. Thus the optimisation suggests a fractional volume 34 times that given by Eq.(6.48).

Values of B_η/B_L were found from Eqs. (6.12) and (6.65), with Pr equal to 0.7, c equal to 0.25, r_f equal to 0.95, $n_L V_L$ equal to unity and b equal to 44. The results are plotted in Figs. 6.18 to 6.21, for different values of R_L. Values of δ_t/L given by Eq. (6.34), are also presented in these figures.

In order to obtain a theoretical form for the number density of the dissipative eddies, Eq. (6.64) should be introduced into Eq.(6.42) to replace the experimentally determined intermittency ratio, γ_η/γ_L . This, with Eqs. (6.13) and (6.58), leads to

$$y \alpha \frac{b\ c}{1.681\ Pr} \left(\frac{u'}{u_\ell}\right)^2 R_L^{-1} \qquad (6.67)$$

Again, the value of the right hand side of this equation for a particular condition was divided by that associated

with the experimental condition of 5000 r.p.m. fan speed in the present experimental work and a value of u_ℓ/u' equal to 0.12. Theoretical values normalised in this way for two values of R_L are shown by the two curves in Fig.6.23, whilst experimental points are shown for four ranges of R_L, as in Fig.6.17.

The theoretical values of Y, at a given u_ℓ/u', decrease with increase in R_L. Some experimental support for this trend can be observed. It is contrary to that indicated by the broken curves in Fig.6.17, which are based upon the approach of Section 6.7.

6.10 CONCLUSIONS

Two theoretical analyses have been employed to obtain the ratio u_t/u_ℓ. In the first approach, laminar flame propagation across a vortex tube was envisaged, whilst in the second the concept of a reaction time in the vortex tube was used. The former would appear to be more valid in the régime where $\eta >> \delta_\ell$, to the right of the dotted curve in Fig.6.12, whilst the latter probably is more valid where the laminar flame thickness and Kolmogorov microscale become comparable, or when the former is greater than the latter.

With regard to the experimental observations on flammability limits, there are two relevant theoretical aspects. First, a decrease in the probable fraction of a small eddy which reacts before the eddy is dissipated is

represented by a leftwards shift in the combustion régime towards a régime to the left of the dotted curve of $\tau_{c\eta} = k\tau_{d\eta}$ (which is the same as $\tau_{c\eta} = c\ \tau_{d\eta}$) in Fig.6.12. This is illustrated by the dashed curve on the figure representing the flammability limit for run 5. . Ignition becomes more difficult as the ratio $\tau_{c\eta}/\tau_{d\eta}$ increases. At the highest value of R_L for the dashed flammability limit curve, Eq.(6.26) yields a value of $\tau_{c\eta}/\tau_{d\eta}$ of 1.663k , in terms of the first approach, whilst in terms of the second approach, Eqs. (6.13) and (6.58) give

$$\frac{\tau_{c\eta}}{\tau_{d\eta}} = \frac{c}{1.681\ Pr}\left(\frac{u'}{u_\ell}\right)^2 R_L^{-0.5} \qquad (6.68)$$

and at the same flammability limit this yields a value of $\tau_{c\eta}/\tau_{d\eta}$ equal to 3.949c. Thus, both approaches, with the optimised values for "k" and "c" of 0.5 and 0.25, respectively, suggest that the limit occurs at $\tau_{c\eta} \sim \tau_{d\eta}$.

The experimental results of Chapter 4 show that the tendency of a spark kernel to be quenched with increase in turbulence can be countered by an appreciable increase in spark energy. This effectively creates an electrically augmented chemical plasma with a smaller value of $\tau_{c\eta}/\tau_{d\eta}$, consequent upon a decrease in the numerator. Another counter which is suggested by the results is to shield the spark kernel from the full turbulence. This increases the value of $\tau_{d\eta}$ and allows the flame to become established before emergence into the fully turbulent region.

The second, yet related, theoretical aspect is that before a flame can be capable of self-sustaining propagation,

it must attain a certain critical diameter, which is related to the flame thickness. The theoretical values of δ_t/L in Figs. 6.2 to 6.11, 6.14 to 6.16 and 6.18 to 6.21 show the ratio to increase with decrease of u_ℓ/u'. A limited number of measurements of limit flame kernel sizes, when the flame just quenched on emergence from the shielded region, were made. The associated theoretical values of δ_t/L were calculated and both approaches suggest that quenching occurs in highly turbulent flames when the diameter of the kernel is less than approximately four times the flame thickness. Clearly, an increase in δ_t/L creates greater difficulties for the establishment of a propagating flame.

Returning now to the theoretical derivation of u_t/u_ℓ, theoretical support has been obtained for the use of the three dimensionless parameters employed in Chapter 5 to correlate experimental values of turbulent burning velocity. The increasing importance of small eddy burning, as R_L is increased and as u_ℓ/u' is decreased, becomes clear. Considering the assumptions that, of necessity, have had to be made to obtain numerical solutions, the correspondence between theoretical and experimental values of u_t/u_ℓ is satisfactory. The experimental values are of limited accuracy, particularly those close to flammability limits, and the theoretical values are capable of further refinement. Associated refinements to the theory might include the generation of pdfs, as a function of mean reactedness, for chemical lifetimes and allowance for the changing turbulence through the reaction zone.

Nevertheless, although the theoretical curves of the first approach (Figs.6.2 to 6.11) follow the same trends as the experimental ones, the values of u_t/u_ℓ of the former are consistently low. These were obtained on the bases of experimentally determined values of γ_L and γ_η and assumed values of chemical lifetimes in dissipative eddies. The last parameter is a particularly challenging one, for which no data are available, whilst values of u_t/u_ℓ are particularly sensitive to the value of intermittency factor of the small eddies and less so to the factor for large eddies. Inevitably, the signals which give rise to the values of these factors can be interpreted differently depending on the amplitude threshold.

It might be anticipated that values of γ_L asymptotically approach unity with increase of R_L and the question arises whether there exists a similar asymptotic value of γ_η. Values of γ_η were selected which made the theoretical value of u_t/u_ℓ coincide with the experimental one at three different values of R_L and for u_ℓ/u' equal to 0.1. A value of 0.5 was also selected for k as this seemed to give a closer parallel with the experimental values of u_t/u_ℓ. These values are shown in Table 6.4. Although the values are higher than the original measured values, they are not unreasonably different. The values to be assigned to such intermittency factors and chemical lifetimes in dissipative eddies seems a challenging area for future research.

However, the use of measured values of intermittencies is not satisfactory in a theoretical analysis and in this regard the second approach is preferable. Our limited understanding of the physical nature of turbulence creates problems in assigning an accurate value for the volume fraction occupied by the dissipative eddies. Some adjustment of theoretical values for this was necessary to obtain harmony of theory and experiment. This approach seems to hold more promise than the first one but the theory is capable of further improvement and more experimental studies are required.

TABLE 6.1 Fractional Volume Occupied by Small Dissipative Eddies

Author	Ref.	Eq.No.	Fractional Volume Occupied by Small Eddies	
			$R_L = 875$	$R_L = 2500$
Corrsin Saffman (tubes)	21 22	(6.45)	8.062×10^{-3}	3.668×10^{-3}
Saffman (sheets)	22	(6.48)	43.847×10^{-3}	25.940×10^{-3}
Tennekes	10	(6.49)	1.339×10^{-3}	0.792×10^{-3}

TABLE 6.2 Values of u_t/u_ℓ Calculated on the Basis of Eq. (6.56)

u_ℓ/u'	k = 1.0		k = 0.5	
	R_L = 875	R_L = 2500	R_L = 875	R_L = 2500
.025	2.961	2.398	3.143	2.561
.05	2.086	1.681	2.170	1.746
.10	1.455	1.164	1.483	1.183
.20	1.007	0.801	1.014	0.806
.30	0.802	0.638	0.805	0.640
.40	0.674	0.536	0.676	0.537
.50	0.584	0.464	0.585	0.464
.60	0.515	0.409	0.516	0.409

TABLE 6.3 Values of u_t/u_ℓ Calculated on the Basis of Eq.(6.59)

u_ℓ/u'	c = 1.0		c = 0.25	
	R_L = 875	R_L = 2500	R_L = 875	R_L = 2500
.025	2.771	2.215	2.853	2.323
.05	1.979	1.592	2.084	1.705
.10	1.423	1.149	1.482	1.189
.20	1.007	0.803	1.018	0.809
.30	0.804	0.640	0.807	0.641
.40	0.676	0.537	0.677	0.538
.50	0.585	0.464	0.585	0.465
.60	0.516	0.410	0.516	0.410

TABLE 6.4 Values of γ_η for Agreement with Experiment at $u_\ell/u' = 0.1$ and $k = 0.5$ for Typically Three Values of R_L

R_L	γ_η measured	γ_η for agreement
425	0.095	0.72
875	0.190	0.73
1750	0.435	1.15

6.11 NOMENCLATURE

a	constant, Eq.(6.63)
b	constant, Eq.(6.64)
B	dimensionless volumetric rate of burning
c	constant of proportionality for chemical lifetime in small eddy, Eq.(6.57)
d	pipe diameter
k	constant of proportionality for chemical lifetime in small eddy, Eq.(6.16)
L	integral scale of turbulence
n	eddy number density
p	probable fraction of an eddy which burns during the eddy lifetime
Pr	Prandtl number
R_L	$u'L/\nu$
R_λ	$u'\lambda/\nu$
r	mean reactedness
r_f	final reactedness
t	time
t_f	time to attain r_f
t_η	Kolmogorov time scale
u'	r.m.s. turbulent velocity
u_ℓ	laminar burning velocity
u_t	turbulent burning velocity
V	volume of an eddy
y	number of small eddies photographed, Eq. (6.42)

Y	normalised number density of small eddies
γ	intermittency factor
η	Kolmogorov microscale
ε	turbulent diffusivity
δ	characteristic length scale, Eq.(6.46)
δ_ℓ	laminar flame thickness
δ_t	turbulent flame thickness
κ	eddy decay constant
λ	Taylor microscale of turbulence
ν	kinematic viscosity
τ	dimensionless time ($u'^2 t/\nu$)
τ_c	dimensionless chemical lifetime
τ_d	dimensionless eddy lifetime
τ_f	dimensionless time to attain r_f

Subscripts

L	large eddy
t	total
y	radial direction
η	small eddy

6.12 REFERENCES

1. G.E.ANDREWS, D. BRADLEY and S.B.LWAKABAMBA, Turbulence and turbulent flame propagation – a critical appraisal, Combustion and Flame 24, 285 (1975).

2. A.H.LEFEBVRE and R.REID, The influence of turbulence on the structure and propagation of enclosed flames, Combustion and Flame 10, 355 (1966).

3. J.CHOMIAK, A possible propagation mechanism of turbulent flames at high Reynolds number, Combustion and Flame 15, 319 (1970).

4. B.F.MAGNUSSEN, An investigation into the behavior of soot in a turbulent free jet C_2H_2-flame, Fifteenth Symposium (International) on Combustion, p.1415, The Combustion Institute: Pittsburgh (1975).

5. J.CHOMIAK, On a hypothesis concerning the structure of a turbulent flame front at high Reynolds numbers, Fluid Dynamics Transactions 5, 47 (1971).

6. J.CHOMIAK, Application of chemiluminescence measurement to the study of turbulent flame structure, Combustion and Flame 18, 429 (1972).

7. G.E.ANDREWS, Laminar and turbulent flame propagation, Ph.D. thesis, Dept. Mechanical Engineering, Univ. Leeds (1972).

8. S.B.LWAKABAMBA, Turbulent flame propagation in closed vessels, Ph.D. thesis, Dept.Mechanical Engineering, Univ.Leeds (1975).

9. F.C.LOCKWOOD and O.O.ODIDI, Measurements of mean and fluctuating temperature and of ion concentration in round free-jet turbulent diffusion and premixed flames, Fifteenth Symposium (International) on Combustion, p.561, The Combustion Institute: Pittsburgh (1975).

10. H. TENNEKES, Simple model for the small-scale structure of turbulence, The Physics of Fluids 11, 669 (1968).

11. A.Y-S. KUO and S.CORRSIN, Experiment on the geometry of the fine-structure regions in fully turbulent fluid, J.Fluid Mech. 56, 447 (1972).

12. J.CHOMIAK, Dissipation fluctuations and the structure and propagation of turbulent flames in premixed gases at high Reynolds numbers, Sixteenth Symposium (international) on Combustion, p.1665, The Combustion Institute: Pittsburgh (1977).

13. P.O.A.L. DAVIES and A.J.YULE, Coherent structures in turbulence, J. Fluid Mech. 69, 513 (1975).

14. A. ROSHKO, Structure of turbulent shear flows: a new look, AIAA J.14, 1349 (1976).

15. D.B.SPALDING, Mixing and chemical reaction in steady confined turbulent flames, Thirteenth Symposium (International) on Combustion, p.649, The Combustion Institute: Pittsburgh (1971).

16. B.F.MAGNUSSEN and B.H.HJERTAGER, On mathematical modelling of turbulent combustion with special emphasis on soot formation and combustion, Sixteenth Symposium (International) on Combustion, p.719, The Combustion Institute: Pitssburgh (1977)

17. S.CORRSIN and A.L.KISTLER, Free stream boundaries of turbulent flows, NACA Report 1244 (1955).

18. F.R.MOBBS, Spreading and contraction at the boundaries of free turbulent flows, J.Fluid Mech. 33, 227 (1968).

19. P.BRADSHAW, Conditions for the existence of an inertial subrange in turbulent flow, Aeronautical Research Council Reports and Memoranda, Her Majesty's Stationary Office, London, 1969.

20. A.A.TOWNSEND, On the fine-scale structure of turbulence, Proc. Roy. Soc. (London), Ser.A208, 534 (1951).

21. S.CORRSIN, Turbulent dissipation fluctuations, Physics of Fluids 5, 1301 (1962).

22. P.G.SAFFMAN, Lectures on homogeneous turbulence, Topics in Nonlinear Physics (Ed.N.J. Zabusky), Proceedings of the Physics Session International School of Nonlinear Mathematics and Physics, p.485, Springer-Verlag: Berlin (1968).

23. T.SMITH, private communication.

24. C.J.LAWN, discussion on paper by R.G.ABDEL-GAYED and D.BRADLEY, Derivation of turbulent transport coefficients from turbulent parameters in isotropic turbulence, Trans.Am.Soc.Mech.Engrs 100, 139 (1978). (Series I, Journal of Fluids Engineering.)

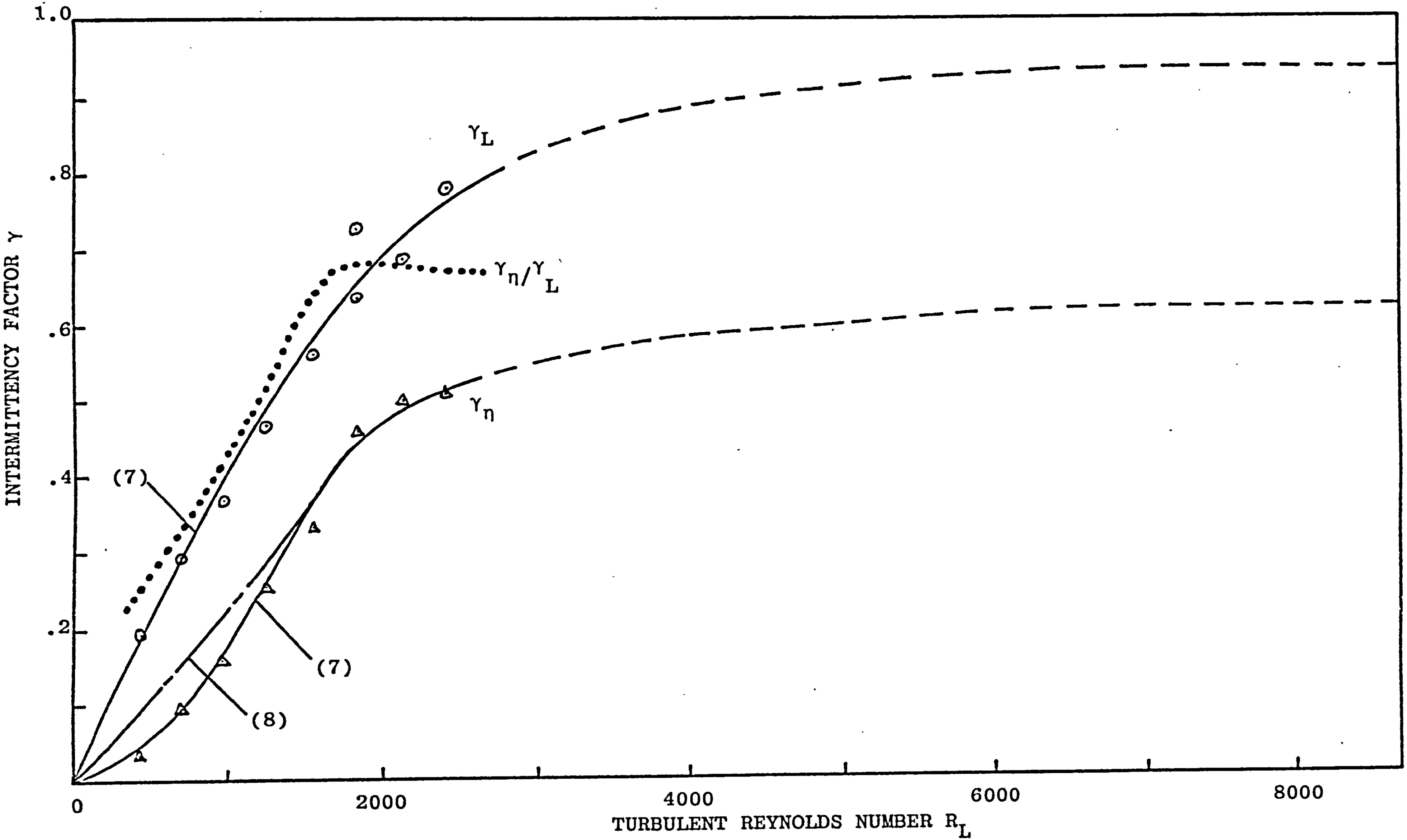

FIG.6.1 VARIATION OF γ_L, γ_η AND γ_η/γ_L WITH R_L

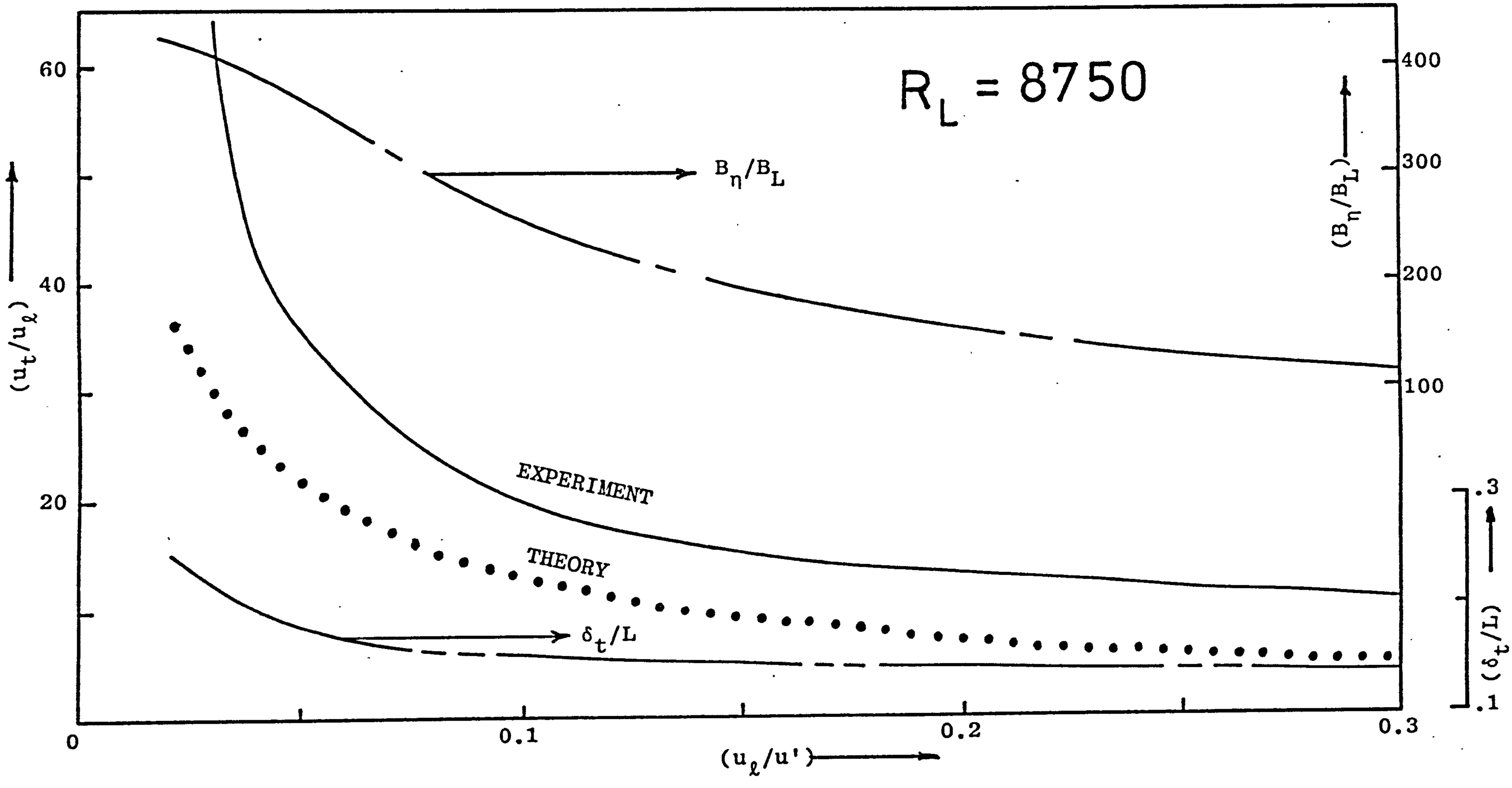

FIG.6.2 THEORETICAL AND EXPERIMENTAL TURBULENT FLAME DATA FOR R_L = 8750 (k = 1)

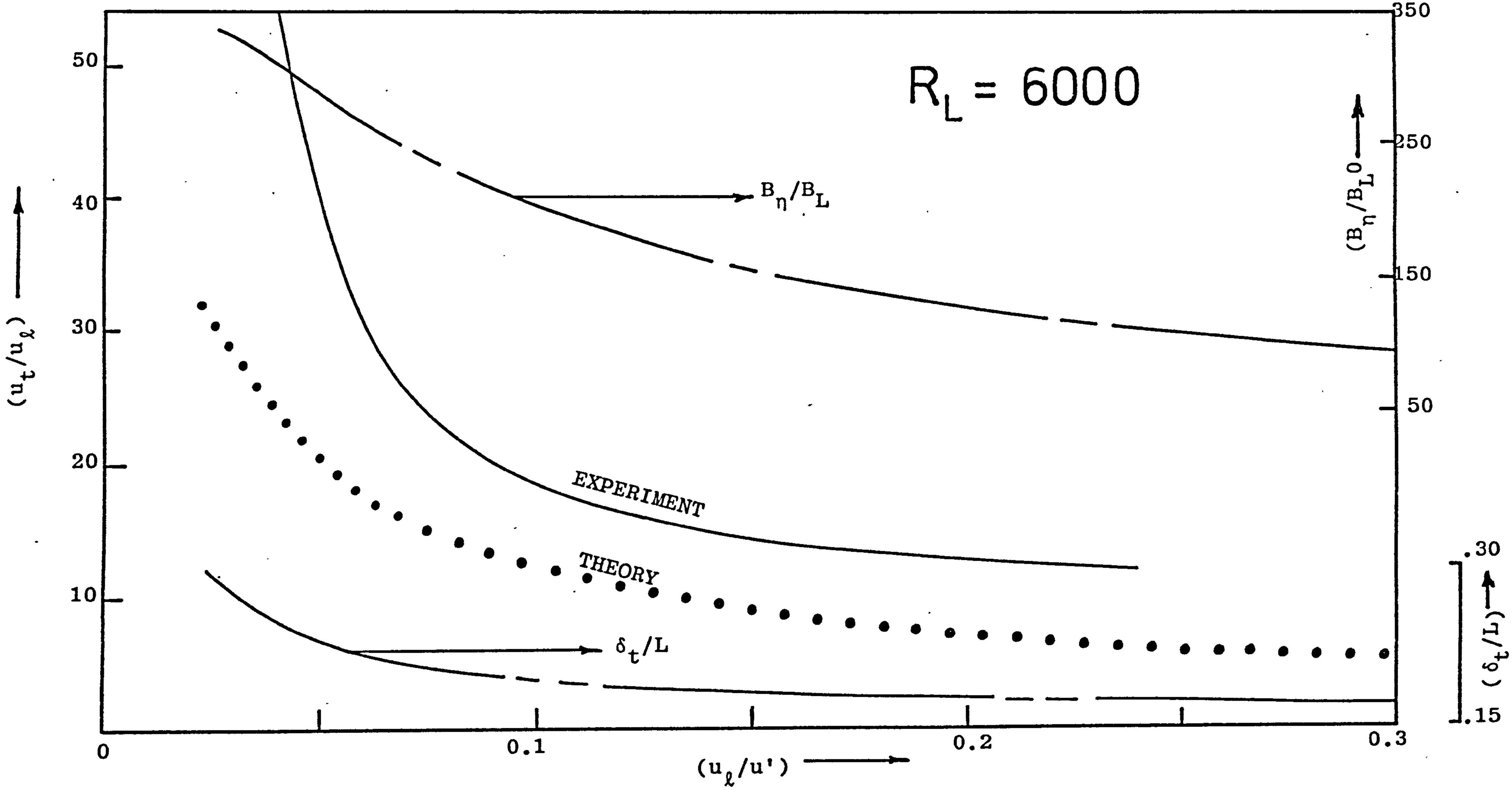

FIG.6.3 THEORETICAL AND EXPERIMENTAL TURBULENT FLAME DATA FOR R_L = 6000 (k = 1)

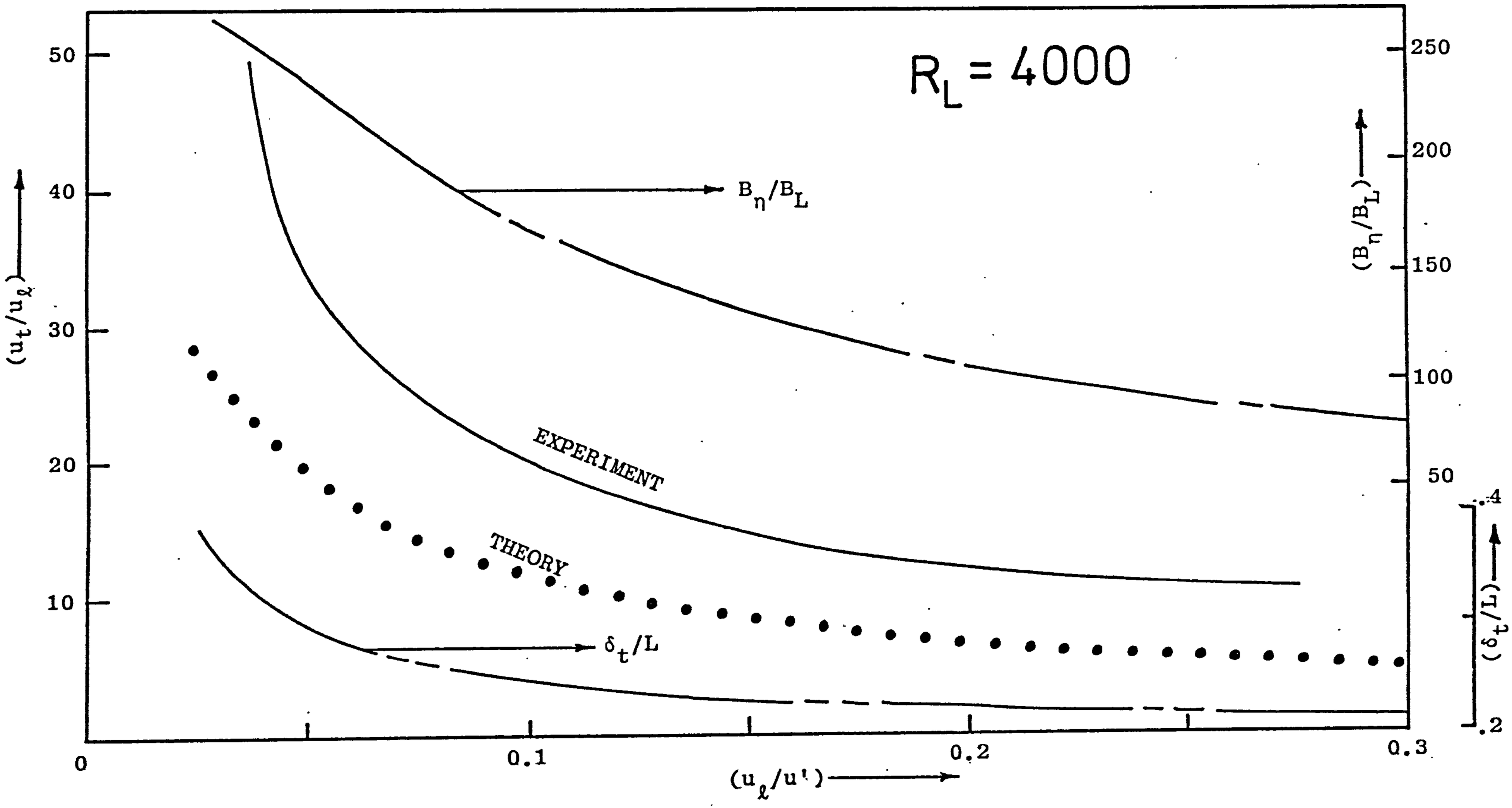

FIG.6.4 THEORETICAL AND EXPERIMENTAL TURBULENT FLAME DATA FOR R_L = 4000 (k = 1)

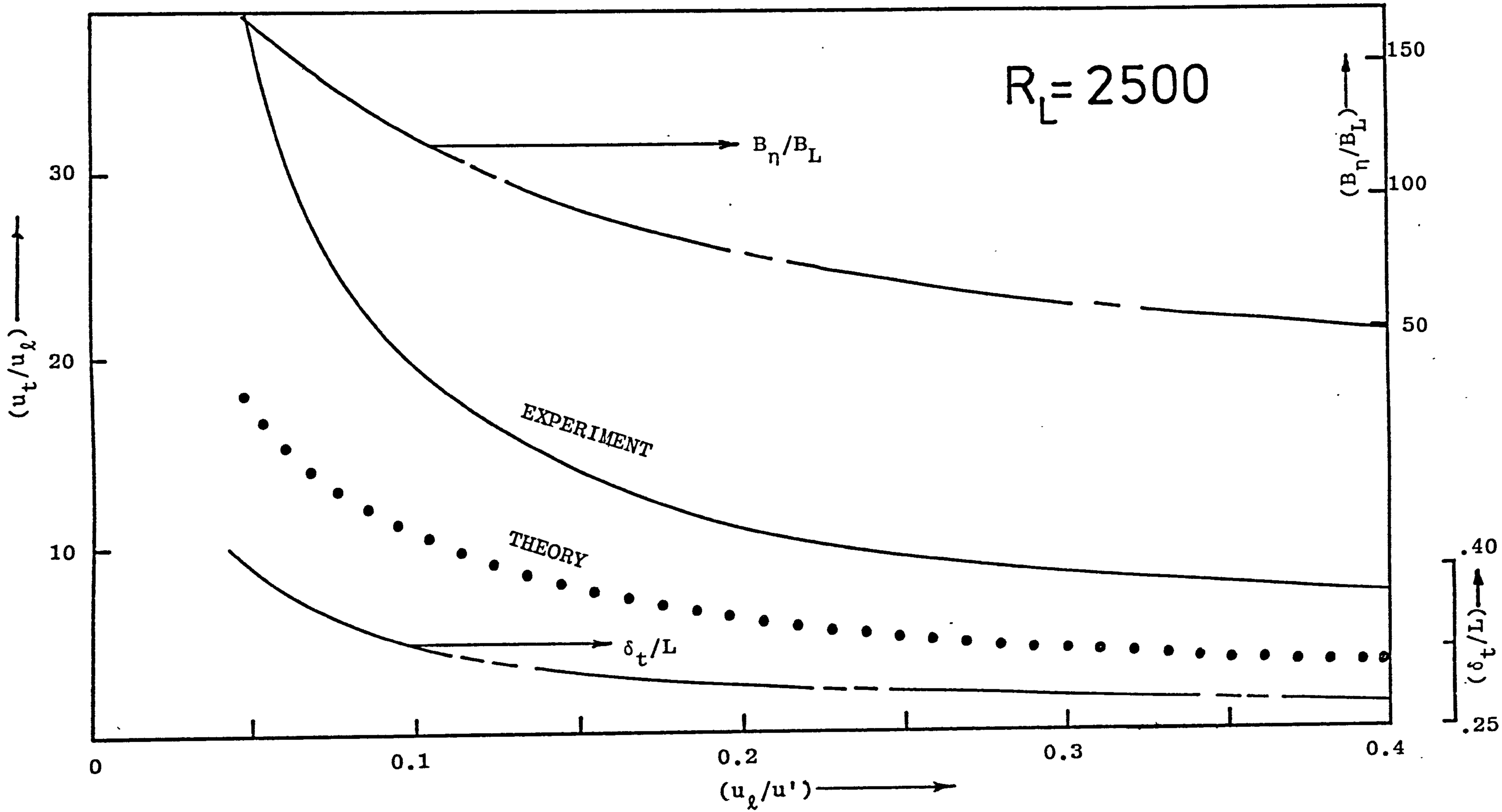

FIG.6.5 THEORETICAL AND EXPERIMENTAL TURBULENT FLAME DATA FOR R_L = 2500 (k = 1)

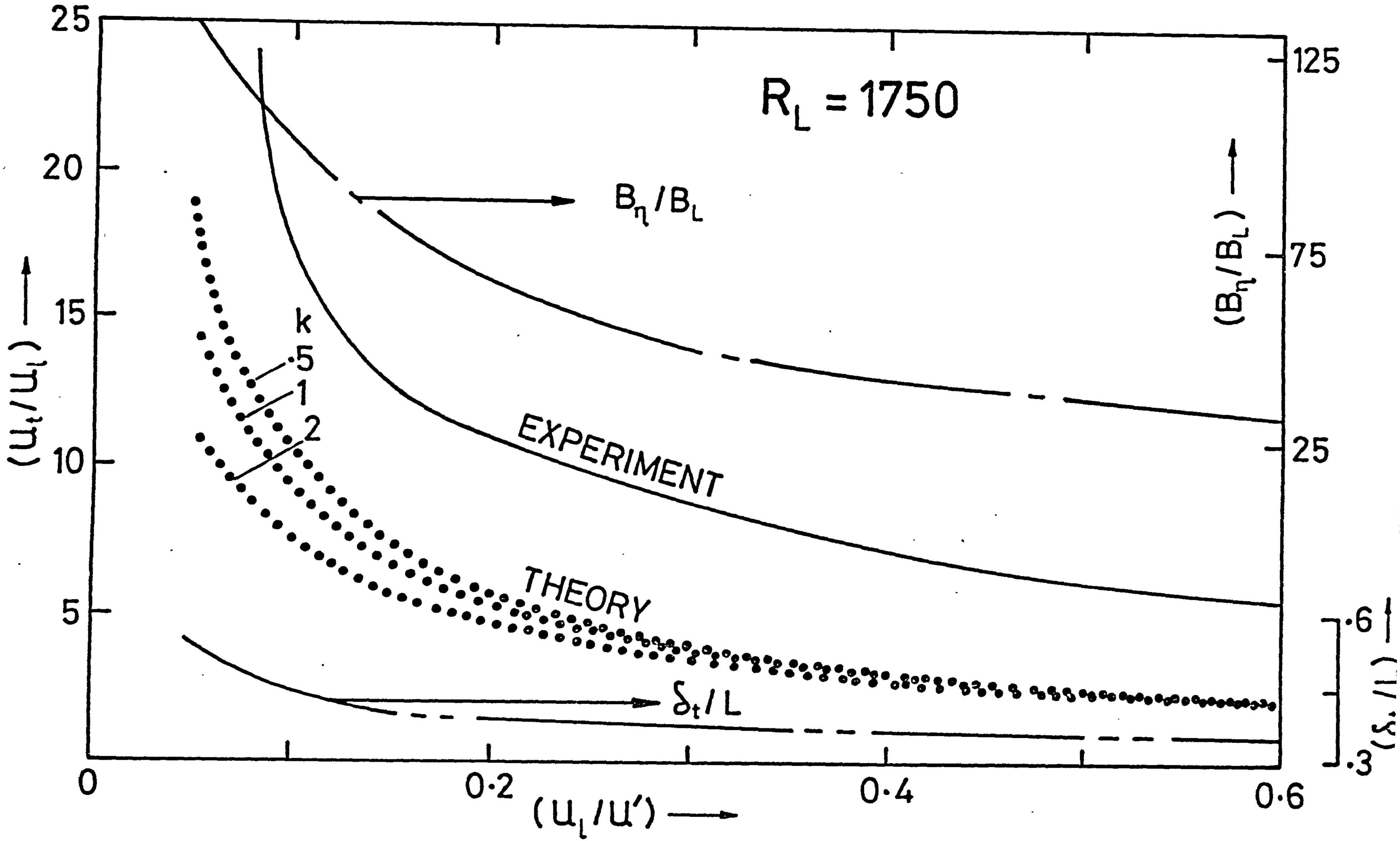

FIG.6.6 THEORETICAL AND EXPERIMENTAL TURBULENT FLAME DATA FOR R_L = 1750 (k = .5, 1 and 2)

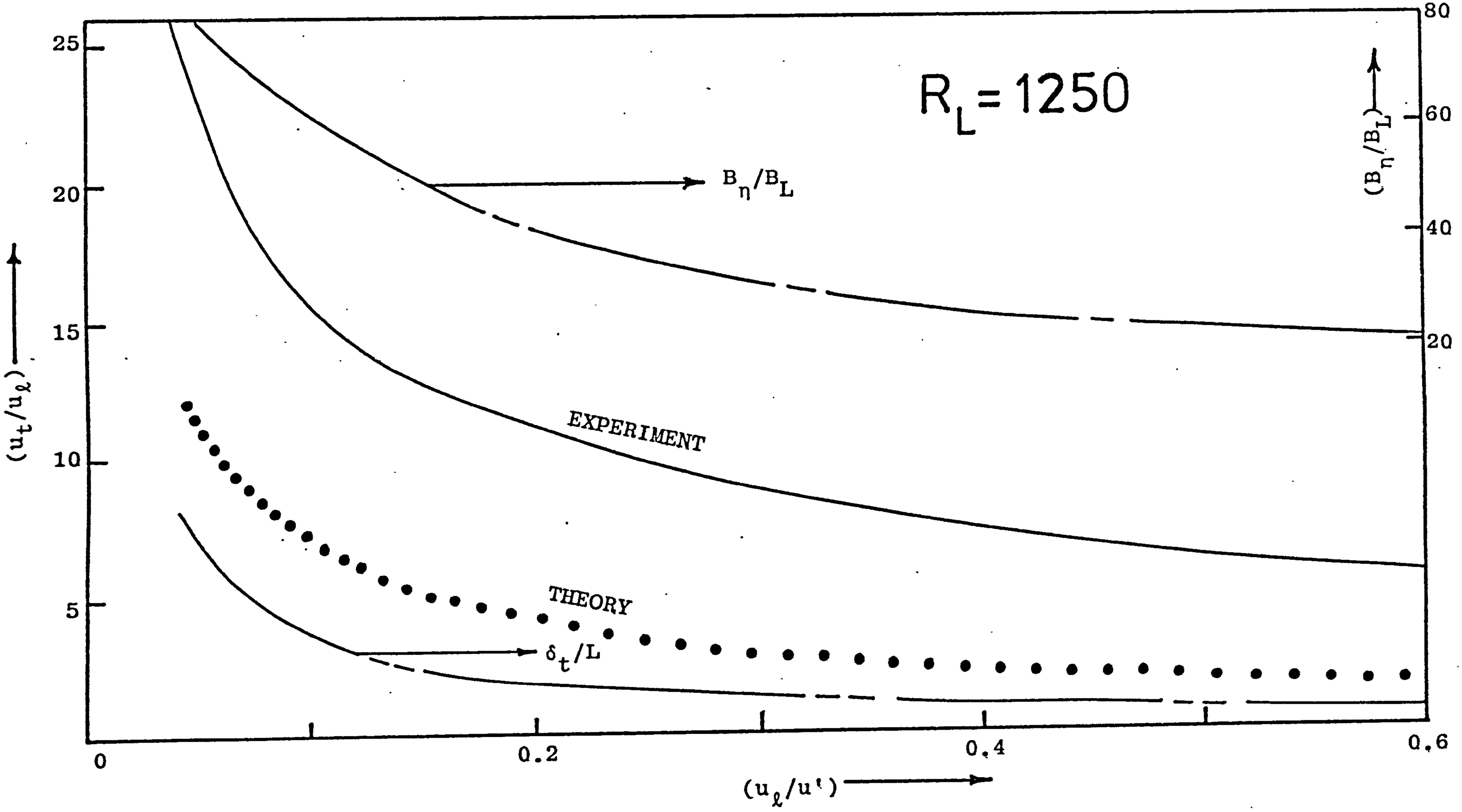

FIG.6.7 THEORETICAL AND EXPERIMENTAL TURBULENT FLAME DATA FOR $R_L = 1250$ (k = 1)

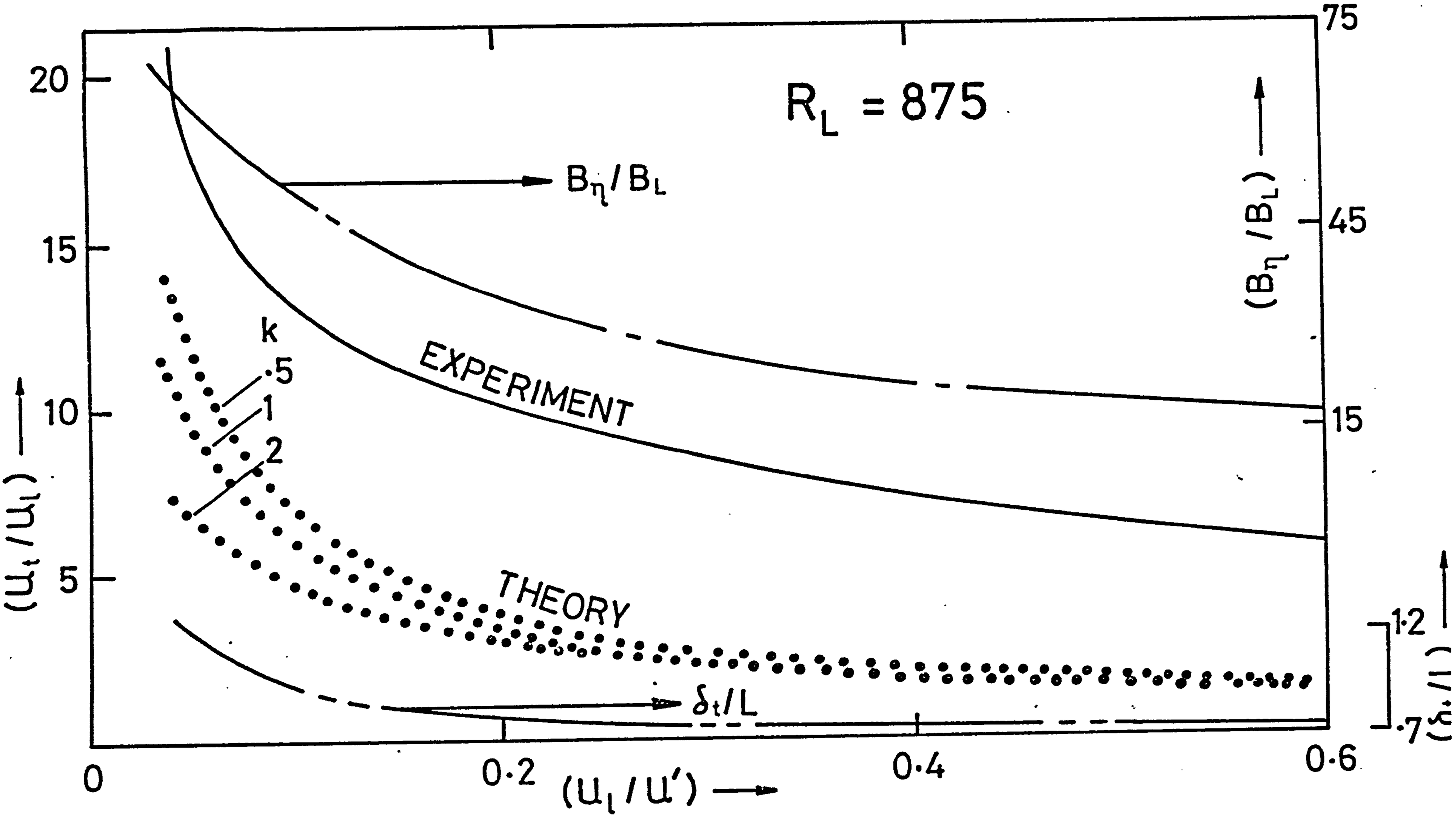

FIG.6.8 THEORETICAL AND EXPERIMENTAL TURBULENT FLAME DATA FOR R_L = 875 (k = .5, 1 and 2)

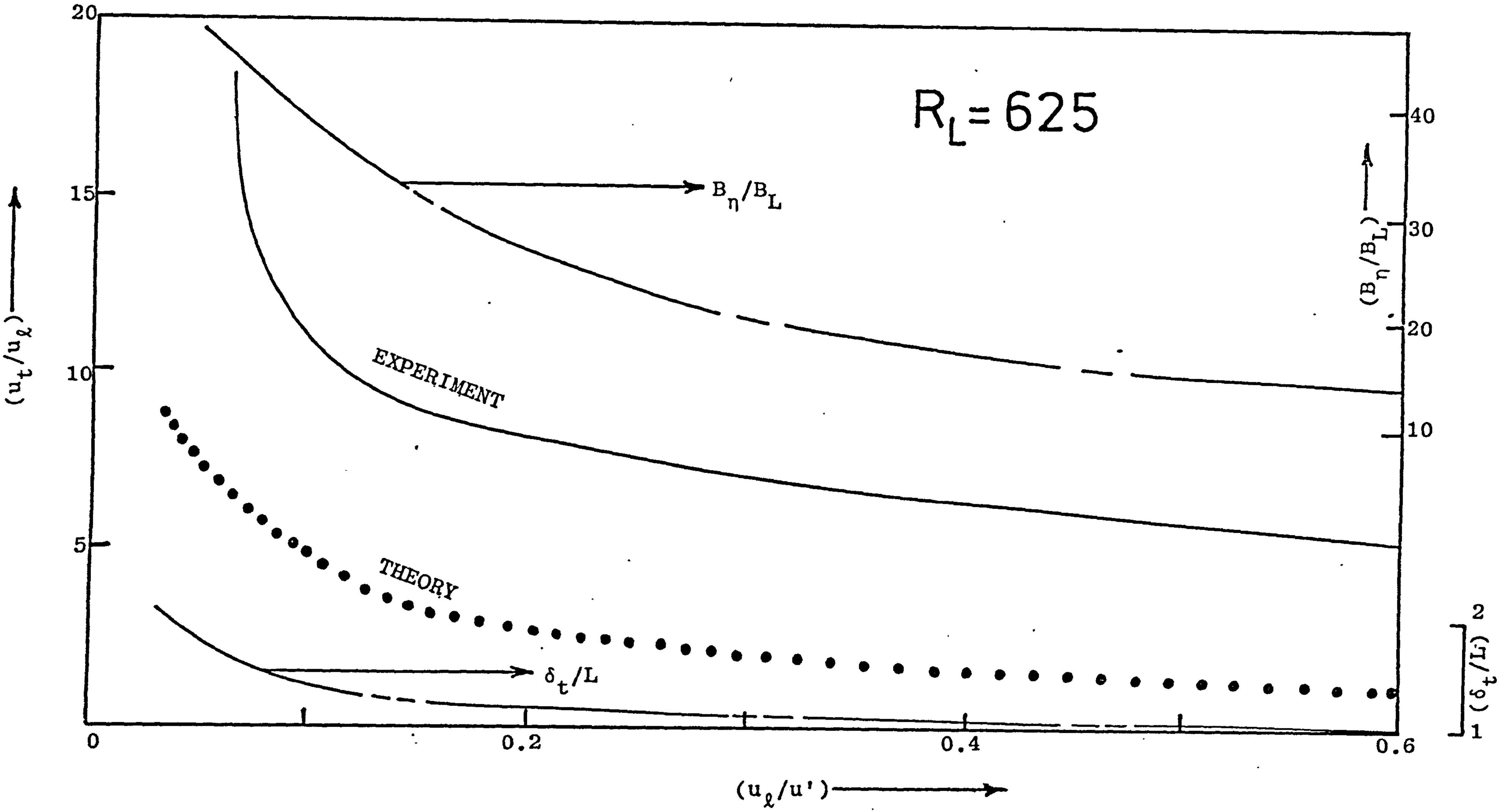

FIG.6.9 THEORETICAL AND EXPERIMENTAL TURBULENT FLAME DATA FOR $R_L = 625$ (k = 1)

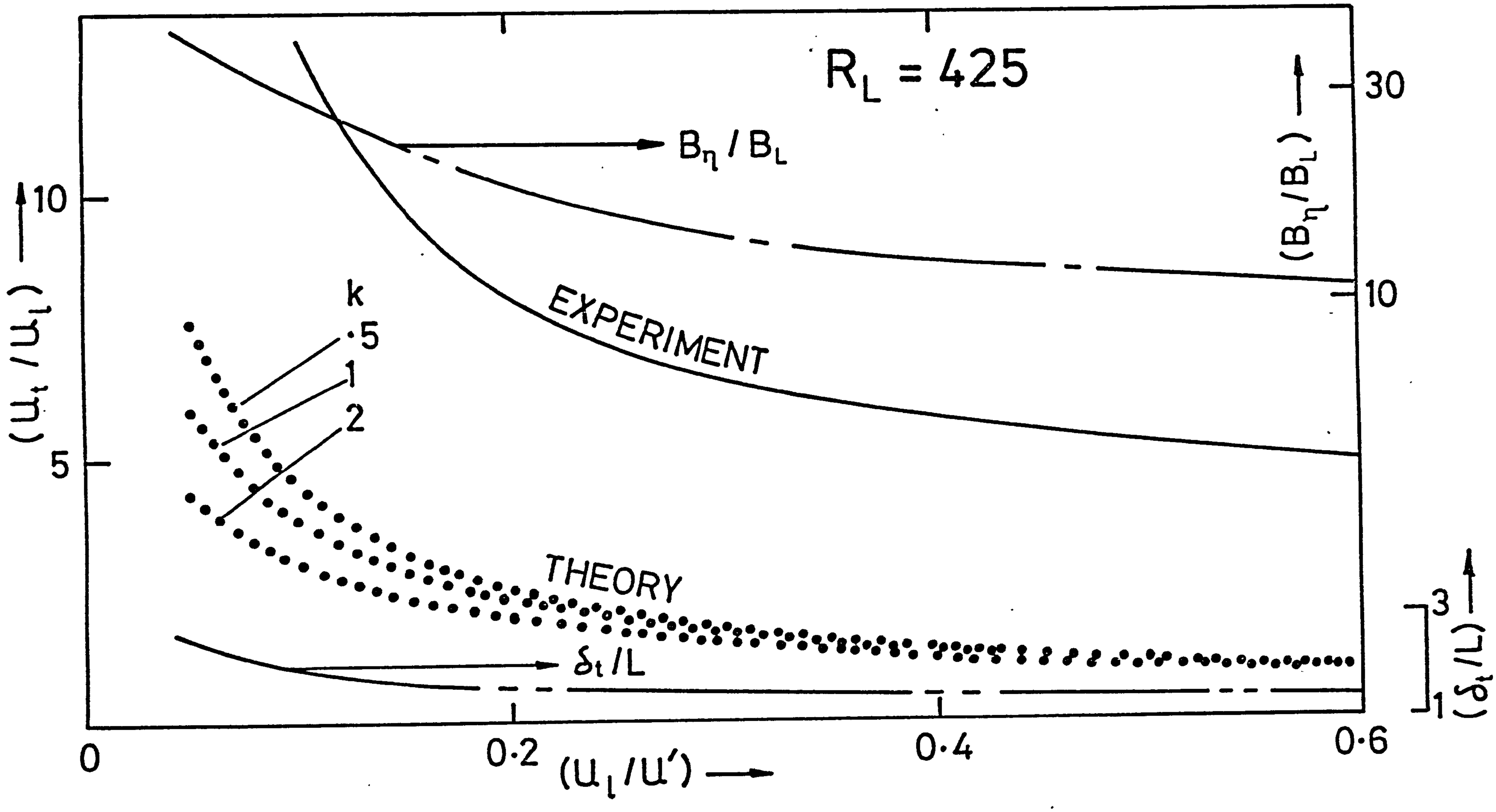

FIG.6.10 THEORETICAL AND EXPERIMENTAL TURBULENT FLAME DATA FOR R_L = 425 (k = .5,1 and 2)

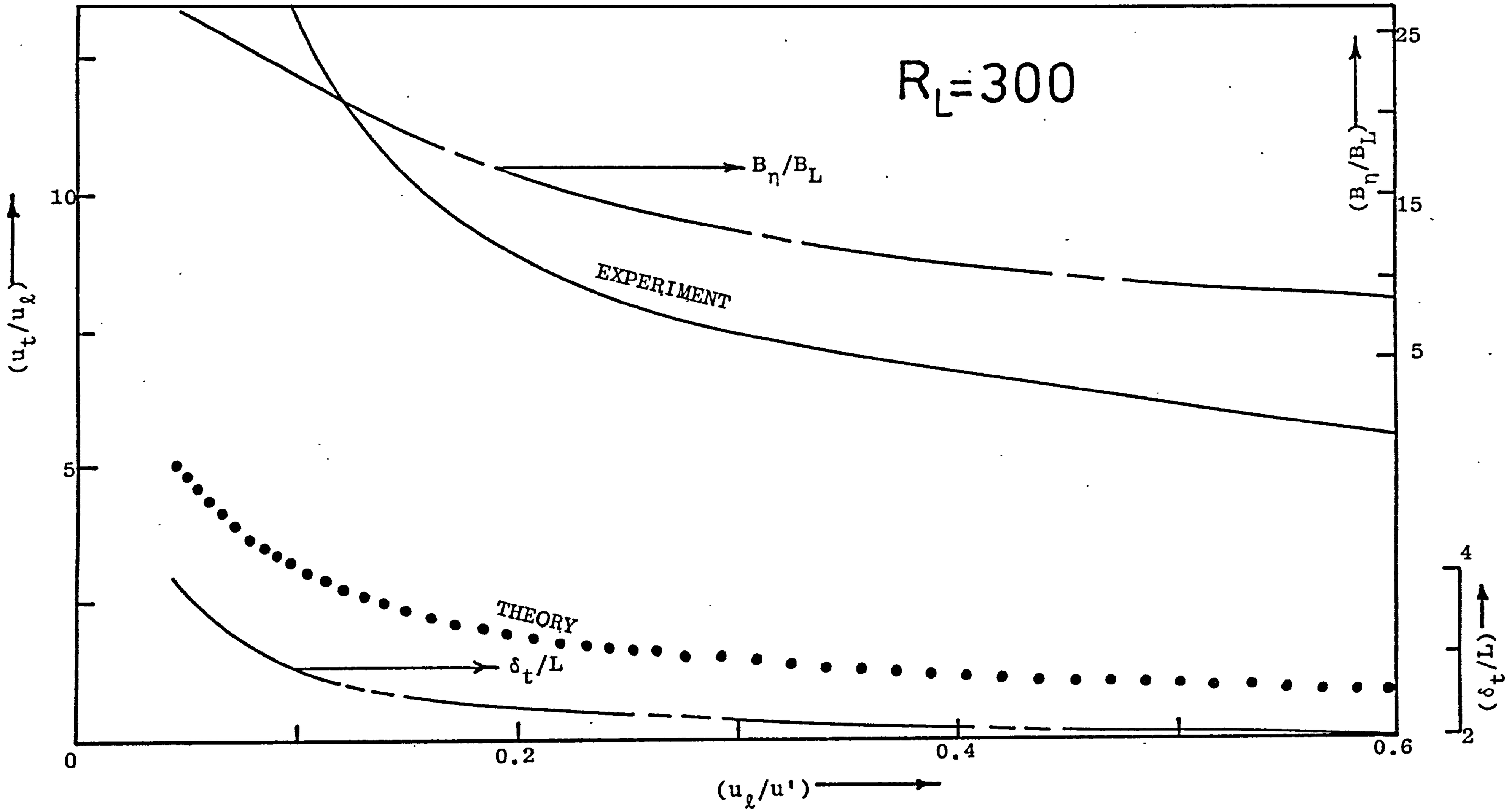

FIG.6.11 THEORETICAL AND EXPERIMENTAL TURBULENT FLAME DATA FOR R_L = 300 (k = 1)

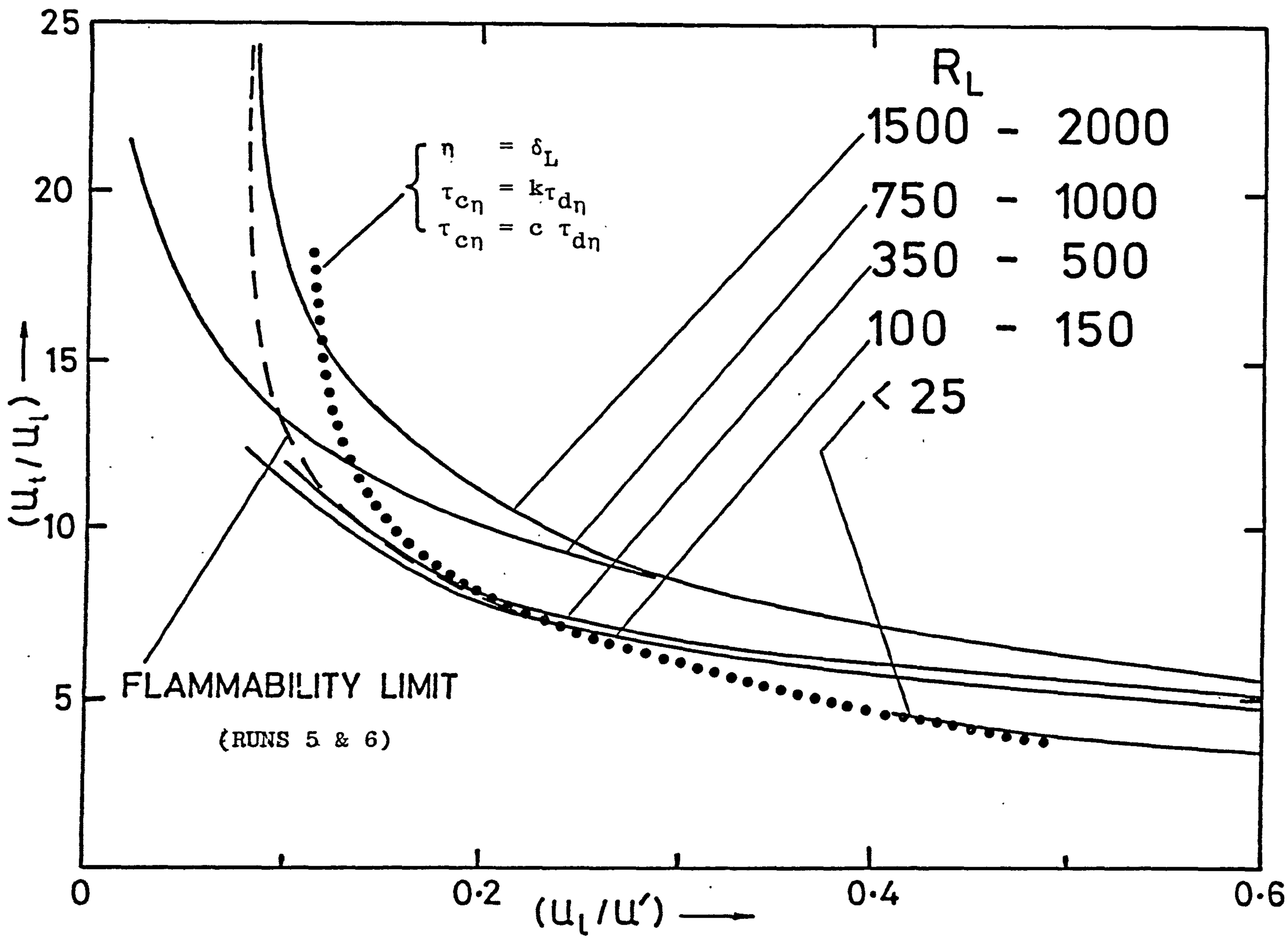

FIG.6.12 FLAMMABILITY LIMITS FOR RUNS 5 AND 6 (FIG.4.15) IN TERM OF BURNING VELOCITIES.

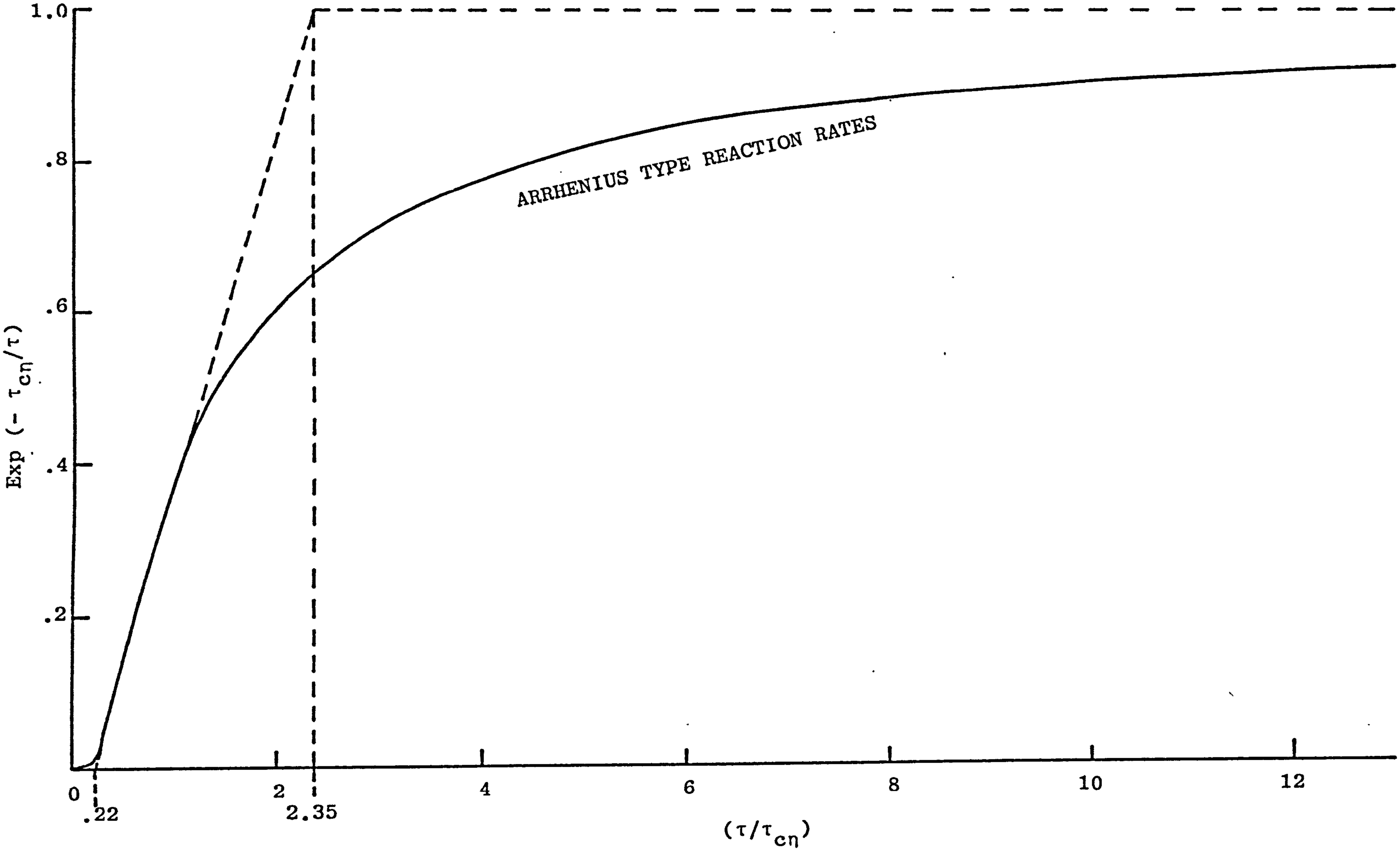

FIG.6.13 ARRHENIUS TYPE REACTION RATES WITHIN SMALL EDDIES

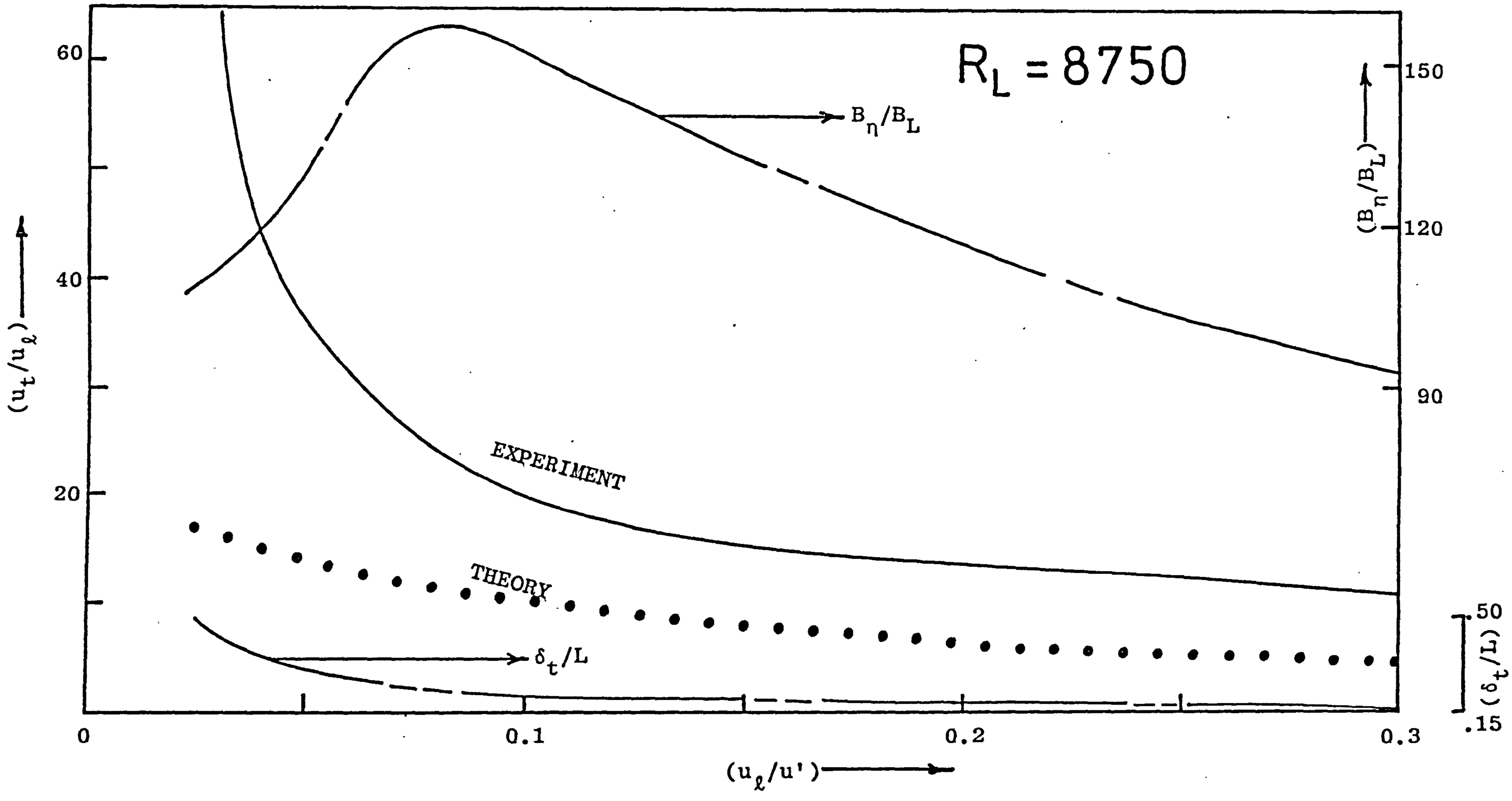

FIG.6.14 THEORETICAL AND EXPERIMENTAL TURBULENT FLAME DATA FOR R_L = 8750 (ARRHENIUS)

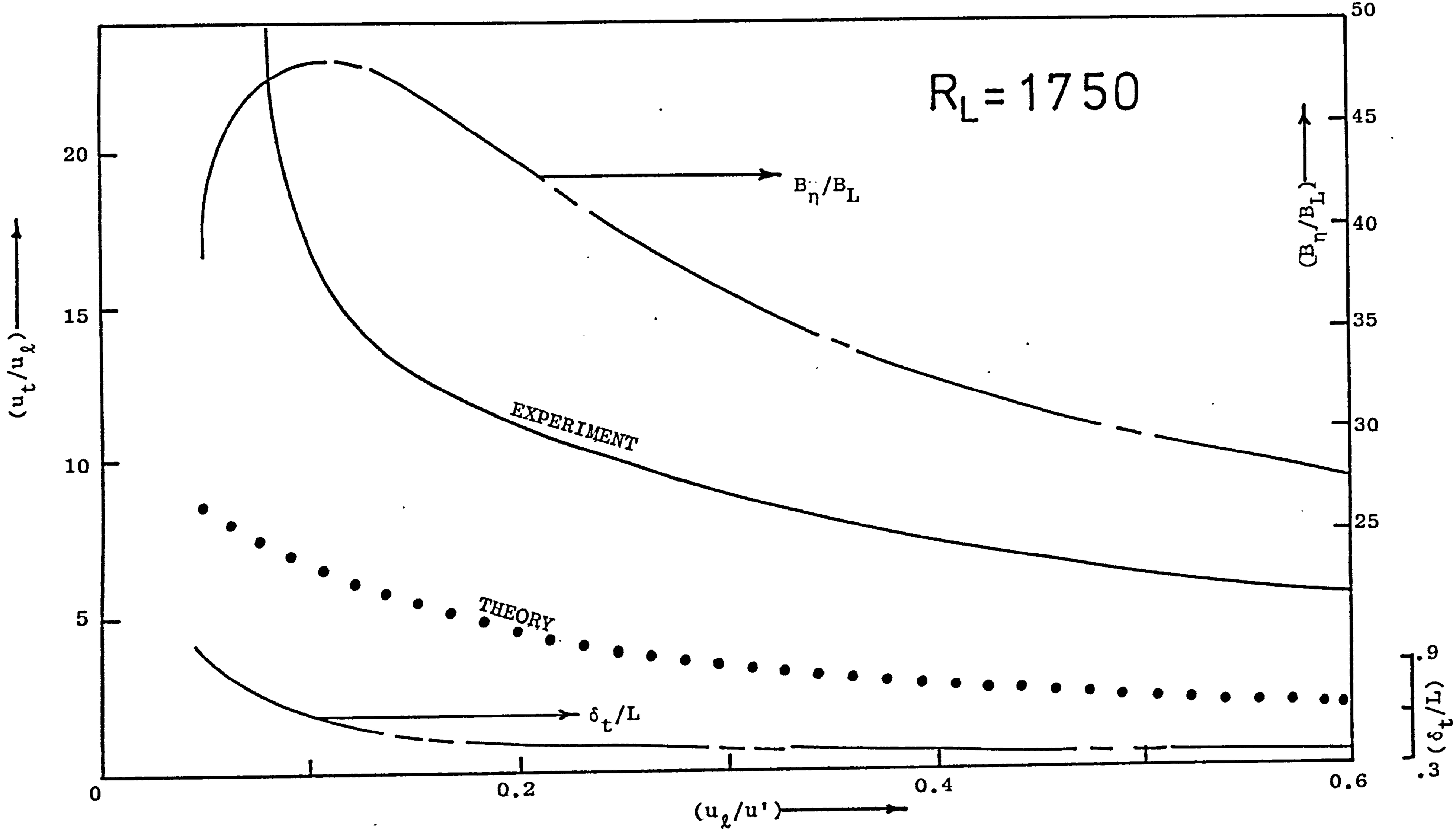

FIG.6.15 THEORETICAL AND EXPERIMENTAL TURBULENT FLAME DATA FOR R_L = 1750 (ARRHENIUS)

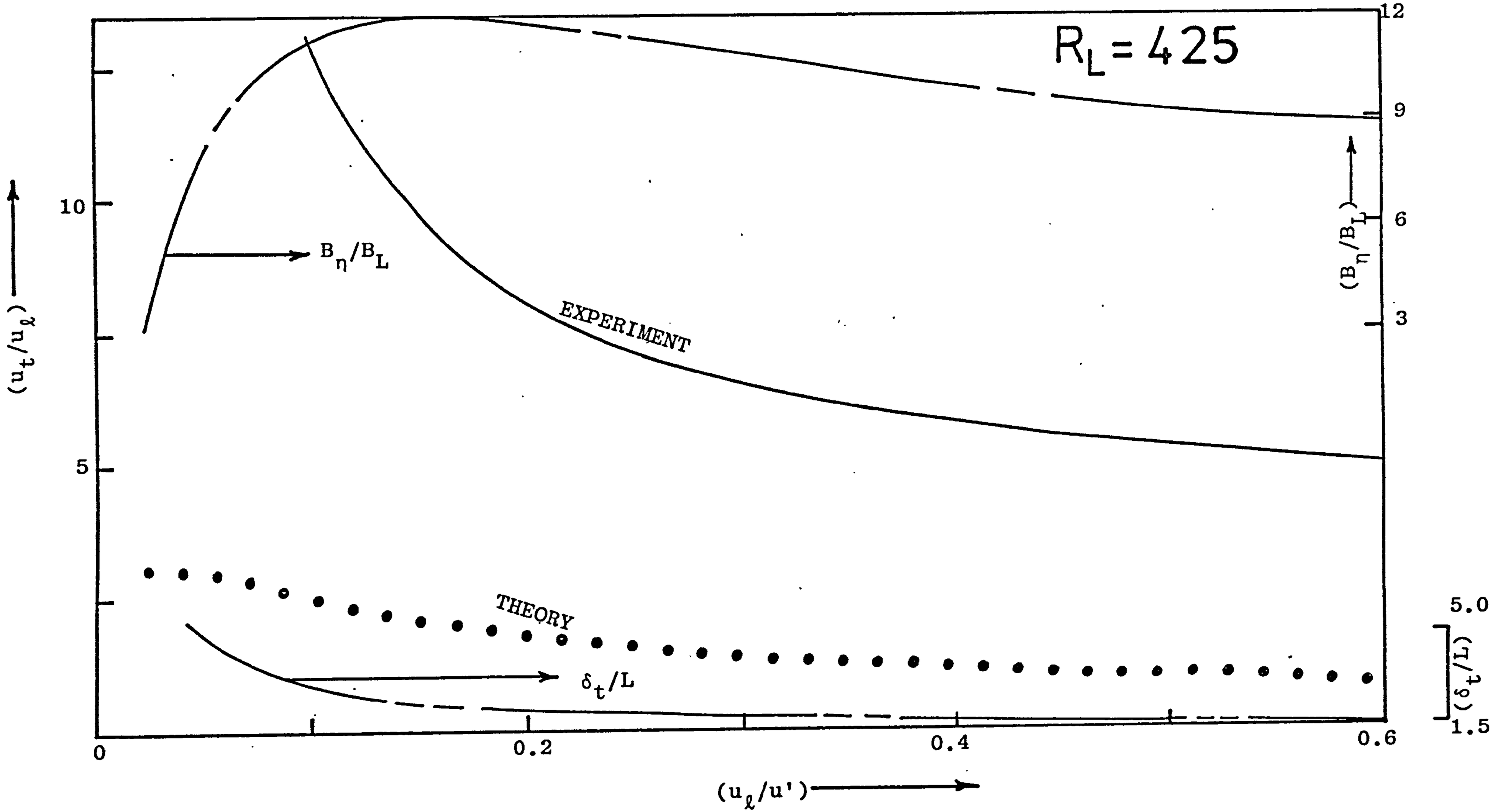

FIG.6.16 THEORETICAL AND EXPERIMENTAL TURBULENT FLAME DATA FOR R_L = 425 (ARRHENIUS)

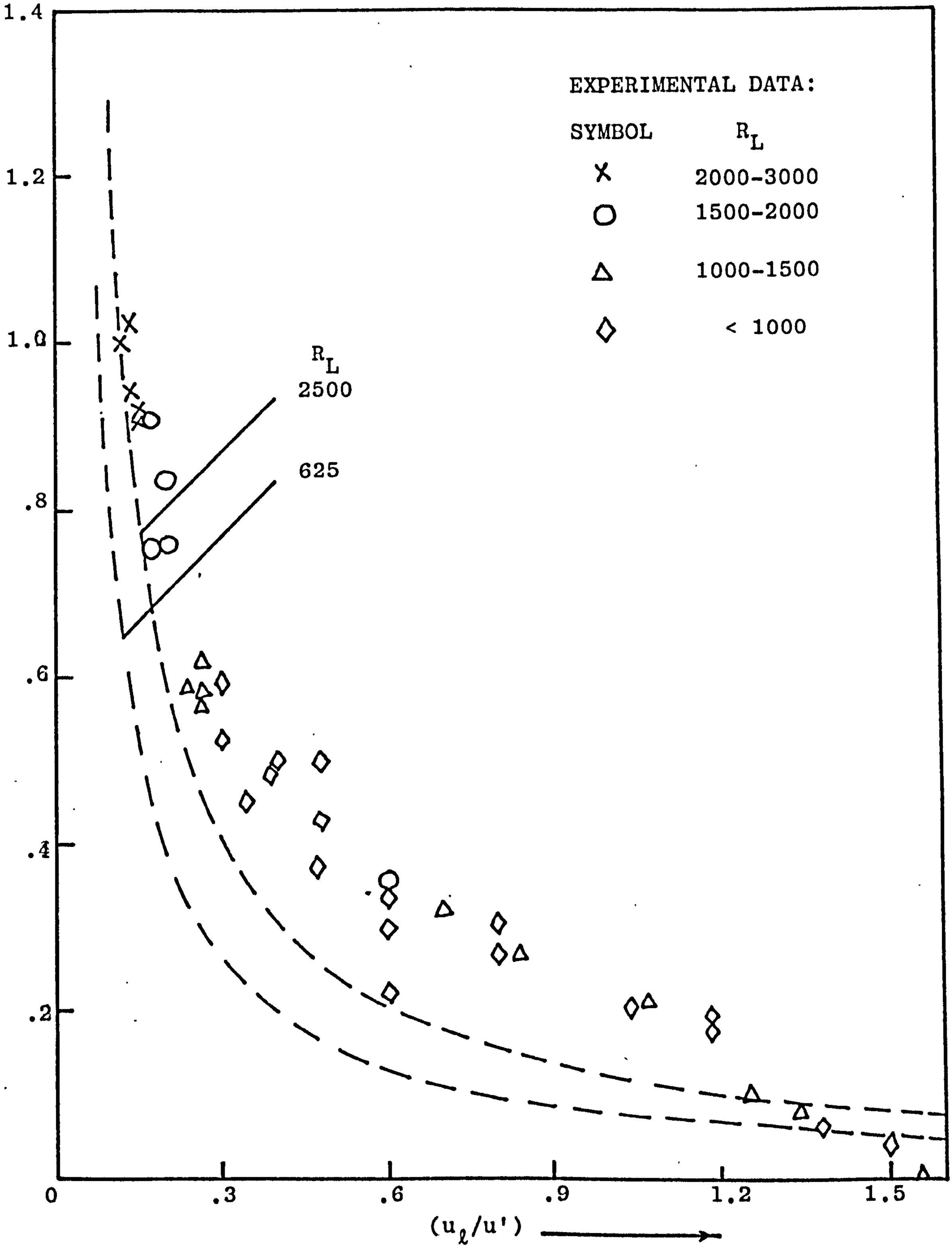

FIG.6.17 SEMI-THEORETICAL AND EXPERIMENTAL DATA FOR Y

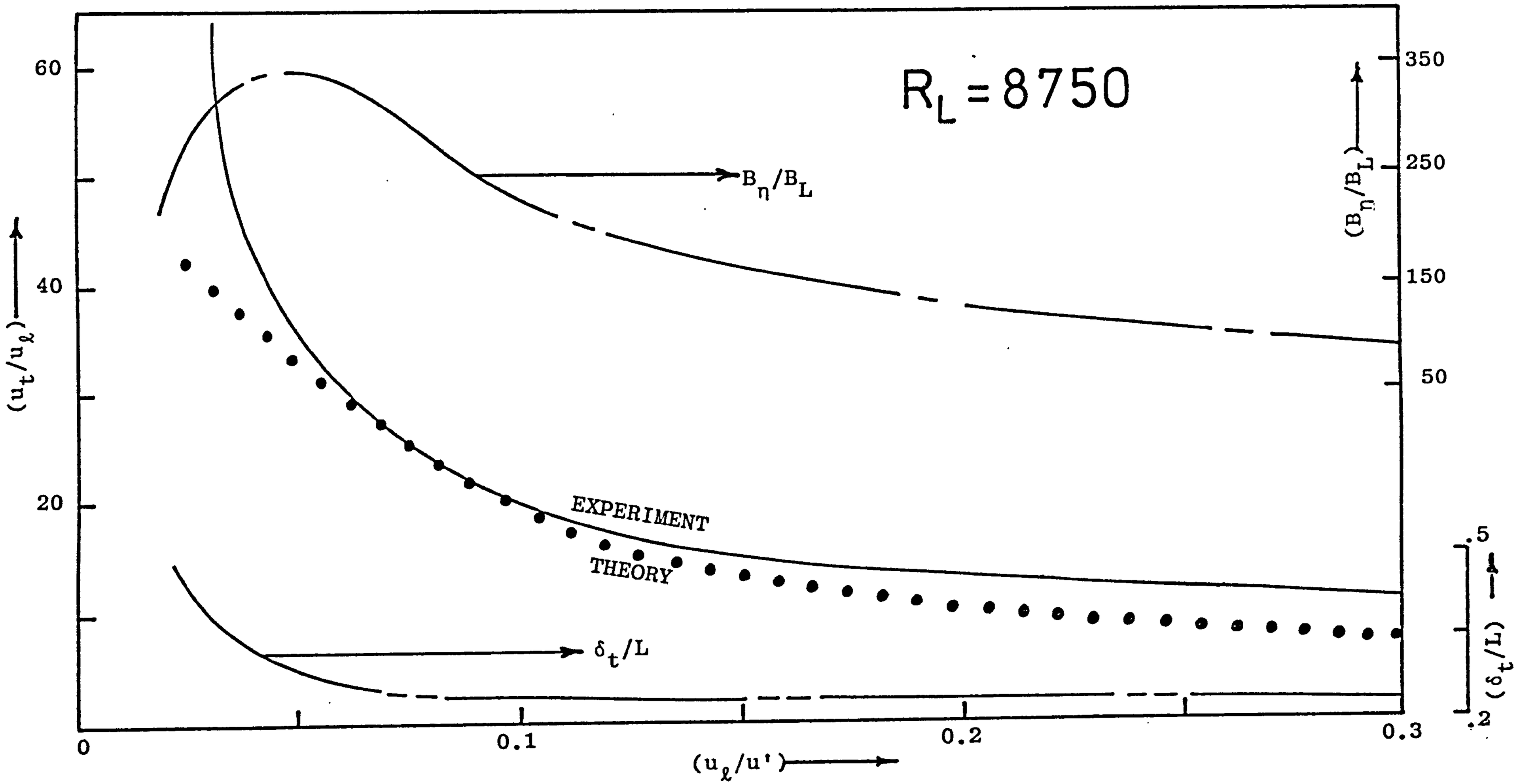

FIG.6.18 THEORETICAL AND EXPERIMENTAL TURBULENT FLAME DATA FOR R_L = 8750 (c = .25)

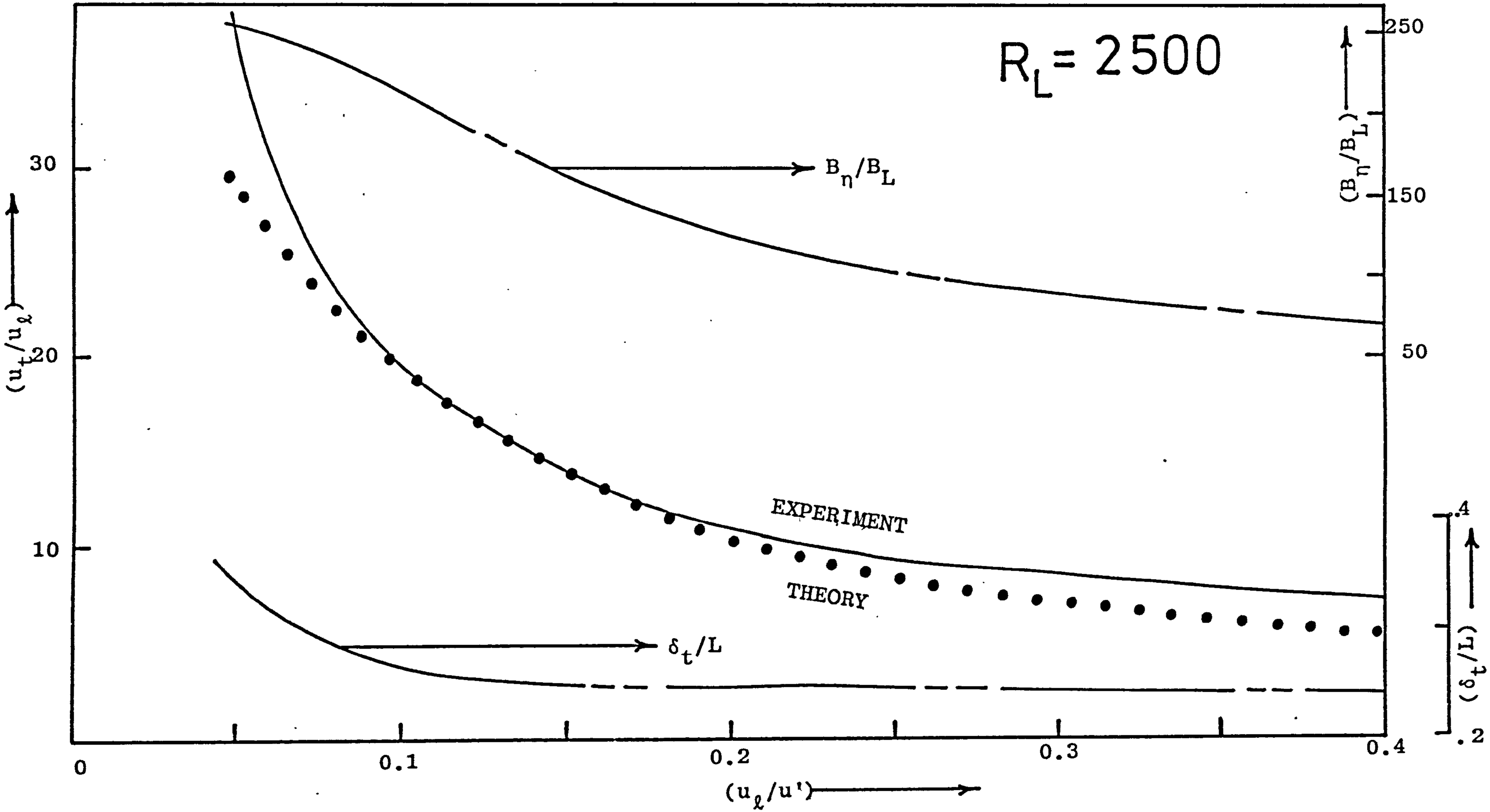

FIG.6.19 THEORETICAL AND EXPERIMENTAL TURBULENT FLAME DATA FOR R_L = 2500 (c = .25)

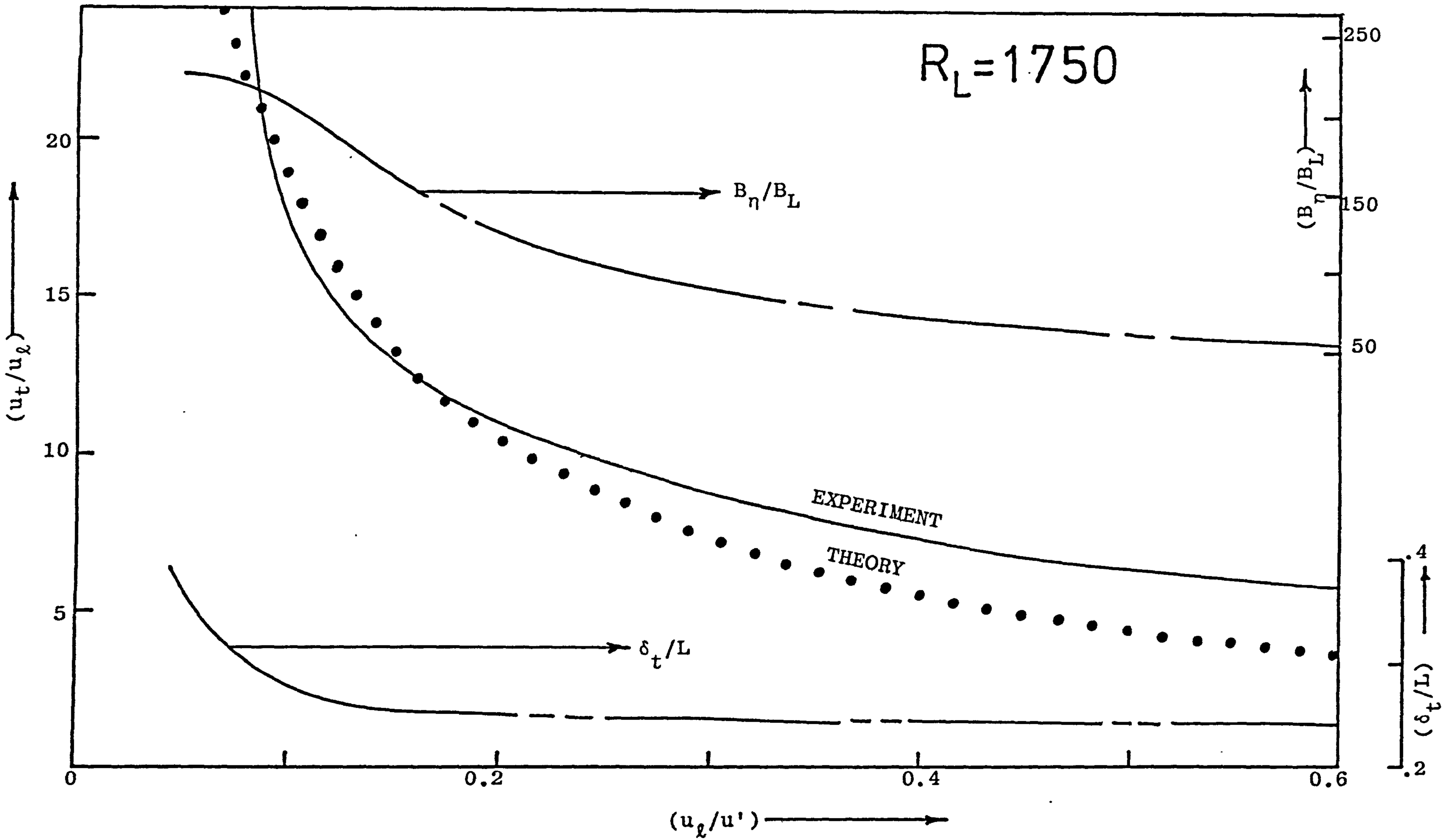

FIG.6.20 THEORETICAL AND EXPERIMENTAL TURBULENT FLAME DATA FOR R_L = 1750 (c = .25)

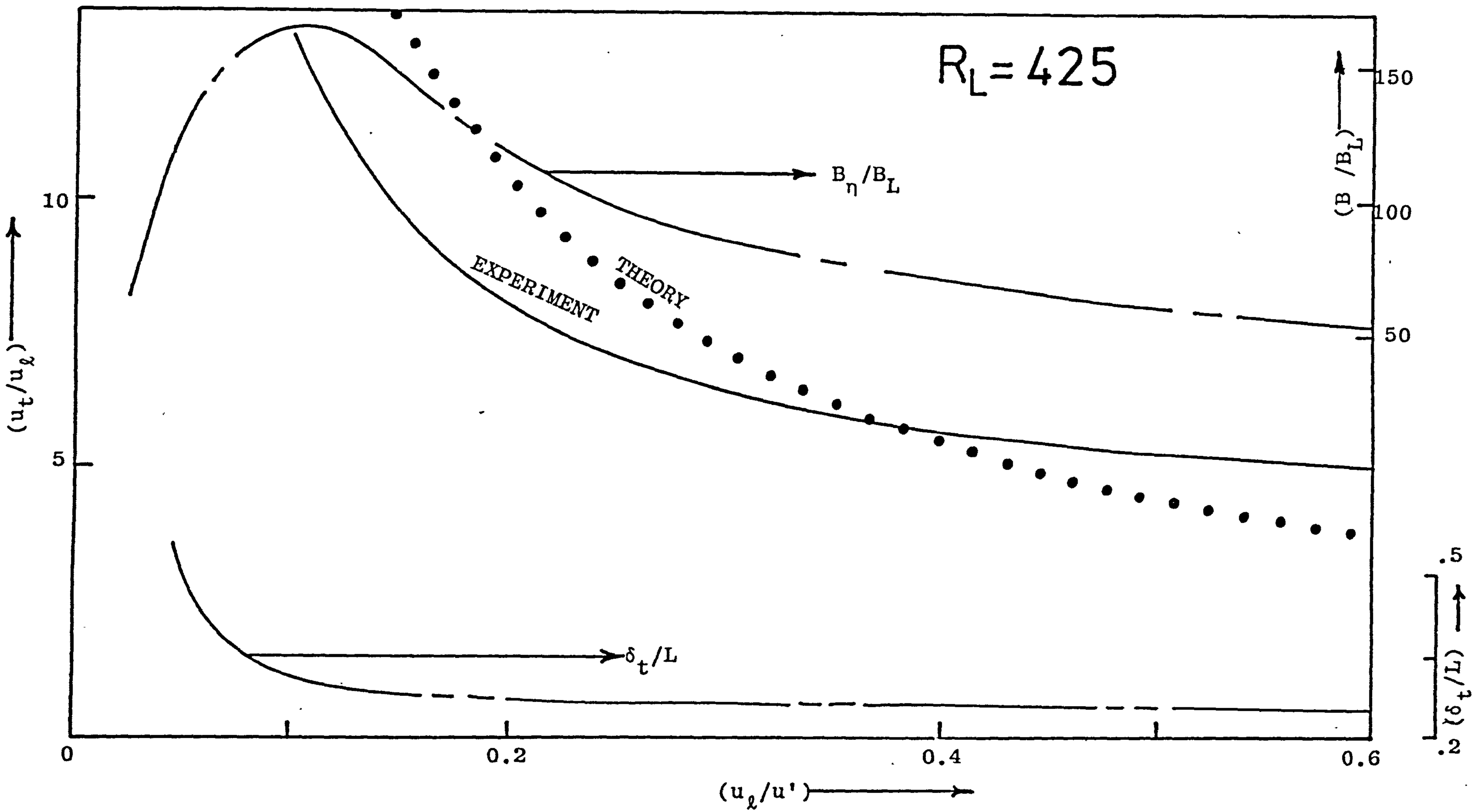

FIG.6.21 THEORETICAL AND EXPERIMENTAL TURBULENT FLAME DATA FOR $R_L = 425$ (c = .25)

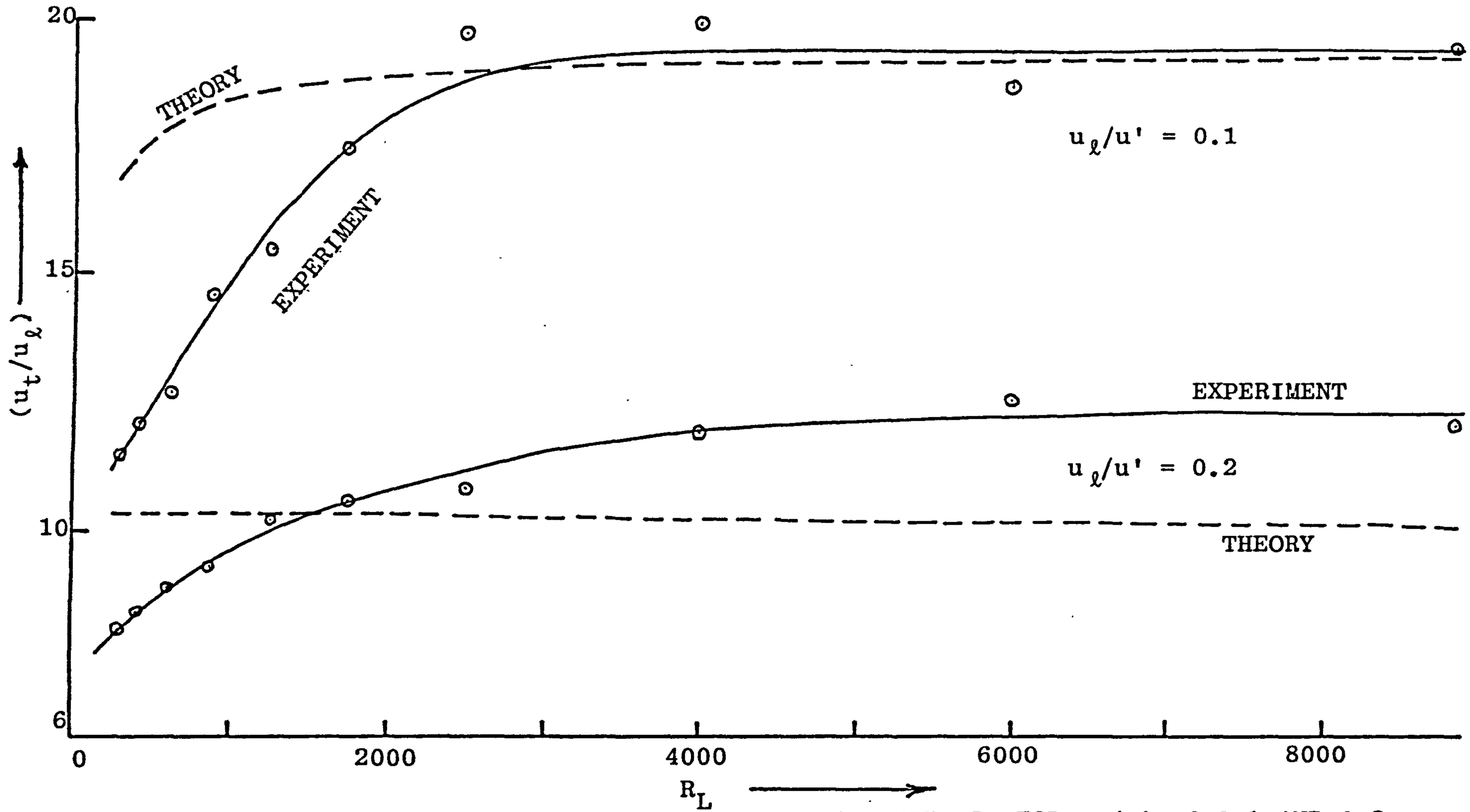

FIG.6.22 THEORETICAL AND EXPERIMENTAL VARIATION OF u_t/u_ℓ WITH R_L FOR u_ℓ/u' of 0.1 AND 0.2

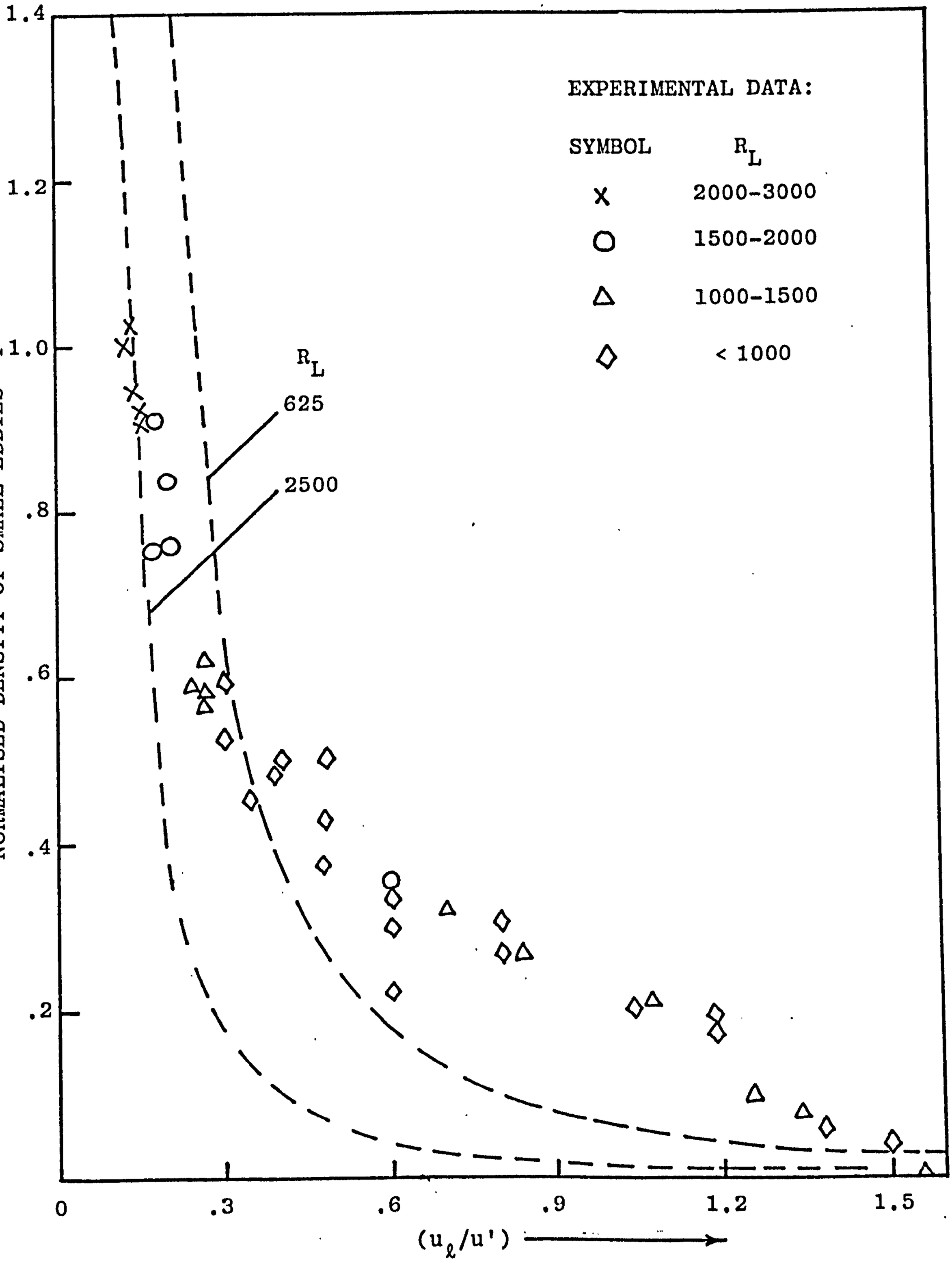

FIG.6.23 THEORETICAL AND EXPERIMENTAL DATA FOR Y

CHAPTER 7

TURBULENT COMBUSTION IN GASOLINE ENGINES

CHAPTER 7

TURBULENT COMBUSTION IN GASOLINE ENGINES

7.1 INTRODUCTION

Pressure to improve the gasoline engine, though always present, has been intensified in recent years by exhaust emission standards as well as the energy crisis. Since the combustion process is a key to both fuel consumption and exhaust emissions, it is logical that much engine research is focused on this. The combustion in a gasoline engine is an important example of the development of a turbulent flame in an enclosed volume and in this Chapter some of the knowledge gained in the previous ones is applied to practical combustion problems in such engines.

The extent to which the flame propagation data of Chapter 5 are relevant is now examined in relation to current attempts to produce spark ignition engines capable of running on weak mixtures, in contrast to traditional mixtures which are either close to stoichiometric or, more usually, slightly rich.

In traditional operation CO and hydrocarbon emissions are excessive by contemporary standards. To

reduce these, weak mixtures are preferred but these can have the unfortunate side effect of increasing the NO emission. This is a maximum when the mixture is slightly fuel-lean and a further increase in the proportion of air decreases this emission (1,2), (see Fig. 7.1). However, the main disadvantage of the lean burn engine is that its power output is low ((3) and see Fig. 7.1).

Hence, in principle the reduction of emissions of hydrocarbons, CO and NO can be achieved by operating with weak mixtures, close to the misfire limit. In order to obtain an adequate rate of burning with a lean mixture, it is necessary to compensate for the associated reduction in burning velocity by an increase in the intensity of turbulence. This will become apparent later.

The correlation of u_t/u_ℓ with u_ℓ/u' and unburnt gas R_L, demonstrates a need to measure unburnt gas turbulent parameters in engines. However, the use of hot wire anemometers inside a cylinder presents special difficulties because of the fluctuations of pressure and the high temperatures. Consequently, anemometers have only been used in motored engines (4-13) and their calibration has proved difficult.

The high level of turbulence when the mean flow may be zero (11,12) presents problems of data discrimination and interpretation. The conditions close to top centre, when combustion occurs, are of particular interest and

here the mean flow tends to zero (4,14). This leads to problems in the derivation of turbulent parameters, in particular the integral length scale, due to rectification of the signal, as discussed in Chapters 3 and 4.

7.2 THE SOURCE OF TURBULENCE IN ENGINE CYLINDER

The evolution of the gasoline engine to give what is, with the exception of certain emissions, a generally satisfactory performance over a range of powers and speeds has shown the importance of turbulence in the achievement of satisfactory rates of burning. The means by which the necessary turbulence in the charge might be produced are now summarised:

(i) Restriction of the passage-way in a 'turbulent head'. During compression the gasses are forced through a constricted passage and made turbulent. This was the basis of the early 'turbulent head' design of Ricardo (15).

(ii) The motion of the piston, supplemented by a controlled amount of 'squish'. The latter is the ejection of the charge compressed between the piston and a corresponding surface in the cylinder head, as top centre is approached.

(iii) The use of 'swirl' or charge rotation. This arises from the conservation of angular momentum imparted to the charge during induction. It may be encouraged by inlet ports which direct the

charge in a tangential direction, or by the use of a shrouded or masked valve. A large amount of swirl has been used in compression ignition engines and less on spark ignition engines. The angular velocity of swirl might be ten times the engine speed (16), but this does not imply solid body swirl, which is the exception rather than the rule (17).

(iv) The use of sonic throttling intake valves (18). Ma (19) has designed such a turbulence generator, based on shock wave generation. A convergent-divergent passage is formed between a streamlined plunger and a fixed nozzle. Sonic velocity is reached during intake at the annular throat section and a shock wave occurs downstream which is determined by the prevailing manifold vacuum. To vary the engine mass flow, the plunger is moved axially to vary the throat area, whilst the sonic velocity is maintained. Ma concluded that this turbulence generator was capable of producing efficiently small scale, high intensity turbulence inside the combustion chamber.

All of the above flows generate a cascade of turbulent energy, in which the energy finally is dissipated in a small scale, high frequency régime (Chapter 6). There is, however, a tendency for the turbulence which originates in motions imparted in the inlet manifold and valve passages

to decay in the period of time which elapses before top centre and combustion.

Increased turbulence is usually accompanied by a drop in volumetric efficiency. Brown (20) has shown recently that the turbulence produced by a shrouded valve is not necessarily homogeneous, with the result that although the mean burning velocity is increased, in regions of relatively low values of u' the combustion tends to be uncompleted and after-burning occurs during the expansion stroke, with consequent loss of efficiency.

7.3 MEASUREMENTS OF TURBULENCE PARAMETERS IN MOTORED ENGINES

Semenov (4) was the first to measure turbulence with a hot wire anemometer in a motored engine. He found that the flow during intake produced the velocity gradients which generated turbulence. The velocity and spatial velocity gradients during intake were found to vary greatly with location in the chamber, thus illustrating the jet nature of flow through the intake valve. Both intake jet and turbulent velocity at top centre of the compression stroke were found to be affected primarily by engine speed, but also accompanied by effects due to throttling and the value of the compression ratio. The measured velocities were found to vary from cycle to cycle. Semenov also found that the turbulent velocity remained relatively constant with time towards the end of compression and at

the beginning of expansion and that the turbulent parameters did not vary greatly over different locations. Semenov estimated the integral scale to be 2 mm from his data.

Matsuoka et al (10) found that the turbulent velocity varied from cycle to cycle and ranged from 0.3 m sec^{-1} to 4 m sec^{-1} at 500 r.p.m. Induction gas velocities in cylinders have been measured also by Arnold et al (16). Winsor and Patterson (21) measured turbulent velocity in a CFR engine. They concluded that turbulence in the engine cylinder was isotropic and homogeneous, that it existed only at frequencies below 13 KHZ, and was unaffected by volumetric efficiency. The measured velocity variations were found to increase linearly with engine speed, and the decay of turbulence during compression and expansion was observed.

Winsor (22) estimated an integral scale value of between 1.2 mm and 2.5 mm near compression top centre. Recently, Dent and Salama (12) have measured values of u' between 0.13 and 12 m sec^{-1} dependent on the crank angle, engine speed and throttle setting. They also measured values of integral scales of between 0.2 mm and 3.5 mm, dependent on the combustion chamber geometry and crank angle.

A most important consequence of the induced turbulence of the charge is the linear variation of turbulent velocity and mean velocity with engine speed, which is

independent of combustion chamber shape and inlet swirl (14). Thus the indicator diagrams and rates of pressure increase in terms of crank angle during combustion do not change significantly with speed. At the higher speeds, it becomes necessary to slightly advance the spark, but this is largely due to an increase in combustion time during the early stage of propagation only.

It is revealing to identify the régime of burning in gasoline engines on Fig. 5.19, and to do this it is necessary to have accurate values of u' and L in motored engines. Comprehensive, reliable data are available in the recent hot wire anemometry studies of Lancaster (13) and Lancaster et al (23) and it is these data which were utilised.

7.4 THE RÉGIME OF BURNING IN GASOLINE ENGINES

Lancaster's work was carried out at the General Motors Laboratories at Warren, with a motored CFR engine. Readings were obtained over a range of engine speeds, volumetric efficiencies, and compression ratios with both shrouded and unshrouded intake valves. Mean velocities, turbulent velocities, and integral scales of turbulence were computed. The turbulence near compression top centre was found to be isotropic, with values of both turbulent velocity and length scale determined by the intake process.

Figures 7.2 to 7.5 are taken from Ref. 15 and show the effects of engine operating variables on turbulent

velocity and length scale. Figure 7.2 shows u' to increase linearly with engine speed. When the intake pressure and density are reduced the flow velocities through the intake valve decrease along with the volumetric efficiency. One would expect that the turbulent velocity would increase as load increases and the throttle opens, as indeed is shown in Fig. 7.3. This effect is more marked for the shrouded valve. In this case the swirl decays more slowly than initially more randomised motion would decay and the amount of swirl, controlled by throttling, shows a greater dependence upon the throttling and hence upon the volumetric efficiency (14).

The integral scale of turbulence in the axial direction, L_x, was calculated from the measured integral time scale, L_t, by applying Eq. (3.10). The variation of L_x with engine speed is shown in Fig. 7.4. For the unshrouded valve L_x is almost independet of engine speed, but for the shrouded valve L_x shows a decrease with speed. Figure 7.5 shows the integral scale to increase slightly with volumetric efficiency.

In order to plot these experimental points on Fig. 5.19, values of R_L must be calculated. No measurements were reported for the integral scale in the radial direction, L_y. However, Dent and Salama (12) have suggested that the value of L_y should be half that of L_x, as in isotropic flow systems (24). But at top centre there is almost no mean flow (4) and conditions may be approximated

as isotropic and uniform, as in the explosion vessel, and L_y equated to L_x.

Values of density, ρ, were calculated on the basis of compression of air according to the law $PV^{1.35} = a$ constant. Values of the dynamic viscosity, μ, were taken from standard thermodynamic tables (25) for the corresponding temperature. Both ν and u_ℓ were evaluated for conditions of the unburnt charge, just prior to ignition at top centre. This represents the worst condition for flame propagation, as will be demonstrated. As the pressure and temperature of unburnt gas increase due to compression, the value of u_ℓ increases appreciably and it might be expected that an associated increase in u_ℓ/u' will cause the flame propagation to occur in a régime further removed from the flame quench limit shown in Fig. 5.21.

The need for accurate values of u_ℓ, at high temperatures and pressures becomes apparent. So far, only limited data have been published on u_ℓ under engine-like conditions (26,27). The present calculations employ the values given by Lancaster et al (23) for propane-air mixtures with an equivalence ratio, ϕ, of 0.8. Their computation for u_ℓ over a range of ϕ was based on the expression derived by De Soete and Brasselet (26) from the theoretical burning velocity expression proposed by Van Tiggelen (28). This equation accounts for the influences of temperature, pressure and charge dilution. The engine conditions are given in Table 7.1 and the

corresponding values of u_ℓ in Table 7.2.

The results for both unshrouded and shrouded valves, in terms of the dimensionless parameters of Fig. 5.19, are given in Table 7.2 and are also shown graphically in Fig. 7.6, on which the characteristic curves of Fig. 5.19 have been drawn. It is demonstrated clearly that the shrouded valve increases the value of the turbulent burning velocity.

It is of interest to attempt to ascertain whether the increase in u_t/u_ℓ due to shrouding demonstrated by Fig. 7.6 is confirmed by engine tests.

Lancaster et al (23) calculated the turbulent burning velocity for propane-air mixtures from a combustion heat release model which assumed spherical flame propagation and used measured values of cylinder pressures. Values of the measured ratio u_t/u_ℓ obtained by Lancaster et al (23), for ϕ equal to 0.8, are given in Table 7.3 for both shrouded and unshrouded valves. The corresponding values were derived from Fig. 7.6 and these are also given in Table 7.3. Also given is the ratio of u_t/u_ℓ derived from Fig. 7.6 to that measured by Lancaster et al (23) for both cases.

Table 7.3 shows that Fig. 7.6 always predicts values of u_t/u_ℓ which are higher than those measured. Possible explanations are that the turbulence at the measuring position was greater than that close to the

cylinder walls and the turbulent Reynolds number in the radial direction might be less than that in the axial direction, which was used to yield the value of R_L.

Figure 7.7 shows the effect of shrouding on turbulent burning velocity. In this figure the measured ratios of values of u_t/u_ℓ for shrouded to unshrouded valves are compared with those derived from Fig. 7.6.

7.5 LEAN BURNING IN AN ENGINE CYLINDER

In order to identify where a typical operating régime might lie on Fig. 7.6, run 3 of Table 7.1, for the unshrouded valve case, was considered. The corresponding value of R_L is 1246, whilst the computed value of u_ℓ of Lancaster et al (23) for a stoichiometric propane-air mixture, is 1.68 m sec^{-1}. The corresponding ratio of u_ℓ/u' is 0.8 and the associated point is point 1 on Fig. 7.6. The data of the figure give a value of u_t/u_ℓ in the region of 4.45.

Now, in weak running the value of u_ℓ might be halved (38) and if other conditions including the turbulence, are unchanged, for u_ℓ/u' equal to 0.4 the same value of R_L gives a value of u_t/u_ℓ of approximately 6.8. This is shown as point 2 on Fig. 7.6. If it is desired to maintain the same rate of burning with the weak mixture, the halving of u_ℓ necessitates a doubling of u_t/u_ℓ to a value in the region of 8.9. This would maintain u_t at the original value. Figure 7.6 shows that this must involve a decrease

in u_ℓ/u' to a value of 0.25, point 3 on the figure, and this entails an increase in u' of 60% above the original value. Thus sufficiently more turbulence must be generated in order to maintain the same rate of burning with the weak mixture (29,30) and Table 7.2 shows it is possible to do this by shrouding the inlet valve.

The various techniques that might be used to achieve this end are given in Section 7.2. The employment of sonic throttling intake valves has been shown to promote rapid, turbulent combustion of very weak mixtures (18). The turbulence generator used by Ma (19) extended the lean limit up to an air-fuel ratio of 20, with no loss in thermal efficiency and a significant reduction in exhaust emissions, especially NO.

Unfortunately, the effects of turbulence are not solely beneficial. Figure 4.15 shows that there is a narrowing of the limits of propagation as turbulence is increased. An increase in the turbulence in a lean mixture might also result in ignition failure.(19,31,37). Figure 7.6 shows that point 3 is approaching the experimentally determined limit of flame propagation. Thus high levels of turbulence may not be entirely beneficial to lean mixture combustion because of ignition and flame propagation limitations.

It is possible by charge stratification, with an easily ignitable mixture at the spark, to facilitate ignition and burning up to a point where the increases in

pressure and temperature are sufficient to so increase u_ℓ that leaner burning becomes possible, away from the flame propagation limit.

With regard to what are purely ignition problems, with some modifications to the spark plug it is possible to ignite weaker and more turbulent mixtures than those traditionally used. Increases in spark gap, spark gap projection and spark energy, all enable the lean limit to be extended, as a result of a reduction in quenching (32, 33). They also lead, at a given equivalence ratio, to a reduction in hydrocarbon emission (34). An increase in spark duration extends the lean limit and reduces hydrocarbon emission (34). Changes in spark plug location might also (35,36) help to extend the lean operational limit of an engine.

A pulsed plasma jet has been used as the ignition device by Topham et al (39). These workers found significant increases in power output, fuel economy and lean operation limit. More recently Dale et al (40) used a repetitive pulsed laser ignition with a duration of 1 μ sec in a gasoline engine. They concluded that, laser ignition initiates a more rapid rate of pressure rise which results in more engine power and improved efficiency. The lean limit air-fuel ratio was extended from 20 to 23 and cyclic variations were reduced.

The experimental investigations with the tulip (Chapter 4), show that it might be helpful to shield the spark gap from the full turbulence intensity, but thermal quenching must be avoided.

TABLE 7.1 Conditions for Figs. 7.6 and 7.7

Run	Engine Speed r.p.m.	Vol. Eff. %	Compression Ratio	Intake Manifold Pressure atmos.
1	1500	50	8.72	0.73
2	1000	50	8.72	0.73
3	2000	50	8.72	0.73
4	1500	25	8.72	0.40
5	1500	75	8.72	1.07
6	1500	50	6.84	0.73
7	1500	50	10.55	0.73

TABLE 7.2 Turbulence Parameters in Motored Engines for Fig. 7.6

Run	u_ℓ m sec^{-1}	Unshrouded Valve				Shrouded Valve			
		u' m sec^{-1}	u_ℓ/u'	L_x mm	R_{Lx}	u' m sec^{-1}	u_ℓ/u'	L_x mm	R_{Lx}
1	1.45	1.70	0.85	3.55	1274	3.76	0.39	4.91	3896
2	1.45	0.91	1.59	2.73	525	2.73	0.53	4.63	2670
3	1.45	2.11	0.69	2.80	1246	4.96	0.29	5.99	6271
4	1.45	1.21	1.20	2.60	364	3.35	0.43	4.43	1715
5	1.45	1.77	0.82	3.54	1942	3.99	0.36	5.19	6418
6	1.21	1.27	0.95	2.60	565	3.43	0.35	5.31	3114
7	1.70	1.40	1.21	2.81	941	3.32	0.51	3.63	2880

TABLE 7.3 Comparison of u_t/u_ℓ Derived from Fig. 7.6 and those Measured by Lancaster et al (23) for both Shrouded and Unshrouded Valves

Run	Shrouded Valve			Unshrouded Valve		
	u_t/u_ℓ from Fig. 7.6	Measured u_t/u_ℓ	Ratio	u_t/u_ℓ from Fig. 7.6	Measured u_t/u_ℓ	Ratio
1	7.10	4.55	1.56	4.40	2.85	1.54
2	5.80	3.80	1.53	2.90	2.20	1.32
3	8.90	5.85	1.52	4.95	3.30	1.50
4	6.40	4.35	1.47	3.20	2.65	1.21
5	7.60	5.00	1.52	4.60	3.00	1.53

7.6 NOMENCLATURE

L	integral scale of turbulence
L_x	integral scale of turbulence in the axial direction
L_t	integral time scale
L_y	integral scale of turbulence in the radial direction
P	pressure
R_L	$\frac{u'L}{\nu}$
R_{Lx}	$\frac{u'L_x}{\nu}$
u_ℓ	laminar burning velocity
u_t	turbulent burning velocity
u'	r.m.s. turbulent velocity
V	volume
μ	dynamic viscosity
ν	kinematic viscosity
ρ	density
ϕ	equivalence ratio $= \frac{\text{actual fuel-air ratio}}{\text{stoichiometric fuel-air ratio}}$

7.7 REFERENCES

1. J.E.A. JOHN, Lean burn engine concepts - emissions and economy, SAE paper No 750930 (1975).

2. J.B. HEYWOOD, Pollutant formation and control in spark-ignition engines, Prog. Energy Combust. Sci. 1, 135 (1976).

3. R. LINDSAY, A. THOMAS, J.A. WOODWORTH and E.G. ZESCHMANN, Influence of homogeneous charge on the exhuast emissions of hydrocarbons, carbon monoxide, and nitric oxide from a multi-cylinder engine, SAE paper No. 710588 (1971).

4. E.S. SEMENOV, Studies of turbulent gas flow in piston engines, Otedelenie Technicheskikh Nauk No. 8 (1958). (English translation: NASA Technical Translation F97.)

5. E.S. SEMENOV, Combustion in turbulent flow, Ed. L.N. KHITRIN, Moscow. (English Translation: IPST, Jerusalem, 122 (1963).)

6. E.S. SEMENOV and A.S. SOKOLIK, Studies of turbulent gas flows in piston engines, Izv, Akad. Nauk SSSR, Otd. Tekhn. Nauk No. 8, 130 (1958).

7. K.K. MOLCHANOV, On the problem of gas motion and combustion in a light fuel engine, Trudy Moskovskogo Avtomobil'no-dorozhnogo Instituta, Avtotransizdat, Moscow No. 17, 85 (1955). (English translation: Shell Trans. No. 1019.)

8. V.N. IVANOV, Investigation of the rate of air flow in the combustion chamber of the engine, Russian Translating Programme RTS 3953, National Lending Science and Technology (1967). (Izvestiya Vysshikh. Uch. Zavedenii Mash. 3, 91 (1964).)

9. M. HORVATIN and A.W. HUSSMAN, Measurements of air movements in internal combustion engine cylinders, DISA information No. 8, July 1969.

10. S. MATSUOKA, T. YAMAGUCHI and Y. UMEMURA, Factors influencing the cyclic variation of combustion of spark ignition engine, SAE paper No. 710586 (1971).

11. P.O. WITZE, Hot-wire turbulence measurements in a motored internal combustion engine, Second European Combustion Symposium, Orléans-France, 812 (1975).

12. J.C. DENT and N.S. SALAMA, The measurement of turbulence characteristics in an internal combustion engine cylinder, SAE paper No. 750886 (1975).

13. D.R. LANCASTER, Effects of engine variables on turbulence in a spark-ignition engine, SAE paper No. 760159 (1976).

14. R.J. TABACZYNSKI, Turbulence and turbulent combustion in spark-ignition engines, Prog. Energy Combust. Sci. 2, 143 (1976).

15. H.R. RICARDO and J.G.G. HEMPSON, The high-speed internal-combustion engine, Fifth edition, Blackie and Son, London (1968).

16. M.J. ARNOLD, M.J. TINDAL and T.J. WILLIAMS, Measurement of induction gas velocities in a reciprocating engine cylinder, SAE paper No. 720115 (1972).

17. K.H. HUEBNER and A.T. McDONALD, Experimental determination of air flow patterns in piston engine with induction swirl, SAE paper No. 720026 (1972).

18. D.L. STIVENDER, Intake valve throttling (IVT) - a sonic throttling intake valve engine, SAE paper No. 680399 (1968).

19. T.H. MA, Effect of cylinder charge motion on combustion, paper No. C81/75, I. Mech. E. Conference on Combustion in Engines, Cranfield, England (1975).

20. P.G. BROWN, Lean burning in petrol engines, M.Sc. thesis, Dept. Mechanical Engineering, Univ. Leeds (1977).

21. R.E. WINSOR and D.J. PATTERSON, Mixture turbulence, A key to cyclic variation, SAE paper No. 730086 (1973).

22. R.E. WINSOR, Relationship of cyclic combustion variations and mixture motion in a spark-ignition engine, Ph.D. thesis, Univ. of Michigan (1972).

23. D.R. LANCASTER, R.B. KRIEGER, S.C. SORENSON and W.L. HULL, Effects of turbulence on spark-ignition engine combustion, SAE paper No. 760160 (1976).

24. J.O. HINZE, Turbulence - An introduction to its mechanism and theory, McGraw-Hill, New York, p. 172 (1959).

25. Y.R. MAYHEW and G.F.C. ROGERS, Thermodynamic and transport properties of fluids (SI Units), Oxford, Basil Blackwell (1971).

26. G. DE SOETE and J. BRASSELET, Rev. Inst. Fr. Petrole 24, 1507 (1969).

27. M.P. HALSTEAD, D.B. PYE and C.P. QUINN, Laminar burning velocities and weak flammability limits under engine-like conditions, Combustion and Flame 22, 89 (1974).

28. A. VAN TIGGELEN and J. DECKERS, Chain branching and flame propagation, Sixth Symposium (International) on Combustion, Reinhold Publishing, New York, p.61 (1957).

29. W.R. BRANDSTETTER, Experimental results from Volkswagen's prechamber stratified charge engines, paper No. C249/76, I. Mech. E. Conference on Stratified Charge Engines, London (1976).

30. L.A. GUSSAK and M.C. TURKISH, Lag-process of combustion and its application in automobile gasoline engines, paper No. C257/76, I. Mech. E. Conference on Stratified Charge Engines, London (1976).

31. K. IINUMA, A study of turbulence flame propagation in closed vessels, Automobile Exhaust Clarification Study Group, Japan, March 1977.

32. T. TANUMA, K. SASAKI, T. KANEKO and H. KAWASAKI, Ignition, combustion, and exhaust emissions of lean mixtures in automotive spark ignition engines, SAE paper No. 710159 (1971).

33. T.W. RYAN, S.S. LESTZ and W.E. MEYER, Extension of the lean misfire limit and reduction of exhaust emissions of an SI engine by modification of the ignition and intake systems, SAE paper No. 740105 (1974).

34. R.R. BURGETT, J.M. LEPTICH and K.V.S. SANGWAN, Measuring the effect of spark plug and ignition system design on engine performance, SAE paper No. 72007 (1972).

35. A.A. QUADER, Effects of spark location and combustion duration on nitric oxide and hydrocarbon emissions, SAE paper No. 730153 (1973).

36. A.A. QUADER, Lean combustion and the misfire limit in spark ignition engines, SAE paper No. 741055 (1974).

37. Y. HAMAMOTO, T. WAKISAKA and S. OHIGASHI, Limits of flame propagation in spark ignition engines - behaviour of flames and exhaust exmissions, Sixteenth International Congress of FISITA, Tokyo, May 1976.

38. R.G.ABDEL-GAYED, Contribution on "Experimental results from Volkswagen's pre-chamber stratified charge engines", "Conference on Stratified Charge Engines", paper No. C249/76, I.Mech.E.Conference Publications 1976-11, p.225, London (1977).

39. D.R.TOPHAM, P.R.SMY and R.M.CLEMENTS, An investigation of a coaxial spark igniter with emphasis on its practical use, Combustion and Flame 25, 187 (1975).

40. J.D.DALE, P.R.SMY, D.WAY-NEE and R.M.CLEMENTS, Laser-ignited internal combusion engine, Combusion and Flame 30, 319 (1977).

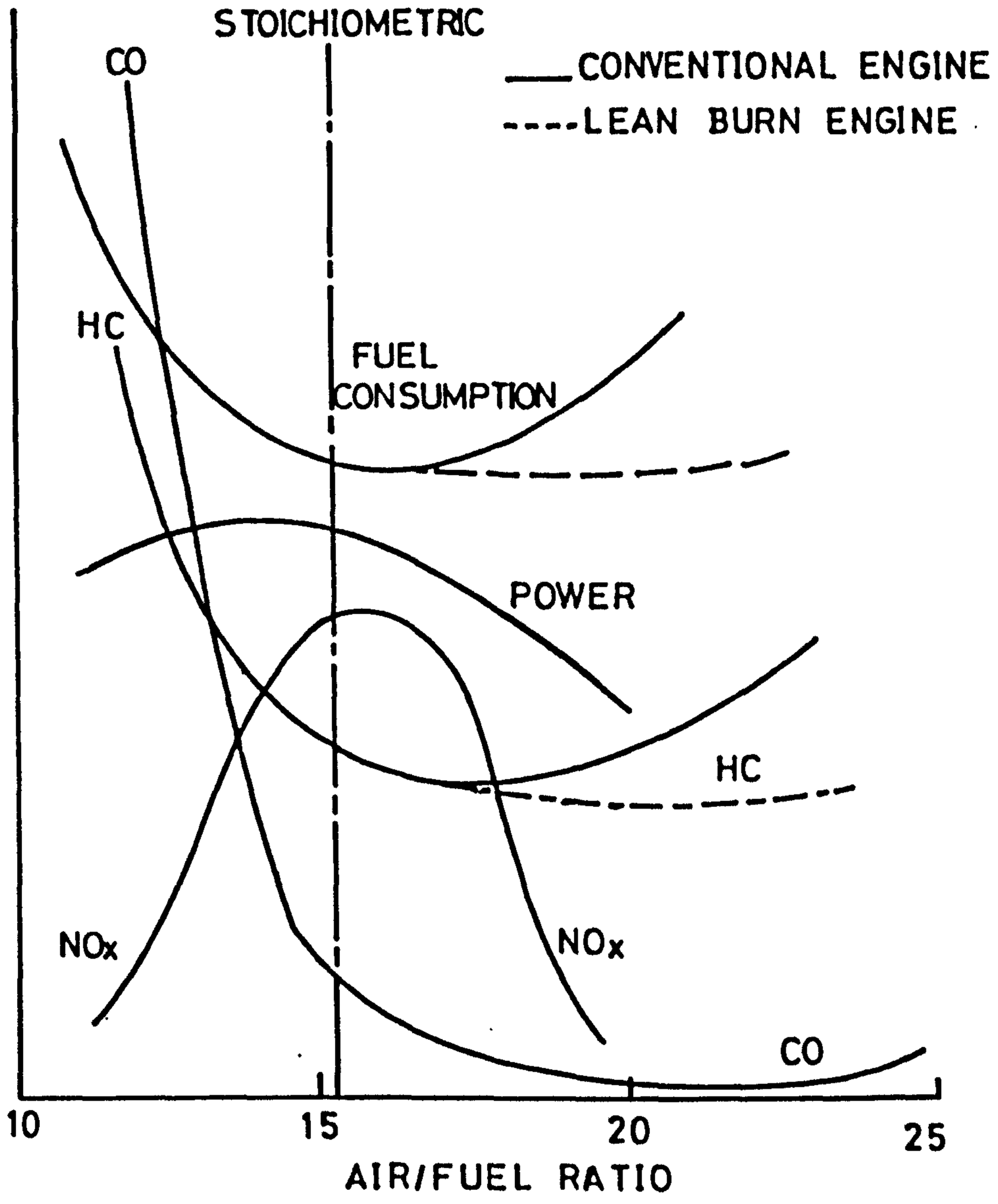

FIG. 7.1 THE RELATIONSHIP OF TYPICAL ENGINE EMISSIONS AND PERFORMANCE TO AIR/FUEL RATIO (TAKEN FROM REF. 1)

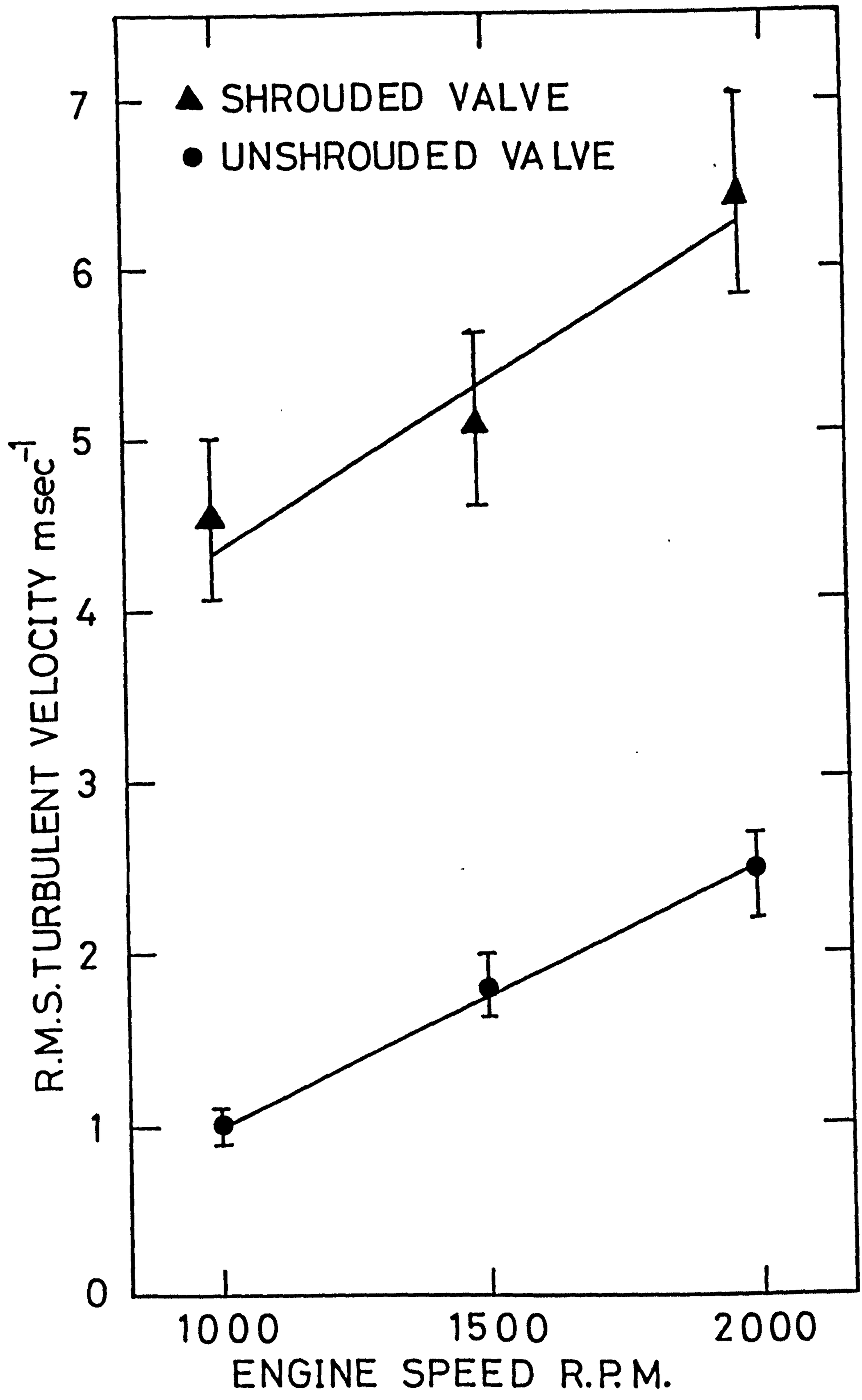

FIG.7.2 VARIATION OF R.M.S.TURBULENT VELOCITY WITH ENGINE SPEED(TAKEN FROM REF.15)

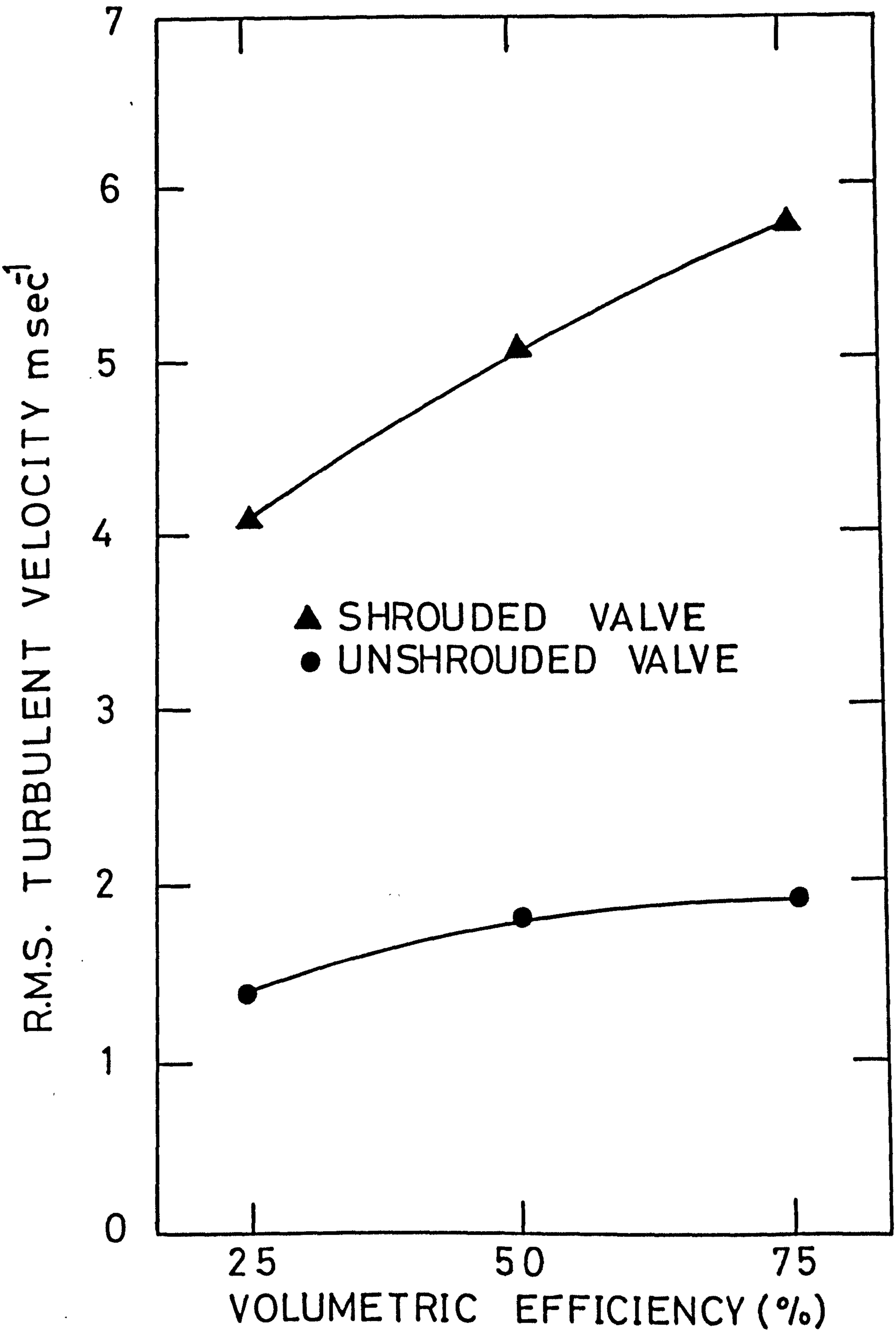

FIG. 7.3 VARIATION OF R.M.S. TURBULENT VELOCITY WITH VOLUMETRIC EFFICIENCY (TAKEN FROM REF. 15)

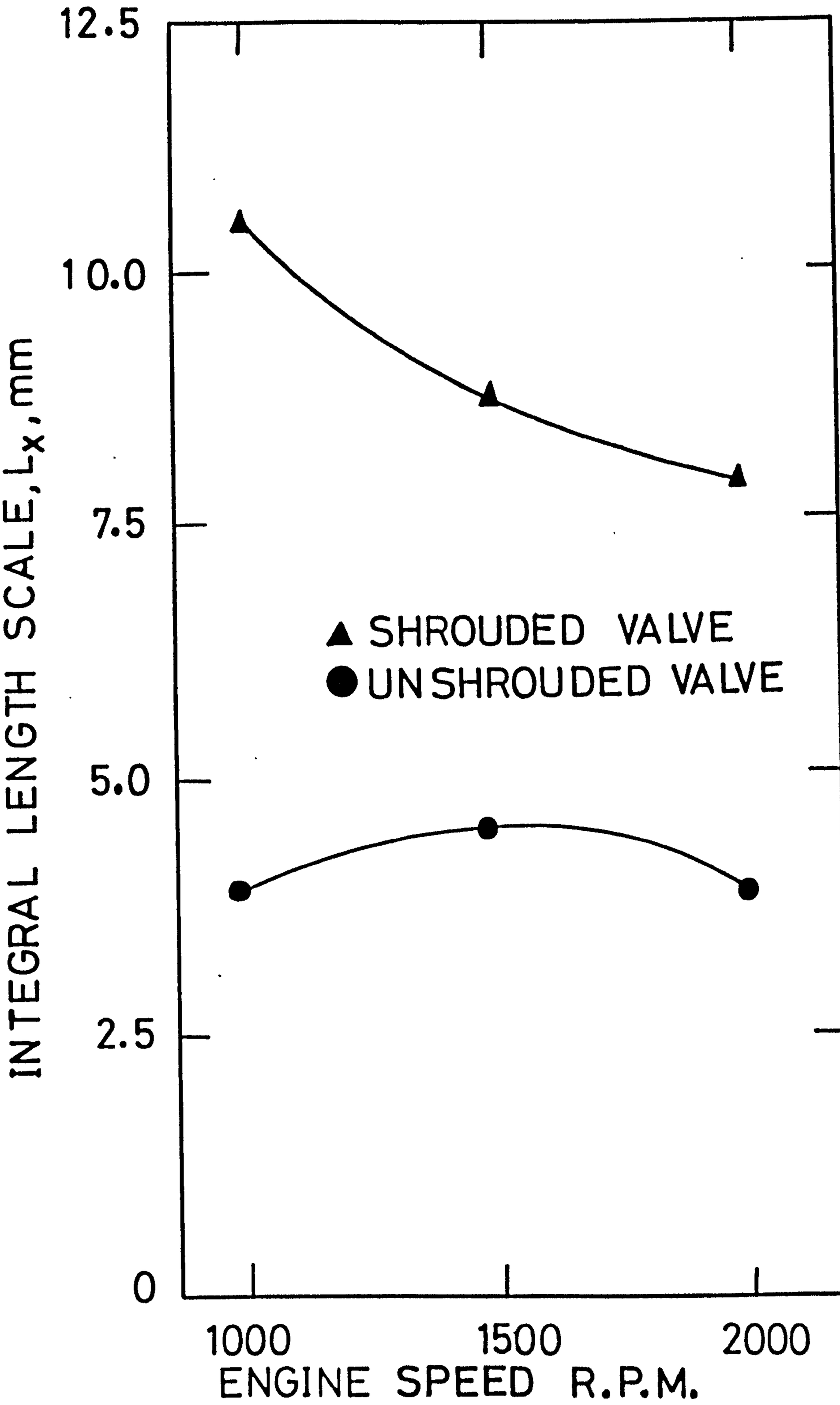

FIG. 7.4 VARIATION OF INTEGRAL LENGTH SCALE WITH ENGINE SPEED (TAKEN FROM REF. 15)

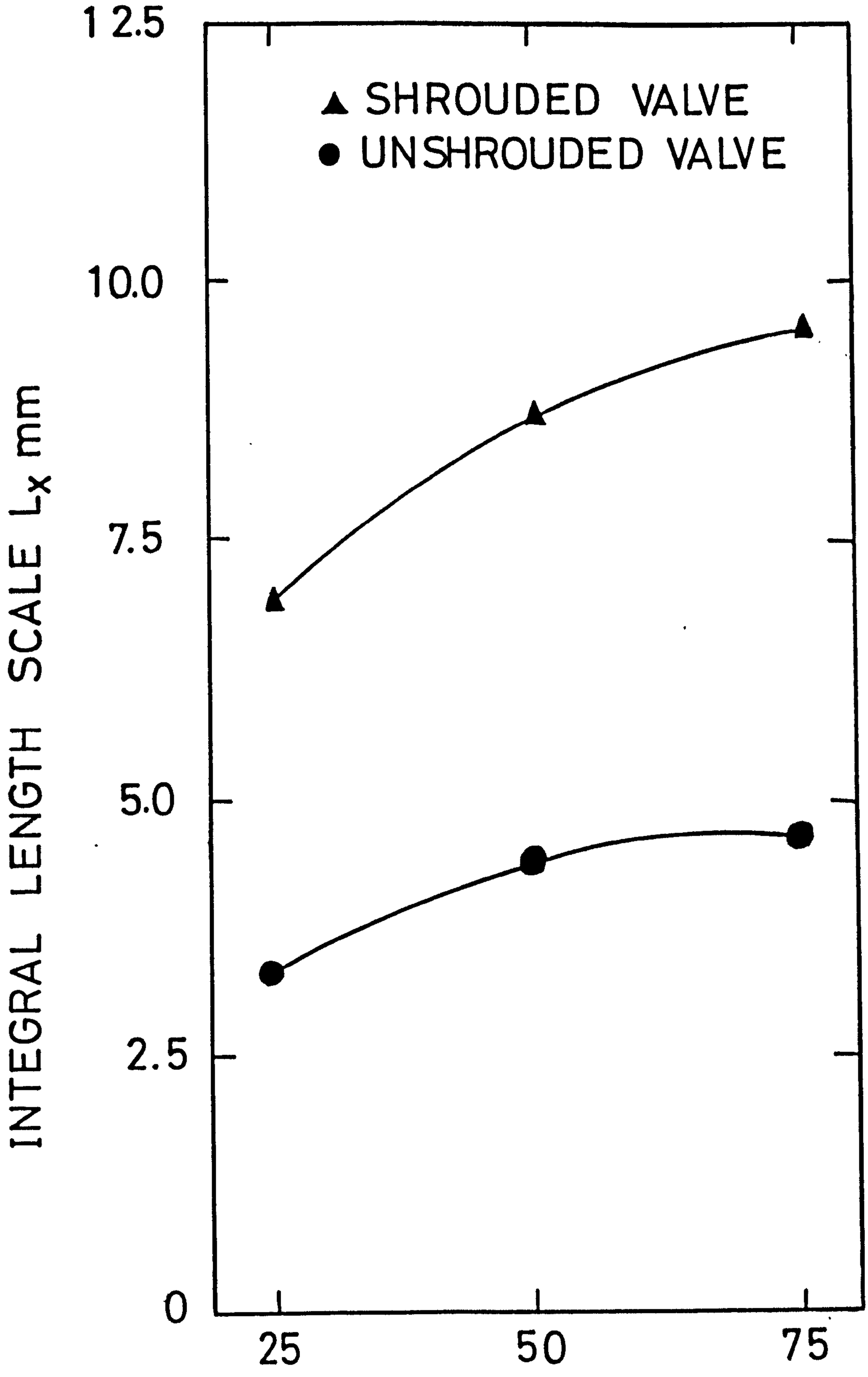

FIG.7.5 VARIATION OF INTEGRAL LENGTH SCALE L_x WITH VOLUMETRIC EFFICIENCY (TAKEN FROM REF.15)

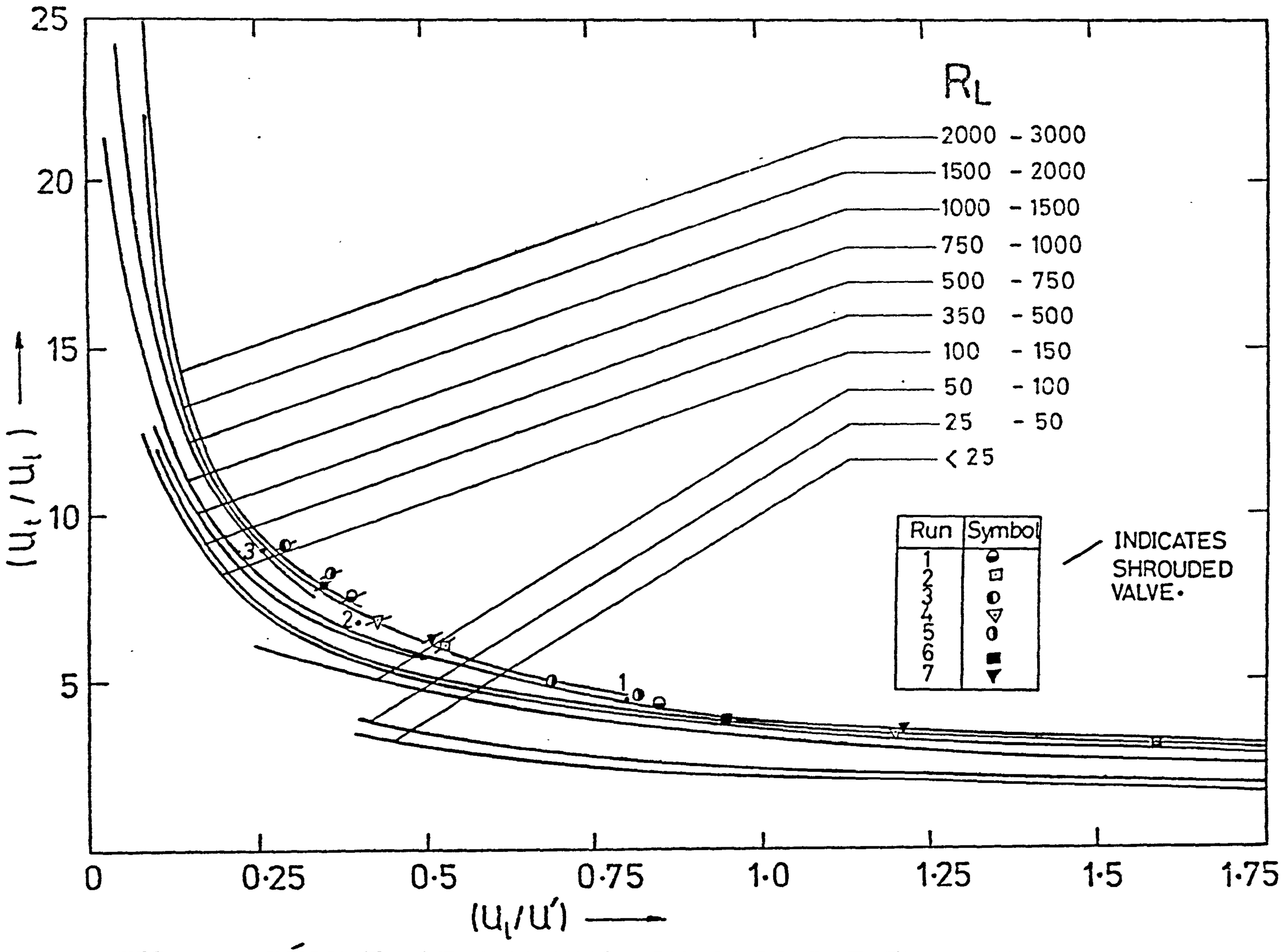

FIG. 7·6 RÉGIME OF BURNING IN GASOLINE ENGINES

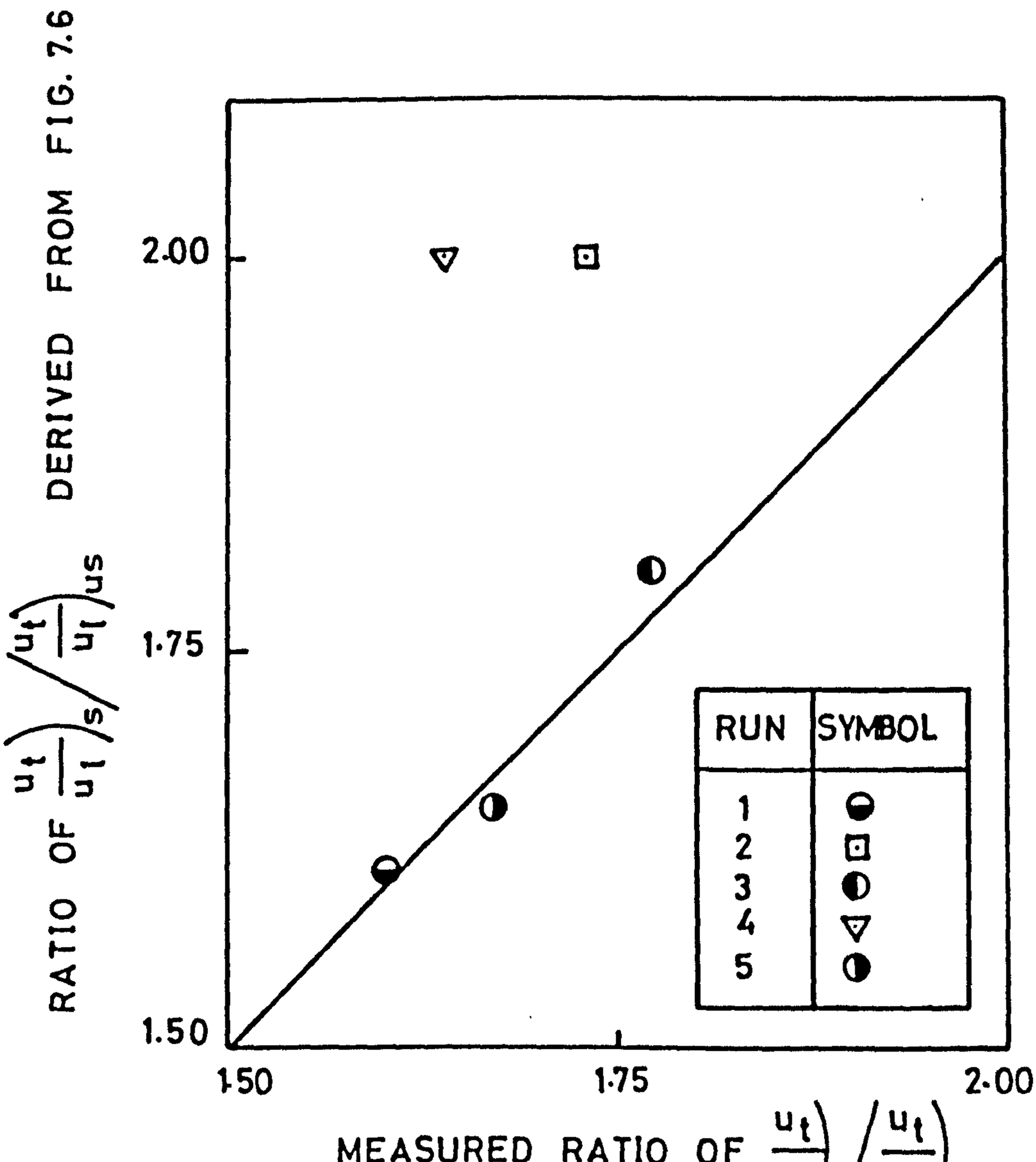

FIG. 7.7 EFFECT OF SHROUDING ON TURBULENT BURNING VELOCITY

CHAPTER 8

CONCLUSIONS

1. A survey of experimental results for non-reacting turbulent flows shows a similar correlation between ϵ_y/ν and either Re or Re_p at the axis of pipes and parallel plate channel respectively, for mass, energy and momentum transfer.

2. For isotropic turbulence a new relationship is proposed between L and λ.

3. Reference to non-reacting turbulent flows suggests a particular relationship between the turbulent transport number, ϵ_y/ν, and turbulent Reynolds number, R_{Ly}.

4. The use of hot wire anemometers in closed vessels, equipped with fans, to obtain turbulence characteristics revealed some practical problems. Limitations were revealed in three different techniques for the measurement of L, primarily because of problems arising from rectification of the signal by the hot wire. It is probable that all values are too low. A greater agreement in values of λ was obtained by the different techniques. There appear to be no problems in obtaining accurate values of u'.

5. Turbulent combustion has been studied experimentally over a wide régime of u_ℓ/u' values. Correlations are shown of u_t/u_ℓ with u_ℓ/u' and R_L.

6. Not all previous experimenters have devoted sufficient attention to the determination of isothermal turbulence parameters. This has resulted in a lack of sufficient

parameters with which to correlate burning velocity results. However, an alternative method of finding u' and L was adopted in cases where circular tube and flat slot burners have been employed. Experimental measurements of integral scale of turbulence and r.m.s. turbulent velocities in non-reacting flows in tubes and between plates were reviewed. Values of $\frac{u'}{U}$ and R_L, with L measured in the transverse direction, were correlated with flow Reynolds numbers, Re and Re_p.

7. The limits of flammability for turbulent methane and hydrogen-air mixtures were determined. Limits were narrowed by an increase in turbulence, but were extended by an increase in spark energy and spark gap. A similar extension was observed when the flame was allowed first to develop under the less turbulent conditions, in a shielded region, before emerging into the fully turbulent region.

8. Theoretical support has been obtained for the use of the three dimensionless parameters employed in correlations of experimental values of turbulent burning velocity. The increasing importance of small eddy burning, as R_L is increased and as u_ℓ/u' is decreased, becomes clear.

9. Important refinements to the theory might include the generation of pdfs, as a function of mean reactedness, for chemical lifetimes and allowance for the changing turbulence through the reaction zone.

10. Theoretical data have been obtained for the variations in turbulent flame thickness.

11. Two theoretical analyses have been employed to obtain the ratio u_t/u_ℓ . In the first approach, laminar flame propagation across a vortex tube was envisaged, whilst in the second the concept of a reaction time in the vortex tube was used. The former would appear to be more valid in the régime where $\eta >> \delta_\ell$, whilst the latter probably is more valid where the laminar flame thickness and Kolmogorov microscale become comparable, or when the former is greater than the latter.

12. In the first approach, the theoretical values of u_t/u_ℓ were obtained on the bases of experimentally determined values of intermittency factors, γ_L and γ_η . In the second approach a volume fraction obtained from available theories of turbulence was employed.

13. Values of u_t/u_ℓ are particularly sensitive to the value of intermittency factor of the small eddies but less so to the value of the factor for large eddies.

14. The experimental measurements of the intermittency factors, show the ratio γ_η/γ_L to increase as R_L increases, whilst the theoretical predictions of the fractional volume occupied by the dissipative eddies, show it to decrease as R_L increases.

15. The use of measured values of intermittencies is not satisfactory in a theoretical analysis and in this

regard the second approach is preferable. The present limited understanding of the physical nature of turbulence creates problems in assigning an accurate value for the volume fraction occupied by the dissipative eddies. Some adjustment of theoretical values for this was necessary to obtain harmony of theory and experiment.

16. Agreement between the theoretical values of u_t/u_ℓ obtained by the second approach and experimental measurements is satisfactory. This approach seems to hold more promise than the first one but the theory is capable of further improvement and more experimental studies are required.

17. Theoretical data have been obtained for the variations in number density of dissipative eddies. This is in accord with experimental measurements.

18. Ignition and flame propagation would be expected to become more difficult as the theoretical ratios $\tau_{c\eta}/\tau_{d\eta}$ and δ_t/L increase. The experimentally measured flammability limits are in accord with this and suggest, for highly turbulent flames, that the limit occurs at $\tau_{c\eta} \sim \tau_{d\eta}$.

19. Comparison of experimental flame propagation limits, and associated flame kernel sizes, with corresponding theoretical values of δ_t/L, suggests that, for highly turbulent flames, a kernel quenches when its diameter is less than approximately four times the flame thickness.

20. More data are required on the unburnt gas turbulent parameters in practical combustors. A knowledge of the value of u_ℓ/u' and R_L in a combustor is valuable in ascertaining practical combustion performance. In the case of lean burning in gasoline engines, it is necessary to generate more turbulence to maintain the same rate of burning in the weak mixture as in the conventional mixture. But high levels of turbulence may not be entirely beneficial to lean mixture combustion because of ignition and flame flammability limitations.

21. It is possible by charge stratification, with an easily ignitable mixture at the spark, to facilitate ignition and burning up to a point where the increases of pressure and temperature are sufficent to so increase u_ℓ that leaner burning becomes possible.

APPENDICES

APPENDIX 1

THE MIXTURES PROGRAMME

APPENDIX 1

THE MIXTURES PROGRAMME

A1.1 DETERMINATION OF THE PROPERTIES OF A MIXTURE FROM THOSE OF INDIVIDUAL CONSTITUENTS

This programme was developed by Draper (1), but it was decided to include a brief description of it for completeness. However, a more complete description is given in Ref.1.

Any homogeneous mixture of gases can be regarded as a single substance if the constituents do not react chemically with one another and are in a fixed proportion by weight. The properties of such a mixture can then be determined as follows:

A1.1.1 Density

At any temperature and pressure, the density, ρ_m, of the mixture was obtained from:

$$\rho_m = \sum_{i=1}^{i=s} \rho_i \qquad \text{(A1.1)}$$

where ρ_i is the density of the constituent, i, and is given by:

$$\rho_i = \frac{P_i}{TR_i} = \frac{P}{T\bar{R}} x_i M_i \qquad \text{(A1.2)}$$

where P is the pressure of the mixture

T is the temperature of the mixture

$\bar{R}$ is the universal gas constant

x_i is the mole fraction of constituent i

M_i is the molecular weight of constituent i

and s is the number of constituents in a mixture.

Substitution for ρ_i in Eq. (A1.1) gives:

$$\rho_m = \frac{P}{T\bar{R}} \sum_{i=1}^{i=s} x_i M_i \qquad \text{(A1.3)}$$

A1.1.2 Specific Heat

At any temperature and 1 atmosphere, the specific heat, C_{p_m}, is given by:

$$C_{p_m} = \sum_{i=1}^{i=s} m_i C_{p_i} \qquad \text{(A1.4)}$$

C_{p_i} is the specific heat of constituent i,

and m_i is the mass fraction of constituent i, and is given by:

$$m_i = \frac{x_i M_i}{\sum_{i=1}^{i=s} x_i M_i} \qquad \text{(A1.5)}$$

That is $$C_{p_m} = \frac{\sum_{i=1}^{i=s} x_i M_i C_{p_i}}{\sum_{i=1}^{i=s} x_i M_i} \qquad \text{(A1.6)}$$

A1.1.3 Viscosity

At any temperature, the viscosity of a mixture, μ_m, is given by Wilke (2) as being:

$$\mu_m = \sum_{i=1}^{i=s} \frac{\mu_i}{1 + \frac{1}{x_i} \sum_{\substack{j=1 \\ j \neq i}}^{j=s} x_j \Phi_{ij}} \qquad \text{(A1.7)}$$

where Φ_{ij} is given by equation:

$$\Phi_{ij} = \frac{\left[1 + (\mu_i/\mu_j)^{\frac{1}{2}} (M_j/M_i)^{\frac{1}{4}}\right]^2}{(8)^{\frac{1}{2}} \left[1 + (M_i/M_j)\right]^{\frac{1}{2}}} \qquad \text{(A1.8)}$$

where μ_i and μ_j are viscosities of pure components.

A1.1.4 Thermal Conductivity

At any temperature, the thermal conductivity of the mixture, k_m, is given by Mason and Saxena (3) as being:

$$k_m = \sum_{i=1}^{i=s} \frac{k_i}{1 + \frac{1}{x_i} \sum_{\substack{j=1 \\ j \neq i}}^{j=s} x_j G_{ij}} \qquad \text{(A1.9)}$$

where G_{ij} is given by the equation:

$$G_{ij} = \frac{1.065}{(8)^{\frac{1}{2}}} \left[1 + \frac{M_i}{M_j}\right]^{-\frac{1}{2}} \left[1 + \left(\frac{\mu_i M_j}{\mu_j M_i}\right)^{\frac{1}{2}} \left(\frac{M_i}{M_j}\right)^{\frac{1}{4}}\right]^2 \qquad \text{(A1.10)}$$

Equation (A1.10) may be written as:

$$G_{ij} = 1.065 \frac{\left[1 + (\mu_i/\mu_j)^{\frac{1}{2}}(M_j/M_i)^{\frac{1}{4}}\right]^2}{(8)^{\frac{1}{2}}\left[1 + (M_i/M_j)\right]^{\frac{1}{2}}} \qquad \text{(A1.11)}$$

Comparison of Eqs. (A1.8) and (A1.11) shows that:

$$G_{ij} = 1.065\Phi_{ij} \qquad \text{(A1.12)}$$

On substituting for G_{ij} in Eq.(A1.9), k_m then becomes:

$$k_m = \sum_{i=1}^{i=s} \frac{k_i}{1 + 1.065 \frac{1}{x_i} \sum_{\substack{j=1 \\ j\neq i}}^{j=s} x_j \Phi_{ij}} \qquad \text{(A1.13)}$$

A1.2 BRIEF DESCRIPTION OF THE PROGRAMME

The programme, named MIXTURES, was written to obtain the density (Kgm^{-3}), specific heat at constant pressure ($J\ Kg^{-1}\ {}^{o}K^{-1}$), viscosity ($N\ s\ m^{-2}$), thermal conductivity ($J\ m^{-1}\ s^{-1}\ {}^{o}K^{-1}$), enthalpy ($J\ kg\ mole^{-1}$) and entropy ($J\ Kg\ mole^{-1}\ {}^{o}K^{-1}$) of any gas mixture from the equations given in A1.1 at atmospheric pressure. These values were determined at different temperatures. The input data are in a convenient form, and require little knowledge of the programme operation. A four figure table is produced for the required property in $10^{o}K$ increments. The operator may select which properties are to be calculated. The data for pure gases were obtained from Svehla (4).

The mixture properties are given the code numbers: 1 for density, 2 for specific heat at constant pressure,

3 for viscosity, 4 for absolute enthalpy and 5 for entropy.

A1.2.1 Language

Algol 60.

A1.2.2 Input Data

The data to be read into the programme are as follows:

(1) The number of gas components present.

(2) The number of gas components required.

(3) The pressure of the mixture in atmosphere.

(4) The code numbers of mixture properties required (as set out in the description above).

(5) The volume percentage of each gas component.

A1.2.3 Output Data

The output is in the form of tables resembling normal four figure mathematical tables, with a difference column. The tables are mainly self-descriptive, the title and units being outputed prior to the main table.

The keywords in the output are: PROPERTIES OF MIXTURE, MOLECULAR WEIGHT OF MIXTURE, DENSITY, VISCOSITY, THERMAL CONDUCTIVITY, SPECIFIC HEAT, ABSOLUTE ENTHALPY and ENTROPY.

A1.2.4 The contents of MIXDATA File

The coefficients of the various polynomials used to

fit the properties of each gas can be accessed by listing the datafile MIXDATA.

These polynomials were either obtained from Prothero (5) and Watson (6) or fitted from Svehla (4).

A1.2.5 Modification to MIXDATA

Should a chemical compound be presented to the programme which does not occur in its "library" of compounds at the beginning of the MIXDATA file, the message

CHEMICAL SYMBOL NOT IN LIBRARY OF COMPOUNDS

is printed on the output from the programme, and the programme is terminated. Should the information for this mixture still be required, the file can easily be modified if the tabulated data are available for that component.

To help the user, a short programme and macro command has been written which will take in the raw data and convert it into a series of polynomials, followed by their inclusion in MIXDATA, so that all the user does is present the commands

```
JOB INMOD,:MEICOMB
IN MODATA,T£££(TG :MANGER ALL)
the data
££££
GASMACRO
****
```

This will prepare the programme for use with the "unknown" gas.

A1.3 THE PROGRAMME MIXTURES

```
'LIBRARY' (ED, SUBGROUPNAGA)
'PMD' (ED, COFFIN)
'INPUT' 0=CR0
'INPUT' 1=CR1
'OUTPUT' 0=LP0
'TRACE' 2
'BEGIN'
   'COMMENT' THE PROGRAM CALCULATES DENSITY, SPECIFIC HEAT,
   VISCOSITY AND THERMAL CONDUCTIVITY OF ANY NUMBER OF  COMPONENTS OF
   GAS MIXTURES AT DIFFERENT TEMPERATURES;
'REAL'
   T, SAVE, HOLD, Z, E, E1, E2, Y, W, MOLM, X, A0, A, B0, B, C,
   PRESS;
'INTEGER'
   I, J, NUM, F1, F2, F3, F4, TOT, IFAIL, H, NOTAB, F5, F6, F7, F8,
   IT, MAX;
'ARRAY'
   LIBCOMP[1:100, 1:10], TABLE[1:10], ASAVE[1:100];
'REAL' 'PROCEDURE' INSYMB(A);
   'ARRAY'
      A;
   'BEGIN'
   'INTEGER'
      I, J;
   'BOOLEAN'
      L, K;
   K:= L:= 'TRUE';
   'FOR' I:= 1 'STEP' 1 'UNTIL' 100 'DO'
     'FOR' J:= 1 'STEP' 1 'UNTIL' 10 'DO'
        'BEGIN'
```

```
  A[I, J]:= READCH;
RPE:
  'IF' NEXTCH = CODE('('SS')') 'OR' NEXTCH = CODE('('E
  L')') 'THEN'
     'BEGIN'
     SKIPCH;
     'GO TO' RPE;
     'END';
  'IF' NEXTCH = CODE('(',')') 'THEN'
     'BEGIN'
     A[I, J + 1]:= - 2;
     J:= 10;
     SKIPCH;
     'END'
  'ELSE' 'IF' NEXTCH = CODE('(';')') 'THEN'
     'BEGIN'
     A[I, J + 1]:= - 2;
     J:= 10;
     INSYMB:= I;
     I:= 100;
     SKIPCH;
     'END';
  'END';
'END';
MAX:= READ;
NUM:= READ;
PRESS:= READ;
SELECTINPUT(1);
TOT:= INSYMB(LIBCOMP);
'BEGIN'
```

```
'ARRAY'
   M, MOL, SOB, HOB, HF, SO[1:MAX], MZ[1:TOT], MUE, K, CP, RO, HC,
   SC[1:MAX, 0:6], CHEMSYM[1:MAX, 1:10], GASDATA[1:TOT, 1:4, 0:6];

'BOOLEAN' 'ARRAY'
   BBE[1:TOT], BEATTIE[1:MAX];
'PROCEDURE' C05AAA(A, B, EPS, ETA, F, X, IFAIL);
   'VALUE'
      A, B, EPS, ETA;
   'INTEGER'
      IFAIL;
   'REAL'
      A, B, EPS, ETA, F, X;
   'ALGOL';
'PROCEDURE' PRINTOUT(X);
   'VALUE'
      X;
   'REAL'
      X;
   'IF' ABS(X) > 1000 'THEN'
      WRITE(0, F5, X)
   'ELSE' 'IF' ABS(X) > 100 'THEN'
      WRITE(0, F6, X)
   'ELSE' 'IF' ABS(X) > 10 'THEN'
      WRITE(0, F7, X)
   'ELSE'
      WRITE(0, F8, X);
'PROCEDURE' TABULATE(N);
   'VALUE'
      N;
```

```
  'INTEGER'
     N;
  'BEGIN'
  'SWITCH' S1:=
     L10, L11, L12, L13, L14, L15;
  'SWITCH' S2:=
     L20, L21, L22, L23, L24, L25;
  'GO TO' S1[N];
L10:
  WRITETEXT('('('('C')'%%DENSITY%%%%%%%%KG/M↑3'('CC')'')');
  'GO TO' FINI;
L11:
  WRITETEXT('('('('C')'%%SPECIFIC%HEAT%AT%CONSTANT%PRESSURE%%%%
  %%%%KJ/KG.DEG.K'('2C')'')');
  'GO TO' FINI;
L12:
  WRITETEXT('('('('C')'%%VISCOSITY%%%%%%%%N.S/M↑2'('2C')'')');
  'GO TO' FINI;
L13:
  WRITETEXT('('('('C')'%%THERMAL%CONDUCTIVITY%%%%%%%
  %J/M.S.DEG.K*10↑3'('2C')'')');
  'GO TO' FINI;
L14:
  WRITETEXT('('('('C')'%%ABSOLUTE%%ENTHALPY%%%%%%%
  %MEGAJ/KG.MOL'('2C')'')');
  'GO TO' FINI;
L15:
  WRITETEXT('('('('C')'%%ENTROPY%%%%%%%
  %KJ/KG.MOL.DEG.K.'('2C')'')');
  'GO TO' FINI;
```

```
FINI:
  WRITETEXT('('%%T%%*%%
  %0'('7S')'10'('6S')'20'('6S')'30'('6S')'40'('6S')'50'('6S')'6
  0'('6S')'70'('6S')'80'('6S')'90%%%'('C')'%%200*'('56S')'')');
  T:= 270;
  'COMMENT' TEMPERATURE STARTS AT 270 DEG K AND IS STEPPED  IN
  INTERVALS OF 10 DEG K TO 2000 DEG K;
  'FOR' I:= 7 'STEP' 1 'UNTIL' 199 'DO'
     'BEGIN'
     E:= 0;
     'GO TO' S2[N];
   L20:
     DENSITY;
     'GO TO' EX;
L21:
   CPCT;
   'GO TO' EX;
L22:
L23:
   MUECT(N);
   'GO TO' EX;
L24:
   ENTHALPY;
   'GO TO' EX;
L25:
   'IF' I = 7 'THEN'
      'FOR' H:= 1 'STEP' 1 'UNTIL' NUM 'DO'
         'BEGIN'
         'FOR' J:= 0 'STEP' 1 'UNTIL' 6 'DO'
            'IF' J = 0 'THEN'
```

```
                SC[H, 0]:= CP[H, 0]
             'ELSE'
                SC[H, J]:= CP[H, J] / J;
          POLY(HOLD, T / 1000, SC, H, 0, 6);
          SOB[H]:= HOLD + SC[H, 0] * (LN(0.293) - 1);
          'END';
   ENTROPY;
EX:
   'IF' I = 7 'THEN'
      E1:= E * W;
   T:= 200 + 10 * (I + 1);
   'IF' (I + 1) '/' 10 * 10 = I + 1 'THEN'
      'BEGIN'
         NEWLINE(1);
         'IF' I # 199 'THEN'
            WRITE(0, F2, T);
         WRITETEXT('('*')');
         'END';
      'END';
   'IF' N = 1 'AND' H = - 1 'THEN'
      'BEGIN'
      WRITETEXT('('''('C')'NOTE%THAT%THE%FOLLOWING%GASES%HAVE
      %BEEN%TREATED%AS%PERFECT%GASES%(%THE%BEATTIE-BRIDGEMAN
      %CONSTANTS%ARE%NOT%AVAILBLE)'('C')''')');
      'FOR' I:= 1 'STEP' 1 'UNTIL' 100 'DO'
         PRINTCH(ASAVE[I]);
      NEWLINE(2);
      'END';
   'END' OF PROCEDURE TABULATE;
'PROCEDURE' SYMBOL(A);
```

```
'ARRAY'
   A;
'BEGIN'
'INTEGER'
   K, J;
'BOOLEAN'
   L;
L:= 'TRUE';
'FOR' K:= 1 'STEp' 1 'UNTIL' 10 'DO'
   'BEGIN'
 RPA:
   'IF' NEXTCH = 16 'OR' NEXTCH = CODE('('EL')') 'THEN'
      'BEGIN'
      SKIPCH;
      'GO TO' RPA;
      'END';
   A[I, K]:= READCH;
   PRINTCH(A[I, K]);
   'IF' NEXTCH = CODE('(',')') 'THEN'
      'BEGIN'
      J:= K;
      K:= 10;
      SKIPCH;
      'END';
   'END';
A[I, J + 1]:= - 1;
'END';
'PROCEDURE' COMPARE(A, B, TOT);
   'VALUE'
      TOT;
```

```
'INTEGER'
   TOT;
'ARRAY'
   A, B;
'BEGIN'
'INTEGER'
   H, J;
'BOOLEAN'
   K, L;
L:= 'TRUE';
K:= 'FALSE';
'FOR' H:= 1 'STEP' 1 'UNTIL' TOT 'DO'
   'BEGIN'
   'FOR' J:= 1 'STEP' 1 'UNTIL' 10 'DO'
      'IF' A[I, J] = B[H, J] 'THEN'
         K:= 'TRUE'
      'ELSE' 'IF' A[I, J] = - 1 'THEN'
         J:= 10
      'ELSE'
         'BEGIN'
         K:= 'FALSE';
         J:= 10;
         'END';
   'IF' K 'THEN'
      'BEGIN'
      X:= H;
      H:= TOT;
      'END';
   'END';
'IF' K 'THEN'
```

```
        H:= H
    'ELSE'
        'BEGIN'
        WRITETEXT('('('C')'CHEMICAL%SYMBOL%NOT%IN%LIBRARY%OF
        %COMPOUNDS.%%%PLEASE%CHECK%YOUR%DATA.'('C')'IF%THE
        %COMPOUND%SYMBOL%IS%CORRECT%THE%DATA%FOR%THIS%GAS%WILL
        %REQUIRE%INPUTTING%INTO%THE%DATAFILE.'('2C')''('20')'THIS
        %IS%EASY'('2C')'SEE%THE%WRITE%UP%IN%THE%LIBRARY%OF
        %COMBUSTION%PROGRAMS%KEPT%IN%ROOM%434.')');
        X:= - 1;
        'END';
    'END';
'REAL' 'PROCEDURE' FUNCT(XX);
    'VALUE'
        XX;
    'REAL'
        XX;
    'BEGIN'
    'REAL'
        BETA, GAMMA, DELTA, DD;
    DD:= C / (T * T);
    BETA:= 0.08206 * (T * BO - DD) - AO;
    GAMMA:= 0.08206 * BO * (B * T - DD) - AO * A;
    DELTA:= 0.08206 * BO * B * DD;
    FUNCT:= DELTA + XX * (GAMMA + XX * (BETA + XX * (0.08206 * T
    - XX * PRESS)));
    'END';
'PROCEDURE' DENSITY;
    'BEGIN'
    'INTEGER'
```

```
   I, J, U;
'BEGIN'
   W:= 1;
   U:= 0;
   'FOR' I:= 1 'STEP' 1 'UNTIL' NUM 'DO'
      'BEGIN'
      'IF' T = 270 'AND' RO[I, 0] = 0 'AND' RO[I, 2] =
      0 'THEN'
         'BEGIN'
         H:= - 1;
         'FOR' J:= 1 'STEP' 1 'UNTIL' 10 'DO'
            'BEGIN'
         ASAVE[J + U]:= CHEMSYM[I, J];
         'IF' CHEMSYM[I, J + 1] = - 1 'THEN'
            'BEGIN'
            ASAVE[J + U + 1]:= CODE('(',')');
            U:= U + J + 1;
            J:= 10;
            'END';
         'END';
   'FOR' J:= U 'STEP' 1 'UNTIL' 100 'DO'
      ASAVE[J]:= 16;
   'END';
'IF' BEATTIE[I] 'THEN'
   'BEGIN'
   AO:= RO[I, 0];
   A:= RO[I, 1];
   BO:= RO[I, 2];
   B:= RO[I, 3];
   C:= RO[I, 4] * 10000;
```

```
            IFAIL:= 1;
            C05AAA(0.08206 * T * 0.5, 0.08206 * T * 3, 1&-6,
            1&-40, FUNCT(HOLD), HOLD, IFAIL);
            HOLD:= M[I] / HOLD;
            'IF' IFAIL = 1 'THEN'
               J:= 1 / (IFAIL - 1);
            'END'
         'ELSE'
            POLY(HOLD, 1000 / T, RO, I, 0, 4);
         'IF' BEATTIE[I] 'THEN'
            E:= HOLD * MOL[I] + E
         'ELSE'
            E:= HOLD * MOL[I] * PRESS + E;
         'END';
      PRINTOUT(E);
   'END';
'PROCEDURE' ENTHALPY;
   'BEGIN'
   'INTEGER'
      I, J;
   W:= 0.1;
   E:= 0;
   'IF' T = 270 'THEN'
      'FOR' I:= 1 'STEP' 1 'UNTIL' NUM 'DO'
         'BEGIN'
         'FOR' J:= 0 'STEP' 1 'UNTIL' 6 'DO'
            HC[I, J]:= CP[I, J] / (J + 1);
         POLY(HOB[I], T / 1000, HC, I, 1, 6);
         'END';
```

```
    'FOR' I:= 1 'STEp' 1 'UNTIL' NUM 'DO'
       'BEGIN'
       POLY(HOLD, T / 1000, HC, I, 1, 6);
       E:= E + MOL[I] * 4.1868 * (HOLD - HOB[I] + HF[I] / 1000);

       'END';
    PRINTOUT(E)
    'END';
'PROCEDURE' ENTROPY;
    'BEGIN'
    'INTEGER'
       I, J;
    W:= 1;
    E:= SAVE:= 0;
    'FOR' I:= 1 'STEp' 1 'UNTIL' NUM 'DO'
       'BEGIN'
       POLY(HOLD, T / 1000, SC, I, 0, 6);
       E:= E + ((HOLD + SC[I, 0] * (LN(T / 1000) - 1) + SO[I] -
       SOB[I]) * 4.1868 - 8.31434 * LN(MOL[I])) * MOL[I] - 8.31434
       * MOL[I] * LN(PRESS);
       'END';
    PRINTOUT(E);
    'END';
'PROCEDURE' CPCT;
    'BEGIN'
    'COMMENT' THIS PROCEDURE CALCULATES THE SPECIFIC HEATS;
    'INTEGER'
       I;
    SAVE:= 0;
    W:= 1;
```

```
    'FOR' I:= 1 'STEp' 1 'UNTIL' NUM 'DO'
       SAVE:= SAVE + MOL[I] * M[I];
    'FOR' I:= 1 'STEp' 1 'UNTIL' NUM 'DO'
       'BEGIN'
       POLY(HOLD, T / 1000, CP, I, 0, 6);
       E:= E + MOL[I] * HOLD * 4.1868;
       'END';
    E:= E / SAVE;
    PRINTOUT(E);
    'END' OF PROCEDURE CpCT;
'PROCEDURE' pOLY(VAR, X, A, I, C, M);
    'VALUE'
       X, I, M, C;
    'REAL'
       VAR, X;
    'INTEGER'
       I, M, C;
    'ARRAY'
       A;
    'BEGIN'
    'INTEGER'
       J;
    VAR:= 0;
    'FOR' J:= 0 'STEP' 1 'UNTIL' M 'DO'
       VAR:= VAR + A[I, J] * X↑(J + C);
    'END';
'PROCEDURE' MUECT(L);
    'VALUE'
       L;
    'INTEGER'
```

```
   L;
'BEGIN'
'INTEGER'
   I, J;
'FOR' I:= 1 'STEP' 1 'UNTIL' NUM 'DO'
   'IF' MOL[I] # 0 'THEN'
      'BEGIN'
      SAVE:= 0;
      'IF' L = 3 'THEN'
         W:= 0.1
      'ELSE'
         W:= 1;
      'FOR' J:= 1 'STEP' 1 'UNTIL' I - 1,
         I + 1 'STEP' 1 'UNTIL' NUM 'DO'
      'IF' MOL[J] # 0 'THEN'
         SAVE:= SAVE + MOL[J] * PHI(I, J);
'COMMENT' THE FACTOR Z CONVERTS FROM VISCOSITY TO
THERMAL CONDUCTIVITY;
'IF' L = 3 'THEN'
   'BEGIN'
   Z:= 1;
   POLY(HOLD, 100 / T, MUE, I, 0, 6);
   HOLD:= SQRT(T) / HOLD;
   'END'
'ELSE'
   'BEGIN'
   Z:= 1.065;
   POLY(HOLD, T / 1000, K, I, 0, 6);
   HOLD:= HOLD * 0.41868;
   'END';
```

```
            E:= E + HOLD / (1 + Z / MOL[I] * SAVE);
            'END';
      PRINTOUT(E);
      'END' OF PROCEDURE MUECT;
'REAL' 'PROCEDURE' PHI(I, J);
      'VALUE'
         I, J;
      'INTEGER'
         I, J;
      'BEGIN'
      'COMMENT' THIS PROCEDURE CALCULATES THE PHI FACTOR IN WILKES
      EQUATION;
      'REAL'
         A, B;
      POLY(A, 100 / T, MUE, I, 0, 6);
      A:= SQRT(T) / A;
      POLY(B, 100 / T, MUE, J, 0, 6);
      B:= SQRT(T) / B;
      PHI:= (1 + SQRT(A / B * SQRT(M[J] / M[I])))↑2 / (2.8285 *
      SQRT(1 + M[I] / M[J]));
      'END' OF PROCEDURE PHI;
'COMMENT' THIS IS THE MAIN CALCULATION BLOCK;
F1:= FORMAT('('NDD.DOOS')');
F2:= FORMAT('('-NDDD')');
F3:= FORMAT('('-ND')');
F4:= FORMAT('('NDD.DO')');
F5:= FORMAT('('-NDDD.DS')');
F6:= FORMAT('('-NDD.DDS')');
F7:= FORMAT('('-ND.DDDS')');
F8:= FORMAT('('-D.DDDDS')');
```

```
'FOR' I:= 1 'STEP' 1 'UNTIL' TOT 'DO'
   'BEGIN'
 CTU:
   SKIPCH;
   'IF' NEXTCH # CODE('(':')') 'THEN'
      'GO TO' CTU
   'ELSE'
      SKIPCH;
   MZ[I]:= READ;
   BBE[I]:= READBOOLEAN;
   'FOR' J:= 1 'STEP' 1 'UNTIL' 4 'DO'
      'FOR' H:= 0 'STEP' 1 'UNTIL' 6 'DO'
         GASDATA[I, J, H]:= READ;
   'END';
  SELECTINPUT(0);
LOOP:
  'FOR' I:= 1 'STEP' 1 'UNTIL' 10 'DO'
     'BEGIN'
     TABLE[I]:= READ;
     'IF' NEXTCH = CODE('('#')') 'THEN'
        'BEGIN'
        NOTAB:= I;
        SKIPCH;
        I:= 10;
        'END';
     'END';
RPT:
  WRITETEXT('('('30S')'PROPERTIES%OF%MIXTURE'('C')')');
  'FOR' I:= 1 'STEP' 1 'UNTIL' NUM 'DO'
     'BEGIN'
```

```
SYMBOL(CHEMSYM);
WRITETEXT('('%:%%')');
SAVE:= READ;
WRITE(0, F4, SAVE);
SPACE(10);
MOL[I]:= SAVE / 100;
'IF' I '/' 4 * 4 = I 'THEN'
   NEWLINE(1);
COMPARE(CHEMSYM, LIBCOMP, TOT);
'IF' X = - 1 'THEN'
   'GO TO' TERMINATE;
'FOR' J:= 0 'STEP' 1 'UNTIL' 6 'DO'
   'BEGIN'
   'IF' J < 5 'THEN'
      RO[I, J]:= GASDATA[X, 1, J];
      CP[I, J]:= GASDATA[X, 2, J];
      MUE[I, J]:= GASDATA[X, 3, J];
      K[I, J]:= GASDATA[X, 4, J];
      'END';
   HF[I]:= GASDATA[X, 1, 5];
   SO[I]:= GASDATA[X, 1, 6];
   M[I]:= MZ[X];
   BEATTIE[I]:= BBE[X];
   'END';
E:= 0;
WRITETEXT('('('C')'MOLECULAR%WEIGHT%OF%MIXTURE=')');
'FOR' I:= 1 'STEP' 1 'UNTIL' NUM 'DO'
   E:= E + M[I] * MOL[I];
WRITE(0, F4, E);
MOLM:= E;
```

```
'FOR' IT:= 1 'STEP' 1 'UNTIL' NOTAB 'DO'
   TABULATE(TABLE[IT]);
'IF' NEXTCH = CODE('('R')') 'THEN'
   'BEGIN'
   PAPERTHROW;
   SKIPCH;
   'GO TO' RPT;
   'END'
'ELSE' 'IF' NEXTCH = CODE('('S')') 'THEN'
   'BEGIN'
   PAPERTHROW;
   SKIPCH;
   NUM:= READ;
   PRESS:= READ;
   'GO TO' LOOP;
      'END';
   'END';
TERMINATE:
'END'
```

A1.4 THE DATAFILE MIXDATA1

```
0. C6H6,AR,HE,H2,O2,N2,CO,CO2,H2O,CH4;
1. *
2. C6H6: 7.81100& +1;'TRUE'
3. 0.00000& +0; 0.00000& +0; 0.00000& +0; 0.00000& +0; 0.00000& +0;-2.48910& +4; 6.43550& +1;
4. 1.65050& +0; 6.84460& +1;-2.95660& +0;-2.37040& +1; 3.74030& +0; 4.84570& +0;-1.41470& +0;
5. 8.79484& -1; 5.53778& +0;-1.65651& +1; 7.78505& +1;-6.23918& +1;-4.75937& +2; 8.95025& +2;
6. 7.94059& +0;-1.18839& +2; 8.06978& +2;-8.31176& +2; 4.48199& +2;-1.25953& +2; 1.44750& +1;
7. AR:39.944,'TRUE'
8. 1.2907,0.02328,0.03931,0,5.99,0,36.983,
9. 4.9681,0,0,0,0,0,0,
10. 0.41974233,2.2568869,-9.853673,27.792396,-27.943493,0,0,
11. 4.462848,150.2578,-89.8525,40.00906,-7.009794,0,0,
12. HE:4.003,'TRUE'
13. 0.0216,0.05984,0.014,0.00,0.004,0,0,
14. 4.9681,0,0,0,0,0,0,
```

```
15. 0.45217235,3.5591461,-15.376631,36.663014,-33.851656,0,0,
16. 84.93506,1177.921,-804.4561,532.049,-194.2285,28.72471,0,
17. H2:2.016,'TRUE'
18. 0.1975,-0.00506,0.02096, -0.04359,0.0504,0,31.208,
19. 6.183042,4.710657,-10.92135,12.54086,-7.016263, 1.923395,-0.2084091,
20. 1.0745515,6.5691392,-19.63902,22.851072,0,0,0,
21. 106.7697,1455.1822,-1222.765,1026.896,-403.866,59.92994,0,
22. 02:32,'TRUE'
23. 1.4911,0.02562,0.04624,0.004208,4.8,0,49.004,
24. 7.361141,-5.369589,20.54179,-25.86526,15.94566,-4.858890,0.5861501,
25. 0.47682327,2.7856246,-15.410077,51.909942,-63.049470,0,0,
26. 10.13991,179.1933,34.02138,-77.21173,38.78089,-6.430318,0,
27. N2:28.02,'TRUE'
28. 1.3445,0.02617,0.05046,-0.00691,4.2,0,45.770,
29. 7.709928,-5.503897,13.12136,-11.67955,5.233997,-1.173185,0.103883,
```

```
30. 0.57956129,2.8474859,-13.232490,37.106107,-37.549675,0,0,
31. 10.00609,212.26,-150.6055,142.0527,-66.38042,11.44726,0,
32. CO:28.01,'TRUE'
33. 1.3445,0.02617,0.05046,-0.00691,4.2,-26417.0,47.214,
34. 7.812249,-6.668293,17.28296,-17.28709,8.860125,-2.314819,0.2447785,
35. 0.570144,3.453801,-18.73535,58.54447,-67.39072,0,0,
36. 12.47864,178.4064,-34.05928,9.307403,-1.708599,0,0,
37. CO2:44.01,'TRUE'
38. 5.0065,0.07132,0.10476,0.07235,66,-94054,51.072,
39. 4.324933,20.80895,-22.94590,16.84483,-7.935665,2.121672,-0.2408713,
40. 0.6247357,1.40257,0.55316129,0,0,0,0,
41. -12.40077,190.9057,-5.093014,-17.60527,4.657475,0,0,
42. H20:18.02,'TRUE'
43. 0,0,0,0,0,-57798.0,45.106,
44. 7.98886,-1.506271,6.661376,-4.655970,1.696464,-0.3706212,0.03992444,
```

```
45. 0.478231,3.611226,8.069244,-44.26806,51.97652,0,0,
46. 15.89631,136.1396,146.383,1.094772,-29.17123,6.649056,0,
47. CH4:16.04,'TRUE'
48. 2.2769,0.01855,0.05587,-0.01587,12.83,-17895,44.49,
49. 7.916404,-11.41722,63.73457,-75.25691,43.29269,-12.56732,1.469695,
50. 0.86778759,3.7839125,-14.473411,42.547274,-44.474225,0,0,
51. 17.42152,89.59157,541.2368,-299.6113,53.82444,0,0,
```

A1.5 NOMENCLATURE

C_p specific heat at constant pressure

k thermal conductivity

m mass fraction

M molecular weight

P pressure

$\bar{R}$ universal gas constant

s number of constituents in a mixture

T temperature

x mole fraction

μ viscosity

ρ density

Subscripts

m mixture

A1.6 REFERENCES

1. M.S.DRAPER, Mathematical modelling of a jet stirred combustor, Ph.D.thesis, Dept. Mechanical Engineering, Univ.Leeds (1977).

2. C.R.WILKE, A viscosity equation for gas mixtures, J.Chem.Phys. 18, 517 (1950).

3. E.A.MASON and S.C.SAXENA, Approximate formula for the thermal conductivity of gas mixtures, Phys.Fluids 1, 361 (1958).

4. R.A.SVEHLA, Estimated viscosities and thermal conductivities of gases at high temperatures, NASA TR 132 (1962).

5. A.PROTHERO, Computing with thermochemical data, Combustion and Flame 13, 399 (1969).

6. J.T.R. WATSON, Viscosities of gases in metric units, N.E.L., H.M.S.O. (1972).

APPENDIX 2

TURBULENT TRANSPORT NUMBER AND TURBULENT REYNOLDS NUMBER AT DIFFERENT RADII FOR PIPE FLOW

APPENDIX 2

TURBULENT TRANSPORT NUMBER AND TURBULENT REYNOLDS NUMBER AT DIFFERENT RADII FOR PIPE FLOW

In Chapter 2, a relationship was proposed between turbulent transport number, ε/ν, and turbulent Reynolds number, R_L, for isotropic turbulence. This is given by Eq.(2.20) which was derived from available measurements of turbulent diffusivity and turbulent parameters at pipe centrelines, where flow is considered to be isotropic. This relationship was applied in Chapter 5 at half radius. In this appendix a justification for this is demonstrated and the validity of Eq.(2.20) is examined away from the centre-line.

A2.1 DESCRIPTION OF THE PROGRAMME

The programme, named NORRL, was written to obtain the variation of ε/ν with R_L at different radius ratios, ($a = r/R$), between 0 and 0.9. The procedure used is similar to that used in Chapter 2 to obtain Eq. (2.20), in which Richardt's expression, Eq.(2.3), was used for the relation between ε/ν and Re at different radius ratio.

A literature survey for the measurements of turbulent parameters in pipes shows that some workers (1-4) used the hot wire anemometer for measuring r.m.s. turbulent

velocity in all the three directions at different radius ratios. These were made for values of Re in the range $0.5 \times 10^5 < Re < 5 \times 10^5$.

Powe et al (5) have more recently used hot wire anemometry in measurements of the integral scale of turbulence, for all three directions for a flow of air in a pipe. These were made at different radius ratios for a value of Re of 1.65×10^5 only. Other workers (6,7) measured integral length scales for all three directions at different values of Re but only at the pipe axis, whilst Mickelsen (8) and Lawn (3) measured the Taylor microscale, λ , from which integral scales were obtained from Eq. (2.16). Since not all measurements include the variation of length scales with pipe radius ratio, apart from those reported in Ref.5, it was assumed that the raio of any length scale at a fixed position to that at the pipe centreline is independent of Re and was taken to be the same as that reported in Ref.5.

These measurements enable R_L, at a given position, to be calculated at different values of Re . From the combination of these with Eq.(2.30), it was possible to relate ε/ν with R_L at different radius ratio. Turbulent Reynolds numbers based on different parameters could be introduced. The programme gives a plot of the normalised turbulent transport number, obtained by dividing the turbulent transport number at a given position by that at the centre-line, against R_L for radius ratios between 0 and 0.9 at intervales of 0.1.

A2.1.1 Language

Algol 60.

A2.1.2 Input Data

The programme uses a permanent input file, in which r.m.s. turbulent velocity and integral length scales for the three coordinates at different values of Re and radius ratios between 0 and 0.9, at 0.1 intervals, are stored. The file may be listed if these values are required for use in any other programme or if more data need to be added.

The file, identified by the name DFRL, is ordered in a form which is convenient for reading both by computer and by eye. The first 10 lines are a list of r.m.s. turbulent velocity in the x-direction, u'. Each line represents a certain radius ratio, in which the first line represents the centreline (r/R=0) and line number 10 represents the position r/R=0.9. Similarly, lines 11 to 20 are a list of r.m.s. turbulent velocity in the y-direction, v', and lines 21 to 30 are a list of r.m.s. turbulent velocity in the z-direction, w'.

Lines 31 and 32 of the file are a list of L_x values obtained from Ref.5, for Re values of 1.65×10^5 and for r/R ranging between 0 and 0.9 at 0.1 intervals. Similarly, lines 33 and 34 give L_y and lines 35 and 36 give L_z. Lines 37 and 38 list integral length scales in the

x-direction at the centreline of the pipe, L_{xc} for fourteen different values of Re in the range 0.23×10^5 to 6.478×10^5. Similarly, lines 39 and 40 list L_{yc} and lines 41 and 42 list L_{zc}. With a value of kinematic viscosity, ν, of 1.568×10^{-5}, values of R_L were calculated by the programme.

A2.1.3 Output Data

Figure A2.1 shows an output from computer plot graphs in which R_L is defined as $u'L_y/\nu$, whilst Fig.A2.2 is for R_L based on the total kinetic energy, given by Eq.(2.22), as $\frac{1}{\sqrt{3}} (u'^2+v'^2+w'^2)^{\frac{1}{2}} L_y/\nu$. Both figures show that Eq.(2.20) is reasonably valid away from the pipe centreline up to a radius ratio of 0.8. As the radius ratio increases, Eq.(2.20) becomes less valid and this is probably not surprising because of the development of boundary layers close to the pipe internal surface.

The following expressions for R_L were used and the correlation with ε/ν examined:

(a) $R_L = \frac{v'L_y}{\nu}$

(b) $R_L = \frac{1}{\sqrt{3}} (u'^2+v'^2+w'^2)^{\frac{1}{2}} \frac{L_y}{\nu}$

(c) $R_L = \frac{1}{\sqrt{3}} (u'^2+v'^2+w'^2)^{\frac{1}{2}} \frac{(L_x+L_y+L_z)}{3\ \nu}$

(d) $R_L = \frac{1}{\sqrt{3}} (u'^2+v'^2+w'^2)^{\frac{1}{2}} \frac{(L_x \cdot L_y \cdot L_z)^{1/3}}{\nu}$

(e) $$R_L = \frac{v'(L_x+L_y+L_z)}{3\ \nu}$$

(f) $$R_L = \frac{v'(L_x \cdot L_y \cdot L_z)^{1/3}}{\nu}$$

(g) $$R_L = \frac{v'L_x}{\nu}$$

(h) $$R_L = \frac{u'L_x}{\nu}$$

(i) $$R_L = \frac{(u' \cdot v')^{\frac{1}{2}}\ (L_x \cdot L_y)^{\frac{1}{2}}}{\nu}$$

(j) $$R_L = \frac{(u' \cdot v' \cdot w')^{1/3}\ (L_x \cdot L_y \cdot L_z)^{1/3}}{\nu}$$

No better correlations were obtained than those given by cases (a) and (b) and shown in Figs.A2.1 and A2.2, respectively. Accordingly, a correlation based on a turbulent Reynolds number defined by (a) is recommended.

A2.2 THE PROGRAMME NORRL

```
'LIBRARY' (ED,SUBGROUPNAGA)
'LIBRARY'(ED,SUBGROUPLDSA)
'PMD'(ED,COFFIN)
'TRACE'2
'BEGIN'
    'PROCEDURE' E01ACA(M, N, G, A, B, X, Y, F, VAL, VALL, IFAIL);
        'VALUE'
            M, N, G;
        'INTEGER'
            M, N, G, IFAIL;
        'REAL'
            A, B, VAL, VALL;
        'ARRAY'
            X, Y, F;
        'ALGOL';
'PROCEDURE' E01AAA(N, X, A, B, C);
    'VALUE'
        N, X;
    'INTEGER'
        N;
    'REAL'
        X;
    'ARRAY'
        A, B, C;
    'ALGOL';
'PROCEDURE' E02ABA(M, X, F, W, K, N, SI, P, L);
    'VALUE'
        M, K;
```

```
    'INTEGER'
        M, K, N;
    'ARRAY'
        X, F, W, SI, P;
    'BOOLEAN'
        L;
    'ALGOL';
'PROCEDURE' EXCHANGE(A, B, N);
    'VALUE'
        N;
    'INTEGER'
        N;
    'ARRAY'
        A, B;
    'BEGIN'
    'INTEGER'
        I;
    'FOR' I:= 0 'STEP' 1 'UNTIL' N 'DO'
        B[I]:= A[I];
    'END';
'REAL'
    U1, U2, V1, V2, W1, W2, ALX, ALY, ALZ, NU, EPSILON, R2, RL, L0;
'INTEGER'
    R, I, IFAIL, ZZ, J;
'ARRAY'
    AEPSCL, ARL, AEPS, RE1, RE3[0:7], RAD[0:9], RE2[0:13], U, V,
    W[0:9, 0:7], LX, LY, LZ[0:9], LX0, LY0, AAA, BBB, LZ0[0:13],
    LXC, LYC, LZC[0:45], LX0C, LY0C, LZ0C[0:91], WW, BRL,
    BEPS[1:80], P, SI[0:1];
RE1[0]:= 0.5&5;
```

```
RE1[1]:= 0.9&5;
RE1[2]:= 1&5;
RE1[3]:= 2&5;
RE1[4]:= 2.5&5;
RE1[5]:= 3&5;
RE1[6]:= 4&5;
RE1[7]:= 5&5;
NU:= 1.568&-5;
RE3[0]:= 0.52&5;
RE3[1]:= 0.92&5;
RE3[2]:= 1.01&5;
RE3[3]:= 2.01&5;
RE3[4]:= 2.51&5;
RE3[5]:= 3.01&5;
RE3[6]:= 4.01&5;
RE3[7]:= 4.99&5;
ZZ:= 1;
WRITETEXT('('('C')'U'('C')')');
'FOR' R:= 0 'STEP' 1 'UNTIL' 9 'DO'
    'BEGIN'
    'FOR' I:= 0 'STEP' 1 'UNTIL' 7 'DO'
        'BEGIN'
        U[R, I]:= READ;
        PRINT(U[R, I], 0, 3);
        'END';
    NEWLINE(1);
    RAD[R]:= R / 10;
    'END';
WRITETEXT('('('C')'V'('C')')');
'FOR' R:= 0 'STEP' 1 'UNTIL' 9 'DO'
```

```
    'FOR' I:= 0 'STEP' 1 'UNTIL' 7 'DO'
        'BEGIN'
        V[R, I]:= READ;
        PRINT(V[R, I], 0, 3);
        'END';
WRITETEXT('('('C')'W'('C')')');
'FOR' R:= 0 'STEP' 1 'UNTIL' 9 'DO'
    'FOR' I:= 0 'STEP' 1 'UNTIL' 7 'DO'
        'BEGIN'
        W[R, I]:= READ;
        PRINT(W[R, I], 0, 3);
        'END';
WRITETEXT('('('C')'LX'('C')')');
'FOR' R:= 0 'STEP' 1 'UNTIL' 9 'DO'
    'BEGIN'
    LX[R]:= READ;
    'IF' R = 0 'THEN'
        LO:= LX[0];
    LX[R]:= LX[R] / LO;
    PRINT(LX[R], 0, 3);
    'END';
WRITETEXT('('('C')'LY'('C')')');
'FOR' R:= 0 'STEP' 1 'UNTIL' 9 'DO'
    'BEGIN'
    LY[R]:= READ;
    'IF' R = 0 'THEN'
        LO:= LY[0];
    LY[R]:= LY[R] / LO;
    PRINT(LY[R], 0, 3);
    'END';
```

```
WRITETEXT('('''('C')'LZ'('C')''')');
'FOR' R:= 0 'STEP' 1 'UNTIL' 9 'DO'
    'BEGIN'
    LZ[R]:= READ;
    'IF' R = 0 'THEN'
        L0:= LZ[0];
    LZ[R]:= LZ[R] / L0;
    PRINT(LZ[R], 0, 3);
    'END';
NEWLINE(1);
RE2[0]:= 0.23&5;
RE2[1]:= 0.4&5;
RE2[2]:= 0.61&5;
RE2[3]:= 0.9&5;
RE2[4]:= 1.65&5;
RE2[5]:= 1.975&5;
RE2[6]:= 2.8676&5;
RE2[7]:= 2.9625&5;
RE2[8]:= 3.95&5;
RE2[9]:= 4.1869&5;
RE2[10]:= 4.819&5;
RE2[11]:= 5.332&5;
RE2[12]:= 6.3199&5;
RE2[13]:= 6.478&5;
WRITETEXT('('''('C')'LX0'('C')''')');
'FOR' I:= 0 'STEP' 1 'UNTIL' 13 'DO'
    'BEGIN'
    LX0[I]:= READ;
    PRINT(LX0[I], 0, 3);
    'END';
```

```
WRITETEXT('('('C')'LYO'('C')')');
'FOR' I:= 0 'STEP' 1 'UNTIL' 13 'DO'
    'BEGIN'
    LYO[I]:= READ;
    PRINT(LYO[I], 0, 3);
    'END';
WRITETEXT('('('C')'LZO'('C')')');
'FOR' I:= 0 'STEP' 1 'UNTIL' 13 'DO'
    'BEGIN'
    LZO[I]:= READ;
    PRINT(LZO[I], 0, 3);
    'END';
NEWLINE(1);
IFAIL:= 0;
REGION( - 1.5, 5.2, 0.2, 3.9);
LIMITS(0, 15, 0, 10);
CRSIZE(0.075);
PLOTNI(1, .9, 10);
PLOTNI(2, .9, 10);
SUPFIX;
TYPENI(2);
NORMAL;
PLOTNI(3, .9, 10);
SUPFIX;
TYPENI(3);
NORMAL;
PLOTNI(4, .9, 10);
SUPFIX;
TYPENI(4);
NORMAL;
```

```
PLOTNI(.9, 1, 0);
PLOTNI(.9, 2, 1);
PLOTNI(.9, 3, 2);
CRSIZE(.06);
POSITN(2.1, .75);
TYPEAS('('TURBULENT%REYNOLDS%NUMBER%%')');
CRSIZE(.08);
TYPENC(28);
SUFFIX;
TYPENC(22);
NORMAL;
CRSIZE(.06);
ROTATE(.6, .7, 3.1412 / 2);
POSITN(1.5, .7);
TYPEAS('('NORMALISED%TURBULENT%TRANSPORT%NUMBER%%')');
CRSET(4);
ROTATE(.6, .7, 0);
CRSIZE(0.05);
REGION( - 1.5, 5.2, - 0.8, 2.9);
'FOR' R:= 0 'STEP' 1 'UNTIL' 9 'DO'
    'BEGIN'
    'FOR' I:= 0 'STEP' 1 'UNTIL' 7 'DO'
        'BEGIN'
        R2:= (R - 4.5) * 4.48 / 4.5 + 4.5;
        EPSILON:= .006666 * (1 - R2↑2 / 100) * (1 + 2 * R2↑2 /
        100) * (RE3[I]↑.875);
        E01ACA(7, 9, 9, R2 / 10, RE3[I], RAD, RE1, U, U1, U2,
        IFAIL);
        E01ACA(7, 9, 9, R2 / 10, RE3[I], RAD, RE1, V, V1, V2,
        IFAIL);
```

```
E01ACA(7, 9, 9, R2 / 10, RE3[I], RAD, RE1, W, W1, W2,
IFAIL);
EXCHANGE(LX, AAA, 9);
EXCHANGE(RAD, BBB, 9);
E01AAA(9, R2 / 10, BBB, AAA, LXC);
EXCHANGE(LY, AAA, 9);
EXCHANGE(RAD, BBB, 9);
E01AAA(9, R2 / 10, BBB, AAA, LYC);
EXCHANGE(LZ, AAA, 9);
EXCHANGE(RAD, BBB, 9);
E01AAA(9, R2 / 10, BBB, AAA, LZC);
EXCHANGE(LXO, AAA, 13);
EXCHANGE(RE2, BBB, 13);
E01AAA(13, RE3[I], BBB, AAA, LXOC);
EXCHANGE(LYO, AAA, 13);
EXCHANGE(RE2, BBB, 13);
E01AAA(13, RE3[I], BBB, AAA, LYOC);
EXCHANGE(LZO, AAA, 13);
EXCHANGE(RE2, BBB, 13);
E01AAA(13, RE3[I], BBB, AAA, LZOC);
U1:= (U1 + U2) / 2;
V1:= (V1 + V2) / 2;
W1:= (W1 + W2) / 2;
ALX:= LXC[45] * LXOC[91];
ALY:= LYC[45] * LYOC[91];
ALZ:= LZC[45] * LZOC[91];
RL:= SQRT((U1 * U1 + V1 * V1 + W1 * W1) / 3) * ALY / NU;
WW[ZZ]:= 1;
BRL[ZZ]:= ARL[I]:= LN(RL) / 2.302585;
BEPS[ZZ]:= AEPS[I]:= LN(EPSILON) / 2.302585;
```

```
    ZZ:= ZZ + 1;
    'END';
CRSIZE(0.075);
'IF' R = 0 'THEN'
    'BEGIN'
    'FOR' J:= 0 'STEP' 1 'UNTIL' 7 'DO'
        AEPSCL[J]:= AEPS[J];
    'END';
'FOR' J:= 0 'STEP' 1 'UNTIL' 7 'DO'
    AEPS[J]:= AEPS[J] / AEPSCL[J];
CURPTO(ARL, AEPS, 0, 7, 50 + R);
    PLOTNC(3.3, 0.7 - R * 0.07, 50 + R);
    CRSIZE(0.055);
    PLOTNF(3.5, 0.7 - R * 0.07, R / 10, 2);
    'END';
CRSET(2);
PLOTNC(3.5, 0.83, 28);
CRSET(0);
TYPENC(46);
TYPENC(28);
RFGION( - 1.5, 5.2, 0.2, 3.9);
POINT(1, 3);
JOIN(4, 3);
POINT(4, 2);
JOIN(1, 2);
POINT(1, 1);
JOIN(4, 1);
POINT(4, 1);
JOIN(4, 3);
POINT(3, 3);
```

```
    JOIN(3, 1);
    POINT(2, 1);
    JOIN(2, 3);
    POINT(1, 3);
    JOIN(1, 1);
    BORDER;
    GREND;
'END'
```

A2.3 THE DATAFILE DFRL

1. 0.25463,0.361998,0.51854,0.7517,0.60204,1.157475,1.4959,1.81003,
2. 0.29323,0.367982,0.5170,1.01858,0.62028,1.43527,1.88585,2.29795,
3. 0.30094,0.40089,0.55559,1.14205,0.671365,1.75936,2.23745,2.71504,
4. 0.35882,0.448758,0.67134,1.25007,0.758935,1.87511,2.4612,3.0377,
5. 0.38583,0.502609,0.81795,1.43527,0.8392,2.08315,2.68495,3.28166,
6. 0.42441,0.550477,0.88739,1.54331,0.9121817,2.17605,2.79366,3.46266,
7. 0.47456,0.6013363,0.93369,1.65134,1.03624,2.40755,3.13244,3.83254,
8. 0.46299,0.658179,0.97999,1.7748,1.058131,2.59274,3.32422,4.09224,
9. 0.55559,0.7060465,1.07259,1.8674,1.1311,2.70849,3.45207,4.24963,
10. 0.590312,0.7718645,1.11117,2.08346,1.258811,3.05573,3.89956,4.80051,
11. 0.231495,0.2884215,0.37039,0.47547,0.36613,0.73213,0.9462,1.14487,
12. 0.235353,0.2901982,0.37348,0.636612,0.38444,0.89704,1.178656,1.436218,
13. 0.23766,0.3050042,0.42441,0.6149499,0.38809,0.947347,1.2047807,1.461944,
14. 0.26236,0.3209948,0.46299,0.6707692,0.402743,1.006125,1.3206439,1.629985,
15. 0.27779,0.3434999,0.46299,0.717635,0.421049,1.041575,1.342475,1.64083,

16. 0.31637,0.3630439,0.50929,0.784202,0.45034,1.1057164,1.4195426,1.759481,
17. 0.32409,0.3814034,0.54016,0.8166626,0.49794,1.1906429,1.5491339,1.895365,
18. 0.32409,0.39798618,0.55559,0.8422779,0.48695,1.230452,1.577595,1.94208,
19. 0.32795,0.4086465,0.54787,0.88778,0.549195,1.287642,1.641148,2.020315,
20. 0.32409,0.4086465,0.56176,0.845462,0.530888,1.2400064,1.58243,1.948033,
21. 0.23149,0.288425,0.40897,0.47547,0.36613,0.73213,0.9462,1.14487,
22. 0.23535,0.2961206,0.42595,0.636612,0.36962,0.89704,1.178656,1.436218,
23. 0.25078,0.3109267,0.42749,0.7099229,0.41843,1.093656,1.390847,1.687727,
24. 0.28551,0.3393543,0.46299,0.7738528,0.453304,1.160782,1.5236,1.8804809,
25. 0.30866,0.375481,0.50312,0.904844,0.52304,1.31329,1.692685,2.068872,
26. 0.32795,0.4045008,0.54016,1.0267989,0.575347,1.447775,1.858685,2.303785,
27. 0.33953,0.4323361,0.57874,1.0769608,0.5927819,1.5701413,2.042896,2.499483,
28. 0.36267,0.4560258,0.61115,1.082929,0.62765,1.5820108,2.02833,2.49696,
29. 0.37811,0.479715,0.6559,1.174654,0.662521,1.703727,2.171463,2.673154,
30. 0.39199,0.5241336,0.66362,1.2562038,0.714825,1.842425,2.351205,2.894425,

```
31. 0.020563,0.025636,0.029454,0.03229,0.033709,0.033272,0.032182,0.030545,
32. 0.003109,0.0033109,
33. 0.01189,0.01188,0.012163,0.013472,0.014727,0.014836,0.012873,0.010909,
34. 0.010363,0.0090,
35. 0.006709,0.008727,0.0099818,0.010363,0.009436,0.0080727,0.006,0.005836,
36. 0.00709,0.009272,
37. 0.002057,0.002667,0.0041148,0.016248,0.020563,0.014305,0.029809,
38. 0.021133,0.02682,0.03535,0.03186,0.04328,0.046939,0.0408,
39. 0.0010287,0.0013335,0.002057,0.008124,0.01189,0.007152,0.0149,
40. 0.010566,0.013411,0.017678,0.01593,0.02164,0.023469,0.0204,
41. 0.0010287,0.0013335,0.002057,0.008124,0.006709,0.007152,0.0149,
42. 0.010566,0.013411,0.017678,0.01593,0.02164,0.023469,0.0204,
    ****

    ********************************************************************************************************************
```

A2.4 NOMENCLATURE

a pipe radius ratio, Eq.(2,3)

L integral scale of turbulence

r radius

R pipe radius

Re pipe flow Reynolds number

R_L turbulent Reynolds number based on integral scale, L

u' r.m.s. turbulent axial velocity

v' r.m.s. turbulent radial velocity

w' r.m.s. turbulent velocity in third orthogonal direction

ε turbulent diffusivity

λ Taylor microscale of turbulence

ν kinematic viscosity

ε/ν turbulent transport number

Subscripts

x axial direction

y radial direction

z third orthogonal direction

c pipe centreline

A2.5 REFERENCES

1. J.LAUFER, The structure of turbulence in fully developed pipe flow, NACA Rep. 1174 (1954).

2. V.A.SANDBORN, Experimental evaluation of momentum terms in turbulent pipe flow, NACA TN3266 (1955).

3. C.J.LAWN, The determination of the rate of dissipation in turbulent pipe flow, J.Fluid Mech.48, 477 (1971).

4. H.W.TOWNES, J.L.GOW, R.E.POWE and N.WEBER, Turbulent flow in smooth and rough pipes, Trans.Am.Soc.Mech. Engrs 94, 353 (1972). (Series D, Journal of Basic Engineering.)

5. R.E.POWE and H.W.TOWNES, Turbulence structure for fully developed flow in rough pipes, Trans.Am.Soc. Mech.Engrs 95, 255 (1973). (Series I, Journal of Fluid Engineering.)

6. L.V.BALDWIN and T.J.WALSH, Turbulent diffusion in the core of fully developed pipe flow, A.I.Ch.E.J. 7, 53 (1961).

7. J.M.ROBERTSON, J.H.BURKHART and J.D.MARTIN, Study of turbulent flow in rough pipes, University of Ill., Theoretical and Applied Mechanics Rep.No.279, Urbana (1965).

8. W.R.MICKELSEN, An experimental comparison of Lagrangian and Eulerian correlation coefficients in homogeneous isotropic turbulence, NACA TN 3570 (1955).

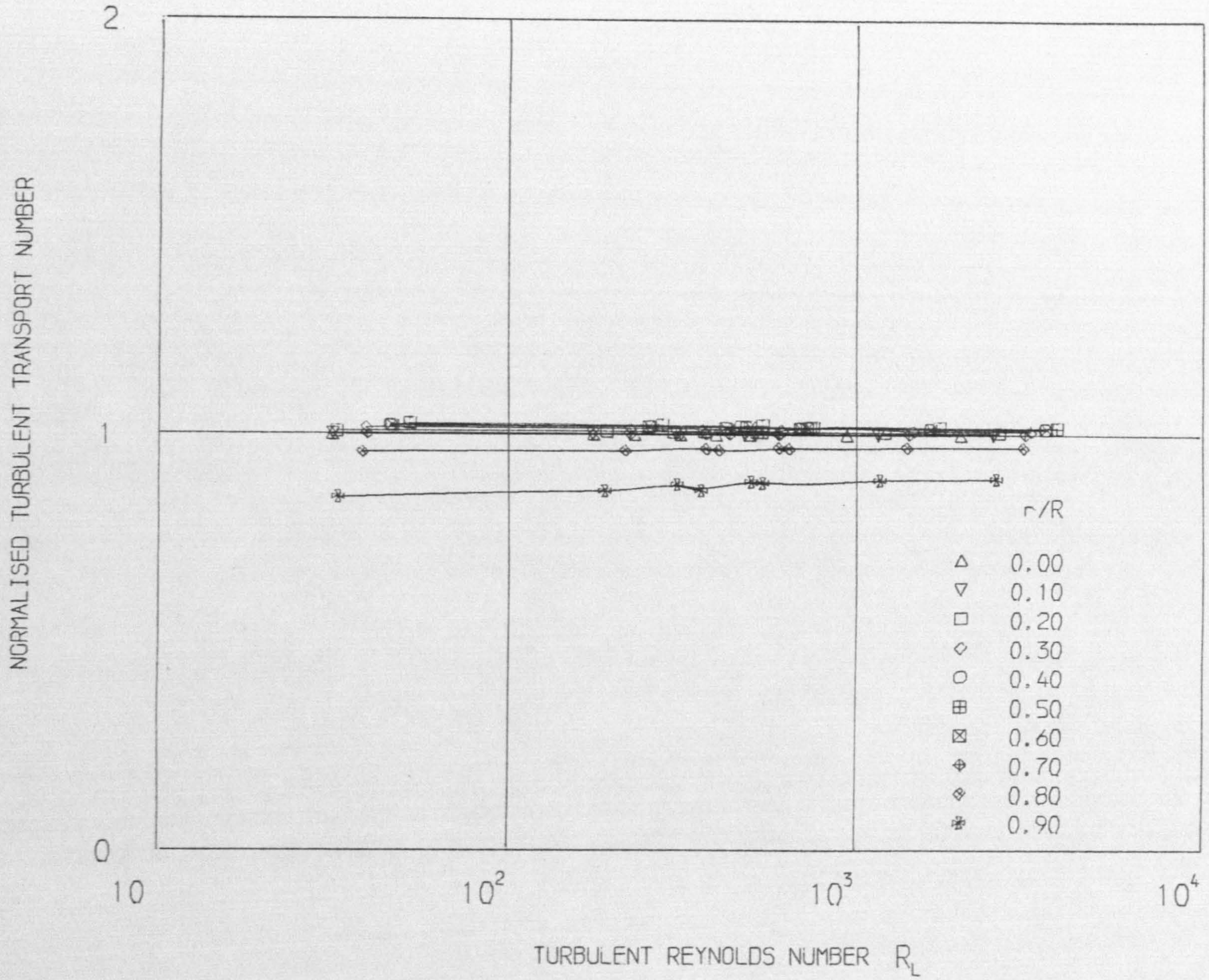

FIG.A2.1 VARIATION OF ε/ν WITH $R_L(=v'L_y/\nu)$ AT DIFFERENT RADII FOR PIPE FLOW

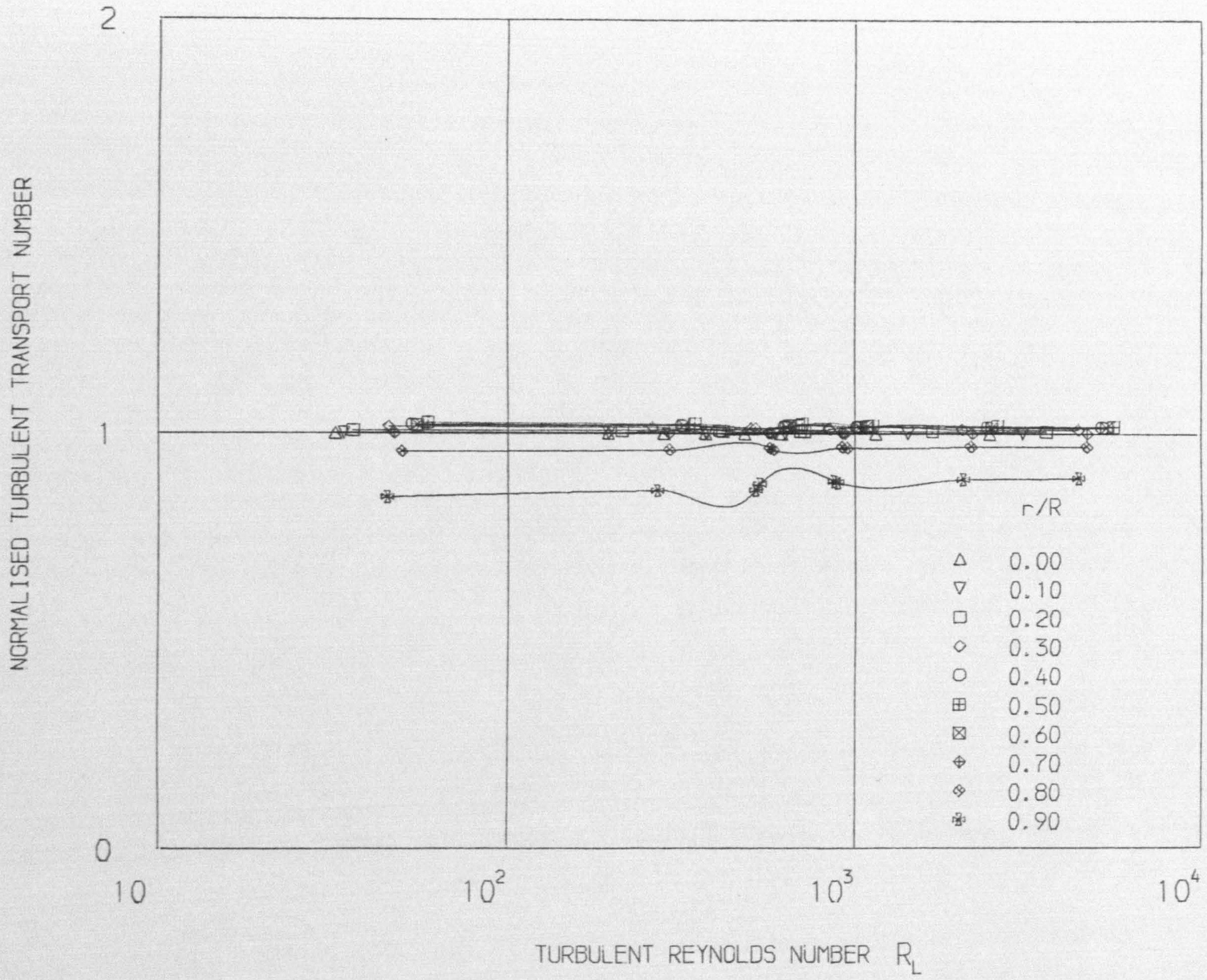

FIG. A2.2 VARIATION OF ε/ν WITH $R_L(=1/\sqrt{3}\ (u'^2+v'^2+w'^2)L_y/\nu)$ AT DIFFERENT RADII FOR PIPE FLOW

"There are more questions than answers,

And the more I find out the less I know"

Pop Song (1972)